

# UC Davis

## Research Reports

### Title

Guidance for Selection of Unbound Pavement Layer Seasonal Stiffnesses

### Permalink

<https://escholarship.org/uc/item/4k2551p7>

### Authors

Curran, Hannah M.

Harvey, John T.

Wu, Rongzong

### Publication Date

2018-11-01

Research Report – UCD-ITS-RR-18-26

---

# Guidance for Selection of Unbound Pavement Layer Seasonal Stiffnesses

November 2018

Hannah M. Curran  
John T. Harvey  
Rongzong Wu

# Guidance for Selection of Unbound Pavement Layer Seasonal Stiffnesses

**Authors:**  
Hannah M. Curran, John T. Harvey, and Rongzong Wu

Partnered Pavement Research Center (PPRC) Project Number 3.30 (DRISI Task 2667):  
Standard Materials Library and Guidance

---

**PREPARED FOR:**

California Department of Transportation  
Division of Research, Innovation, and System  
Information  
Office of Materials and Infrastructure

**PREPARED BY:**

University of California  
Pavement Research Center  
UC Davis, UC Berkeley








## TECHNICAL REPORT DOCUMENTATION PAGE

1. REPORT NUMBER UCPRC-RR-2017-11	2. GOVERNMENT ASSOCIATION NUMBER	3. RECIPIENT'S CATALOG NUMBER
4. TITLE AND SUBTITLE Guidance for Selection of Unbound Pavement Layer Seasonal Stiffnesses		5. REPORT PUBLICATION DATE November 2018
		6. PERFORMING ORGANIZATION CODE
7. AUTHOR(S) H.M. Curran, J.T. Harvey (ORCID 0000-0002-8924-6212), and R. Wu (ORCID 0000-0001-7364-7583)		8. PERFORMING ORGANIZATION REPORT NO. UCPRC-RR-2017-11
9. PERFORMING ORGANIZATION NAME AND ADDRESS University of California Pavement Research Center Department of Civil and Environmental Engineering, UC Davis 1 Shields Avenue Davis, CA 95616		10. WORK UNIT NUMBER
		11. CONTRACT OR GRANT NUMBER 65A0542
12. SPONSORING AGENCY AND ADDRESS California Department of Transportation Division of Research, Innovation, and System Information P.O. Box 942873 Sacramento, CA 94273-0001		13. TYPE OF REPORT AND PERIOD COVERED Research Report 2014 to 2017
		14. SPONSORING AGENCY CODE
15. SUPPLEMENTAL NOTES		
16. ABSTRACT <p>One of the benefits of using mechanistic-empirical (ME) design methods for pavements is the ability to calculate pavement response to various loading and climate conditions, and then in turn to model the entire damage process that is expected to occur over the pavement lifetime. One property that is currently not accounted for within California's ME design software (<i>CaME</i>) is the change in stiffness of unbound materials that may occur due to seasonal moisture patterns. The engineering properties of unbound material may change due to a variety of factors, such as fluctuations in water content, changes in suction during wetting or drying periods, changes in overburden stress, and they are also dependent on geologic setting. Before moving to develop and implement more complex relationships to model assumed changes in the properties of unbound layers due to seasonal moisture changes, the University of California Pavement Research Center (UCPRC) evaluated the extent of variation that is observed in the field. The goals of this research are to evaluate whether or not these speculated seasonal changes in unbound material properties warrant further design optimization, and if so, how research to characterize such optimization should proceed in the future.</p> <p>In this research, an experiment was performed to evaluate if noticeable changes in subgrade stiffness can be identified and explained using available, pertinent, and easy-to-use pavement monitoring equipment. Testing was performed twice on sections across California, once in the wet season and once in the dry season, to get a broad picture of the types of materials present and their corresponding properties during wet and dry seasons. Monitoring of a test section at UC Davis was also performed more frequently to observe changes in stiffness occurring after rainfall events and during wetting and drying cycles.</p> <p>The literature and various laboratory experiments investigating the influence of moisture and suction on the resilient response of unbound materials strongly suggest that a large degree of variability in stiffness should be encountered in different moisture conditions. However, the results of the study revealed that a majority of the unbound material tested experienced minor, if any, changes at all in stiffness between the two rounds of testing seasonal testing. The most susceptible materials to stiffness variation were not necessarily the compacted subgrade material, but were the stabilized and unstabilized granular materials directly underlying the asphalt surface. While changes in moisture content and penetration resistance were observed between the two rounds of testing, they did not necessarily correspond to significant fluctuation in the field-tested stiffness of the unbound materials; rather, other factors such as spatial variability, drainage conditions, soil type, and influences from overlying layers tended to have a much larger influence on the resilient response of these materials than did seasonal moisture change.</p> <p>It is therefore recommended that <i>CaME</i>'s current assumption of constant stiffness for unbound layers continue to be used, except in cases where the designer identifies issues with drainage, irrigation, or other likely causes of seasonal variation of stiffness. Performing FWD testing for backcalculation of unbound layer stiffnesses after the rainy season, or at other times of highest moisture contents where rainfall is not the main source of moisture, will impart some conservatism into designs.</p>		
17. KEY WORDS Subgrade, unbound layers, seasonal variation, stiffness, backcalculation, asphalt pavement, ME design		18. DISTRIBUTION STATEMENT No restrictions. This document is available to the public through the National Technical Information Service, Springfield, VA 22161
19. SECURITY CLASSIFICATION (of this report) Unclassified	20. NUMBER OF PAGES 194	21. PRICE None

Reproduction of completed page authorized

## UCPRC ADDITIONAL INFORMATION

1. DRAFT STAGE Final	2. VERSION NUMBER 1				
3. PARTNERED PAVEMENT RESEARCH CENTER STRATEGIC PLAN ELEMENT NUMBER 3.30	4. DRISI TASK NUMBER 2667				
5. CALTRANS TECHNICAL LEAD AND REVIEWER(S) Raghubar Shrestha	6. FHWA NUMBER CA192667B				
7. PROPOSALS FOR IMPLEMENTATION It is recommended that the current assumed constant values for stiffness of unbound layers in the <i>CalME</i> design software remain unchanged, and that more complex models for seasonal stiffness changes of unbound layers do not need to be developed. It is recommended that stiffness using deflection testing only be measured once as part of project development at whatever is expected to be the time with lowest stiffness of the unbound materials, which is Caltrans current practice. That time of lowest stiffness will depend on rainfall, drainage, agricultural irrigation, and other local conditions that affect moisture contents.					
8. RELATED DOCUMENTS					
9. LABORATORY ACCREDITATION The UCPRC laboratory is accredited by AASHTO re:source for the tests listed in this report					
10. SIGNATURES					
H.M. Curran <b>FIRST AUTHOR</b>	J.T. Harvey <b>TECHNICAL REVIEW</b>	D. Spinner <b>EDITOR</b>	J.T. Harvey <b>PRINCIPAL INVESTIGATOR</b>	R. Shrestha <b>CALTRANS TECH. LEAD</b>	T.J. Holland <b>CALTRANS CONTRACT MANAGER</b>

Reproduction of completed page authorized

# TABLE OF CONTENTS

<b>LIST OF FIGURES .....</b>	<b>vii</b>
<b>LIST OF TABLES .....</b>	<b>xi</b>
<b>PROJECT OBJECTIVES.....</b>	<b>xiv</b>
<b>EXECUTIVE SUMMARY.....</b>	<b>xv</b>
<b>LIST OF ABBREVIATIONS.....</b>	<b>xxiii</b>
<b>LIST OF TEST METHODS AND SPECIFICATIONS USED IN THE REPORT .....</b>	<b>xxiv</b>
<b>1 INTRODUCTION.....</b>	<b>1</b>
1.1 Background .....	1
1.2 Problem Statement, and Project Goals, and Objectives .....	4
1.3 Organization of Report.....	5
<b>2 LITERATURE REVIEW.....</b>	<b>7</b>
2.1 Introduction .....	7
2.2 Geotechnical Pavement Design Considerations.....	7
2.3 Unbound Pavement Material Properties.....	7
2.3.1 Characterization .....	8
2.3.2 Resilient Response .....	8
2.3.2.1 Definition of Resilient Modulus.....	9
2.3.2.2 Falling Weight Deflectometer and Backcalculation.....	11
2.3.2.3 Factors Affecting Resilient Response .....	13
Moisture and Suction .....	13
2.4 Current Modeling of Seasonal Variability in Modulus .....	17
2.4.1 Enhanced Integrated Climatic Model.....	17
2.4.2 South Africa Pavement Design Method.....	19
2.4.3 WesTrack Experiment.....	20
2.5 CalME .....	20
2.6 Knowledge Gaps .....	23
2.7 Additional Questions from the Literature .....	23
<b>3 EXPERIMENT DESIGN AND LABORATORY TESTING .....</b>	<b>25</b>
3.1 Introduction .....	25
3.2 Research Instruments .....	25
3.2.1 Deflection Testing and Backcalculation.....	25
3.2.2 Dynamic Cone Penetrometer .....	27
3.3 Experiment Design.....	29
3.3.1 Long-Term Assessment of Seasonal Changes .....	29
3.3.1.1 Section Information, Location, and Schedule .....	30
3.3.1.2 Section Descriptions.....	32
3.3.1.3 Field Testing Procedures.....	32
Initial Condition Survey .....	32
Falling Weight Deflectometer Testing.....	32
Coring and Sampling Procedure .....	33
3.3.1.4 Laboratory .....	34
Moisture Content.....	34
Soil Properties .....	34
3.3.1.5 Analyses .....	36
3.3.2 Small-Scale Assessment of Seasonal Changes .....	37
3.3.2.1 Outside Track Description .....	37
3.3.2.2 Testing Factorial.....	39
3.3.2.3 Limitations of Experiment .....	39

<b>4</b>	<b>RESULTS .....</b>	<b>41</b>
4.1	Seasonal Behavior .....	41
4.1.1	Colusa 20.....	43
4.1.1.1	Structure .....	44
4.1.1.2	Unbound Material Properties .....	45
4.1.1.3	Falling Weight Deflectometer .....	46
4.1.2	El Dorado 193 .....	49
4.1.2.1	Structure .....	50
4.1.2.2	Unbound Material Properties .....	51
4.1.2.3	Falling Weight Deflectometer.....	53
4.1.3	Sierra 89 .....	56
4.1.3.1	Structure .....	56
4.1.3.2	Unbound Material Properties .....	58
4.1.3.3	Falling Weight Deflectometer .....	59
4.1.4	Plumas 70 .....	64
4.1.4.1	Structure .....	65
4.1.4.2	Unbound Material Properties .....	66
4.1.4.3	Falling Weight Deflectometer.....	67
4.1.5	Ventura 33 .....	70
4.1.5.1	Structure .....	71
4.1.5.2	Unbound Material Properties .....	72
4.1.5.3	Falling Weight Deflectometer.....	73
4.1.6	San Luis Obispo 166 .....	76
4.1.6.1	Structure .....	77
4.1.6.2	Unbound Material Properties .....	78
4.1.6.3	Falling Weight Deflectometer .....	80
4.1.7	Santa Barbara 166 .....	80
4.1.7.1	Structure .....	81
4.1.7.2	Unbound Material Properties .....	82
4.1.7.3	Falling Weight Deflectometer.....	84
4.1.8	San Luis Obispo 46 .....	87
4.1.8.1	Structure .....	88
4.1.8.2	Unbound Material Properties .....	89
4.1.8.3	Falling Weight Deflectometer .....	91
4.1.9	Lassen 44.....	94
4.1.9.1	Structure .....	95
4.1.9.2	Unbound Material Properties .....	96
4.1.9.3	Falling Weight Deflectometer.....	98
4.1.10	Modoc 395 .....	101
4.1.10.1	Structure .....	102
4.1.10.2	Unbound Material Properties .....	103
4.1.10.3	Falling Weight Deflectometer.....	105
4.1.11	Modoc 299 .....	108
4.1.11.1	Structure .....	109
4.1.11.2	Unbound Material Properties .....	110
4.1.11.3	Falling Weight Deflectometer.....	112
4.2	Short-Term Seasonal Behavior Measured at ATIRC Test Track.....	115
4.3	DCP Correlated Stiffness Evaluation .....	119
4.4	Asphalt-Bound Materials .....	121
4.4.1	Damage in Hot Mix Asphalt .....	121
4.4.2	Temperature Susceptibility of Hot Mix Asphalt .....	123

4.4.3	Temperature Susceptibility of Full-Depth Reclamation with Foamed Asphalt .....	125
4.5	Summary of Results .....	125
<b>5</b>	<b>CONCLUSIONS AND RECOMMENDATIONS .....</b>	<b>133</b>
5.1	Summary and Conclusions .....	133
5.1.1	Seasonal Changes in Unbound Material Properties .....	133
5.1.2	DCP-Correlated Stiffness .....	134
5.1.3	Asphalt-Bound and Lightly Stabilized Materials .....	135
5.2	Recommendations .....	135
	<b>REFERENCES .....</b>	<b>137</b>
	<b>ADDITIONAL SOURCES .....</b>	<b>142</b>
	<b>APPENDIX A: SITE DESCRIPTIONS .....</b>	<b>146</b>
	Colusa 20 .....	146
	El Dorado 193 .....	146
	Sierra 89 .....	147
	Plumas 70 .....	148
	Ventura 33 .....	149
	State Route 166 .....	150
	San Luis Obispo 46 .....	152
	Lassen 44 .....	153
	Modoc 395 .....	154
	Modoc 299 .....	155
	Appendix A References .....	156
	<b>APPENDIX B: ASPHALT-BOUND MATERIAL .....</b>	<b>158</b>



## LIST OF FIGURES

---

Figure 1.1: Example of <i>CalME</i> design modeling damage (longer trend) and seasonal climate variation. ....	2
Figure 1.2: California pavement climate regions. ....	3
Figure 2.1: Definition of resilient modulus. ....	9
Figure 2.2: Typical plots showing the stress sensitivity of the resilient modulus: (a) stress stiffening and (b) stress softening. ....	11
Figure 2.3: Typical FWD testing setup (14). ....	12
Figure 2.4: Simplified schematic of suction under pavements (5). ....	14
Figure 2.5: Conceptual distribution of pore air and water in a soil matrix (18). ....	14
Figure 2.6: Effective stress in unsaturated soil (21). ....	14
Figure 2.7: Air-soil-water interface in unsaturated soils (24) showing menisci under (a) wetting and (b) drying. ....	15
Figure 2.8: Soil-water characteristic curve (18). ....	18
Figure 2.9: Effective stress in partially saturated unbound granular material (21). ....	19
Figure 2.10: WesTrack seasonal variation of foundation-soil modulus for (a) south tangent and (b) north tangent. ....	20
Figure 2.11: Discrete element modeling of unbound material under a stiff material (11). ....	21
Figure 3.1: Example of load normalization for unbound layer stiffness. ....	27
Figure 3.2: Graphical representation of relationships of DN versus corrected resilient modulus for typical range of DN. ....	28
Figure 3.3: Locations of test sites (yellow boundaries indicate Caltrans districts). ....	29
Figure 3.4: Plan view of FWD testing locations (for one lane). ....	33
Figure 3.5: Field sampling flow chart. ....	34
Figure 3.6: Linear shrinkage mold. ....	36
Figure 3.7: Outside track DCP. ....	38
Figure 3.8: GPR scans of outside track. ....	38
Figure 3.9: ATIRC outside track. ....	40
Figure 4.1: Precipitation graph of California climate regions (55). ....	42
Figure 4.2: Drainage conditions at Colusa 20 PM 15.35 in (a) May 2015 and (b) April 2016. ....	43
Figure 4.3: Drainage conditions at Colusa 20 PM 15.35 in (a) May 2015 and (b) April 2016. ....	43
Figure 4.4: Cores from Colusa 20. ....	44
Figure 4.5: Unbound materials testing and sampling results for Colusa 20. ....	45
Figure 4.6: Colusa 20 backcalculated stiffnesses, May 14, 2015. ....	46
Figure 4.7: Colusa 20 backcalculated stiffnesses, April 5, 2016. ....	47
Figure 4.8: Colusa 20 unbound layer stiffnesses between the wheelpaths. ....	47
Figure 4.9: Colusa 20 unbound layer stiffnesses in the wheelpath. ....	48
Figure 4.10: Colusa 20 overlying layer effect. ....	49
Figure 4.11: Road conditions on El Dorado 193 during (a) May 2015 and (b) May 2016. ....	50
Figure 4.12: Cores from El Dorado 193. ....	51
Figure 4.13: Unbound materials testing and sampling results for El Dorado 193. ....	52
Figure 4.14: El Dorado 193 backcalculated stiffnesses, May 21, 2015. ....	53
Figure 4.15: El Dorado 193 backcalculated stiffnesses, May 10, 2016. ....	54
Figure 4.16: El Dorado 193 unbound layer stiffnesses between the wheelpaths. ....	54
Figure 4.17: El Dorado 193 unbound layer stiffnesses in the wheelpath. ....	55
Figure 4.18: El Dorado 193 overlying layer effect. ....	56
Figure 4.19: Road conditions on Sierra 89 PM 28.05 on May 11, 2016. ....	57
Figure 4.20: Cores from Sierra 89. ....	58
Figure 4.21: Unbound materials testing and sampling results for Sierra 89. ....	59
Figure 4.22: Sierra 89 backcalculated stiffnesses, July 23, 2015. ....	60

Figure 4.23: Sierra 89 backcalculated stiffnesses, May 11, 2016.....	61
Figure 4.24: Sierra 89 unbound layer stiffnesses between the wheelpaths.....	61
Figure 4.25: Sierra 89 unbound layer stiffnesses in the wheelpath.....	62
Figure 4.26: Sierra 89 overlying layer effect.....	63
Figure 4.27: Road condition on Sierra 89N PM 28.06 in 2010.....	64
Figure 4.28: Plumas 70 surrounding area road conditions in (a) July 2015 (b) and April 2016.....	64
Figure 4.29: Cores from Plumas 70.....	65
Figure 4.30: Unbound materials testing and sampling results for Plumas 70.....	66
Figure 4.31: Plumas 70 backcalculated stiffnesses, July 21, 2015.....	67
Figure 4.32: Plumas 70 backcalculated stiffnesses, April 26, 2016.....	68
Figure 4.33: Plumas 70 unbound layer stiffnesses between the wheelpaths.....	68
Figure 4.34: Plumas 70 unbound layer stiffnesses in the wheelpath.....	69
Figure 4.35: Plumas 70 overlying layer effect.....	70
Figure 4.36: Road conditions near Ventura 33 (a) PM 51.5 and (b) PM 52.2 in June 2016.....	70
Figure 4.37: Cores from Ventura 33.....	71
Figure 4.38: Unbound materials testing and sampling results for Ventura 33.....	72
Figure 4.39: Ventura 33 backcalculated stiffnesses, July 28, 2015.....	74
Figure 4.40: Ventura 33 backcalculated stiffnesses, June 9, 2016.....	74
Figure 4.41: Ventura 33 unbound layer stiffnesses between the wheelpaths.....	75
Figure 4.42: Ventura 33 unbound layer stiffnesses in the wheelpath.....	75
Figure 4.43: Ventura 33 overlying layer effect.....	76
Figure 4.44: Road conditions on San Luis Obispo 166 near (a) PM 41.5 and (b) PM 42.5 in May 2016.....	77
Figure 4.45: Cores from San Luis Obispo 166.....	78
Figure 4.46: Unbound materials testing and sampling results for San Luis Obispo 166.....	79
Figure 4.47: Site conditions at Santa Barbara 166 in May 2016.....	81
Figure 4.48: Cores from Santa Barbara 166.....	82
Figure 4.49: Unbound materials testing and sampling results for Santa Barbara 166.....	83
Figure 4.50: Santa Barbara 166 backcalculated stiffnesses, July 29, 2015.....	84
Figure 4.51: Santa Barbara 166 backcalculated stiffnesses, May 5, 2016.....	85
Figure 4.52: Santa Barbara 166 unbound layer stiffness between the wheelpaths.....	85
Figure 4.53: Santa Barbara 166 unbound layer stiffness in the wheelpath.....	86
Figure 4.54: Santa Barbara 166 overlying layer effect.....	87
Figure 4.55: Site and drainage conditions at San Luis Obispo 46 in May 2016.....	88
Figure 4.56: Cores from San Luis Obispo 46.....	89
Figure 4.57: Unbound materials testing and sampling results for San Luis Obispo 46.....	90
Figure 4.58: San Luis Obispo 46 backcalculated stiffnesses, July 31, 2015.....	91
Figure 4.59: San Luis Obispo 46 backcalculated stiffnesses, May 3, 2015.....	92
Figure 4.60: San Luis Obispo 46 unbound layer stiffnesses between the wheelpaths.....	92
Figure 4.61: San Luis Obispo 46 unbound layer stiffnesses in the wheelpath.....	93
Figure 4.62: San Luis Obispo overlying layer effect.....	94
Figure 4.63: Surface conditions at Lassen 44 in August 2015.....	95
Figure 4.64: Drainage conditions at Lassen 44 in (a) August 2015 and (b) April 2016.....	95
Figure 4.65: Cores from Lassen 44.....	96
Figure 4.66: Unbound materials testing and sampling results for Lassen 44.....	97
Figure 4.67: Lassen 44 backcalculated stiffnesses, August 3, 2015.....	98
Figure 4.68: Lassen 44 backcalculated stiffnesses, April 21, 2016.....	99
Figure 4.69: Lassen 44 unbound layer stiffness between the wheelpaths.....	99
Figure 4.70: Lassen 44 unbound layer stiffnesses in the wheelpath.....	100
Figure 4.71: Lassen 44 overlying layer effect.....	101
Figure 4.72: Site conditions at Modoc 395.....	102
Figure 4.73: Cores for Modoc 395.....	103



Figure 4.74: Unbound materials testing and sampling results for Modoc 395. ....	104
Figure 4.75: Modoc 395 backcalculated stiffnesses, August 4, 2015. ....	105
Figure 4.76: Modoc 395 backcalculated stiffnesses, April 20, 2016. ....	106
Figure 4.77: Modoc 395 unbound layer stiffnesses between the wheelpaths. ....	106
Figure 4.78: Modoc 395 unbound layer stiffnesses in the wheelpath.....	107
Figure 4.79: Modoc 395 overlying layer effect.....	108
Figure 4.80: Middle Alkali Lake next to Modoc 299 during testing in August 2015 (a) and April 2016 (b).....	109
Figure 4.81: Cores for Modoc 299.....	110
Figure 4.82: Unbound materials testing and sampling results for Modoc 299. ....	111
Figure 4.83: Modoc 299 backcalculated stiffnesses, August 5, 2015. ....	112
Figure 4.84: Modoc 299 backcalculated stiffnesses, April 19, 2016. ....	113
Figure 4.85: Modoc 299 unbound layer stiffness between the wheelpaths.....	113
Figure 4.86: Modoc 299 unbound layer stiffnesses in the wheelpath. ....	114
Figure 4.87: Modoc 299 overlying layer effect.....	115
Figure 4.88: ATIRC stiffness time history.....	116
Figure 4.89: ATIRC AB overlying layer effect. ....	117
Figure 4.90: ATIRC outside tracks drainage conditions.....	118
Figure 4.91: Lime-treated subgrade and subgrade overlying layer effect.....	119
Figure 4.92: DN median versus backcalculated stiffness between the wheelpaths (EBWP).....	120
Figure 4.93: DN median versus backcalculated stiffness in the wheelpath (EWP). ....	120
Figure 4.94: Comparison of backcalculated modulus with DCP-correlated stiffness.....	121
Figure 4.95: Temperature susceptibility of HMA from backcalculated master curves.....	124
Figure 4.96: Asphalt aging and temperature susceptibility from backcalculated master curves. ....	124
Figure 4.97: Temperature susceptibility of asphalt-stabilized base (full-depth reclamation with foamed asphalt).....	125
Figure 4.98: Summary of base stiffness by type (Round 1 at end of 2015 dry season, Round 2 at end of 2016 wet season). ....	126
Figure 4.99: Summary of unbound material stiffness by type (Round 1 at end of 2015 dry season, Round 2 at end of 2016 wet season).....	127
Figure 4.100: Summary of base stiffness by climate region (Round 1 at end of 2015 dry season, Round 2 at end of 2016 wet season).....	127
Figure 4.101: Summary of soil stiffness by climate region (Round 1 at end of 2015 dry season, Round 2 at end of 2016 wet season).....	128
Figure 4.102: Unbound layer stiffness versus days since last rainfall event (a) between the wheelpaths and (b) in the wheelpath. ....	129
Figure 4.103: Influence of shoulder distance on stiffness.....	130
Figure 4.104: Unbound material stiffness compared with MEPDG-correlated values (Round 1 at end of 2015 dry season, Round 2 at end of 2016 wet season). ....	131
Figure A.1: Test section on Colusa 20. ....	146
Figure A.2: Test section on El Dorado 193.....	147
Figure A.3: Test section on Sierra 89.....	148
Figure A.4: Test section on Plumas 70. ....	149
Figure A.5: Test section on Ventura 33. ....	150
Figure A.6: Test section on San Luis Obispo 166.....	151
Figure A.7: Test section on Santa Barbara 166.....	152
Figure A.8: Test section on San Luis Obispo 46.....	153
Figure A.9: Test section on Lassen 44. ....	154
Figure A.10: Test section on Modoc 395.....	155
Figure A.11: Test section on Modoc 299.....	156
Figure B.1: Colusa 20 asphalt stiffness versus temperature.....	158
Figure B.2: El Dorado 193 asphalt stiffness versus temperature. ....	158

Figure B.3: Sierra 89 asphalt stiffness versus temperature. ....	159
Figure B.4: Plumas 70 asphalt stiffness versus temperature. ....	159
Figure B.5: Ventura 33 asphalt stiffness versus temperature. ....	160
Figure B.6: Santa Barbara 166 asphalt stiffness versus temperature. ....	160
Figure B.7: San Luis Obispo 46 asphalt stiffness versus temperature. ....	161
Figure B.8: Lassen 44 asphalt stiffness versus temperature. ....	161
Figure B.9: Modoc 395 asphalt stiffness versus temperature. ....	162
Figure B.10: Modoc 299 asphalt stiffness versus temperature. ....	162
Figure B.11: Asphalt stiffness versus temperature for ATIRC. ....	163
Figure B.12: Colusa 20 FDR-FA stiffness versus temperature. ....	163
Figure B.13: Sierra 89 FDR-FA stiffness versus temperature. ....	164
Figure B.14: Ventura 33 FDR-fly ash stiffness versus temperature. ....	164
Figure B.15: Santa Barbara 166 FDR-FA stiffness versus temperature. ....	165
Figure B.16: San Luis Obispo 46 LCB stiffness versus temperature. ....	165
Figure B.17: Modoc 299 FDR-C stiffness versus temperature. ....	166

## LIST OF TABLES

---

Table 3.1: FWD Sensor Locations .....	26
Table 3.2: Relationships between DN and Resilient Modulus .....	28
Table 3.3: Test Site Locations .....	30
Table 3.4: California Climate Regions (52) .....	31
Table 3.5: Sieve Sizes .....	35
Table 3.6: Outside Track Structure .....	39
Table 4.1: Structure from Caltrans Plans for Colusa 20 .....	44
Table 4.2: Observed Structure for Colusa 20 (mm) .....	44
Table 4.3: Median DN (mm/blow) for Colusa 20 .....	45
Table 4.4: Backcalculated Stiffnesses (MPa) for Colusa 20 (in MPa) .....	46
Table 4.5: Structure from Caltrans Plans for El Dorado 193 .....	50
Table 4.6: Observed Structure for El Dorado 193 (in mm) .....	51
Table 4.7: Median DN (mm/blow) for El Dorado 193 .....	52
Table 4.8: Backcalculated Stiffnesses for El Dorado 193 (in MPa) .....	53
Table 4.9: Structure from Caltrans Plans for Sierra 89 .....	57
Table 4.10: Observed Structure for Sierra 89 (in mm) .....	57
Table 4.11: Median DN (mm/blow) for Sierra 89 .....	59
Table 4.12: Backcalculated Stiffnesses for Sierra 89 (in MPa) .....	60
Table 4.13: Structure from Caltrans Plans for Plumas 70 .....	65
Table 4.14: Observed Structure for Plumas 70 (mm) .....	65
Table 4.15: Median DN (mm/blow) for Plumas 70 .....	66
Table 4.16: Backcalculated Stiffnesses for Plumas 70 (in MPa) .....	67
Table 4.17: Structure from Caltrans Plans Ventura 33 .....	71
Table 4.18: Observed Structure for Ventura 33 (in mm) .....	71
Table 4.19: Median DN (mm/blow) for Ventura 33 .....	72
Table 4.20: Backcalculated Stiffnesses for Ventura 33 (in MPa) .....	73
Table 4.21: Structure from Caltrans Plans for San Luis Obispo 166 .....	77
Table 4.22: Observed Structure for SLO 166 (in mm) .....	78
Table 4.23: Median DN (mm/blow) for San Luis Obispo 166 .....	79
Table 4.24: Structure from Caltrans Plans for Santa Barbara 166 .....	81
Table 4.25: Observed Structure for Santa Barbara 166 (in mm) .....	82
Table 4.26: Median DN (mm/blow) for Santa Barbara 166 .....	83
Table 4.27: Backcalculated Stiffnesses for Santa Barbara 166 (in MPa) .....	84
Table 4.28: Structure from Caltrans Plans for San Luis Obispo 46 .....	88
Table 4.29: Observed Structure for San Luis Obispo 46 (in mm) .....	89
Table 4.30: Median DN (mm/blow) for San Luis Obispo 46 .....	90
Table 4.31: Backcalculated Stiffnesses for San Luis Obispo 46 (in MPa) .....	91
Table 4.32: Structure from Caltrans Plans for Lassen 44 .....	96
Table 4.33: Observed Structure for Lassen 44 (in mm) .....	96
Table 4.34: Median DN (mm/blow) for Lassen 44 .....	97
Table 4.35: Backcalculated Stiffnesses for Lassen 44 (in MPa) .....	98
Table 4.36: Structure from Caltrans Plans for Modoc 395 .....	102
Table 4.37: Observed Structure for Modoc 395 (in mm) .....	103
Table 4.38: Median DN (mm/blow) for Modoc 395 .....	104
Table 4.39: Backcalculated Stiffnesses (MPa) for Modoc 395 (in MPa) .....	105
Table 4.40: Structure from Caltrans Plans for Modoc 299 .....	109
Table 4.41: Observed Structure for Modoc 299 (in mm) .....	110
Table 4.42: Median DN (mm/blow) for Modoc 299 .....	111

Table 4.43: Backcalculated Stiffnesses (MPa) for Modoc 299 (in MPa) .....	112
Table 4.44: Range of Stiffnesses for Outside Track (MPa) .....	119
Table 4.45: Equivalent Asphalt Stiffness and Damage Assessment .....	122
Table 4.46: Asphalt Age and Temperature Susceptibility .....	123

## **DISCLAIMER**

---

This document is disseminated in the interest of information exchange. The contents of this report reflect the views of the authors who are responsible for the facts and accuracy of the data presented herein. The contents do not necessarily reflect the official views or policies of the State of California or the Federal Highway Administration. This publication does not constitute a standard, specification or regulation. This report does not constitute an endorsement by the Department of any product described herein.

For individuals with sensory disabilities, this document is available in alternate formats. For information, call (916) 654-8899, TTY 711, or write to California Department of Transportation, Division of Research, Innovation and System Information, MS-83, P.O. Box 942873, Sacramento, CA 94273-0001.

## **ACKNOWLEDGMENTS**

---

The authors would like to thank Raghubar Shrestha and Imad Basheer for technical review of this report and technical oversight of the project, and Joe Holland for overall technical oversight. They would also like to thank Stefan Louw, Jonny van Hoang, and Julian Brotschi for collecting FWD data, Jillian Walke for help with the soils testing, and Jeremy Lea, David Jones, Mark Hannum, Julio Paniagua, Fabian Paniagua and Jeff Buscheck for laboratory and field support.

## PROJECT OBJECTIVES

---

This study is part of Strategic Plan Element (SPE) 3.30, which is titled “Mechanistic-Empirical (ME) Design: Standard Materials Library and Guidance.” This project is a continuation of Strategic Plan Element 3.18.1 titled “Updated Standard Materials Library.” The goal of this project is to continue improving the standard materials library being developed by the UCPRC. In addition, guidance will be developed to help design engineers select materials from the library for use in a given project. Guidance will also be developed to help design asphalt concrete mixes for meeting performance-based specifications as part of the ME design method.

The objectives for this project will be achieved by completion of the following tasks:

1. Laboratory testing of materials sampled from selected construction projects across the state.
2. Field testing of the same materials during and after construction.
3. Guidance regarding the selection of materials from the standard materials library in the *CalME* design software.
4. Guidance regarding possible approaches for improving the laboratory testing results for asphalt mixes in order to meet performance-related specifications.
5. Documentation in project reports.

Publication of this report provides partial completion of the Tasks 3 and 5.

## EXECUTIVE SUMMARY

---

In 2005, the California Department of Transportation (Caltrans) approved an issue memorandum titled “Adoption of Mechanistic-Empirical (ME) Pavement Design Method.” Since that time, Caltrans has continued the development and improvement of mechanistic-empirical (ME) pavement design methods and instituted their more widespread use to replace traditional empirical pavement design methods. This effort has included use of the incremental-recursive ME method implemented in the software program now known as *CalME*, which is used to design asphalt-surfaced pavements for new pavement projects and rehabilitation of existing pavements. The incremental-recursive design approach used in *CalME* has the ability to model the entire life and the damage processes that take place within the pavement structure. This includes the damaging effects of traffic, and the interaction of traffic loading with changes in moisture and temperature conditions.

Pavement designers do not usually have the opportunity to select or modify the underlying base and subgrade materials for projects when they involve the rehabilitation or reconstruction of an existing road, the most common case for the most of the projects done in the state. However, knowing the properties of these unbound materials—as well as of any changes that might have taken place over the pavement life—is important when designing rehabilitation and reconstruction projects. As of 2016, the unbound standard materials present in *CalME* consist of four types of aggregate base, three types of aggregate subbase, and twelve types of soil as defined by the United Soil Classification System (USCS).

Unbound pavement materials generally exist above the water table in a partially saturated state; thus their engineering properties may change due to a variety of environmental factors such as fluctuations in moisture content, wetting and drying seasons, drainage conditions, and changes in overburden stress—depending on the soil type and geologic setting. These factors may result in significant variability in the stiffness of the materials over time, and this could have a considerable impact on the resulting response of the entire structure. Yet, while initial pavement material properties can be fairly well established using backcalculation or other methods at the time of the site investigation, variations in situ moisture conditions and the long-term behavior of water beneath pavement structures continues to be an elusive concept in pavement design across the world.

The default assumption in *CalME* currently does not take into account the seasonal variation of unbound materials properties over time, and leaves it to the designer to change that default if he or she has information regarding seasonal variation. Yet, depending on the degree of variation and its level of importance on the associated response, the long-term design of a pavement structure may not be optimized if seasonal changes in unbound materials properties are ignored. This can potentially result in increased and unnecessary expenditures from costly

overdesign or, worse, from premature failure. By comparison, the AASHTO *PavementME* software handles this design consideration by including pavement moisture prediction models, though this comes at a cost of considerably increased computation time and code complexity. Prior to this study it was unknown whether there is much seasonal variation in unbound materials properties in typical Caltrans pavements.

One of the questions in ME design is the extent to which the stiffness of unbound layers (subgrade and granular base and subbase layers) is actually affected by seasonal changes in the environment. Answering that question will provide information to designers and will help guide the UCPRC and Caltrans in deciding what level of attention those effects warrant in the *CalME* standard materials library and code.

Presented in this report is an investigation of the extent and potential consequences of seasonal variations on asphalt-surfaced pavement. This work was completed as part of Partnered Pavement Research Center Strategic Plan Element (PPRC SPE) 3.30, which is titled “Mechanistic-Empirical (ME) Design: Standard Materials Library and Guidance.” The goal of SPE 3.30 is to continue improving the standard materials library being developed by the UCPRC. The project includes the development of guidance that helps design engineers select materials from the library for use in a given project, and to assist in the design of asphalt concrete mixes that meet performance-based specifications as part of the ME design method. The results documented in this report are part of Task 3 listed in the Project Objectives: “Guidance regarding the selection of materials from the standard materials library in the *CalME* design software.” Publication of this report provides partial completion of Tasks 3 and 5.

The following are the primary questions this research is intended to answer:

- What types of changes in unbound material properties (i.e., moisture content, penetration resistance) are seen seasonally and what are the variables that affect those properties?
- Do these seasonal changes correspond to significant changes in stiffness at the design scale?
- Can trends of seasonal stiffness variation in unbound materials be seen using available and pertinent pavement engineering equipment?
- If these trends are seen, what are they and how they can be further characterized for use in design?
- What is the range of unbound layers stiffnesses seen for different soil types, and for bases and subbases?

The questions posed in the research problem statement were answered by the results of the following completed tasks:

- Perform in situ testing and sampling to evaluate and compare changes in material properties at specific locations
- Perform laboratory index testing to characterize materials



- Assess trends between unbound material properties and in situ stiffness
- Perform an experiment to evaluate short-term changes after specific events
- Evaluate the significance of any changes observed
- Provide recommendations for future work, if it is needed

The scope of this research did not involve the following:

- Analysis of quantitative relationships between stiffness and soil properties
- Development of numerical models
- Use of testing procedures that are not generally available to pavement engineers

Chapter 2 presents a literature review of unbound pavement material properties and behavior. This chapter also discusses some of the current pavement design models that incorporate seasonal changes in unbound material properties.

Chapter 3 presents the field and laboratory testing procedures used to evaluate seasonal changes. The experiment had two phases. The first consisted of full-scale field testing on existing pavement structures located around the state. This required two trips—one at the end of the rainy season and the other in the middle of the dry season—to 11 test sites to evaluate changes in moisture conditions, in the materials' resistance to penetration, and their in situ stiffnesses, the latter of which was assessed by means of falling weight deflectometer backcalculation methods. This portion of the study was used to gauge the scale and breadth of the properties and materials, and to examine any corresponding changes that were evaluated from one season to the next. The second portion of the study was a smaller-scale field test performed on the UCPRC test track to evaluate any changes in stiffness that occurred throughout the year, after rainfall events, and during wetting and drying cycles.

Field testing consisted of deflection testing using the falling weight deflectometer (FWD), which was later used to backcalculate in situ layer moduli. Dynamic cone penetrometer (DCP) testing (ASTM D 6951) was also performed to obtain the subsurface pavement structure and to provide a secondary measure of stiffness. Lastly, unbound materials were taken and sampled for processing in the laboratory.

In order to assess the range of properties that might be encountered throughout the state, 11 different field locations across California were chosen to assess in situ backcalculated stiffnesses of materials and their relationship to various soil properties such as water content, grain size distribution, Atterberg limits, and soil type, as well as geologic setting and drainage conditions. The first round of field testing occurred in the late spring and summer of 2015 (May through August), a drought year; data collected during this time is intended to serve as the “dry”

sampling. The second round of field testing occurred during the spring of 2016 (April through June) after a rainy season with near normal rainfall, and the data collected is intended to serve as the “wet” sampling.

The test site locations are shown in the following table.

Location		Test Section			Site Information		Testing Schedule	
County	Route	Direction	Post Miles Tested	Lane Number	Climate Region	Base Material	Round 1	Round 2
Colusa	20	East	15.35 – 14.35	1/1	Inland Valley	FDR-FA	5/14/15	4/5/16
El Dorado	193	East	10.4 – 11.4	1/1	Low Mountain	CIR	5/21/15	5/10/16
Sierra	89	North	28 – 29	1/1	High Mountain	FDR-FA	7/23/15	5/11/16
Plumas	70	East	82 – 83	1/1	High Desert	PAB	7/21/15	4/26/16
Ventura	33	North	51.5 – 52.5	1/1	South Mountain	FDR	7/28/15	6/9/16
Santa Barbara	166	East	55 – 56	1/1	South Coast	FDR-FA	7/29/15	5/5/16
San Luis Obispo	166	East	41.5 – 42.5	1/1	South Coast	CIR	7/30/15	5/4/16
San Luis Obispo	46	East	36.6 – 37.6	2/2	Inland Valley	LCB	7/31/15	5/3/16
Lassen	44	West	9.5 – 10.5	1/1	High Mountain	PAB	8/3/15	4/21/16
Modoc	395	North	13.5 – 14.5	1/1	High Desert	PAB	8/4/15	4/20/16
Modoc	299	East	59.5 – 60.5	1/1	High Desert	FDR-C	8/5/15	4/19/16

A full-scale and more closely analyzed test section at the Advanced Transportation Infrastructure Research Center (ATIRC) at UC Davis was used to assess whether or not significant changes in backcalculated subgrade stiffness could be noticed over shorter periods of time or were correlated to specific rainfall events and wetting/drying periods. The pavement structure consisted of asphalt concrete (AC) placed on aggregate base and a clay subgrade that was lime stabilized in places. Baseline testing of the outside track began in May 2015 and continued until April 2016. The test section was divided into four subsections based on the extent of lime stabilization and deflection testing results. The small-scale experiment on the ATIRC test track was conducted in an attempt to bridge the gap between the two seasonal field tests with more frequent testing; however, substructure variability and periods of inactivity have left room for a degree of uncertainty.

Chapter 4 presents the results from the field and lab testing procedures from the 11 field test sections. Organization of each section is as follows:

- A brief description of the site, conditions, and any notable visual or circumstantial information
- The structure of the site as provided by the Caltrans plan and the observed structure (Note that core photos are inverted.)

- A summary of the properties of the unbound material with depth including:
  - DCP total number of blows versus depth
  - DCP DN versus depth
  - Moisture content versus depth
  - Structure and material type
- Backcalculated stiffness for materials for each site

All base materials except for lean concrete base (LCB) experienced a decrease in stiffness between the two rounds of testing, whereas the underlying unbound materials did not seem to show any trends in variability based purely on soil type. When assessing the sites in terms of climate regions, it became clear that the sites in the High Mountain climate region experienced reductions in both base and unbound material stiffnesses after the wet season, while all the other climate regions experienced consistent reductions in the base material stiffness in the wet season. The one site that did not appear to reveal any consistent trend in seasonal variation of stiffness is San Luis Obispo 46; this was the only two-lane highway tested and was the only site to have notable side drains present along the length of the section, which likely played a role in its consistent behavior.

By assessing the influence of specific rainfall events on the stiffness of the material, it was found that the stiffness of unbound material between the wheelpaths generally tended to decrease with time after rainfall, while the opposite was true for the stiffness of material in the wheelpath, which increased with time after rainfall.

Generally the material between the wheelpaths did not show a clear relationship between the distance to the unpaved portion of the road and changes in stiffness, while the wheelpath material tended to be softer in the wet season when the site had narrower shoulders. Roadway conditions and rainfall events tended to influence the patterns of stiffness of the material; for the wheelpaths (where most pavement distresses are typically observed), the variability of the unbound layers seemed to be heavily influenced by the width of the shoulder as well as the climate and precipitation. Materials in the wheelpath tended to be softer shortly after rainfall and increased in stiffness as time elapsed after the rainfall, while material between the wheelpaths did not follow any specific pattern, seemingly validating the inherent complexities of water flow beneath pavement structures noted in the literature.

The unbound material stiffnesses obtained through backcalculation are shown in the report compared to the average and the range typically attributed to the specific soil type in the AASHTO Mechanistic-Empirical Pavement Design Guide (*MEPDG*). From this comparison, it is apparent that the backcalculated values measured in this study were consistently higher than those in *MEPDG*, with the exception of the silty sand material. The

resilient modulus ranges provided in *MEPDG* correspond to stiffnesses correlated to California Bearing Ratio (CBR) and are calibrated from soil index testing and laboratory testing. It is noted in the *MEPDG* design guide document that the correlations were originally intended to obtain realistic  $M_R$ , including consideration of frozen material using a limited database of triaxial test data, and that caution should be exercised when extrapolating these values for nonfrozen soils. While oftentimes the moduli values listed in the *MEPDG* tables are used for design, there seems to be relatively little relation to the values that were observed during field testing in this study.

The main results of the study and answers to the questions posed from the literature can be summarized as follows.

#### *Seasonal Changes in Unbound Material Properties*

Questions were posed pertaining to what kinds of seasonal changes in unbound materials properties could be observed and whether or not they corresponded to significant changes in stiffness observed in the field. The data indicate that changes in both moisture content and penetration resistance occurred, which is indicative of the seasonal fluctuations in moisture conditions and shear strength expected for soils. However, these small-scale changes did not necessarily correspond to significant fluctuations or noticeable trends in measured deflections or the backcalculated stiffness of the unbound materials; rather, spatial variability, observed drainage and site conditions, and soil type tended to have a much larger influence on the resilient response of the materials tested than did observed changes in moisture or penetration resistance.

In almost all cases, the stabilized and unstabilized granular base and subbase materials, not the subgrade, experienced the largest changes in stiffness between the two rounds of testing. This result may be rooted in the relative permeability of the materials: the more permeable granular materials were expected to experience quicker changes in moisture conditions (and therefore suction and stress state) and the less permeable subgrade materials were expected to not experience these changes as quickly. The data also suggest that in some cases, the stiffness of, and additional confinement from, the overlying layers may play an important role in the resulting resilient response of the unbound material.

Summarizing the work completed in the report, it appears that while the literature consistently indicates that significant changes in resilient modulus can occur with changing moisture regime, the field testing results presented in this report indicated that changes in stiffness at different moisture conditions did not seem to be as large as those evaluated in the laboratory testing found in the literature. This could be due to the nature of the in situ testing performed: FWD testing takes place on a larger scale than resilient modulus testing and therefore the averaging of material properties, the specific stress state conditions (particularly lateral and overburden confining stresses), and the greater chances of nonhomogeneity in materials may each be a part of the reason why stark

changes in subgrade stiffness magnitude were not seen from field testing. While it was outside the scope of this project to perform resilient modulus tests on these materials, this finding may help shed light on some of the discrepancies between field and laboratory testing conditions, results, and appropriate design applications.

Regarding the range of materials properties observed for different soil types, spatial variability and geologic conditions appeared to contribute the most to the range of subgrade stiffnesses seen within each test site. Sites constructed using cut/fill methods tended to exhibit a much wider degree of variability in backcalculated stiffnesses, while sites situated in more level or alluvial plains had much lower standard deviations for unbound material stiffness. Gravelly materials and pulverized asphalt base (PAB) consistently exhibited the highest stiffnesses of the unbound materials. Stiffness tended to decrease with increasing fines, and the unbound material stiffness values obtained from backcalculation did not show a strong relationship to the  $M_R$  values typically assumed in the *MEPDG* design method.

This research did not aim to provide additional relationships between DCP penetration index and backcalculated stiffness, but rather evaluated the effectiveness and reliability of some of the DCP-stiffness relationships expressed in the literature. Backcalculated stiffnesses of the unbound material tested seemed to correlate well with DCP penetration resistance (DN). Of the relationships proposed in the literature, those developed by Chen et al. in two separate references produced the estimated stiffnesses most consistent with the data obtained in this study. The relationships proposed by CSIR and Chai and Roslie also fit well with the data, but tended to overestimate stiffness.

Because of the quantity of information obtained, it was of interest to assess whether field data could be useful for evaluating the damage, aging, and temperature susceptibility of asphalt-bound and lightly stabilized materials. The field data revealed that FWD test data can be used to roughly estimate a field asphalt concrete (AC) master curve that can then be used to evaluate the effects of aging and damage. Evaluating the effects of aging revealed a strong relationship between asphalt age and temperature susceptibility for asphalt concrete. Calculation of “equivalent” asphalt stiffness also showed that damage was observed in the asphalt concrete at about one-third of the sites tested. Little to no relation to temperature was observed for full-depth reclamation materials stabilized with foamed asphalt, which have shown as much sensitivity to stress state as temperature in previous research. This research does not necessarily intend to propose new methods or models for evaluating these phenomena, but rather sheds light on the potential usefulness of field data for investigating them.

The results revealed that many of the unbound materials tested experienced minor, if any, changes in stiffness between the two rounds of testing in the “dry” and “wet” conditions. This indicates that the current assumption

within *CalME*, that unbound material stiffness does not change seasonally, is evidently not far off from the behavior that was observed in the finer subgrade materials evaluated during field testing, despite noted changes in moisture content and penetration resistance. The results indicate that this assumption does not necessarily hold true for the shallower granular base and subbase materials, and it is recommended that further assessment of the causes and degrees of variability in modulus of these coarser materials be evaluated. *CalME*'s model for the effects of overlying layer stiffness tended to be more applicable to these granular materials as well; however, material stiffening from increased confinement did appear to occur in some of deeper materials tested, and this phenomenon may be worth investigating further depending on the importance of the proposed structure. It is therefore recommended that *CalME*'s current assumption of constant stiffness for unbound layers continue to be used, except in cases where the designer identifies issues with drainage, irrigation, or other likely causes of seasonal variation of stiffness. Performing FWD testing for backcalculation of unbound layer stiffnesses after the rainy season, or other times of highest moisture contents where rainfall is not the main source of moisture, will impart some conservatism into designs.

While the results of the field investigations revealed that the subgrade backcalculated stiffness experienced minor changes between the two rounds of testing, DCP testing consistently revealed patterns of decreased penetration resistance when material had higher moisture contents and when material had greater fines content. Though the objectives of the research did not involve evaluating the change in the shear strength of the materials, the DCP data collected reveal seasonal fluctuation in the in situ shear strength of both granular and subgrade materials.

The results of this research provide field data characterizing the stiffnesses of subgrades, granular material, FDR-FA, and lean concrete bases that should be used to update options for designers in the *CalME* Standard Materials Library.

## LIST OF ABBREVIATIONS

---

AC	Asphalt concrete
AB	Aggregate base
APCS	Automated Pavement Condition Survey
ATIRC	Advanced Transportation Infrastructure Research Center
CBR	California Bearing Ratio
CIR	Cold in-place recycling
CSIR	Council for Scientific and Industrial Research
DCP	Dynamic cone penetrometer
DEM	Discrete element modeling
DN	Dynamic cone penetrometer penetration rate
EBWP	Eastbound wheelpath
EICM	Enhanced Integrated Climatic Model
FDR	Full-depth reclamation
FDR-FA	Full-depth reclamation-foamed asphalt stabilization
FDR-PC	Full-depth reclamation-portland cement stabilization
FEM	Finite element model
FWD	Falling weight deflectometer
GPR	Ground-penetrating radar
HMA	Hot mix asphalt
HVS	Heavy Vehicle Simulator
IRI	International Roughness Index
LCB	Lean concrete base
LS	Lime-stabilized subgrade
ME	Mechanistic-empirical
MEPDG	Mechanistic-Empirical Pavement Design Guide
PAB	Pulverized asphalt base
PM	Post Mile
PPRC	Partnered Pavement Research Center
SANRAL	South African National Roads Authority Limited
SAPDM	South African Pavement Design Method
SWCC	Soil-water characteristic curve
UCPRC	University of California Pavement Research Center
USCS	United Soil Classification System

## **LIST OF TEST METHODS AND SPECIFICATIONS USED IN THE REPORT**

AASHTO T 89-13 (2013)	Standard Method of Test for Determining the Liquid Limit of Soils
ASTM C136/C136M-14 (2014)	Standard Test Method for Sieve Analysis of Fine and Coarse Aggregates
ASTM D1140-14 (2014)	Standard Test Methods for Determining the Amount of Material Finer than 75- $\mu$ m (No. 200) Sieve in Soils by Washing
ASTM D2216-10 (2010)	Standard Test Methods for Laboratory Determination of Water (Moisture) Content of Soil and Rock by Mass
ASTM D2487-11 (2011)	Standard Practice for Classification of Soils for Engineering Purposes (Unified Soil Classification System)
ASTM D2488-09a (2009)	Standard Practice for Description and Identification of Soils (Visual-Manual Procedure)
ASTM D4318-10 (2010)	Standard Test Methods for Liquid Limit, Plastic Limit, and Plasticity Index of Soils
ASTM D6913-04(2009)	Standard Test Methods for Particle-Size Distribution (Gradation) of Soils Using Sieve Analysis
ASTM D6951/D6951M-09 (2015)	Standard Test Method for Use of the Dynamic Cone Penetrometer in Shallow Pavement Applications



## SI\* (MODERN METRIC) CONVERSION FACTORS

### APPROXIMATE CONVERSIONS TO SI UNITS

Symbol	When You Know	Multiply By	To Find	Symbol
<b>LENGTH</b>				
in	inches	25.4	Millimeters	mm
ft	feet	0.305	Meters	m
yd	yards	0.914	Meters	m
mi	miles	1.61	Kilometers	Km
<b>AREA</b>				
in <sup>2</sup>	square inches	645.2	Square millimeters	mm <sup>2</sup>
ft <sup>2</sup>	square feet	0.093	Square meters	m <sup>2</sup>
yd <sup>2</sup>	square yard	0.836	Square meters	m <sup>2</sup>
ac	acres	0.405	Hectares	ha
mi <sup>2</sup>	square miles	2.59	Square kilometers	km <sup>2</sup>
<b>VOLUME</b>				
fl oz	fluid ounces	29.57	Milliliters	mL
gal	gallons	3.785	Liters	L
ft <sup>3</sup>	cubic feet	0.028	cubic meters	m <sup>3</sup>
yd <sup>3</sup>	cubic yards	0.765	cubic meters	m <sup>3</sup>
NOTE: volumes greater than 1000 L shall be shown in m <sup>3</sup>				
<b>MASS</b>				
oz	ounces	28.35	Grams	g
lb	pounds	0.454	Kilograms	kg
T	short tons (2000 lb)	0.907	megagrams (or "metric ton")	Mg (or "t")
<b>TEMPERATURE (exact degrees)</b>				
°F	Fahrenheit	5 (F-32)/9 or (F-32)/1.8	Celsius	°C
<b>ILLUMINATION</b>				
fc	foot-candles	10.76	Lux	lx
fl	foot-Lamberts	3.426	candela/m <sup>2</sup>	cd/m <sup>2</sup>
<b>FORCE and PRESSURE or STRESS</b>				
lbf	poundforce	4.45	Newtons	N
lbf/in <sup>2</sup>	poundforce per square inch	6.89	Kilopascals	kPa

### APPROXIMATE CONVERSIONS FROM SI UNITS

Symbol	When You Know	Multiply By	To Find	Symbol
<b>LENGTH</b>				
mm	millimeters	0.039	Inches	in
m	meters	3.28	Feet	ft
m	meters	1.09	Yards	yd
km	kilometers	0.621	Miles	mi
<b>AREA</b>				
mm <sup>2</sup>	square millimeters	0.0016	square inches	in <sup>2</sup>
m <sup>2</sup>	square meters	10.764	square feet	ft <sup>2</sup>
m <sup>2</sup>	square meters	1.195	square yards	yd <sup>2</sup>
ha	Hectares	2.47	Acres	ac
km <sup>2</sup>	square kilometers	0.386	square miles	mi <sup>2</sup>
<b>VOLUME</b>				
mL	Milliliters	0.034	fluid ounces	fl oz
L	liters	0.264	Gallons	gal
m <sup>3</sup>	cubic meters	35.314	cubic feet	ft <sup>3</sup>
m <sup>3</sup>	cubic meters	1.307	cubic yards	yd <sup>3</sup>
<b>MASS</b>				
g	grams	0.035	Ounces	oz
kg	kilograms	2.202	Pounds	lb
Mg (or "t")	megagrams (or "metric ton")	1.103	short tons (2000 lb)	T
<b>TEMPERATURE (exact degrees)</b>				
°C	Celsius	1.8C+32	Fahrenheit	°F
<b>ILLUMINATION</b>				
lx	lux	0.0929	foot-candles	fc
cd/m <sup>2</sup>	candela/m <sup>2</sup>	0.2919	foot-Lamberts	fl
<b>FORCE and PRESSURE or STRESS</b>				
N	newtons	0.225	Poundforce	lbf
kPa	kilopascals	0.145	poundforce per square inch	lbf/in <sup>2</sup>

\*SI is the symbol for the International System of Units. Appropriate rounding should be made to comply with Section 4 of ASTM E380 (Revised March 2003).



# 1 INTRODUCTION

---

## 1.1 Background

The California Department of Transportation (Caltrans) has continued the development and improvement of mechanistic-empirical (ME) pavement design methods, and instituted their more widespread use to replace traditional empirical pavement design methods since 2005, when Caltrans management approved an issue memorandum titled “Adoption of Mechanistic-Empirical (ME) Pavement Design Method” (1). Since then, Caltrans has used the incremental-recursive ME method implemented by the software program now known as *CalME* when designing asphalt-surfaced pavements for new pavement projects and rehabilitation of existing pavements.

By utilizing incremental-recursive design methods, *CalME* has the ability to model the entire life and the damage processes that take place within the pavement structure. Incremental-recursive design updates damage on a load repetition-to-repetition basis through the entire life of the pavement, providing a more realistic estimation of the pavement’s life and an estimate of the stiffnesses of the layers after each loading which can be used for a number of purposes. This estimation includes the effects of traffic, which permanently damage the pavement, and their interaction with the effects of moisture and temperature conditions from the environment. Figure 1.1 graphically shows an example of how *CalME* models the fluctuation of layer stiffnesses in a generic pavement structure over time as well as daily temperature changes and seasonal moisture changes.

One important feature of *CalME* is its capacity to allow designers to select input data for a specific geographic region from a collection of regional data in the program’s standard materials library. This allows a designer to account for regional and site-specific conditions such as materials, traffic, and climate.

California is a large state with many different climates. Regional climatic conditions—such as temperature, precipitation, freeze/thaw, and solar radiation—can also have large effects on pavement performance. To help account for these varied climatic conditions, Caltrans has divided California into nine climate regions, as shown in Figure 1.2 (2), which are incorporated into the climate database for *CalME*.

Particular materials for a given project will likely be dominated largely by the inventories of local quarries, refineries, and asphalt mixing plants, and by regional geologic conditions. To account for regional differences in materials, *CalME* utilizes a library that contains the standard materials used from various regions throughout the state and their corresponding properties. This helps designers account for regional differences in materials such as aggregate type and source, PG binder grading, and soil type that may influence performance. This library is

continually updated, expanding the number and variety of materials used throughout the state and providing designers with a comprehensive and representative selection of materials.

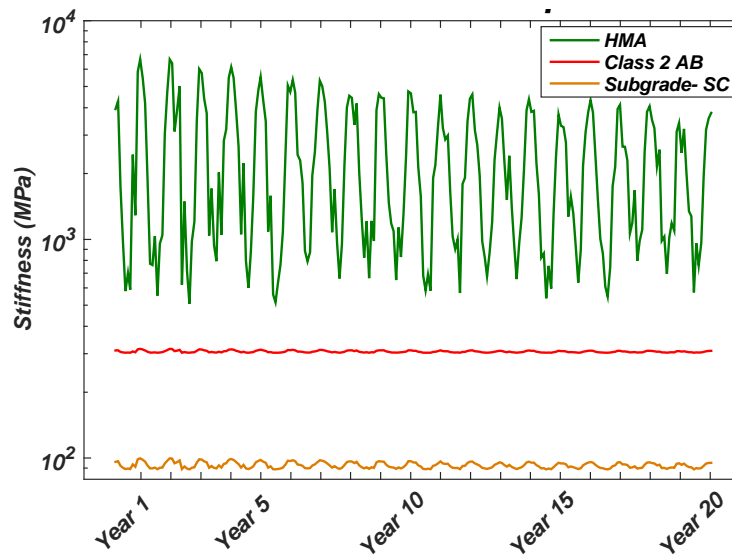


**Figure 1.1: Example of CalME design modeling damage (longer trend) and seasonal climate variation.**

Designers usually do not have the opportunity to select or modify the underlying base and subgrade materials for their project when it involves rehabilitation or reconstruction of an existing road, which is the case for the most of the projects done in the state. Knowing the properties of these unbound materials, as well as any changes that might have taken place over the pavement life, will therefore be of key importance when designing rehabilitation and reconstruction projects. As of 2016, the unbound standard materials present in CalME consist of four types of aggregate base, three types of aggregate subbase, and twelve types of soil as defined by the United Soil Classification System (USCS).

Unbound pavement materials generally exist above the water table in a partially saturated state; thus their engineering properties may change due to a variety of environmental factors such as fluctuations in moisture content, wetting and drying seasons, drainage conditions, and changes in overburden stress, depending on the soil type and geologic setting. These factors may result in significant variability in the stiffness of the materials over time, and this could have a considerable impact on the resulting response of the entire structure. Yet, while initial pavement material properties can be fairly well-established using backcalculation or other methods at the time of the site investigation, variations in situ moisture conditions and the long-term behavior of water beneath pavement structures continues to be an elusive concept in pavement design across the world (3).

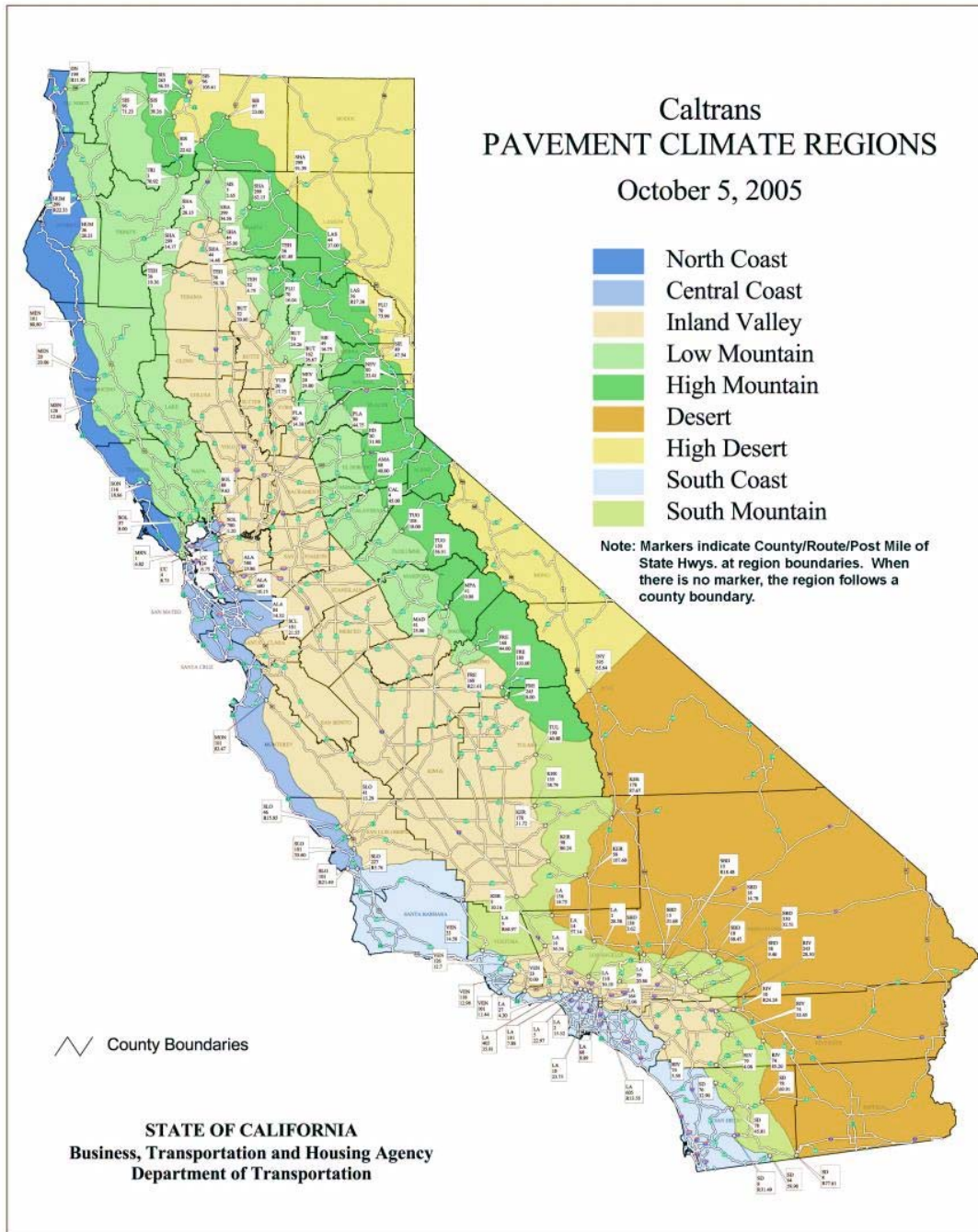


**Figure 1.2: California pavement climate regions.**

Because these soil moisture conditions and relationships are inherently complex, the default assumption in *CalME* currently is to not take into account the seasonal variation of unbound materials properties over time, and to leave it to the designer to change that default if he or she has information regarding seasonal variation. Yet, depending on the degree of variation and its level of importance on the associated response, the long-term design of a pavement structure may not be optimized if seasonal changes in unbound materials properties are ignored. This

can potentially result in increased and unnecessary expenditures from costly over-design or, worse, from premature failure. In comparison, the AASHTO *PavementME* software handles this design consideration by including pavement moisture prediction models, at the cost of considerably increased computation time and code complexity. On the other hand, it is unknown whether there is much seasonal variation in unbound materials properties in typical Caltrans pavements.

One of the questions in ME design is the extent to which the stiffness of unbound layers (subgrade and granular base and subbase layers) is actually affected by seasonal changes in the environment. Answering that question will provide information to designers and will help guide the UCPRC and Caltrans in deciding what level of attention those effects warrant in the *CalME* standard materials library and code.

## **1.2 Problem Statement, and Project Goals, and Objectives**

Before implementing more complex relationships to model changes in unbound material stiffness associated with different environmental factors, the extent and potential consequences of seasonal variations were investigated as part of Partnered Pavement Research Center Strategic Plan Element (PPRC SPE) 3.30, which is titled “Mechanistic-Empirical (ME) Design: Standard Materials Library and Guidance.” The goal of SPE 3.30 is to continue improving the standard materials library being developed by the UCPRC. In addition, guidance will be developed to help design engineers select materials from the library for use in a given project. Guidance for helping design asphalt concrete mixes to meet performance-based specifications as part of the ME design method will also be developed. The results documented in this report are part of Task 3 listed in the Project Objectives: “Guidance regarding the selection of materials from the standard materials library in the *CalME* design software.” Publication of this report provides partial completion of Tasks 3 and 5.

The goals of the research presented in this report are to evaluate how the stiffness of unbound materials varies seasonally, to identify which factors might be most influential in causing seasonal changes (if any), and to provide guidance for any further work if it is found to be needed. The following are the primary questions this research is intended to answer:

- What types of changes in unbound material properties (i.e., moisture content, penetration resistance) are seen seasonally and what are the variables that affect those properties?
- Do these seasonal changes correspond to significant changes in stiffness at the design scale?
- Can trends of seasonal stiffness variation in unbound materials be seen using available and pertinent pavement engineering equipment?
- If these trends are seen, what are they and how they can be further characterized for use in design?
- What is the range of unbound layers stiffnesses seen for different soil types, and for bases and subbases?

The questions posed in the research problem statement will be answered by the results of the following completed tasks:

- Perform in situ testing and sampling to evaluate and compare changes in material properties at specific locations
- Perform laboratory index testing to characterize materials
- Assess trends between unbound material properties and in situ stiffness
- Perform an experiment to evaluate short-term changes after specific events
- Evaluate the significance of any changes observed
- Provide recommendations for future work, if it is needed

The scope of this research does not involve the following:

- Analysis of quantitative relationships between stiffness and soil properties
- Development of numerical models
- Use of testing procedures that are not generally available to pavement engineers

There are a number of works in the literature that reveal strong relationships between moisture content, suction, and unbound material stiffness in the laboratory; the body of knowledge on unsaturated soil mechanics also agrees with these findings. However, in a laboratory it is never possible to completely reproduce the internal structure of pavement materials and their moisture conditions in the field. There are limited examples that explore the significance and scale of these relationships in the field, and this research seeks to bridge the gap between the laboratory and the field in order to reveal the impact that the moisture conditions, environmental factors, and climate, can have on the in situ properties of pavement materials at the project design scale.

### **1.3 Organization of Report**

- Chapter 2 presents a literature review of unbound pavement material properties and behavior. This chapter also discusses some of the current pavement design models that incorporate seasonal changes in unbound material properties.
- Chapter 3 presents the field and laboratory testing procedures used to evaluate seasonal changes.
- Chapter 4 presents the results from the field and lab testing procedures.
- Chapter 5 presents conclusions of the research, and recommendations for future work.

*(This page intentionally blank)*



## 2 LITERATURE REVIEW

---

### 2.1 Introduction

This chapter aims to provide a brief summary of information and research in the literature pertaining to seasonal changes in unbound pavement materials, with a focus on the effects of moisture conditions on their resilient response.

### 2.2 Geotechnical Pavement Design Considerations

Pavement structures generally consist of engineered surface wearing courses, such as asphalt concrete or portland cement concrete, overlying layers of granular base material atop the in situ subgrade material. In order to properly design a pavement structure, it is necessary to understand the geotechnical mechanics and properties of the unbound granular materials and the subgrade to be used (4).

Pavement engineering practice in California is more concerned with the evaluation and maintenance of existing roads than with new construction. While the selection of base materials, compaction specifications for new subgrade and subbase, and other geotechnical design considerations for new roads are not as vital in rehabilitation or recycled pavement projects, the role of soil mechanics in pavement design remains of considerable importance in the design process (5).

### 2.3 Unbound Pavement Material Properties

The field and knowledge of soil mechanics have grown substantially in the past 50 years, and the laws of soil mechanics apply directly to both compacted and crushed aggregate base as well as to the subgrade material found in pavements (4). While the underlying mechanics and behavior of soil are universal, the soil mechanics requirements and parameters for pavement engineering differ significantly from those in other geotechnical problems such as foundation design or liquefaction susceptibility analyses. Brown (5, 4) summarized the primary requirements as follows:

- Unbound pavement materials observe the principles of effective stress, which state that

$$\sigma' = \sigma - u$$

where:

$\sigma'$  is the effective stress,  
 $\sigma$  is the total stress, and  
 $u$  is the pore water pressure in the voids.

- Unbound pavement materials are subjected to a large number of repeated loads well beneath their shear strength.
- Unbound pavement materials generally respond to traffic loads in a resilient manner.

- Irrecoverable plastic strains can accumulate under repeated loading.
- Unbound pavement materials usually exist above the water table. While this does not completely inhibit water ingress, most of the soil will be in a partially saturated state.

The subsequent sections of this report provide more in-depth descriptions of the properties of unbound pavement materials and the factors that influence them.

### 2.3.1 Characterization

In the United States, the most commonly used classification systems for soil are the United Soil Classification System (USCS) and the American Association of State Highway and Transportation Officials (AASHTO) specifications. *CalME* classifies subgrade soils according to USCS specifications and aggregate bases and subbases according to Caltrans Standard specifications (2, Topic 614).

### 2.3.2 Resilient Response

The predominant geotechnical factor for evaluating the response of pavement soils to loading is the stiffness and/or strength of the unbound material. The *stiffness* (used interchangeably with *modulus*) of a material is generally defined as that material's resistance to deformation in response to a force. Given the material's expected loading or failure mechanism, the modulus of interest can vary depending on the application. The *elastic modulus* is described by Hooke's law, which states the ratio of the applied stress over the resulting axial strain is a constant ( $E = \sigma/\epsilon$ ). The ratio between the resulting horizontal and vertical strains is also a constant, and is known as Poisson's ratio ( $\nu$ ). Several other parameters that measure a material's resistance to deformation arise from this relationship, such as Young's Modulus ( $E$ ), Bulk Modulus ( $K$ ), and Shear Modulus ( $G$ ), which describe a material's responses to axial stress, uniform compression, and shear stress, respectively (6).

For simplicity and applicability, the theory of elasticity is typically used for pavement design, under the assumptions of static loading, continuous deformation, and that all materials are homogenous, isotropic, and linear elastic (7). However; these assumptions are nearly never fulfilled by real pavement materials and are rarely the case for soils; loading is typically dynamic, materials contain cracks and other deformations, and most unbound pavement materials are in anisotropic stress states and behave nonlinearly (7, 8).

Powrie (8) describes the concept of an elastic modulus as applied to a soil as no more than "a convenient fiction." This is founded upon a body of knowledge and research that consistently reveals soil's inelastic, nonlinear behavior. Despite the inelastic behavior of soils, it has been found to be appropriate in most pavement design

circumstances to model soil as an elastic material if the stiffness modulus is found using methods in which the material is subjected to the same, or similar, loading conditions anticipated in the field, or if the changes in stress and strain are small.

### 2.3.2.1 Definition of Resilient Modulus

Many of the pavement response models that include inherent complexities that make them “more correct” do not yield results that are much more accurate than those from simpler models based solely on the theory of linear elasticity. Hence simpler models are used to evaluate material response in many geotechnical problems.

Because unbound material behaves nonlinearly, the ratio of applied stress to induced strain can vary depending on the conditions at which they are applied; even so, their behavior is still not fully understood (3). Seed, Chan, and Lee (9) first explored the application of the resilient characteristics of subgrade soils in flexible pavements, and thereby introduced the concept of *resilient modulus* ( $M_R$ ) to describe the relationships between applied stress and recoverable strain (10) under repeated loading. Resilient modulus is defined by:

$$M_R = \frac{\Delta\sigma}{\Delta\varepsilon}$$

where:

$\Delta\sigma$  is the resilient (dynamic) deviatoric stress and

$\Delta\varepsilon_r$  is the recoverable elastic axial strain, as illustrated in Figure 2.1 below.

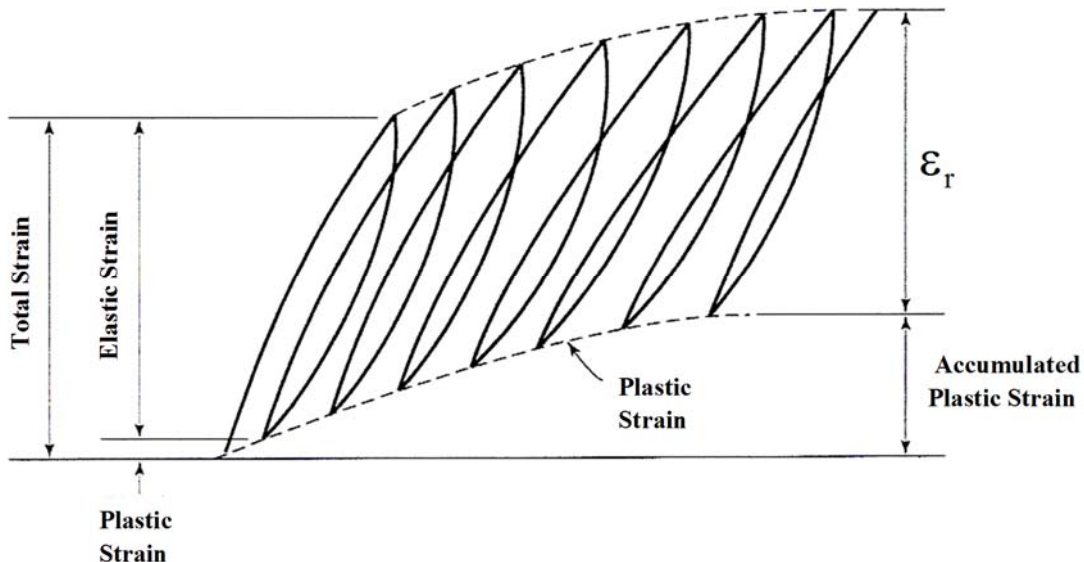


Figure 2.1: Definition of resilient modulus.

Because the permanent deformation of unbound materials has been correlated to the resilient response,  $M_R$  has become the most commonly used parameter in ME design methods for describing an unbound material's response to repeated loads (11, 9).  $M_R$  is commonly evaluated in the laboratory using a cyclic triaxial test setup, although field measurements and USCS correlations can also be used to evaluate  $M_R$ . Examples of these include backcalculation of deflections obtained by falling weight deflectometer tests (Section 2.3.2.2 and Section 3.2.1) and or correlation from in situ penetration tests such as the dynamic cone penetrometer (Section 3.2.2).

Coarse and fine-grained soils have fundamental differences in properties that control behavior: coarse-grained soil behavior is primarily controlled by relative density and confinement, whereas fine-grained soil behavior is primarily controlled by stress history and overburden stress. The resilient behavior of unbound materials is governed by the interparticle behavior of the material; the fabric and frictional slip of the particles themselves play a large role in the resulting resistance to deformation. Most of the valid models for estimating resilient modulus are based upon the universal model developed by Uzan (12) that gives the following relationship for resilient stress dependency of unbound materials:

$$M_R = k_1 p_a \times \left( \frac{\theta}{p_a} \right)^{k_2} \times \left( \frac{\tau}{p_a} + 1 \right)^{k_3}$$

where:

$p_a$  is atmospheric pressure,

$\theta$  is bulk stress  $= \sigma_1 + \sigma_2 + \sigma_3$ ,

$\tau$  is the octahedral shear stress  $\frac{1}{3} \sqrt{(\sigma_1 - \sigma_3)^2 + (\sigma_2 - \sigma_3)^2 + (\sigma_3 - \sigma_1)^2} = \frac{\sqrt{2}}{3} \sigma_d$ , and

$k_1, k_2, k_3$  are regression parameters determined from triaxial testing.

The basic concept of the model is that  $M_R$  is a product of the stress imposed on the system and the shear stress. For granular (coarse-grained) materials,  $M_R$  is primarily a function of bulk stress, where increased confinement and shear stress result in strain hardening and increased modulus. For fine-grained material,  $M_R$  is a function of the shear stress, and increases in deviator stress will result in strain softening and decreased modulus. Figure 2.2 illustrates this stress sensitivity of resilient modulus for granular and fine-grained material.

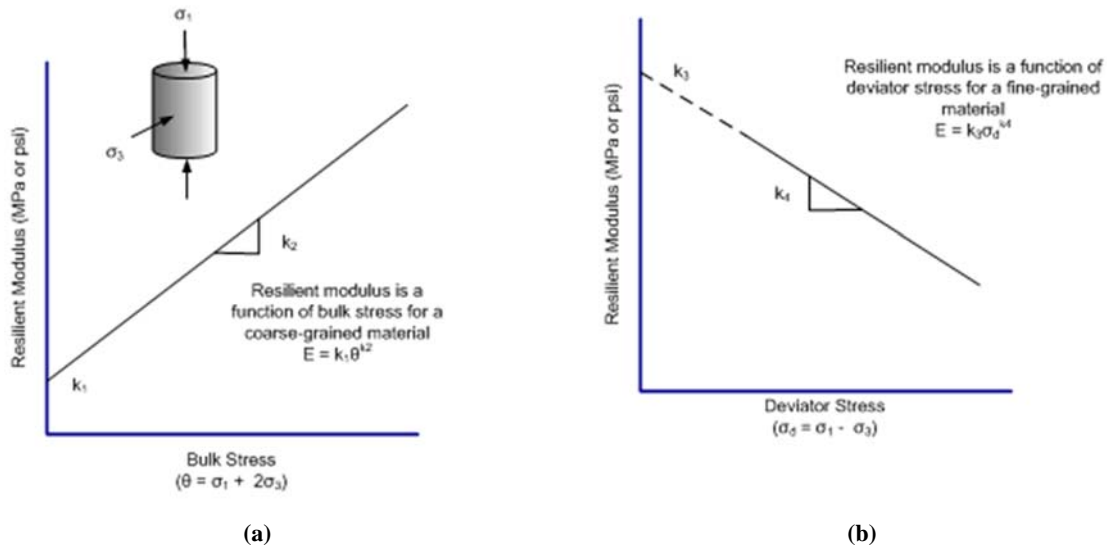


**Figure 2.2: Typical plots showing the stress sensitivity of the resilient modulus: (a) stress stiffening and (b) stress softening.**  
 (Note: illustration is from a CalBack help file).

### 2.3.2.2 Falling Weight Deflectometer and Backcalculation

The falling weight deflectometer (FWD) is the most commonly used tool to evaluate the structural condition of pavements. Testing materials in situ, as opposed to laboratory testing, eliminates the problem of preparing and testing materials at the correct degrees of compaction and moisture content. The FWD and backcalculation of moduli provides a generally realistic measure of the in situ properties of the pavement materials at the time of measurement as they are acting in the total pavement system because the same boundary conditions that apply to design are present while testing.

When using the FWD, a specified load is dropped on the surface of the pavement, creating an impulse force that then generates Rayleigh waves; since these waves produce both vertical and horizontal displacements, the surface is momentarily distorted (13). Placing an array of geophones at known distances away from the load allows accurate measurements of surface deflections to be recorded in time (Figure 2.3). By taking the deflection basin (surface deflections versus distance) and the known pavement structure, the in situ stiffnesses can be evaluated through an inverse analysis known as backcalculation. Figure 2.3 illustrates a typical FWD setup and deflection basin.

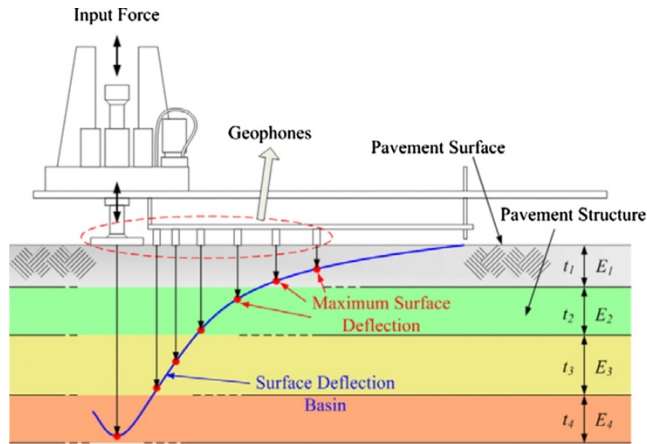


**Figure 2.3: Typical FWD testing setup (14).**

The basic procedure of the inverse analysis (backcalculation) is to assume and vary a set of moduli values until the computed deflections match the measured deflections. A large number of backcalculation programs exist, and most of them are based upon linear elastic theory or finite element methods, modeling the subgrade as a half-space. As described earlier, the assumption of elastic behavior for asphalt materials is approximately correct, while this assumption for inelastic unbound materials may result in incorrect layer moduli. To reduce this error, some programs take into account the nonlinearity of granular material by varying the modulus with the major principal stress; this is commonly applied in the following form (7, 14).

$$E = C \times \left( \frac{\sigma_1}{p_{atm}} \right)^n$$

where:

- $\sigma_1$  is the major principal stress (positive in compression),
- $p_{atm}$  is atmospheric pressure, the reference stress, and
- $C$  and  $n$  are dimensionless constants;  $n$  varies between -1 and +1, depending on whether the material is stress softening (negative) or stress hardening (positive).

While the results of backcalculation analyses are typically attributed as the resilient modulus of the respective material, it should be recognized that backcalculated and laboratory-determined moduli are not the same (15). This should not be a surprise, since it is unlikely that tests performed in the laboratory have precisely the same conditions as the field, such as temperature, stress, moisture, loading rate and duration, and density. Various researchers have found relationships between backcalculated moduli and laboratory-tested moduli, however most studies had slightly different results depending on the conditions at time of testing.

Nonetheless, it has been consistently found that backcalculated moduli are reliable and oftentimes more practical means of evaluating existing pavement material properties (11).

### 2.3.2.3 Factors Affecting Resilient Response

Because  $M_R$  is dependent on the stress state of the material, factors that influence the state of stress can influence the resulting resilient response of the material, making  $M_R$  inherently sensitive to moisture conditions. In their pioneering study, Seed et al. (9) showed that the resilient modulus of compacted soils varies with number of stress applications, age at initial loading, stress intensity, method of compaction, compaction density and water content, and increases in water content after compaction. Further research has found that in addition to the above stated factors, density, soil and aggregate type, shape, material fabric, and soil suction also influence the resilient response (16).

### **Moisture and Suction**

All soils are sensitive to the effects of water, and many issues in geotechnical engineering can be attributed to moisture conditions (3). Richards (17) stressed that for all engineering structures with shallow foundations, it is necessary first to understand and second to predict the moisture movement that will occur during the lifetime of the structure. This section of this report includes a brief summary of moisture and suction behavior in soils, as is pertinent to pavement design.

Any mass of soil consists of solid particles with voids in between that can either be filled with air, water, or some other fluid (such as gas or contaminants). Saturated soils consist only of water and solid particles, while unsaturated soils consist of a mixture of air, water, and solids. In coarse-grained soils, the degree of saturation is one of the primary factors affecting resilient response since it is directly related to the effective stress state of the material. In fine-grained soils, the stiffness characteristics are most dependent on dry density, moisture content and suction, soil structure, and stress state (10).

Because pavement soils exist under a sealed surface and are typically located above the groundwater table, they are usually unsaturated and hence unsaturated soil behavior should be taken into account. Figure 2.4 depicts a simplified schematic of the moisture conditions under a pavement surface.

When a soil is unsaturated, if the void space is small enough, the chemical attraction of water to the particle surface can lead to the development of surface tension at the soil-air-particle interface, causing negative pressures known as suction. Figure 2.5 illustrates the conceptual distribution of pore water and pore air in a soil matrix during drainage from being fully saturated (a) to what is known as the pendular regime (b) where the water is isolated and discontinuous.

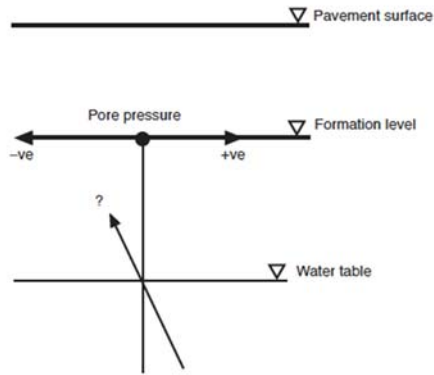


Figure 2.4: Simplified schematic of suction under pavements (5).

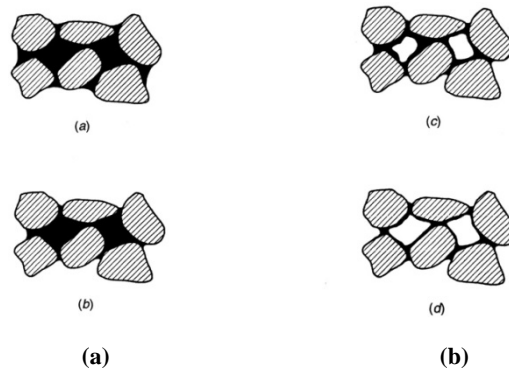


Figure 2.5: Conceptual distribution of pore air and water in a soil matrix (18).

Suction is commonly defined as the “free energy state of soil water” and essentially acts like a vacuum that directly contributes to the effective stress in the soil like an external confining stress, as shown in Figure 2.6; it is probably the most important aspect that differentiates the saturated soil effective stress state and behavior from that of unsaturated soils (19, 20).

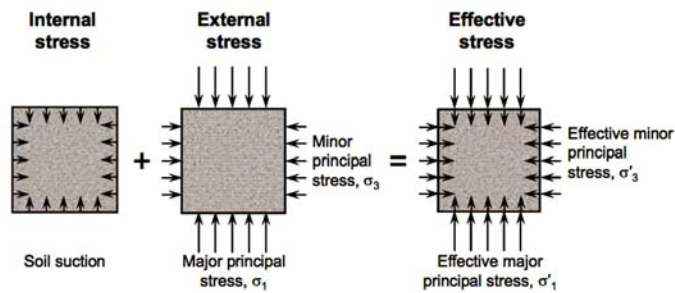


Figure 2.6: Effective stress in unsaturated soil (21).



In engineering problems, the suction present in a soil can be broken up into two components: *osmotic suction* and *matric suction* (also called *matrix suction*) (22). Osmotic suction arises from differences in ionic concentration within the soil and depends on the composition and ability of the particles to restrict the movement of adsorbed cations (23, 19). Typically, in effective stress analyses, osmotic suction is negligible compared to matric suction.

Matric suction arises from negative pore pressures that result from the difference in pore air pressure and pore water pressure (capillary potential), and is defined below.

$$\psi = u_a - u_w = \frac{2T_s}{R_s}$$

where:

- $\psi$  is the matric suction,
- $u_a$  is the air pressure,
- $u_w$  is the pore water pressure,
- $T_s$  is surface tension of the water, and
- $R_s$  is the radius of curvature of the menisci (22)

Figure 2.7 illustrates the soil water between grains with (a) flat menisci and (b) curved menisci. During wetting of the soil, the menisci curvature (and hence radius) at the soil-air-water interface increases, resulting in decreased suction; while drying, the radius of curvature of the menisci decrease, resulting in increased suction; the radius of curvature is dependent on temperature, water content, and state of packing for a given soil (24).

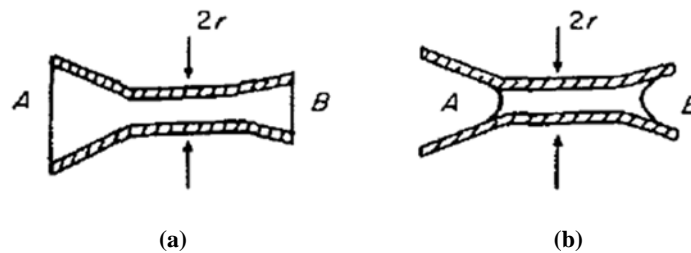


**Figure 2.7: Air-soil-water interface in unsaturated soils (24) showing menisci under (a) wetting and (b) drying.**

The implications of suction and moisture conditions are particularly important during the compaction process. In compacted fine-grained soils, at water contents drier than optimum (for particular compactive efforts), clay particles are arranged in a flocculated structure, and increased capillary tension at the particle interfaces effectively holds the particles together through means of negative pore water pressures, thus increasing the effective stress within the soil (24, 25). At water contents wet of optimum, the water film at the air-particle-water interface grows and effectively acts as a lubricant for the rearranging particles, resulting in a more oriented, or “dispersed” particle

orientation, decreased suction, and lower effective stresses within the soil. Thus the resulting behavior of soils compacted wet and dry of optimum can differ significantly. (25, 23).

Taking into account the influence of matric suction, the resulting effective stress state of unsaturated soils can be simply explained through the equation proposed by Bishop (26):

$$\sigma' = (\sigma - u_a) + \chi(u_a - u_w)$$

where  $\chi$  is a parameter that is a function of saturation levels equal to 0 for a dry soil and 1 for a saturated soil.

While Bishop's equation is "appealingly intuitive," the usefulness of it is often limited in practice due to the uncertainties about  $\chi$  for intermediate degrees of saturation levels and dependence on soil type (19). Despite the complexities involved in design applications and practice, the nature and behavior of unsaturated soils and their implications for specific geotechnical conditions has been shown to be of importance in design considerations. In some cases, neglecting unsaturated soil mechanics properties may result in an incorrect understanding of the actual material behavior and in a consequent misapplication of saturated soil mechanics behavior in design.

The influence of suction on the stress state of the material will influence its resilient response. Recent laboratory experiments have again displayed that the resilient behavior of soils is influenced by suction and moisture variation (27, 28, 29, 5, 30). These researchers have in general found that increased suction typically results in increased resilient moduli, while decreased suction results in decreased moduli. Wetting and drying patterns will also influence the resilient behavior of the material; for a given water content, resilient modulus is typically greater for a soil in a drying state than in a wetting state (7, 30), even for the same water content.

Because unsaturated soils are located above the water table and near or at the ground surface, moisture conditions and suction are closely related to the surrounding environment. While the basic mechanisms of unsaturated soil mechanics can often be readily explained, the actual water–soil interaction underneath pavements is complex and usually uncertain. Beneath an existing pavement structure, moisture condition and suction patterns can vary depending on the following (19):

- Soil type
- Density
- Compaction conditions
- Environmental conditions, such as seasonal fluctuation and drainage conditions
- Location of the water table

- Vegetation
- Surface layer condition
- Spatial variability of all of the above

Because of suction's impact on the effective stress within a soil, and therefore its resilient behavior, several researchers/institutions have sought to integrate unsaturated soil mechanics properties into ME pavement design methods. These are further described in Section 2.4.

## **2.4 Current Modeling of Seasonal Variability in Modulus**

It is acknowledged within ME design that subgrade stiffness should be adjusted due to seasonal changes in moisture conditions. The universal model presented earlier, while indirectly taking into account the effect of moisture by means of the stress state, does not explicitly take into consideration the variation of moisture content or saturation. Several resilient modulus models exist that take into account modulus variation with moisture conditions and density; frost-prone regions also typically take into account effects of freeze/thaw on resilient modulus in their pavement design methods.

### *2.4.1 Enhanced Integrated Climatic Model*

Within the MEPDG (*PavementME* software), the input resilient modulus is estimated using either laboratory determined  $M_R$ , the  $M_R$  obtained from correlations with California Bearing Ratio (CBR), or through correlations to index properties. The MEPDG guidelines and software have been revised several times to include a model known as the *Enhanced Integrated Climatic Model* (EICM) that aims to fine-tune the modulus adjustment factor for unbound material by considering the change in moisture content in the subgrade over the design life of the pavement (12).

EICM requires two primary sources of input parameters to accurately predict environmental factors on modulus: materials property information and climatic information. The necessary climatic information is readily available to designers through a database within MEPDG; historically the unbound materials' requirements range from routine index properties performed by the engineer for parameters in lower-level designs to more complicated parameters, such as the soil-water characteristic curve (SWCC) for higher levels of analysis. The SWCC is a simple way to visualize how matric suction changes with saturation and water content, as shown in Figure 2.8. The shape of the curve depends on the soil type, grain size distribution, soil fabric, and friction angle.

NCHRP project 9-23A, *Development of a National Catalog of Subgrade Soil-Water Characteristic Curves (SWCC) Default Inputs to Use in the Mechanistic-Empirical Pavement Design Guide (MEPDG)*, created a

publically accessible database of SWCC parameters and soil index properties needed for all hierarchical levels of the EICM, and subsequently NCHRP 9-23B was directed at integrating an enhanced GIS-enabled database in order to query this information for specific sites (32).

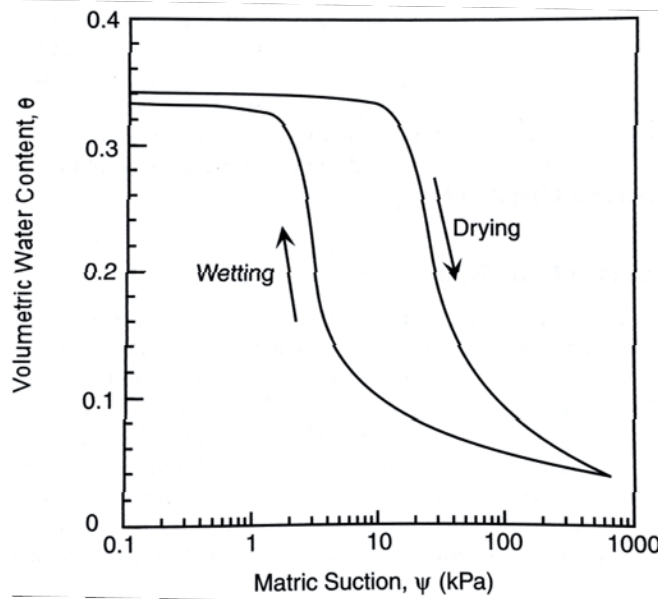


Figure 2.8: Soil-water characteristic curve (18).

The MEPDG uses the climatic and soil information to account for changes in moisture content in the subgrade over the design life by using an environmental factor that represents the modulus ratio for unfrozen, unbound materials. The environmental factor is a function of climate, soil type, and moisture regime, and is represented by the following relationship:

$$\text{Log } F_u = a + \frac{b - a}{1 + e^{\ln(-\frac{b}{a}) + k_m \times (S - S_{opt})}}$$

where:

$F_u = \frac{M_R}{M_{Ropt}}$ , the  $M_R$  at any time divided by  $M_R$  at optimum conditions,

$a$  = minimum of  $\text{Log } F_u$ ,

$b$  = maximum of  $\text{Log } F_u$ ,

$k_m$  is a regression parameter, and

$S - S_{opt}$  is the variation in degree of saturation.

In this model, the saturation at any point in time is calculated by computing the negative pressure head as the unit weight of water multiplied by the distance to the groundwater table from the point of interest. The soil-specific SWCC is then used to evaluate the saturation at that specific level of suction (12). Further descriptions of this equation are described in Witczack, Andrei, and Houston (33) and Cary and Zapata (34).

Although the method utilizes unsaturated soil properties, MEPDG uses a total stress approach to evaluate the stress state of the unbound material. Cary and Zapata (34) noted that in doing so, the stress state, and therefore the resulting stiffness, depends only on the pavement structure and the effective temperature of the asphalt surface at the time of loading. They suggested that by including matric suction as a stress variable in the models, the influence of stress state level would be further refined. This method of design, while predicting the change in stiffness due to change in saturation, does not combine effects of the stress state and water content (27).

#### 2.4.2 South Africa Pavement Design Method

South Africa has had a long history of developing methodologies and solutions for pavement engineering; over the past 10 years they have been working on developing and refining improved ME design methods based on the latest available local data, international research, and design trends. The most recent revision of South African Pavement Design Method (SAPDM) developed for the South African National Roads Authority Limite (SANRAL) discusses the improvements made on their ME design methods for flexible pavements (21). In the SAPDM, both the resilient response model and the shear strength models for unbound granular material incorporate the effects of saturation on the material behavior. The resilient response model accommodates strain-hardening for low saturation and strain-softening for high saturation; the shear strength model includes a term for suction pressure that results from the partial saturation of the material. The response models also account for other influences in the effective stress of the unbound granular material that may result from residual compaction stress, internal suction pressure, and load induced stresses (Figure 2.9) (21).

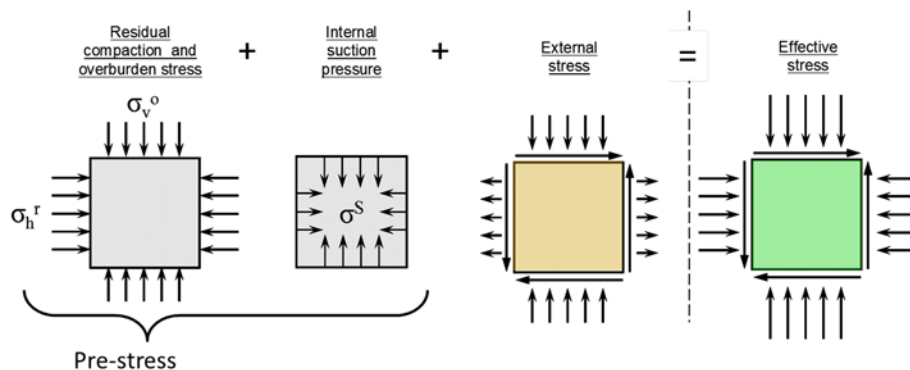


Figure 2.9: Effective stress in partially saturated unbound granular material (21).

For subgrade materials, the material is modeled as a semi-infinite half-space with predetermined stiffnesses based on material type provided in the design manual, or by using backcalculated stiffnesses for existing subgrades. The SAPDM also includes a subgrade stiffness reduction model, which takes into account the influence of loading on subgrade stiffness.

### 2.4.3 WesTrack Experiment

Chapter 2 of *WesTrack: Performance Models for Permanent Deformation and Fatigue* (35) describes the procedure that was used to arrive at the variation of subgrade soil stiffness throughout the year for performance modeling (36). The base material stiffness at the site was found to be independent of temperature and season while the subgrade soil stiffness was found to be sensitive to seasonal changes but not to temperature influences. These conclusions were made based on multilayer linear elastic analyses of FWD data obtained over the course of a year. The resulting subgrade soil stiffness for the WesTrack section was represented as a discrete function of the measurement period and a sinusoidal function represented by:

$$E = D_0 + D_1 \left[ \frac{\sin(\text{day} - D_2)}{365 \times 2\pi} \right]$$

where:

$\text{day}$  = day of the year and  
 $D_0, D_1$  and  $D_2$  are regression parameters.

It was noted in the report that at the time conventional backcalculation analysis routines might underestimate base moduli; it was suggested that an additional investigation for backcalculation of untreated base moduli was warranted but beyond the scope of the study. Figure 2.10 shows the results from backcalculation analyses and the sinusoidal function for the WesTrack foundation soils (35).

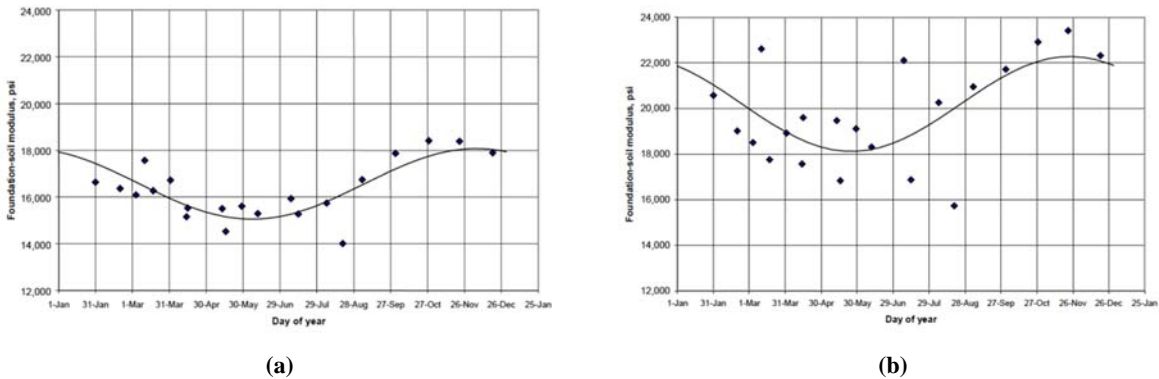


**Figure 2.10: WesTrack seasonal variation of foundation-soil modulus for (a) south tangent and (b) north tangent.**

## 2.5 CalME

*CalME* is California's new ME design method software. In order to implement unbound material behavior into *CalME*, Ullidtz et al. (11) studied the effects of the relationship between resilient modulus and the material strength of unbound pavement material by evaluating the differences between a Finite Element Model (FEM) simulation (using a simple 2-D Drucker Prager model with nonlinear elasticity) and Discrete Element Modeling (DEM) analyses compared with results from full-scale Heavy Vehicle Simulator (HVS) testing, as shown in Figure 2.11. The results of FEM analyses indicated that increased loading resulted in decreased modulus of the

granular layer, which was contradictory to the results from the full-scale HVS tests. These results were likely due to the simplicity of the constitutive model used, and revealed that the particulate nature of the material and the additional confinement from overlying layers also had an influence on the change in modulus. To further refine the findings and model, they evaluated what would occur in the discrete element case (11), which revealed that the stiffness of the upper layer (i.e., asphalt-bound material) may be important to the resulting displacement, and hence the stiffness, of the granular material.

The DEM analyses suggested that stiffer asphalt-bound layers tended to decrease the displacement of the granular particles, and thus increased the effective stiffness. FWD testing also indicated that some of the unbound layer stiffnesses decreased as asphalt stiffness decreased, confirming that the empirical evidence for the influence of overlying layer stiffness may be an important consideration in design, although it is not discussed in the literature or used in any other pavement design methodologies.

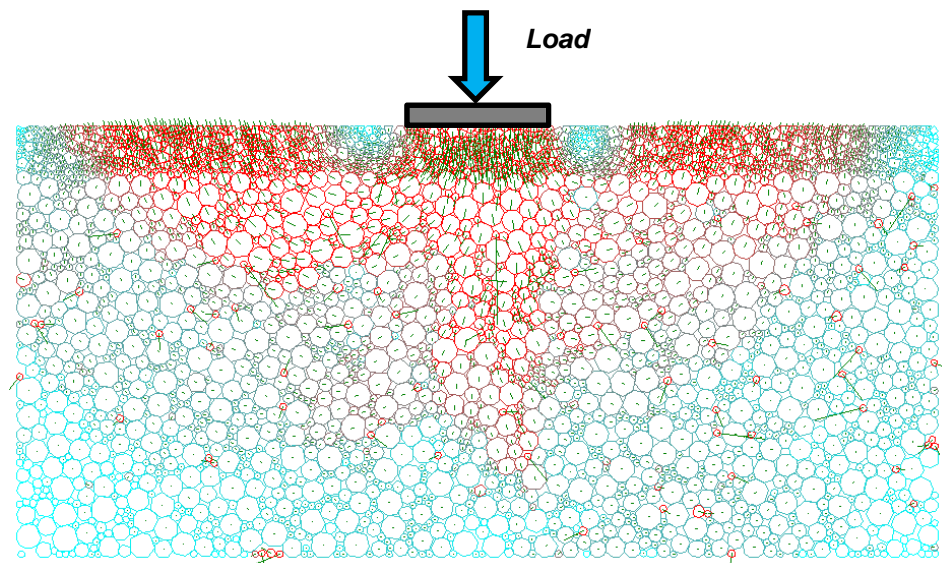


**Figure 2.11: Discrete element modeling of unbound material under a stiff material (11).**

To capture this effect of overlying layer stiffness, within *CalME* the stiffness of unbound materials are calculated from the equation

$$E_n = E_{nref} \times \left( 1 - \left( 1 - \frac{S}{S_{ref}} \right) \times Stiffness\ Factor \right)$$

where:

$E_{nref}$  is the reference stiffness of the material, in a given layer  $n$ ,

$$S = \left( \sum_1^{n-1} h_i \times \sqrt[3]{E_i} \right)^3,$$

$S_{ref}$  is some reference stiffness, typically 3500 MPa<sup>1/3</sup>\*mm,

*Stiffness Factor* is a factor that can be evaluated through FWD testing (between 0 and 1), and  $i$  represents the layers above layer  $n$ .

The study also revealed that the moduli of the unbound layers were not constant under different wheel loads, as would be expected by the stress-hardening or stress-softening behavior representative of granular and fine-grained materials, respectively. The resulting function used within *CalME* to evaluate the modulus at load level  $P$  was calculated as:

$$E_P = \left( \frac{P}{40kN} \right)^\alpha \times E_{40kN}$$

where the power  $\alpha$  is 0.6 for granular layers and -0.3 for the subgrade, which are typical values for granular and cohesive materials, respectively (11).

The aforementioned relationships are what *CalME* currently uses to model the resilient response of unbound material (11). Within the program, there is also a framework available to vary the resilient modulus of unbound material for seasonal effects such as moisture factors or freeze/thaw; however, for the standard materials there is currently no seasonal variation available. Expanding from the model found in the WesTrack experiments, seasonal variation attributed to the material follows either a sinusoidal variation, modeled as

$$E = E_{mean} \times \left( 1 + \frac{Range E}{2} \times \sin \left( \frac{2\pi(Day - Day of Max E)}{365} + \frac{\pi}{2} \right) \right)$$

or an exponential relation for freeze-thaw conditions, modeled as

$$R = 1 - (1 - Max\ frost\ reduction) \times EXP(Recovery\ rate \times Days\ since\ frost)$$

where:

$$Range\ E = (E_{max} - E_{min})/E_{mean},$$

*Day of Max E* is counted from January 1,

*Max frost reduction* is the ratio between the lowest and the highest modulus, and

*Recovery rate* is a modulus adjustment factor representing the change in modulus per day since the day of last frost (0 to 1).

*CalME* also takes into account modulus reduction due to moisture ingress; if the overlying asphalt stiffness reaches a specified limit (indicative of cracking), the unbound materials' moduli will be reduced by some fraction of their original stiffness. These relationships of seasonal variations, while better than nothing, require further investigation and optimization regarding their importance in design and corresponding pavement response.



## 2.6 Knowledge Gaps

While unsaturated soil mechanics in and of itself is a complex phenomenon, and implementation of its principles can prove to be more complicated; implementing these relationships into practical—yet efficient—resilient modulus models for design has not been included in most ME design methods. Soil suction should be expected to vary spatially throughout the soil (even over very short distances) as grain size distributions or pore size distributions vary, hence varying effective stress over short distances (37) yet most models typically average unbound material properties across a design section and therefore do not take into account the spatial variability of the materials or the response (38, 39). Some degree of uncertainty in soil properties, characterization, specific moisture conditions, and spatial variability will undoubtedly exist; however, errors in evaluating very specific responses can sometimes lead to undesirable errors in performance prediction. While the assumption that suction is equal to the negative pressure head may be fairly accurate for shallow groundwater conditions, it neglects other sources of water infiltration such as those from inadequate drainage conditions, agricultural parameters, or influx of water beneath the pavement after rainfall events (12).

Many experiments have been performed to relate the effects of moisture and suction conditions on the resilient response of unbound pavement material in the laboratory; however, relatively few studies have reported the impacts on in situ stiffness (40, 41). In their study, Salour and Erlingsson (40) acknowledged that the ability to reproduce the internal structure of unbound materials for laboratory preparation is not fully possible and the use of field data may prove useful in evaluating moisture effects on pavement structures.

## 2.7 Additional Questions from the Literature

From the literature study, the following questions have been identified:

- While the properties of unsaturated soil mechanics are fairly well-established and changes in resilient response have been tied to changes in moisture and suction, how do these phenomena extrapolate to the loads and conditions experienced in the field?
- If the literature suggests that the stiffness of a material can increase fivefold during drying seasons, as shown through suction-controlled resilient modulus testing using reconstituted samples and laboratory testing, does this behavior occur in the same way under full-scale pavement conditions?
- Does neglecting unsaturated behavior result in more conservative pavement response models and designs, or less conservative pavement response models and designs? How does this result in conservatism influence performance, and what are the respective costs economically?

*(This page intentionally blank)*

## **3 EXPERIMENT DESIGN AND LABORATORY TESTING**

---

### **3.1 Introduction**

In response to the literature and to meet the stated objectives under the aforementioned scope, an experiment was designed and executed to assess seasonal changes in in situ unbound materials. This chapter describes the methods used to evaluate seasonal changes in unbound layer moduli and its associated factors. The experiment had two phases. The first consisted of full-scale field testing on existing pavement structures located around the state. This required two trips—one at the end of the rainy season and the other in the middle of the dry season—to 11 test sites to evaluate changes in moisture conditions, in the materials' resistance to penetration, and their in situ stiffnesses, the latter of which was assessed by means of falling weight deflectometer backcalculation methods. This portion of the study was used to gauge the scale and breadth of the properties and materials, and to examine any corresponding changes that were evaluated from one season to the next. The second portion of the study was a smaller-scale field test performed on the UCPRC test track to evaluate any changes in stiffness that occurred throughout the year, after rainfall events, and during wetting and drying cycles.

### **3.2 Research Instruments**

Field testing consisted of deflection testing using the falling weight deflectometer (FWD), which was later used to backcalculate in situ layer moduli. Dynamic cone penetrometer (DCP) testing (ASTM D 6951) was also performed to obtain the subsurface pavement structure and to provide a secondary measure of stiffness. Lastly, unbound materials were taken and sampled for processing in the laboratory.

#### *3.2.1 Deflection Testing and Backcalculation*

FWD testing provided the primary means of assessing the layer stiffness of the pavement structure, as it captures information about the in situ material with appropriate boundary conditions present in the field. Although triaxial testing of unbound materials is commonly used to obtain alternative measures of material stiffness, the scope of this project was such that stiffness measurements were limited to FWD analysis (11). A Dynatest 8082 Heavy Weight Deflectometer (referred to in this report as the “FWD”) was used to perform all deflection tests; this device has a 150 mm diameter plate and eight geophones attached at the locations specified in Table 3.1. Two drops at three loading levels were used at each test station, which amounted to six drops at each station, corresponding to loadings of approximately 30 to 35 kN, 40 to 45 kN, and 55 to 60 kN. For each test point, the FWD generated load-deflection data (e.g., actual force applied, deflections, time history, etc.) that were used to estimate the pavement layer stiffness.

**Table 3.1: FWD Sensor Locations**

Geophone	Distance from center of load (mm)
1	0
2	200
3	300
4	450
5	600
6	900
7	1,200
8	1,500

Because asphalt is a viscoelastic material, stiffness changes with temperature. Typically, the temperature of asphalt-bound layers is taken as the temperature at 1/3 the height of the layer. If in-depth measurements are unavailable, a relationship known as the BELLS equation can be used to calculate the temperature of the asphalt at depth. The BELLS equation has several forms, and BELLS3 is used to evaluate the asphalt temperature at depth for testing that takes approximately 30 seconds and is described by the following relationship:

$$T_d = 0.95 + 0.892 \times IR + (\log(d) - 1.25) \times [-0.448 \times IR + 0.621 * + 1.83 \times \sin(hr_{18} - 15.5)] + 0.042 \times IR \times \sin(hr_{18} - 13.5) T_{prev}$$

where:

$T_d$  = Pavement temperature at depth  $d$  (°C),

$IR$  = Pavement surface temperature (°C),

$d$  = Depth at which material temperature is to be predicted (mm),

$T_{prev}$  = Average air temperature the day before testing (°C),

$\sin$  = Sine function on an 18-hr clock system, with  $2\pi$  radians equal to one 18-hr cycle, and

$h_{18}$  = Decimal time of day, in a 24-hr clock system, calculated using an 18-hr asphalt concrete (AC) temperature rise-and-fall time cycle (42)

The original source of the backcalculation software used in the analysis, *CalBack*, was developed for Caltrans and uses the Odemark-Boussinesq method to calculate deflections for comparison with measured deflections. Odemark's method is based upon the assumption that the stresses and strains below a layer are also dependent on the stiffness of the layer above it; by transforming a multilayered system to an equivalent semi-infinite half-space, Boussinesq's equations may be used to calculate the corresponding stresses, strains, and deformations of the system, which makes the calculations extremely fast. Backcalculation analyses were conducted using a software program called *KalmanBack*, which uses the Kalman filter search criterion. The Kalman filter is a set of mathematical equations that provide an efficient means to estimate the state of a dynamic system from a series of noisy and incomplete measurements. Choi et al. (14) developed the software and performed sensitivity analyses that indicated this method is fast, consistent, robust, and not highly sensitive to seed values.

Because of the nonlinearity of granular and subgrade material, the stiffness will change depending on the load level. Because the load level fluctuated slightly with each drop, location, and test site, for each test point the average stiffnesses obtained from backcalculation analyses provide little means for comparison across the different sites. For this reason a power relationship was found for the variation of stiffness with load and an equivalent stiffness at a load of 40 kN was calculated (Figure 3.1).

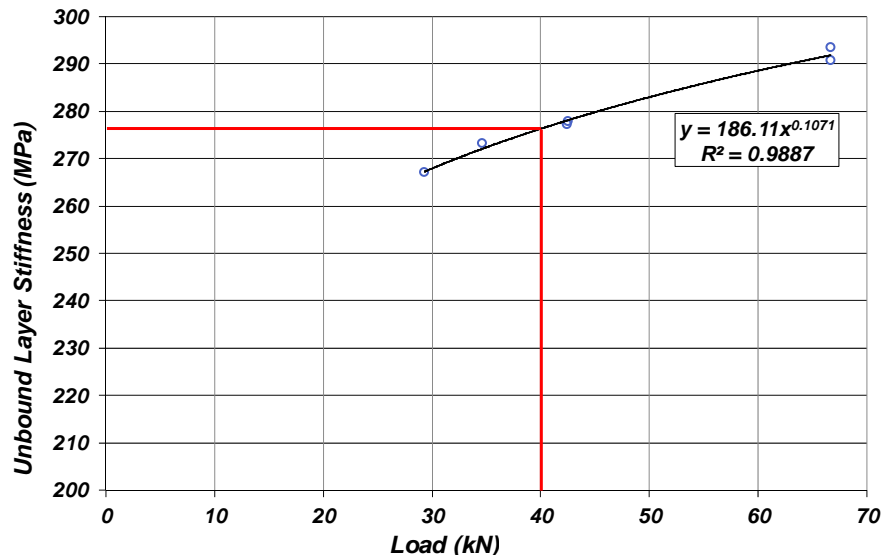


Figure 3.1: Example of load normalization for unbound layer stiffness.

### 3.2.2 Dynamic Cone Penetrometer

The dynamic cone penetrometer (DCP) was used to evaluate the pavement substructure as well as to provide an estimate of penetration resistance and a gauge of the shear strength of the unbound materials. The DCP is a relatively simple penetration test that was developed in the 1950s in Australia—and later improved in South Africa (43)—for evaluating the shear strength of material properties. The DCP data collected were the penetration depth versus the number of blows, with the penetration rate (DN) calculated according to the following, calculated for every five blows:

$$DN = \frac{\Delta Penetration (mm)}{\Delta Blows}$$

A large number of comparative tests have been performed to correlate DN with resilient modulus ( $M_R$ ) from both laboratory and field methods. Table 3.2 and Figure 3.2 summarize some of the relationships between DN and resilient modulus found in the literature.

DCP testing was performed after the coring of the bound material, and extended to the maximum extent of the rod, approximately 1 m below the starting depth. Readings were taken every five blows, unless more frequent measurements were warranted. Because of the passive failure zone beneath the cone tip, the DCP can only distinguish layers whose thickness is at least 6 to 8 times the diameter of the DCP, therefore at least 120 to 160 mm thick.

**Table 3.2: Relationships between DN and Resilient Modulus**

Correlation	Reference	Modulus Type
$\log(E_{eff}) = 3.04758 - 1.06166 \times \log(DN)$	CSIR (1997) (44)	Backcalculated from FWD
$E = 17.6 \left(\frac{269}{DN}\right)^{0.64}$	Chai and Roslie (1998) (45)	Elastic Modulus
$E = 338(DN)^{-0.39}$	Chen et al. (1999) (46)	Backcalculated from FWD
$E = \frac{537.76}{DN^{0.66}}$	Chen et al.(2005) (47)	Backcalculated from FWD
$\ln(M_{FWD}) = 2.35 + \frac{5.21}{\ln(DN)}$	Abu-Farsakah et al. (48)	Backcalculated from FWD
$M_R = \frac{151.8}{(DN)^{1.096}}$	Mohammad et al. (2007) (49)	Lab and backcalculated from FWD
$E_{LFW D} = \frac{5301.54}{DN^{1.44} + 8.31}$	Nazzal et al. (2007) (50)	Backcalculated from lightweight FWD
$M_R = \frac{668.27}{DN^{-0.556}}$	Mejías-Santiago et al. (2015) (51)	Backcalculated from FWD

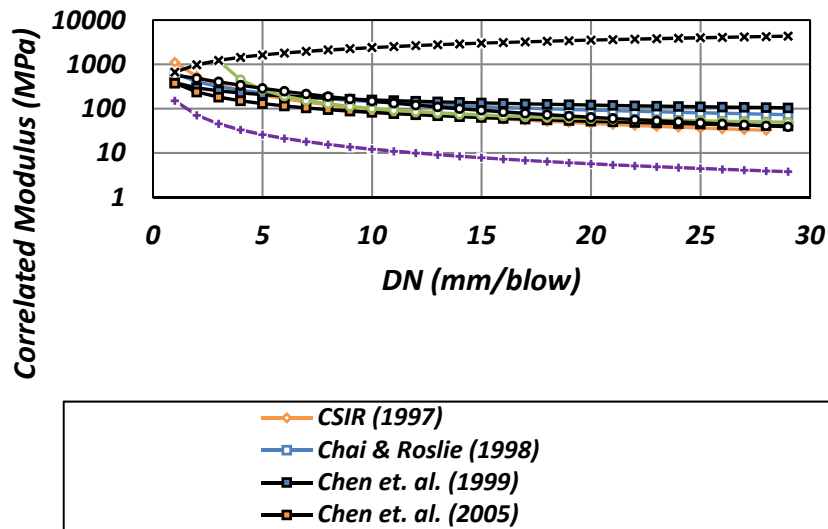


**Figure 3.2: Graphical representation of relationships of DN versus corrected resilient modulus for typical range of DN.**

### 3.3 Experiment Design

#### 3.3.1 Long-Term Assessment of Seasonal Changes

In order to assess the range of properties that might be encountered throughout the state, 11 different field locations across California, shown in Figure 3.3, were chosen to assess in situ backcalculated stiffnesses of materials and their relationship to various soil properties such as water content, grain size distribution, Atterberg limits, and soil type, as well as geologic setting and drainage conditions. The first round of field testing occurred in the late spring and summer of 2015 (May through August), a drought year; data collected during this time is intended to serve as the “dry” sampling. The second round of field testing occurred during the spring of 2016 (March through June) after a rainy season with near normal rainfall, and the data collected is intended to serve as the “wet” sampling.

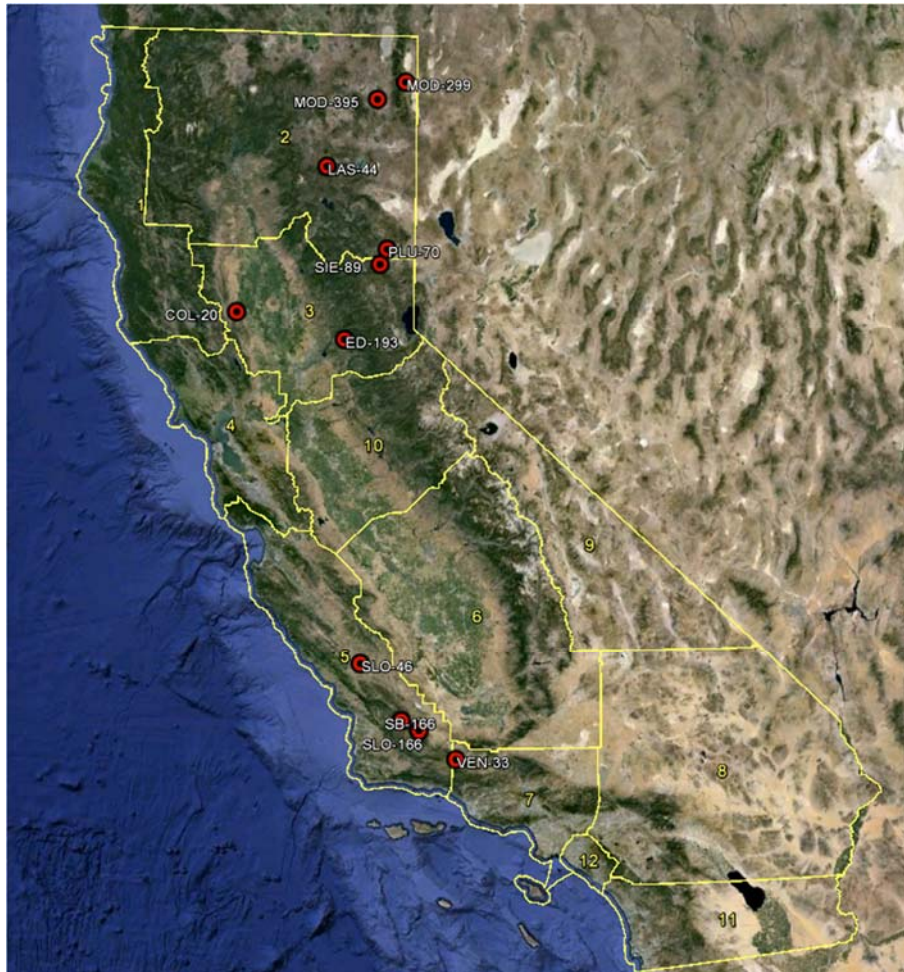


Figure 3.3: Locations of test sites (yellow boundaries indicate Caltrans districts).

### 3.3.1.1 Section Information, Location, and Schedule

The test site locations and the testing dates are summarized in Table 3.3. Testing locations were selected based on the following attributes:

- Stabilized base material
- Location within state
- Proximity to other field sites
- Soil type
- Climate region (Table 3.4)

This field testing for this project fell under Task 2 in Partnered Pavement Research Center Strategic Plan Element (PPRC SPE) 3.30, “Standard Materials Library and Guidance.” The UCPRC and Caltrans are working to further expand their ME standard materials library to encompass additional asphalt-bound and lightly cemented materials. To efficiently evaluate seasonal changes of unbound layers in conjunction with other needs of the project, field testing was conducted at sites with lightly cemented and/or recycled/reclaimed base material. These base materials consisted of full-depth reclaimed material (FDR; FDR-FA signifies foamed asphalt-stabilized, FDR-C signifies cement stabilized); cold in-place recycling (CIR); pulverized asphalt base, which is full-depth reclaimed material with no stabilization (FDR-NS, which is also referred to as PAB); lime-stabilized subgrade (LS); or lean concrete base (LCB).

**Table 3.3: Test Site Locations**

Location		Test Section			Site Information		Testing Schedule	
County	Route	Direction	Post Miles Tested	Lane Number	Climate Region	Base Material	Round 1	Round 2
Colusa	20	East	15.35 – 14.35	1/1	Inland Valley	FDR-FA	5/14/15	4/5/16
El Dorado	193	East	10.4 – 11.4	1/1	Low Mountain	CIR	5/21/15	5/10/16
Sierra	89	North	28 – 29	1/1	High Mountain	FDR-FA	7/23/15	5/11/16
Plumas	70	East	82 – 83	1/1	High Desert	PAB	7/21/15	4/26/16
Ventura	33	North	51.5 – 52.5	1/1	South Mountain	FDR	7/28/15	6/9/16
Santa Barbara	166	East	55 – 56	1/1	South Coast	FDR-FA	7/29/15	5/5/16
San Luis Obispo	166	East	41.5 – 42.5	1/1	South Coast	CIR	7/30/15	5/4/16
San Luis Obispo	46	East	36.6 – 37.6	2/2	Inland Valley	LCB	7/31/15	5/3/16
Lassen	44	West	9.5 – 10.5	1/1	High Mountain	PAB	8/3/15	4/21/16
Modoc	395	North	13.5 – 14.5	1/1	High Desert	PAB	8/4/15	4/20/16
Modoc	299	East	59.5 – 60.5	1/1	High Desert	FDR-C	8/5/15	4/19/16



**Table 3.4: California Climate Regions (52)**

<b>Climate Region</b>	<b>Weather Station Location</b>	<b>Average Annual Rainfall in mm (inches)</b>
North Coast	Arcata	1,604 (41.9)
High Desert	Reno	191 (7.5)
High Mountain	Callahan	544 (21.5)
South Mountain	Cuyamaca	869 (34.2)
Low Mountain	Trinity River	828 (32.6)
Inland Valley	Sacramento	449.6 (17.7)
Central Coast	San Francisco	541 (21.3)
Desert	Daggett	99 (3.9)
South Coast	Los Angeles	330 (13.0)

Preliminary section and materials information was obtained to provide guidance in site selection. The information used included the following:

- Structure from Caltrans Project Plans
- Construction history at the location from the Caltrans Contract Cost Database
- Soil type from *SoilWeb*, a GPS-based soil survey of the continental United States, from the USDA Natural Resources Conservation Service (Soil Staff)
- Construction information from previous UCPRC projects (15)
- iGPR, a database of ground-penetrating radar (GPR) scans for PaveM

This information was also used to aid coring and in situ testing and sampling during field testing, and provided a means to estimate pavement structure if field data were difficult to interpret or lacking. While the aforementioned sources of information provided a comprehensive idea of the structure and materials to be encountered at the site, as-built drawings were not always complete or detailed enough, and thus the actual variability of materials and structure across the site is relatively unknown.

### 3.3.1.2 Section Descriptions

A brief description of all the sites tested can be found in Appendix A. These descriptions include the following:

- Test section location (county, post miles, nearest city)
- Pavement structure and most recent construction date
- Geologic setting
- Caltrans climate region (Table 3.4)
- Approximate annual rainfall
- Elevation
- Aerial photograph

In summary:

- The sections tested covered six of the nine climate regions.
- Five of the test sections were expected to be constructed using cut/fill methods.
- Two of the test sections were located near agriculture.
- Five of the test sections were constructed approximately even with the surrounding ground.
- One of the test sections was an embankment road.

### 3.3.1.3 Field Testing Procedures

In order to streamline the protocol of field testing, a standard field work plan was created. The field work consisted of an initial survey of the test section followed by FWD testing on the one mile long section. To minimize lane closures, sample extraction took place concurrently with the FWD testing, and was spaced approximately 50 feet (15 m) from the outer limits of the one-mile test section. DCP testing was performed after the extraction of bound material from each core hole and prior to unbound material sampling.

#### **Initial Condition Survey**

On arrival at the test site, testing personnel performed a visual survey of the section, which included any observations of pavement quality, drainage conditions, safety, unexpected circumstances, or other pertinent information.

#### **Falling Weight Deflectometer Testing**

The FWD testing plan, shown in Figure 3.5, was developed in order to efficiently capture layer stiffnesses in the center lane and wheelpath over a representative temperature range as well as at specific coring locations.

The FWD testing sequence was as follows:

- Test at Mile 0-50ft (Mile 0 minus 50 ft) and take a core. (*Note: Mile 0 is referred to as Station 0 in some figures, and other locations are labeled similarly.*)
- Test between wheelpath of Mile 0.5 to 1.0.
- Test at Mile 1+50ft, and take a core.
- Test the right wheelpath (unless otherwise specified) for Mile 0.0 to 1.0.
- Test between wheelpath for Mile 0.0 to 1.0.
- For all test sections except for Colusa 20, drop intervals were spaced 40 meters apart.

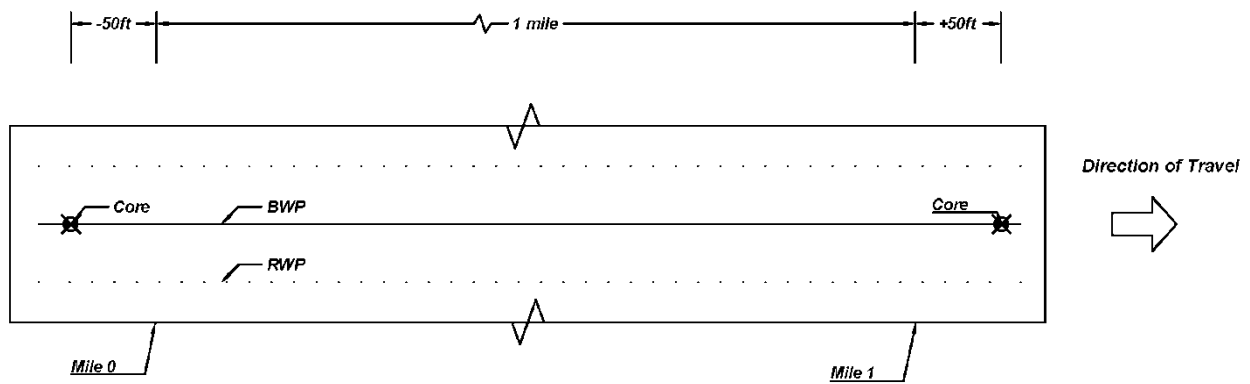
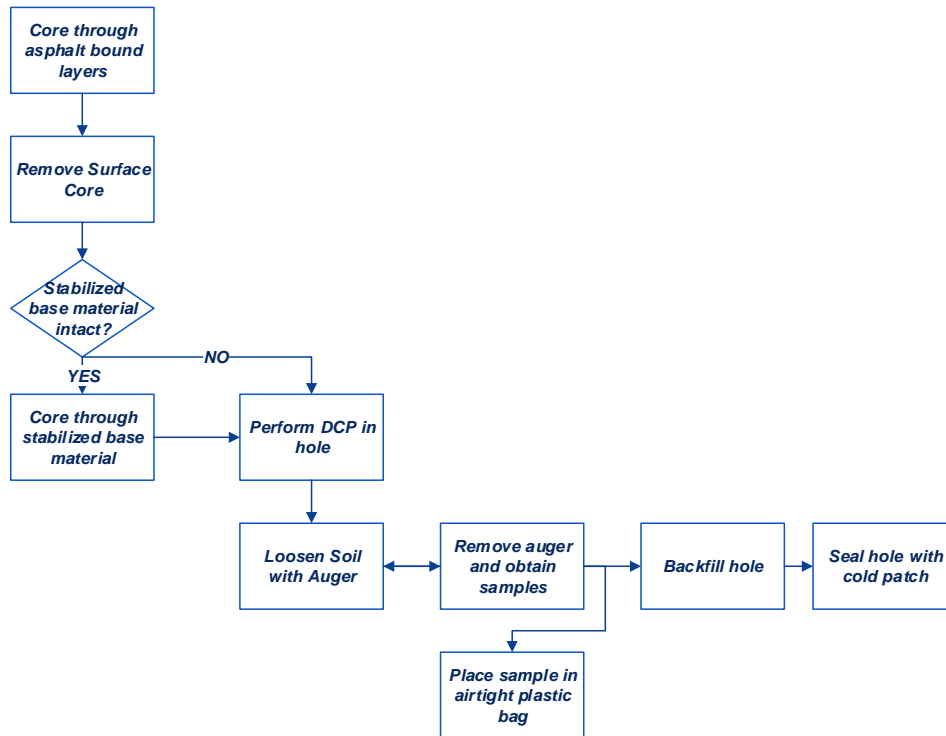


FIGURE NOT TO SCALE

Figure 3.4: Plan view of FWD testing locations (for one lane).

### Coring and Sampling Procedure

Coring and sampling took place at Mile 0-50ft and Mile 1+50ft such that a representative structure of the pavement could be identified for use in backcalculating the layer moduli. Coring and sampling procedures were followed as shown in Figure 3.5.



**Figure 3.5: Field sampling flow chart.**

#### 3.3.1.4 Laboratory

After the in situ testing and sampling procedures were completed, the sampled materials were taken to the laboratory for further processing. The laboratory test results were used to evaluate both in situ properties, such as moisture content, as well as material characteristics, such as soil type, Atterberg limits, and linear shrinkage. The following section describes the laboratory methods used to characterize the sampled material.

#### Moisture Content

The in situ soil moisture content for unbound material was evaluated in accordance with ASTM D2216, *Standard Test Methods for Laboratory Determination of Water (Moisture) Content of Soil and Rock by Mass*. Field moisture content with depth was measured. The results were used for comparison to the liquid limit, plastic limit, and shrinkage limit of the soil and any effects that these parameters might have on the stiffness or penetration resistance of the material. Moisture content was also evaluated to provide a comparison between the two different rounds of field testing to assess changes in moisture content and their influence on in situ stiffness.

#### Soil Properties

In order to evaluate the effects and changes present in different soil types, soils were classified both visually in accordance with ASTM D2488, *Standard Practice for Description and Identification of Soils (Visual-Manual*

Procedure), and through use of the United Soil Classification System (USCS) in D2487, *Standard Practice for Classification of Soils for Engineering Purposes (Unified Soil Classification System)*. In order to classify the soils in accordance with USCS, a sieve analysis and Atterberg limits testing were required, and these are described below.

#### *Sieve Analysis*

A particle-size analysis was performed in accordance with ASTM D6913 (*Standard Test Methods for Particle-Sieve Distribution of Soils using Sieve Analysis*), ASTM C136 (*Sieve Analysis of Fine and Coarse Aggregate*), ASTM D6913 (*Standard Test Methods for Particle-Size Distribution [Gradation] of Soils Using Sieve Analysis*), and ASTM D1140 (*Standard Test Methods for Determining the Amount of Material Finer than 75  $\mu\text{m}$  [No. 200] Sieve in Soils by Washing*) in order to characterize the soil according to USCS specifications and to evaluate the effect that fines content and gradation may have on seasonal stiffness variation. Sieve sizes used are listed in Table 3.5.

**Table 3.5: Sieve Sizes**

Sieve Size	Sieve Size	
	in.	mm
2"	2.000	50.800
3/4"*	0.750	19.050
3/8"	0.375	9.525
#4*	0.187	4.750
#8	0.094	2.388
#10*	0.079	1.999
#16	0.046	1.180
#20	0.033	0.850
#40*	0.017	0.425
#50	0.012	0.295
#100	0.006	0.152
#200*	0.003	0.075

\*Sieve sizes required by ASTM D2487.9.7.

#### *Atterberg Limits*

The Atterberg limits of the material passing the #40 sieve were evaluated for the sampled material. Atterberg limits testing was performed in accordance with the wet preparation method described in ASTM D4318. For some of the tests, the grooving tool used was the one specified in AASHTO T 89 (*Standard Method of Test for Determining the Liquid Limit of Soils*). Atterberg limits were evaluated in order to characterize the soil in accordance with USCS and to assess the impact that plasticity may have on seasonal stiffness variation.

### *Linear Shrinkage*

Linear shrinkage testing of the material passing the #40 sieve was performed in accordance with South Africa Standard Test Method A4 (53). While not a typical American test standard, linear shrinkage is an additional indicator of plasticity and a measure of material sensitivity to water. Linear shrinkage of the material was evaluated to assess effects of shrinkage potential on seasonal stiffness variation. A photo of the mold used can be seen in Figure 3.6.

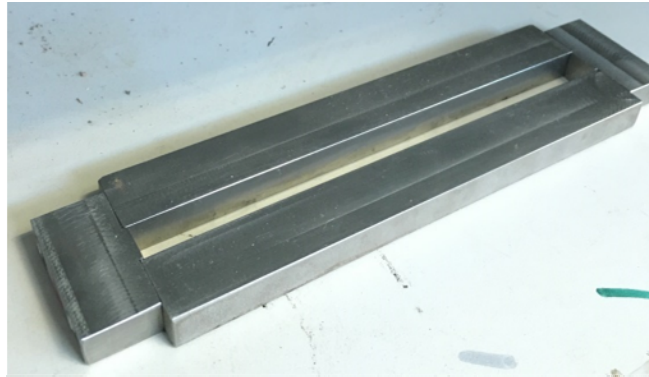


**Figure 3.6: Linear shrinkage mold.**

#### 3.3.1.5 Analyses

In summary, for each section, the following were obtained from the field:

- FWD deflections in the wheelpath for a one mile-long test segment
- FWD deflections between the wheelpath for a one mile-long test segment and 0.5 mile-long test segment
- Layer thicknesses from core samples of bound material
- DCP blow counts versus depth
- Asphalt surface temperature and air temperature from FWD testing

For each section, the following information was obtained through laboratory testing program:

- In situ moisture content of unbound material
- Grain size distribution
- Atterberg limits (Liquid Limit, Plastic Limit, Plasticity Index)
- Linear Shrinkage

For each section, the following were evaluated through means of data comparison and analyses:

- Inferred site structure
- Layer moduli from backcalculation analysis

- DN, DCP Penetration index
- Asphalt temperature at 1/3 depth

Using these data and information, the various factors and properties were compared for the two rounds of field testing to evaluate specific properties that are strongly correlated with changes in unbound material stiffness.

### *3.3.2 Small-Scale Assessment of Seasonal Changes*

A full-scale and more closely analyzed test section at the Advanced Transportation Infrastructure Research Center (ATIRC) at UC Davis was used to assess whether or not significant changes in backcalculated subgrade stiffness could be noticed over shorter periods of time or were correlated to specific rainfall events and wetting/drying periods. The pavement structure consisted of asphalt concrete (AC) placed on aggregate base and a clay subgrade that was lime stabilized in places. Baseline testing of the outside track began in May 2015 and continued until April 2016. While attempts were made to measure at consistent intervals, there were some periods of inactivity due to equipment downtime.

#### 3.3.2.1 Outside Track Description

According to prior construction plans of the outside track, four different pavement structures existed. Initial deflection testing revealed an inconsistent substructure that warranted additional investigation. The construction methods and extent of lime treatment in the subgrade had not been well documented at the time of construction; there were also issues noted concerning the contractor achieving the required relative densities. To verify the structure, cores were taken, DCP testing was performed (Figure 3.7), and GPR data collected by 3D-Radar (Figure 3.8) were analyzed, with the red lines on the GPR plot showing the dividing lines between the asphalt concrete surface, the granular base, and the subgrade. The DCP data revealed that there was spatial variability in the amount of lime stabilization along the track that had varying impacts on the resulting soil properties. From this, the assumed structures can be found in Table 3.6.

As indicated by the GPR scans, the substructure is inconsistent along its length (Figure 3.8). Reference (54), revealed that using specific layer thicknesses does not produce significant improvements in backcalculation, and thus averaged structures, listed in Table 3.6, were used.

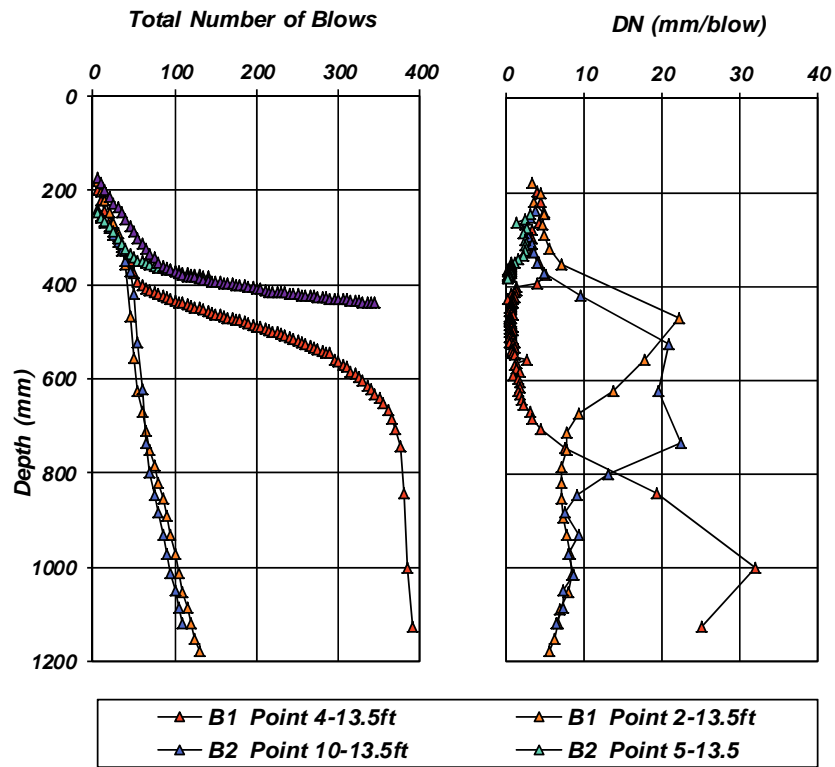


Figure 3.7: Outside track DCP.

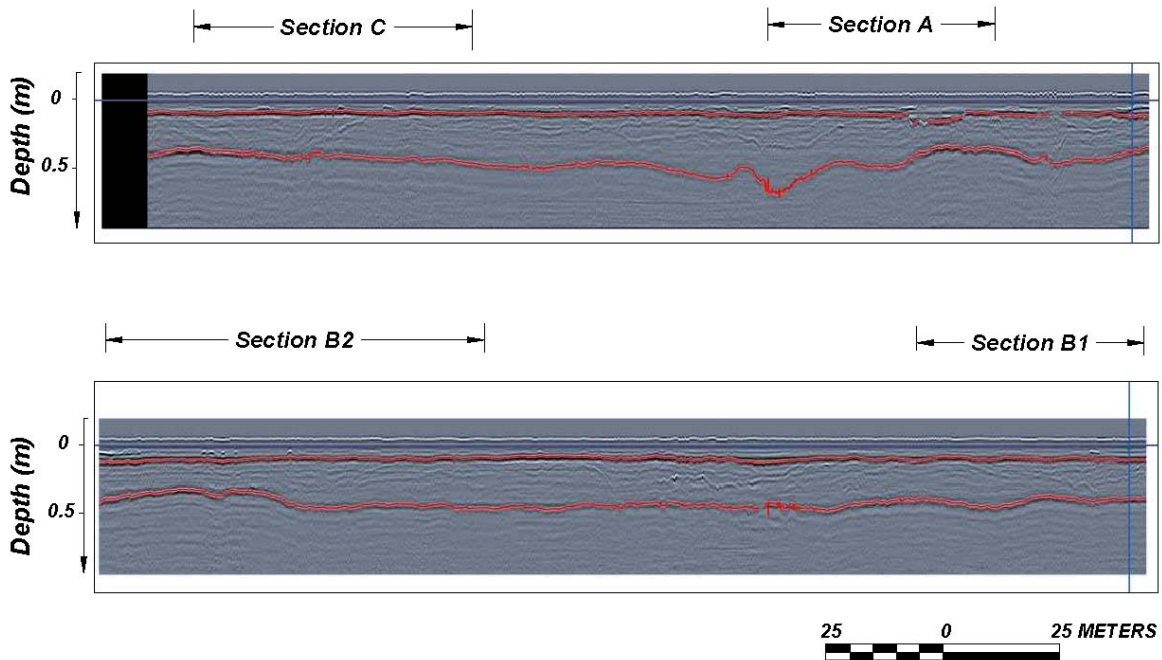


Figure 3.8: GPR scans of outside track.



**Table 3.6: Outside Track Structure**

Material	Section Thickness			
	A	B1	B2	C
Asphalt concrete	110	115	115	105
Aggregate base	300	290	260	290
LS/SG*	-	-	-	-

\*An infinite half-space was used to model both subgrade materials; materials were split into lime-stabilized subgrade (LS) or unstabilized subgrade (SG) after completion of backcalculation.

### 3.3.2.2 Testing Factorial

The four different structures were split into four different sections. The centerline of the sections was tested periodically from May until November. The spacing of the testing dates was slightly irregular due to periods where the deflection equipment was occupied on other projects, downtime at the laboratory, and times when equipment malfunctioned. From November until March/April, the wheelpaths were tested in order to evaluate the influence of the areas of the pavement most susceptible to moisture damage closest to the pavement edge. From March until April, both the centerline and wheelpath were tested. The spacing of test increments was 7.6 m (25ft) between each test point, and for each section a range from 6 to 12 points was tested. A schematic of the testing locations can be seen in Figure 3.9.

### 3.3.2.3 Limitations of Experiment

While the data and results obtained from these tests provide useful insight on what might be thought of as best case and worst case scenarios in terms of seasonal precipitation, these two sets of tests on each field section, likely cannot tell the entire story of what might occur over shorter monthly periods or over the long term of the pavement design life. The small-scale experiment on the ATIRC test track was conducted in an attempt to bridge the gap between the two seasonal field tests with more frequent testing; however, substructure variability and periods of inactivity contribute also leave room for a degree of uncertainty.

Because it was outside the project’s scope and budget to instrument the test sites and perform laboratory testing on samples, quantitative explanations regarding time lag effects and lateral moisture conditions as well as disparities and differences seen in resilient modulus on a broader scale could not be provided. Climatic conditions may also impose a bias on the results obtained, as California had experienced three years of drought prior to the first field testing period and the drier soil conditions for this “dry” sample may have resulted in slower moisture migration than might occur under “normal” climate conditions. These limitations do not necessarily influence the stated goals of the research; however, they should be taken into account before extrapolation and application of the results on a larger scale.

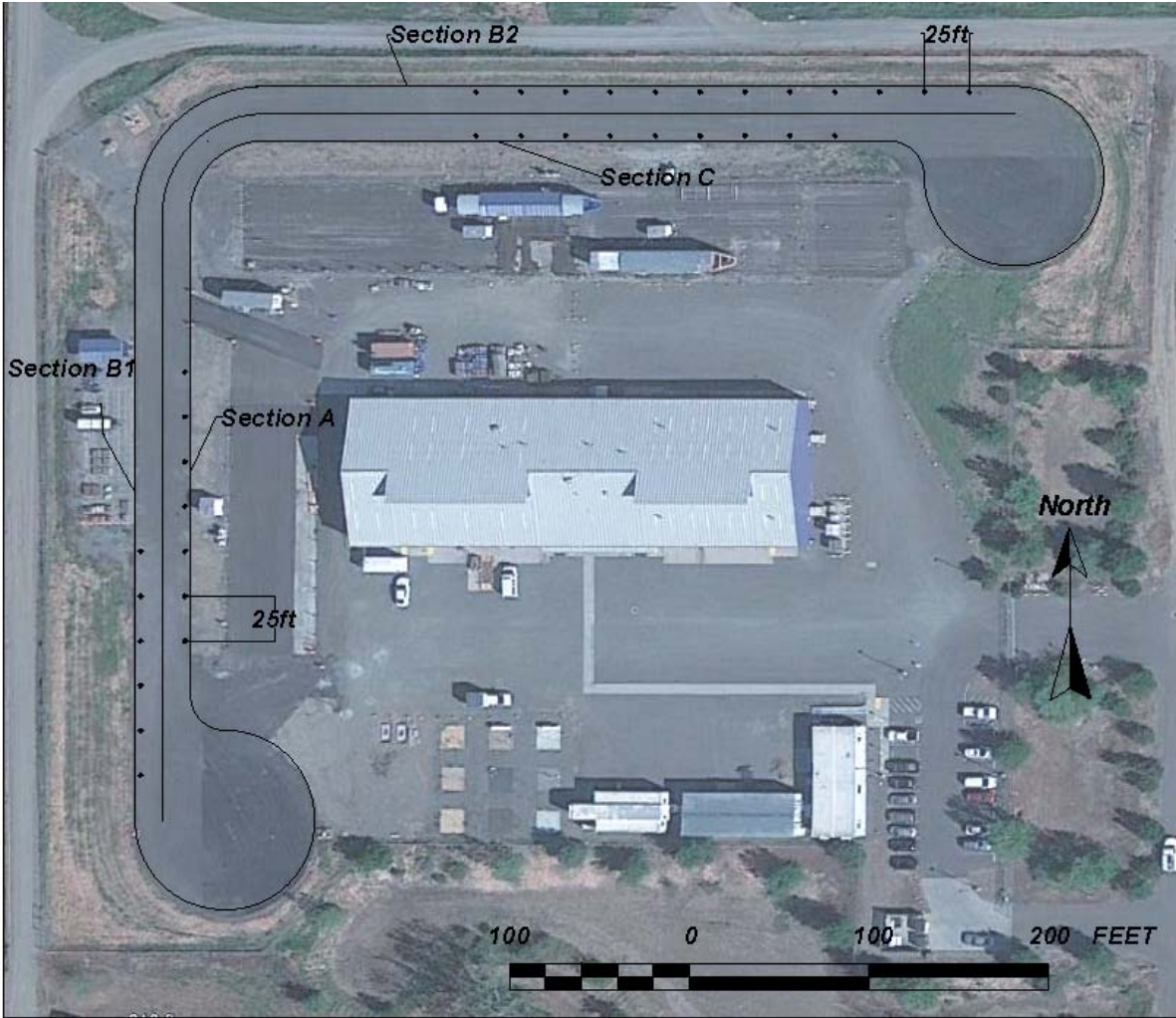


Figure 3.9: ATIRC outside track.

## 4 RESULTS

---

### 4.1 Seasonal Behavior

The following sections include the field and laboratory test results from the 11 test sections. Organization of each section is as follows:

- A brief description of the site, conditions, and any notable visual or circumstantial information
- The structure of the site as provided by the Caltrans plan and the observed structure (Note that core photos are inverted.)
- A summary of properties of the unbound material with depth including:
  - DCP total number of blows versus depth
  - DCP DN versus depth
  - Moisture content versus depth
  - Structure and material type. (V) indicates that the material was classified visually (ASTM 2488).
- Backcalculated stiffness for materials for each site

Figure 4.1 is a precipitation graph for the nine Caltrans climate regions from January 2015 to July 2016, and it shows the testing windows in the context of rainfall patterns over the years.

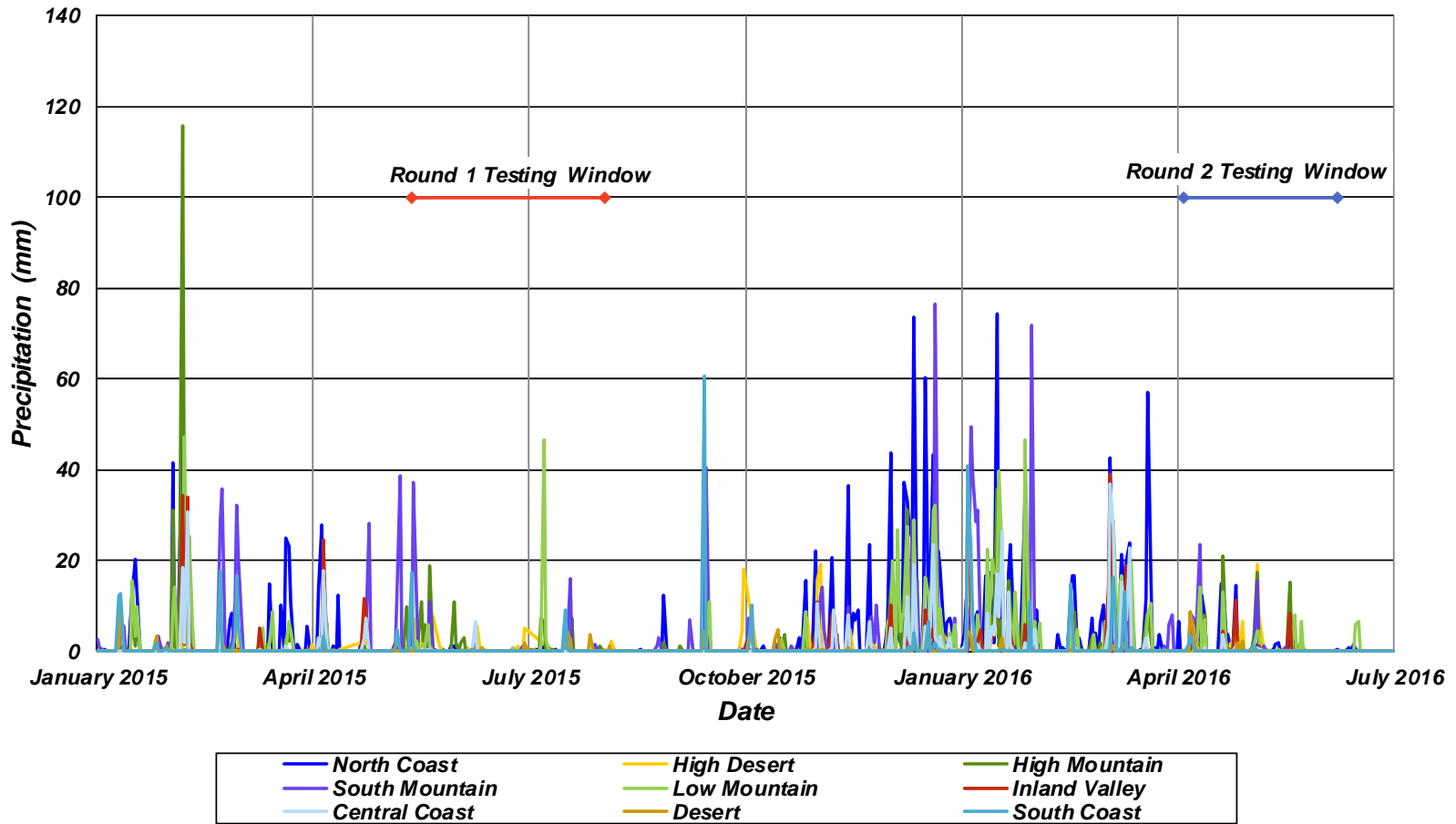


Figure 4.1: Precipitation graph of California climate regions (55).

#### 4.1.1 Colusa 20

Testing and sampling at Colusa 20 (Col 20) took place on May 14, 2015 (Round 1) and April 5, 2016 (Round 2). This road is bordered on both sides by agricultural land that appeared to be planted in nut trees and other crops. The asphalt surface showed minimal evidence of cracking and the wheelpaths showed signs of moderate to heavy traffic. Drainage conditions at the site varied along its length. Along its first 1,000 m (0.6 mi), the road ran higher than the surrounding fields, which included a large drainage ditch; the remaining 600 m (0.4 mi) of the road ran roughly level with the ditch. At the time of the first testing, the fields and the ditch along the first part of the road were bare, fairly dry, and well maintained, but at the time of the second round of testing the soil in the ditch was moist and sparsely vegetated (Figure 4.2). Along the remaining 600 m (0.4 mi) of the site, the elevation of the road ran about even with the drainage ditch, which was more heavily vegetated than the upper part during both rounds of field testing but even wetter in April 2016 (Figure 4.3) during the second round testing.



(a)



(b)

**Figure 4.2: Drainage conditions at Colusa 20 PM 15.35 in (a) May 2015 and (b) April 2016.**



(a)



(b)

**Figure 4.3: Drainage conditions at Colusa 20 PM 15.35 in (a) May 2015 and (b) April 2016.**

#### 4.1.1.1 Structure

The structure and construction history of the test site as indicated from various Caltrans plans and documents are listed in Table 4.1, core photos are shown in Figure 4.4, and the layer thicknesses encountered and evaluated from coring and DCP testing can be found in Table 4.2. The actual structure encountered matched fairly well with that listed in Caltrans documents; thicker layers of FDR-FA material observed at the site could either be a result of spatial and construction variability or indistinguishable base material.

**Table 4.1: Structure from Caltrans Plans for Colusa 20**

EA Number	Construction Began	Construction Completed	Material	Thickness (mm)
03-1F7504	1/20/2012	9/25/2012	AC	91
03-339004	n/a	1/12/2002	AC	49
			FDR-FA	228

**Table 4.2: Observed Structure for Colusa 20 (mm)**

Material	PM 16.35+50ft			PM 15.35-50ft			Source
	May 14, 2015	April 4, 2016	Average	May 14, 2015	April 4, 2016	Average	
AC	85	80	83	90	87	89	Core
AC	45	45	45	45	48	47	
FDR-FA	n/a	296	296	n/a	330	330	DCP
Unbound	n/a	260	-	n/a	n/a	-	
Unbound	Subgrade	Subgrade	-	Subgrade	Subgrade	-	

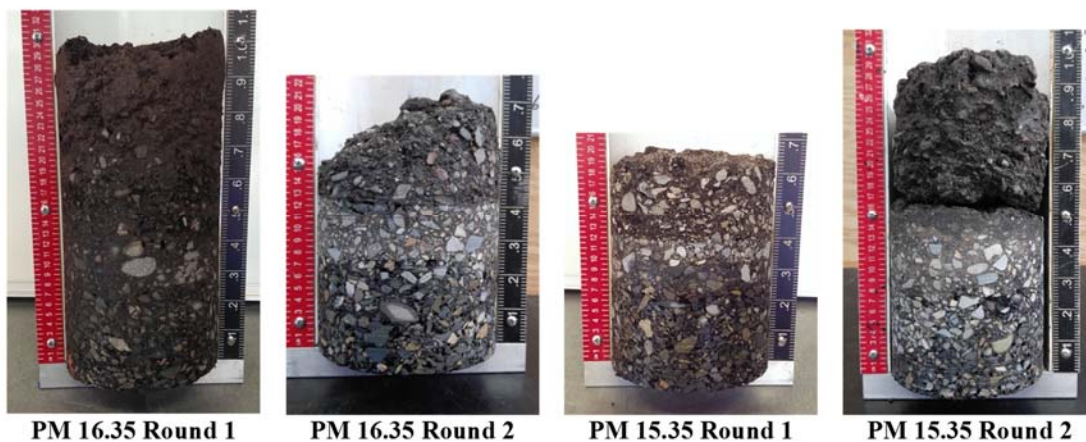


**Figure 4.4: Cores from Colusa 20.**  
(Note: all cores are upside down in the figures.)



4.1.1.2 Unbound Material Properties

Unbound samples of the material at the site were obtained at PM 16.35 for both rounds of field testing and at PM 15.35 in May 2015. The results from DCP testing, moisture content testing, and soils classification can be seen in Figure 4.5. Median DN (mm per blow from the DCP test) values can be seen in Table 4.3.

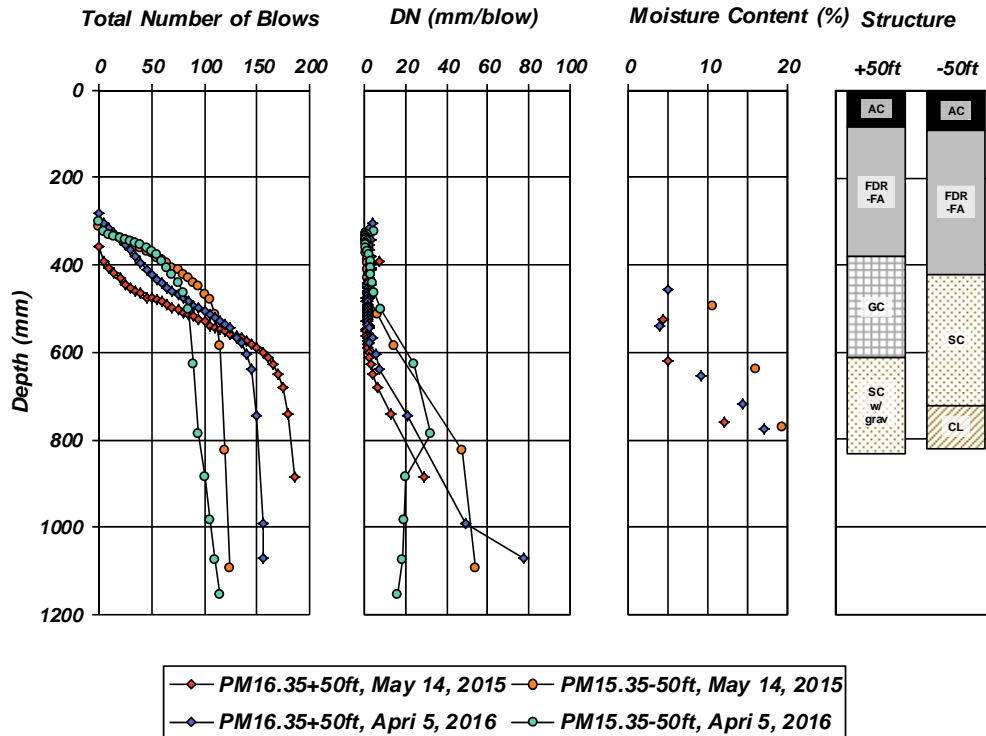


Figure 4.5: Unbound materials testing and sampling results for Colusa 20.

Table 4.3: Median DN (mm/blow) for Colusa 20

Material	DN PM 16.35+50ft		DN PM 15.35-50ft	
	May 14, 2015	April 4, 2016	May 14, 2015	April 4, 2016
FDR-FA	2.7	2.8	1.2	1.4
Unbound	1.2	1.8	31.1	19.2

The unbound material generally consisted of clayey sands and sandy clays with slightly plastic fines, higher gravel contents closer to the surface, and increasing fines content with depth. The clayey gravel encountered at PM 16.35 may be aggregate base from the existing pavement structure, but it consisted of material with plasticity properties similar to deeper material, suggesting that either the gravel is natural in situ material or fines were pumped into the void spaces; the subgrade material encountered between 500 and 600 mm is consistent with what should be expected from site geology. The moisture content at PM 16.35 was slightly higher during the second round of

testing, which corresponds to decreased resistance to penetration. For PM 15.35, no basis for seasonal moisture comparison was obtained because of incomplete data collection. The penetration resistance varies between the two post miles, and corresponds well with the difference in materials classification at both ends.

#### 4.1.1.3 Falling Weight Deflectometer

The backcalculated stiffnesses from the two rounds of falling weight deflectometer (FWD) testing can be found in Figure 4.6 to Figure 4.9. Station 0 corresponds to PM 15.35 and Station 1 corresponds to PM 16.35. A summary of backcalculation results can be seen in Table 4.4.

**Table 4.4: Backcalculated Stiffnesses (MPa) for Colusa 20 (in MPa)**

Material	Thickness Used (mm)	Between Wheelpaths				Wheelpath			
		May 14, 2015		April 5, 2016		May 14, 2015		April 5, 2016	
		Average	Std. Dev.	Average	Std. Dev.	Average	Std. Dev.	Average	Std. Dev.
Asphalt-bound	135	9,481	2,781	12,635	5,334	11,269	5,131	12,806	5,119
FDR-FA	300	355	277	331	268	363	225	285	177
Unbound	0	127	22	126	23	128	21	128	22
Average Asphalt Temp (°C)		32.8		31.7		32.2		29.7	

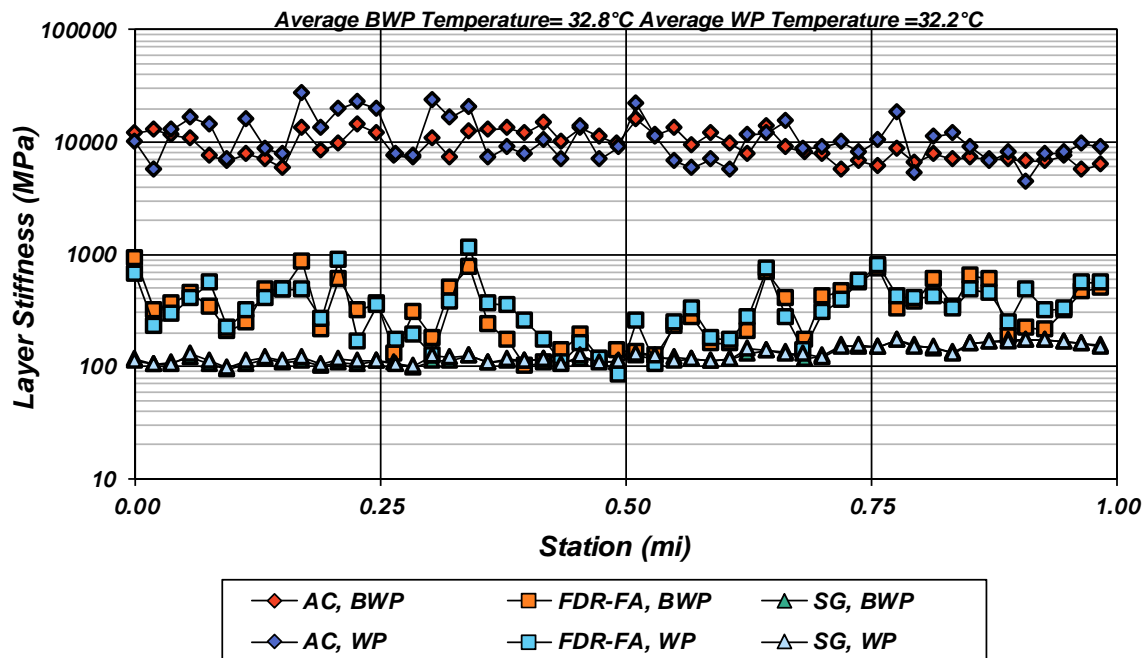


**Figure 4.6: Colusa 20 backcalculated stiffnesses, May 14, 2015.**



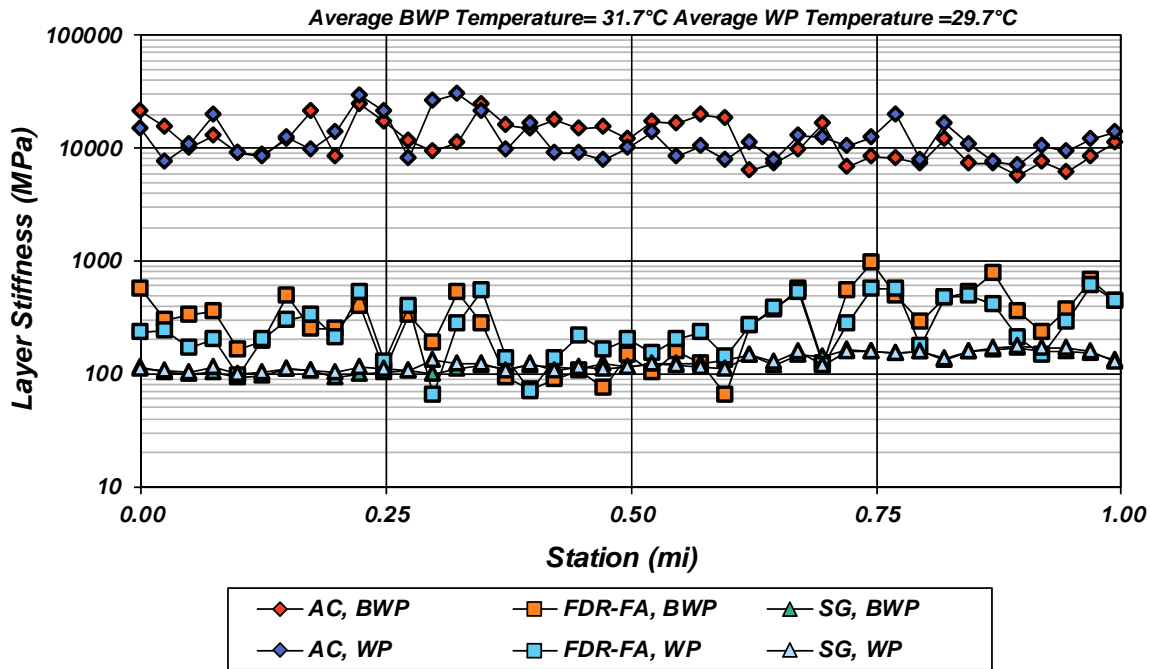


Figure 4.7: Colusa 20 backcalculated stiffnesses, April 5, 2016.

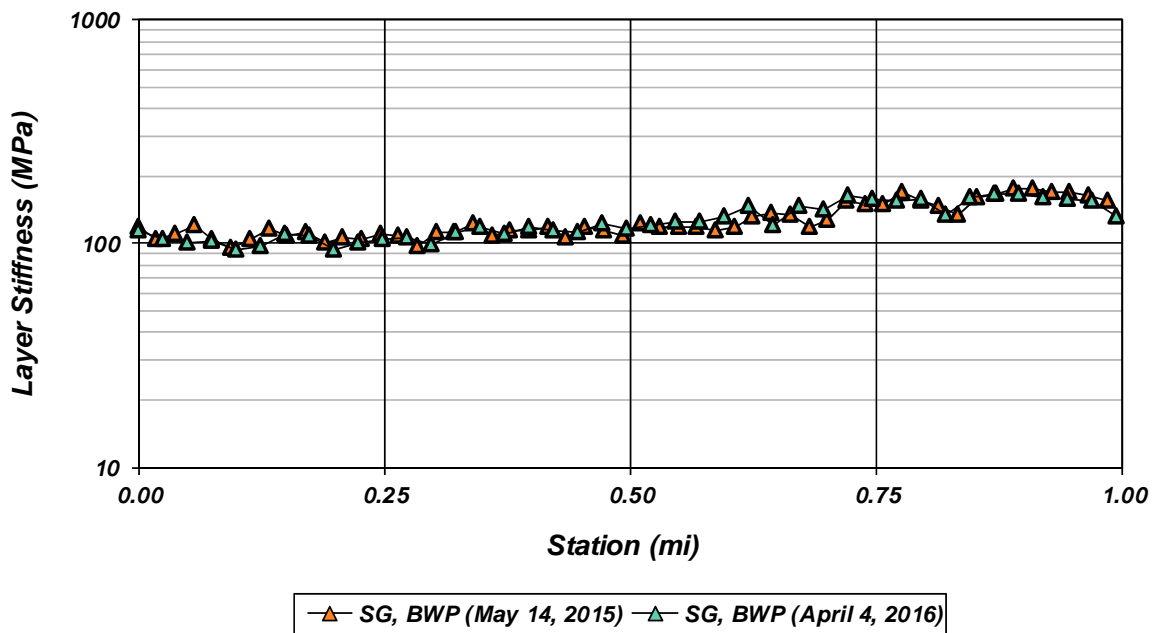


Figure 4.8: Colusa 20 unbound layer stiffnesses between the wheelpaths.

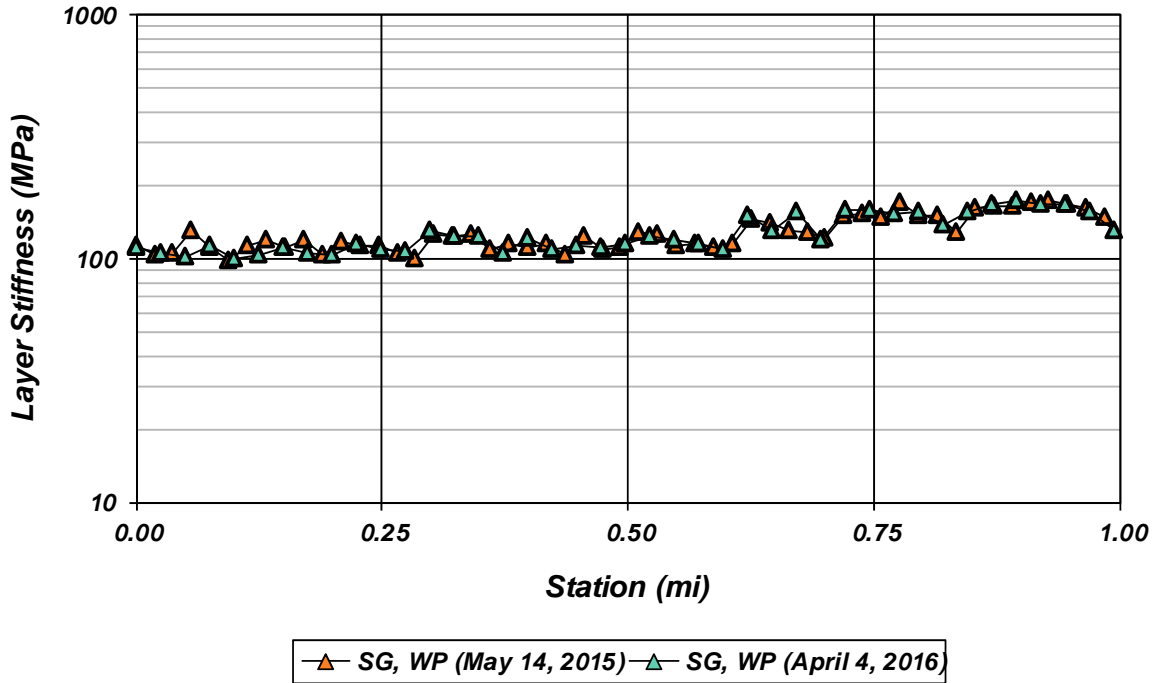
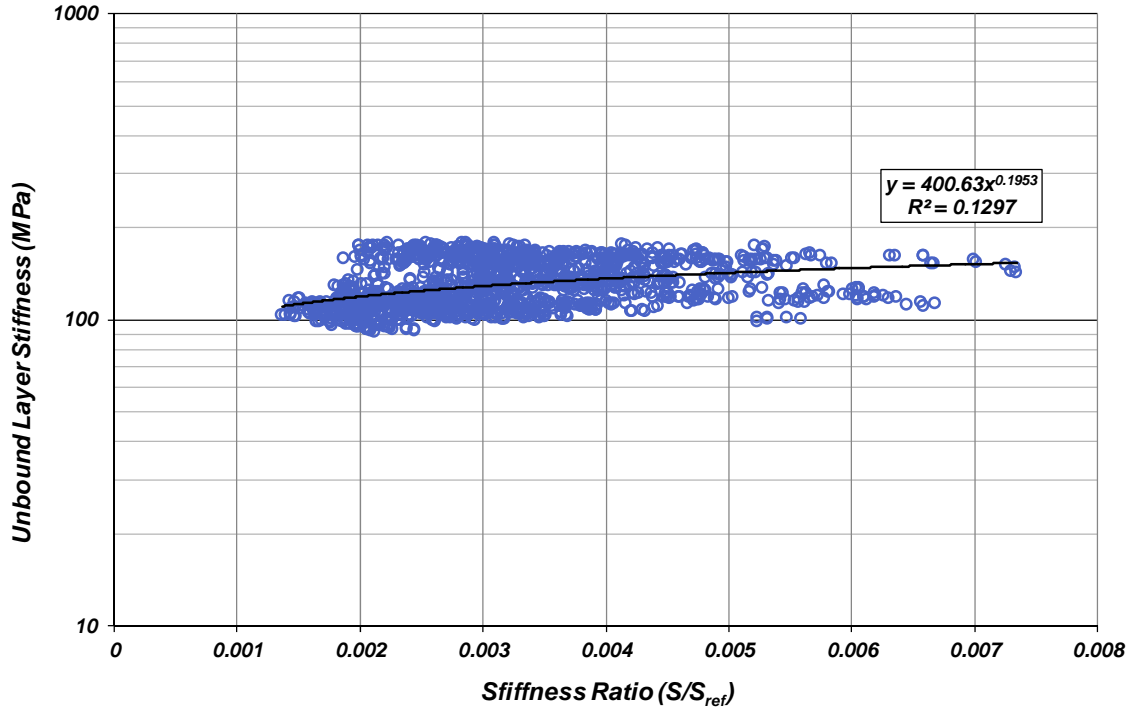


Figure 4.9: Colusa 20 unbound layer stiffnesses in the wheelpath.

The backcalculated stiffnesses reveal fairly consistent material properties for the asphalt and subgrade materials across the length of the section. The FDR-FA material appears to be the most variable material across the site, which may correspond to variable thicknesses or material properties present across the site. A softer portion was encountered from about 0.4 to 0.7 miles (Figure 4.6 and Figure 4.7), which corresponds to changes in agricultural crops and drainage conditions. It was noted that poor drainage and a culvert were encountered near 0.7 miles, which corresponds to a stark decrease of FDR stiffness during both rounds of field testing. The subgrade stiffness increases near the end of the test section, corresponding to the gravelly material encountered beneath the FDR at PM 16.35, which would be stiffer than the clayey and sandy material observed at PM 15.35. The unbound material/subgrade stiffness was fairly consistent between the two rounds of field testing and did not appear to have a distinguishable fluctuation seasonally, despite noted changes in penetration resistance and moisture content. The unbound material showed little to no sensitivity to the overlying layer stiffness, as shown in Figure 4.10.



**Figure 4.10: Colusa 20 overlying layer effect.**  
 (Note: *stiffness ratio* is the ratio of the bending stiffness of the layers above the unbound layer relative [S] to a reference stiffness [S<sub>ref</sub>], giving an indication of the confinement from those layers.)

#### 4.1.2 El Dorado 193

Testing and sampling on El Dorado 193 (ED 193) occurred on May 21, 2015 (Round 1) and May 10, 2016 (Round 2). The structure at the site appeared to be new, with minor detectable damage in the wheelpaths. The road was winding and shaded and appeared to predominantly be on hillside cuts. The westbound sections of the road appeared to have several surficial failures around PM 10.9, which may have been due to slope creep of the surrounding hillsides (Figure 4.11 a), and at PM 11.2, where the surface/CIR material was crumbling into the shoulder. Lush, green vegetation surrounded the site, with little to no shoulder on either side of the road (Figure 4.11 b). Although standing water was observed in the shoulders and drainage areas from approximately 0.6 miles to 0.9 miles in May 2016, in May 2015 conditions had been notably drier and without standing water.



(a)



(b)

**Figure 4.11: Road conditions on El Dorado 193 during (a) May 2015 and (b) May 2016.**

#### 4.1.2.1 Structure

The structure and construction history of the test site as indicated from various Caltrans plans and documents are listed in Table 4.5, and the observed structure from coring, sampling, and DCP testing can be seen in Table 4.6 and Figure 4.12. The observed structure is consistent with the Caltrans records, with the exception of the amount of remaining asphalt concrete (AC) found below the cold in-place recycled (CIR) layers. Asphalt material underlying the CIR ranged from 50 to 100 mm, depending on sampling location. Seeing that the most recent construction occurred in 2014 and no further rehabilitation projects were found, it is likely that the previous structure was not documented accurately.

**Table 4.5: Structure from Caltrans Plans for El Dorado 193**

EA Number	Construction Began	Construction Completed	Material	Thickness (mm)
03-3M9204	6/23/2014	11/18/2014	AC	46
			CIR	76.2
Existing	n/a	n/a	Rem AC	0-15
			AB	0-457.2

**Table 4.6: Observed Structure for El Dorado 193 (in mm)**

Material	PM 11.4+50ft			PM 10.4-50ft			Source
	May 21, 2015	May 10, 2016	Average	May 21, 2015	May 10, 2016	Average	
AC	55	59	57	60	50	55	Core
CIR	90	80	85	80	85	83	
AC	57	41	49	30	65	48	
AC	-	29	-	50	-	50	
AC	-	53	-	-	-	-	
Unbound	695	Unbound	27	550	392	22	DCP
Stiff layer	Stiff layer	-	-	Stiff layer	Stiff layer	-	

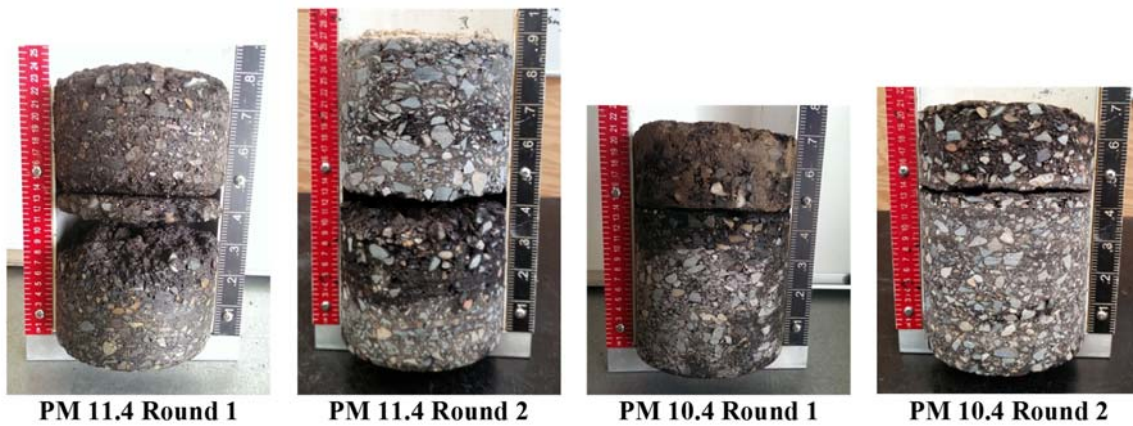


**Figure 4.12: Cores from El Dorado 193.**  
*(Note: all cores are upside down in the figures.)*

#### 4.1.2.2 Unbound Material Properties

Unbound samples of the material at the site were obtained at PM 10.4 and PM 11.4 for both rounds of field testing. The results from DCP testing, moisture content testing, and soils classification can be seen in Figure 4.13, and median DCP values can be seen in Table 4.7.

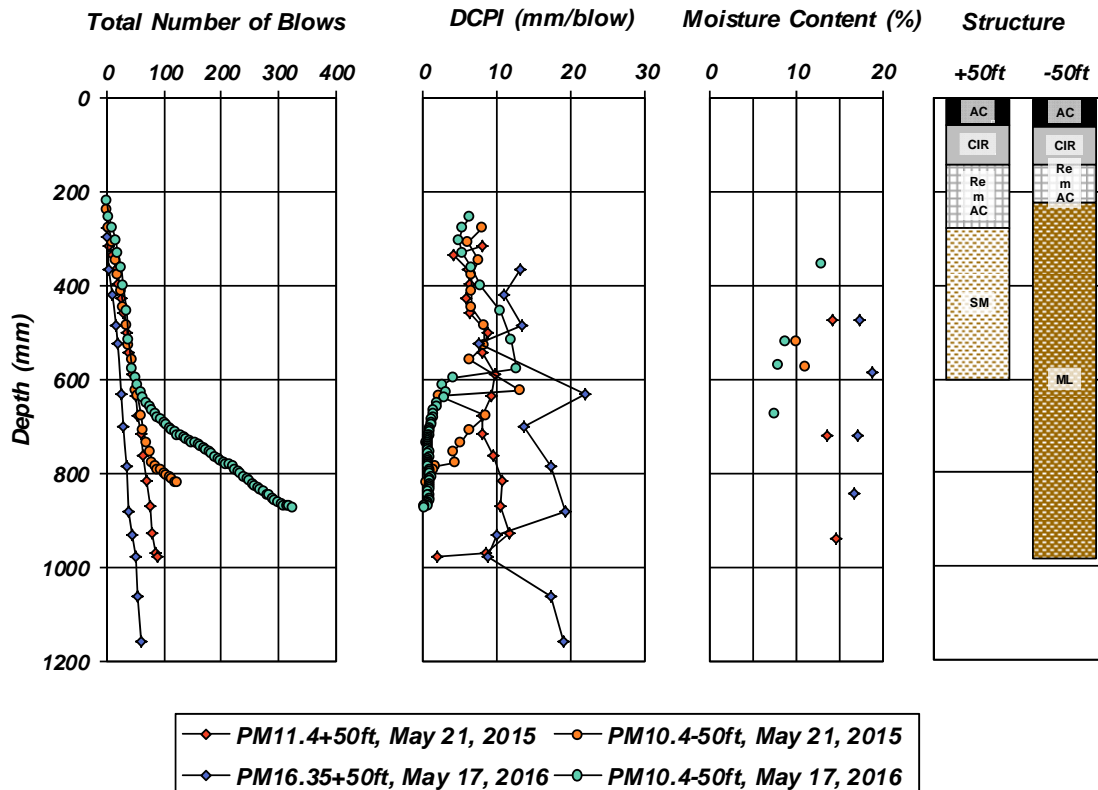


Figure 4.13: Unbound materials testing and sampling results for El Dorado 193.

Table 4.7: Median DN (mm/blow) for El Dorado 193

Material	DN PM 11.2+50ft		DN PM 10.2-50ft	
	May 21, 2015	May 10, 2016	May 21, 2015	May 10, 2016
Unbound	8.0	13.3	6.6	6.6
Subgrade/ Bedrock	10.4	17.2	1.0	1.0

Unbound material at the site consisted of gravelly silt material that appeared to originate from crushed schist and phyllite materials, likely either extremely weathered residual soil, colluvium from surrounding hillslopes, or hillslope material crushed during the cut/fill construction process. The material at both ends had approximately 30 to 60 percent nonplastic fines and were classified as either silty sand or nonplastic silt. Higher moisture contents were observed in the sandier material at PM 11.4 than in the siltier material at PM 10.4. Moisture contents at PM 11.4 were fairly constant with depth during Round 1 and increased slightly closer to the surface during Round 2, while moisture contents at PM 10.4 were higher during May 2015 than May 2016. Penetration resistance was greater for the drier silt material observed at PM 10.4 than for the wetter silty sand observed at PM 11.4. The penetration resistance tended to increase with depth, which is likely an indicator that stiffer and less weathered clasts or parent rock material is encountered.

### 4.1.2.3 Falling Weight Deflectometer

The backcalculated layer stiffnesses for both rounds of field testing can be seen in Figure 4.14 to Figure 4.17. Station 0 corresponds to PM 10.2 while Station 1 corresponds to PM 11.2. A summary of the backcalculation results and parameters can be found in Table 4.8.

**Table 4.8: Backcalculated Stiffnesses for El Dorado 193 (in MPa)**

Material	Thickness Used (mm)	Between Wheelpaths				Wheelpath			
		May 21, 2015		May 10, 2016		May 21, 2015		May 10, 2016	
		Average	Std. Dev.	Average	Std. Dev.	Average	Std. Dev.	Average	Std. Dev.
Asphalt-bound	205	3,545	2,048	4,691	2,889	3,483	2,553	4,773	3,593
Unbound	550	105	76	95	73	77	57	104	89
Subgrade/Bedrock	0	313	145	315	156	327	179	306	137
Average Asphalt Temp (°C)		23.1		29.4		18.5		23.2	

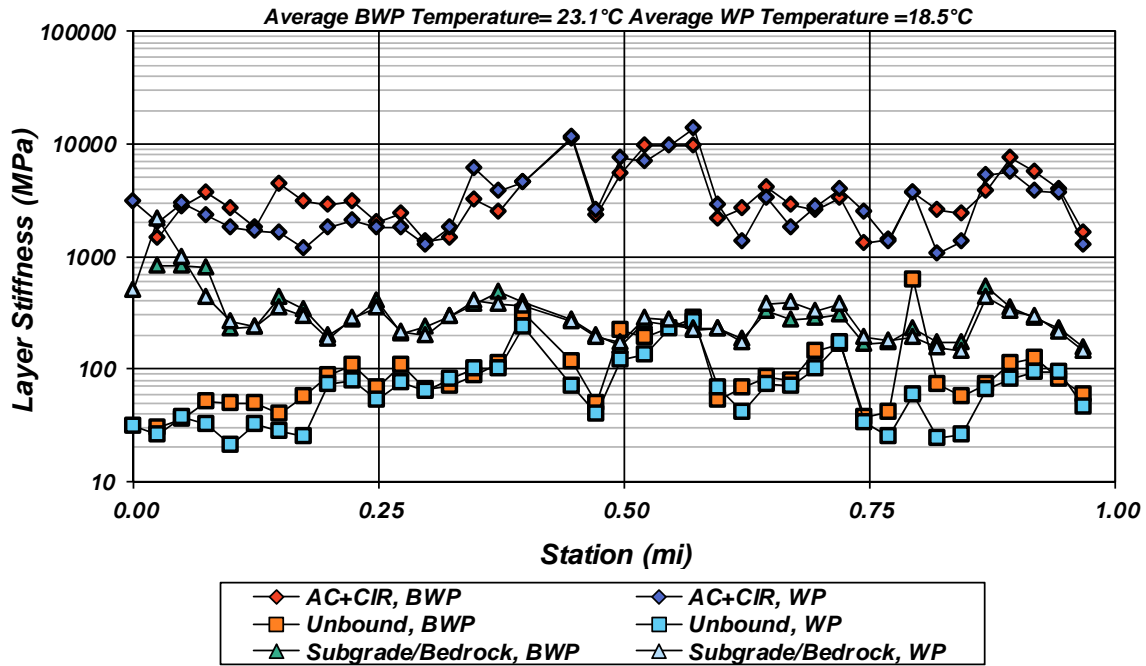


**Figure 4.14: El Dorado 193 backcalculated stiffnesses, May 21, 2015.**

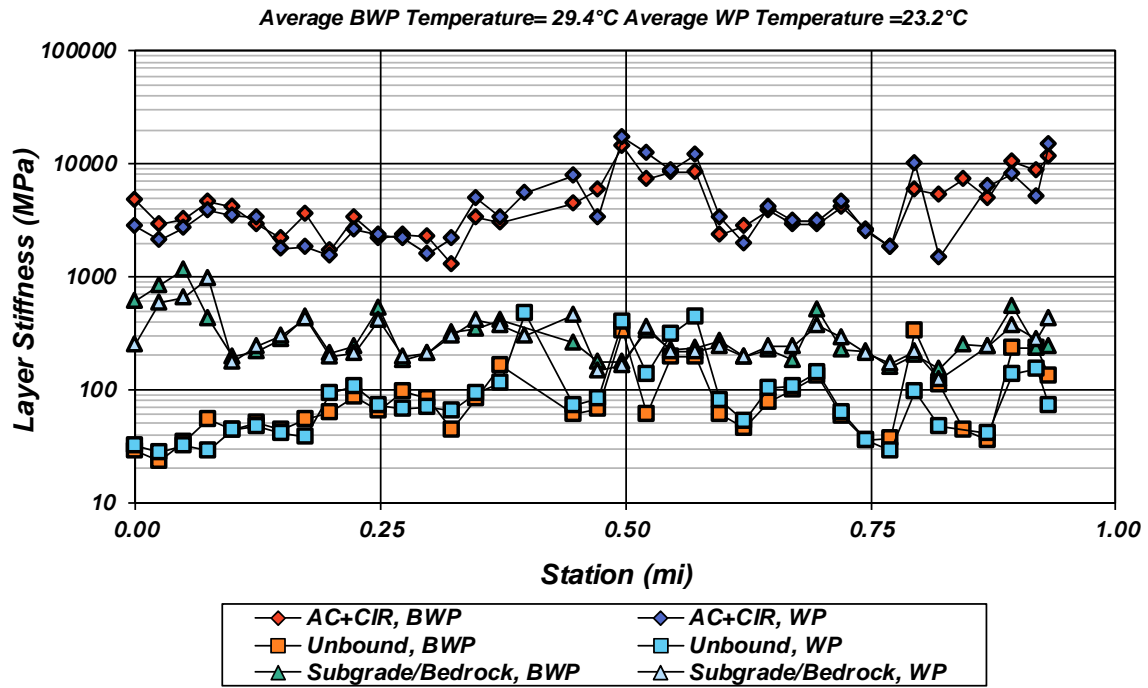


Figure 4.15: El Dorado 193 backcalculated stiffnesses, May 10, 2016.

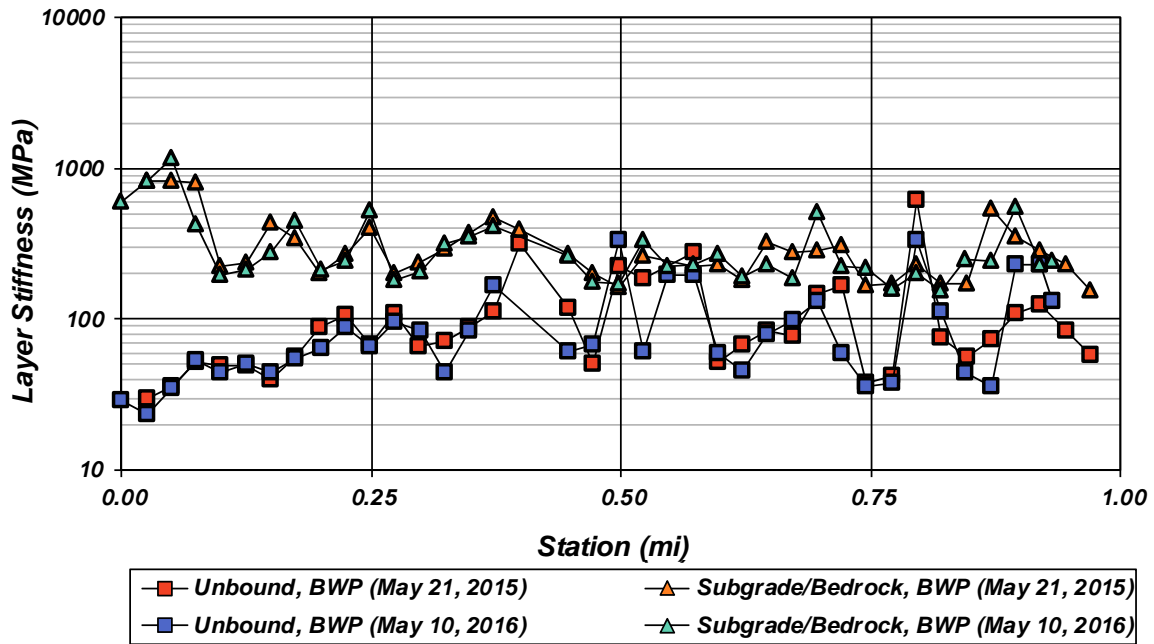


Figure 4.16: El Dorado 193 unbound layer stiffnesses between the wheelpaths.



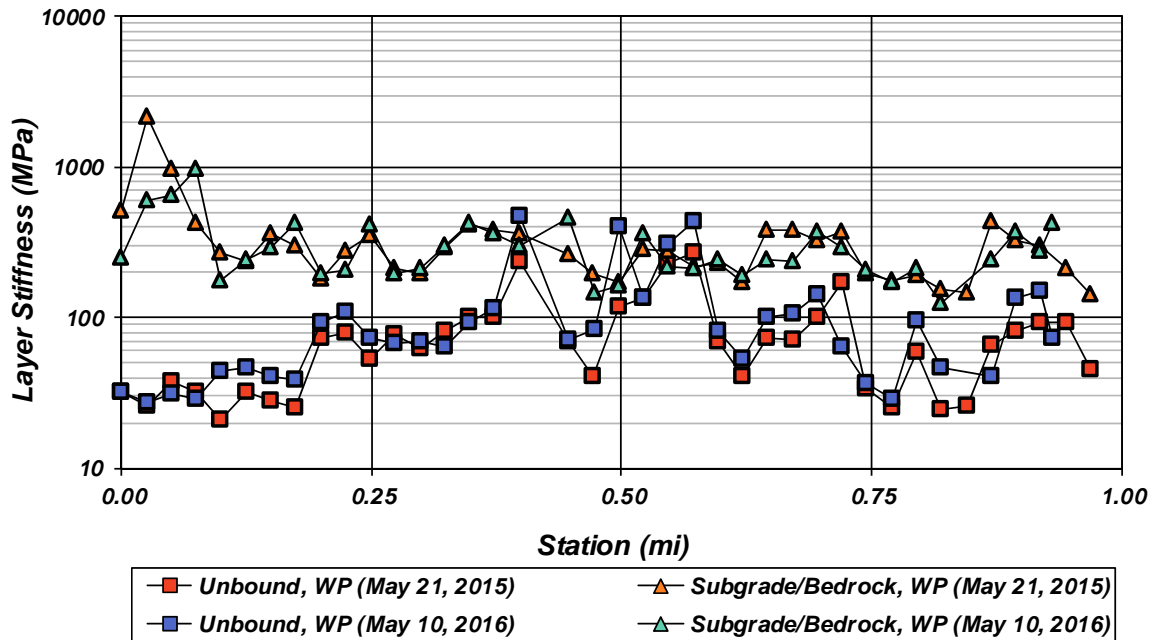
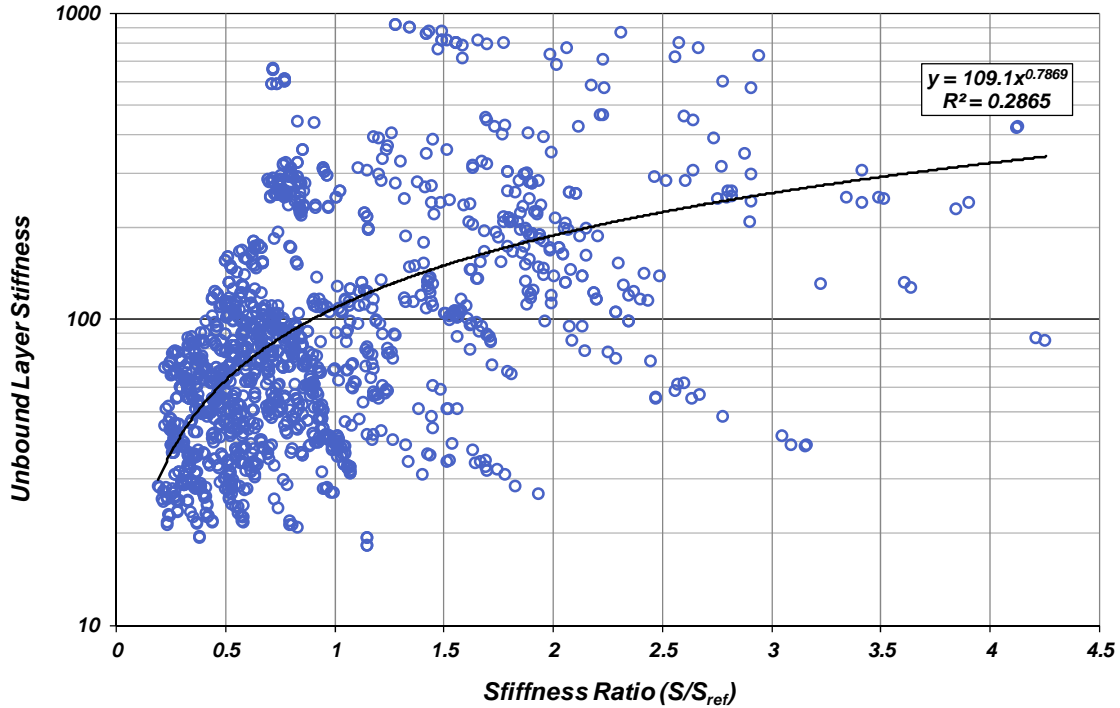


Figure 4.17: El Dorado 193 unbound layer stiffnesses in the wheelpath.

The backcalculated stiffnesses across the section indicate that a wide degree of variability exists across the site: the variability seen in the CIR and asphalt material may be a result of the questionable construction quality that was observed at the site, while the variability seen in the unbound materials is likely a result of the geologic setting of the site, which is in mountainous terrain where rock outcrops are commonly encountered and the road winds through cut and fill portions. The unbound material directly beneath the asphalt-bound layers was less stiff than the subgrade/bedrock material, which is consistent with results obtained from DCP testing indicating that stiffer material is encountered deeper. Average unbound material stiffnesses were similar for material between the wheelpaths and in the wheelpath, and did not have much fluctuation between the two rounds of testing; the unbound materials may have a weak relationship with the stiffness of the overlying layers (Figure 4.18), however, given the scatter in the results it is hard to pinpoint exactly what leads to the variability, whether it be moisture changes or temperature influences.



**Figure 4.18: El Dorado 193 overlying layer effect.**

(Note: *stiffness ratio* is the ratio of the bending stiffness of the layers above the unbound layer relative [S] to a reference stiffness [S<sub>ref</sub>], giving an indication of the confinement from those layers.)

#### 4.1.3 Sierra 89

Testing and sampling at Sierra 89 (Sie 89) were performed on July 31, 2015 (Round 1) and May 11, 2016 (Round 2). Extensive longitudinal and alligator cracking and rutting were present in the wheelpaths on the northbound lane, and less extensive, but still severe, damage was observed in the southbound lanes. The road was bordered by pine trees and vegetation—which appeared significantly greener during May 2016 than July 2015—and had limited drainage on either side of the road.

##### 4.1.3.1 Structure

The structure and construction history of the test site as indicated from various Caltrans plans and documents are listed in Table 4.9, and the structure observed from coring, sampling, and DCP testing can be seen in Table 4.10. Fully intact cores of FDR material were not obtained, and thickness was inferred from DCP testing. The observed structure matches well with the structure provided by Caltrans, with the exception of the asphalt thickness on the surface. The most recent rehabilitation work at the site listed in the Caltrans database was microsurfacing performed in 2008, and it seems unlikely based on the pavement condition that additional overlays were performed in the past eight years. The structure observed also agrees well with cores in the iGPR database, which evidently mistakenly classified the FDR material as aggregate base due to its poor condition.



**Figure 4.19: Road conditions on Sierra 89 PM 28.05 on May 11, 2016.**

**Table 4.9: Structure from Caltrans Plans for Sierra 89**

EA Number	Construction Began	Construction Completed	Material	Thickness (mm)
03-2M3204	n/a	3/16/2008	Micro-surfacing	-
03-0a7001	n/a	8/22/2002	AC	37
			FDR-FA (CFIPR)	200

**Table 4.10: Observed Structure for Sierra 89 (in mm)**

Material	PM 29+50ft			PM 28-50ft			Source
	July 23, 2015	May 11, 2016	Average	July 23, 2015	May 11, 2016	Average	
AC	n/a	63	63	61	66	64	Core
FDR-FA		187	187	200	203	202	Core/DCP
Unbound		505	505	235	266	251	DCP
Unbound		Subgrade	Subgrade	Subgrade	Subgrade	Subgrade	

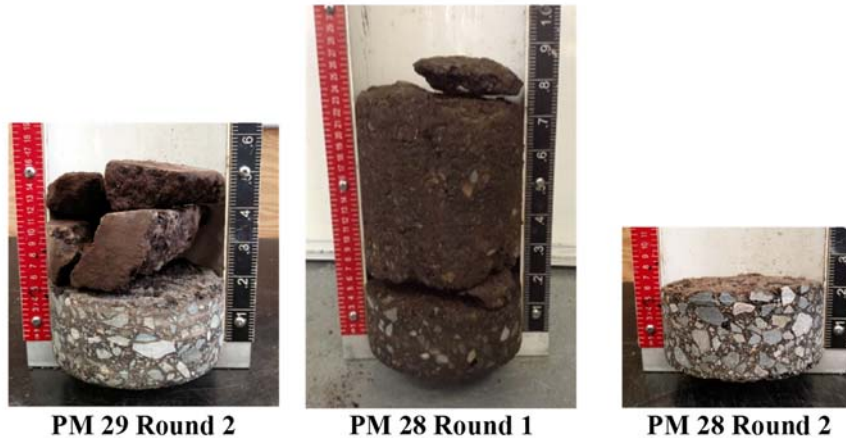


**Figure 4.20: Cores from Sierra 89.**  
 (Note: all cores are upside down in the figures.)

#### 4.1.3.2 Unbound Material Properties

Classification and gradation were only available for PM28-50ft, and samples for PM29+50ft were only obtained in May 2016, as no coring at PM 29 took place in July 2015. The results from DCP testing, moisture content measurement, and soils classification can be seen in Figure 4.21 and median DCP values are listed in Table 4.11.

Unbound material at the site consisted of light-brown to reddish-brown, gravelly clay overlying clayey sands/sandy clays with medium to high plasticity; gravelly clay was only encountered at PM 28, which may be aggregate subbase, as was indicated on iGPR scans, or natural gravelly material. Higher moisture contents and very low penetration resistance were observed during July 2015, most likely because storms had occurred in the area the two days prior to testing.

Penetration resistance was much greater during May 2016, which also corresponded to lower moisture contents. Weather data from Calpine indicated that 44 mm of precipitation was measured from May 3 to 8, 2016, three days prior to Round 2 testing; standing water in the right-hand shoulder was also observed (56). Due to the higher amounts of rainfall preceding the May 2016 testing date, it seems odd that penetration resistance would show such stark increases in comparison to July 2015 and that moisture content would decrease. One possible explanation for this is that the coring progressed slowly, which might have caused excessive wetting of the material in the core hole. Because no additional information about the substructure during July 2015 is available, this is a possibility. Another possible explanation is that the gravelly and sandy material drain well, which would explain why the moisture content two days following precipitation was greater than that measured three to four days following precipitation. Another possible explanation for increased penetration resistance is that the ground might have been partially frozen; climate data near the site indicate that temperatures dropped to -0.5°C the night prior to testing;

however, given the nature of the fines of the material, time spent at subzero temperatures, and the high deflections observed, this explanation is unlikely. However, freeze/thaw of the unbound material may be the cause of much of the damage observed at the site.

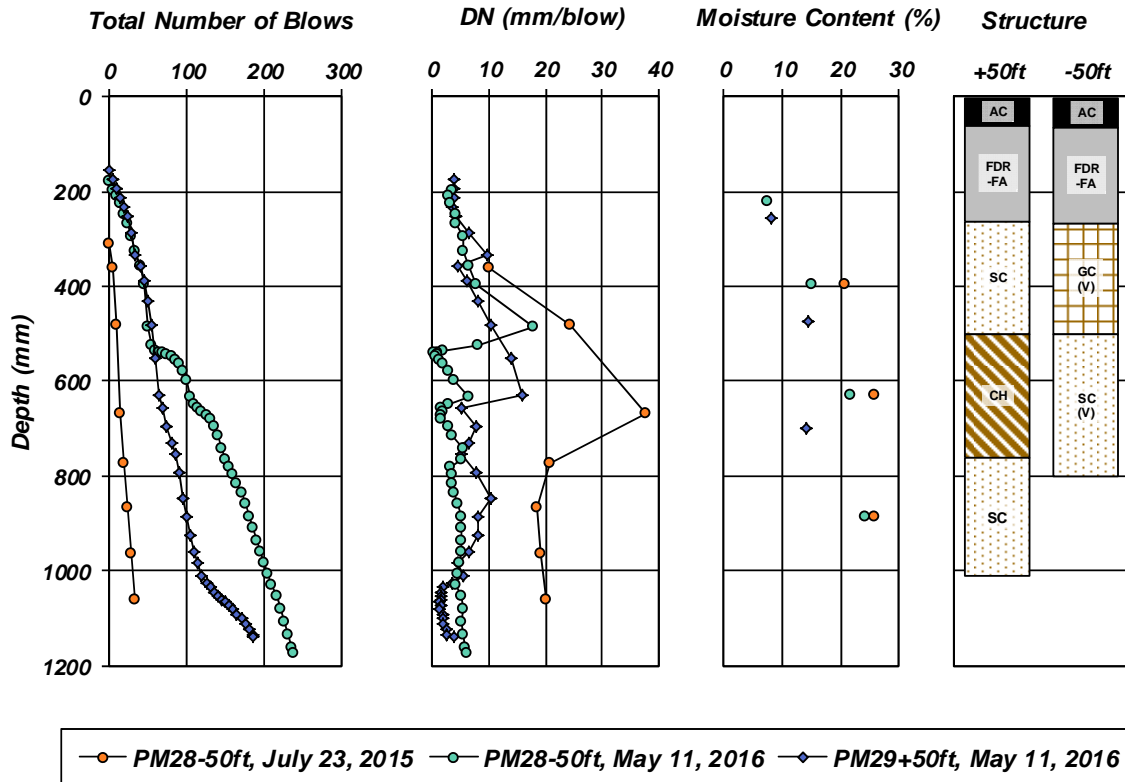


Figure 4.21: Unbound materials testing and sampling results for Sierra 89.

Table 4.11: Median DN (mm/blow) for Sierra 89

Material	DN PM 29+50ft		DN PM 28-50ft	
	July 23, 2015	May 11, 2016	July 23, 2015	May 11, 2016
FDR-FA	n/a	4.0	n/a	4.2
Unbound	n/a	7.8	22.5	3.1

#### 4.1.3.3 Falling Weight Deflectometer

The backcalculated layer stiffnesses for the two testing dates can be seen in Figure 4.22 to Figure 4.25. Station 0 corresponds to PM 28 and Station 1 corresponds to PM 29. A summary of the backcalculation results and parameters can be found in Table 4.12.

Table 4.12: Backcalculated Stiffnesses for Sierra 89 (in MPa)

Material	Thickness Used (mm)	Between Wheelpaths				Wheelpath			
		July 23, 2015		May 11, 2016		July 23, 2015		May 11, 2016	
		Average	Std. Dev.	Average	Std. Dev.	Average	Std. Dev.	Average	Std. Dev.
Asphalt-bound	60	11,704	6,253	20,083	11,807	13,911	7,153	16,286	9,776
FDR-FA	200	225	167	142	113	122	82	71	41
Subgrade	0	142	50	127	29	130	38	110	25
Average Asphalt Temp (°C)		38.4		27.8		42.3		18.6	

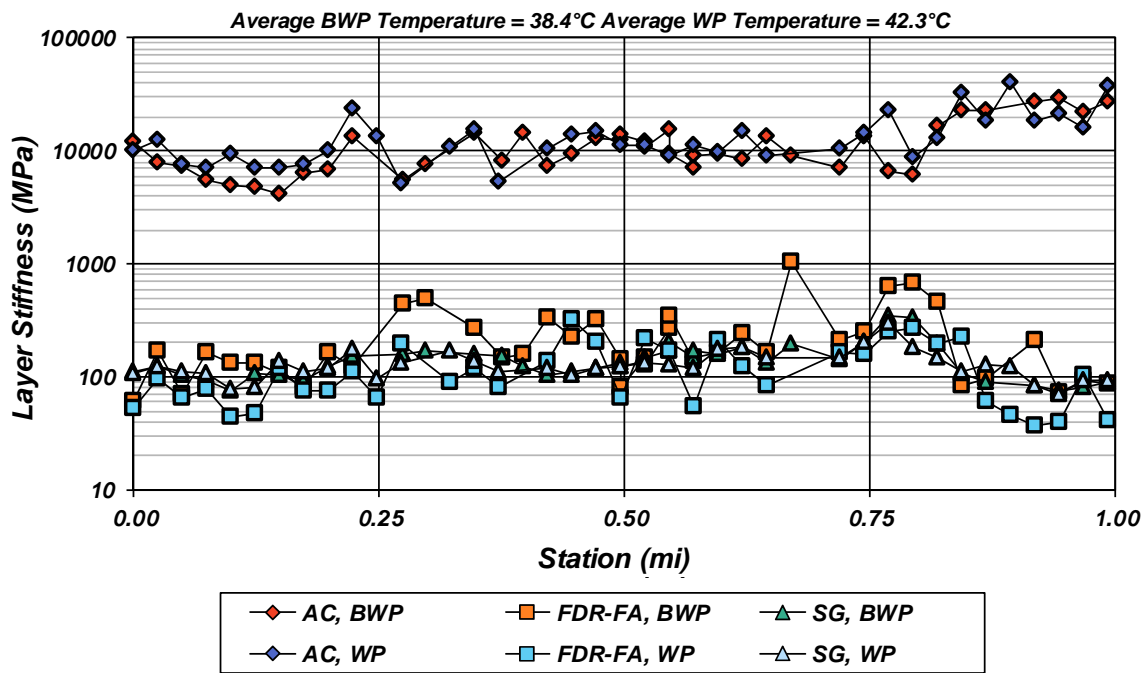


Figure 4.22: Sierra 89 backcalculated stiffnesses, July 23, 2015.

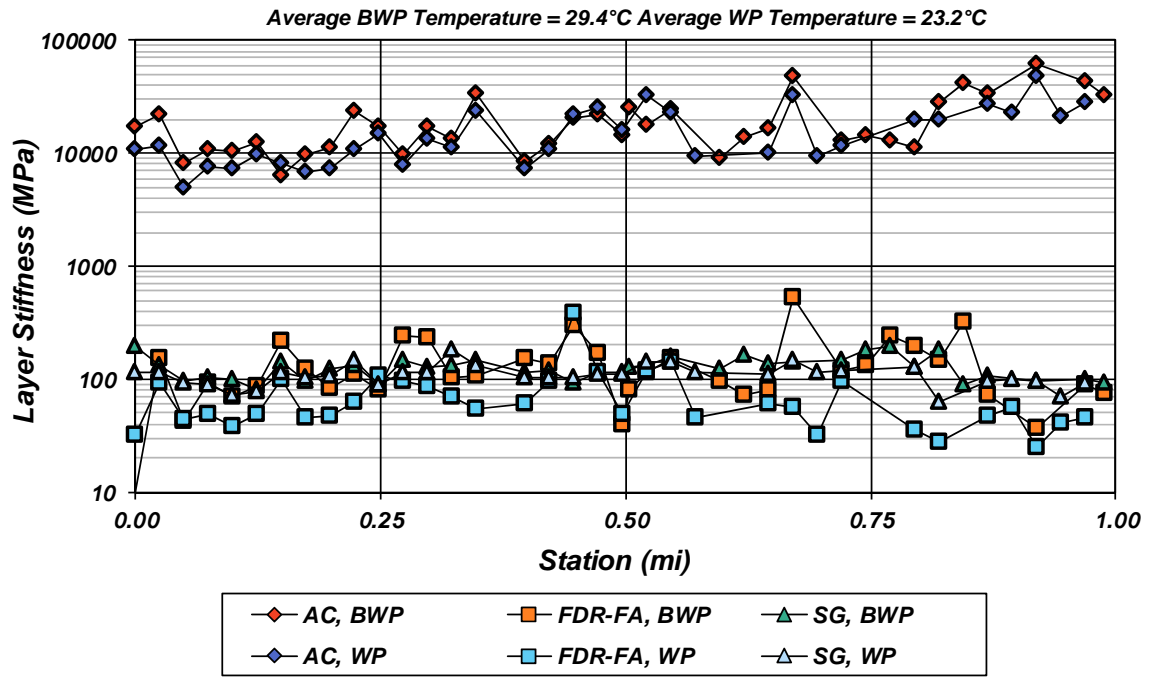


Figure 4.23: Sierra 89 backcalculated stiffnesses, May 11, 2016.

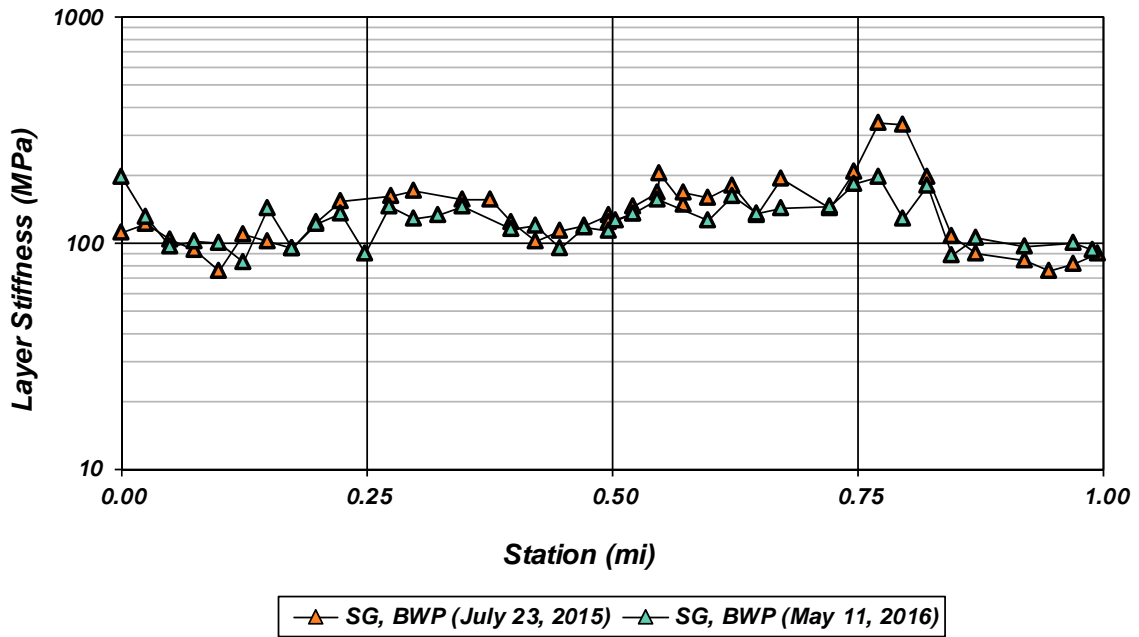


Figure 4.24: Sierra 89 unbound layer stiffnesses between the wheelpaths.

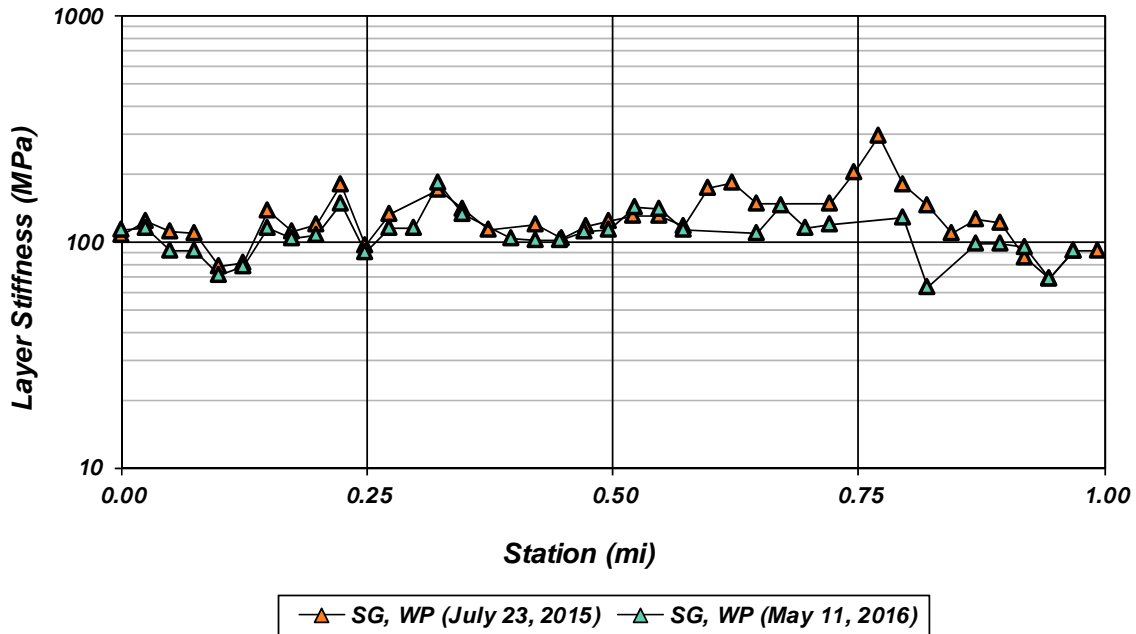


Figure 4.25: Sierra 89 unbound layer stiffnesses in the wheelpath.

The backcalculated stiffnesses across the site were generally consistent for the respective wheelpath locations. As noted earlier, Sierra 89 had the highest deflections and most notable surface distresses of all the sites evaluated. The backcalculated stiffnesses of the FDR and unbound material were consistently higher between the wheelpaths than in the wheelpath, which is indicative of fatigue and/or shear damage accumulation from traffic loadings. Contrary to the DCP test results, all FDR and unbound layer stiffnesses were lower in May 2016 than in July 2015, which is also in agreement with the deflections observed in the two rounds of testing: July 2015 deflections were consistently lower than May 2016 deflections for geophones relevant to the FDR and subgrade.

There appears to be little to no relationship between the subgrade stiffness and the overlying layer stiffness (Figure 4.26), indicating that environmental effects rather than confinement from the overlying layers most likely caused the softer behavior in the subgrade. In those soft locations the asphalt surface was cracked, which would have reduced its ability to provide confinement. The FDR stiffness was surprisingly low and the subgrade stiffness was also low, which may both be due to moisture entering via the cracked surface and remaining in the FDR and subgrade. Although FWD testing and coring followed by DCP testing in the core hole are performed during the same traffic closure, FWD testing usually precedes the other two tests. Although it is possible that water used to cool the core barrel during coring may have influenced the DCP testing, it is considered unlikely that water from the coring had sufficient time to move far enough into the FDR and subgrade to influence the DCP results very



much, or to have any effect on the stiffnesses backcalculated from the FWD testing, even if the core had been taken before use of the FWD.

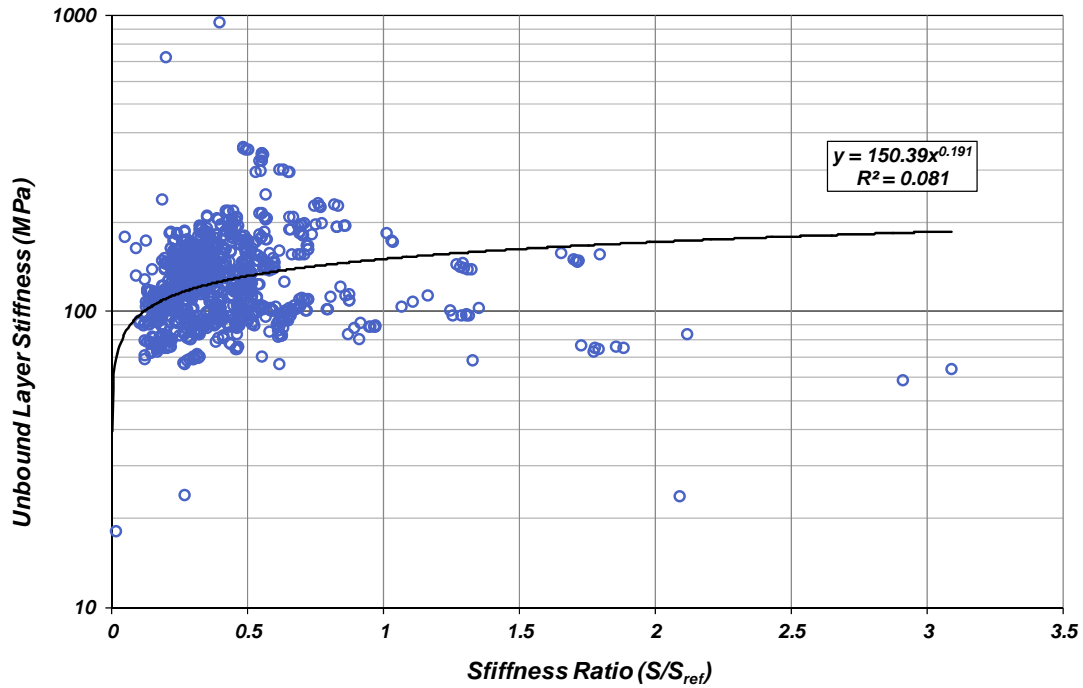


**Figure 4.26: Sierra 89 overlying layer effect.**

(Note: *stiffness ratio* is the ratio of the bending stiffness of the layers above the unbound layer relative [S] to a reference stiffness [S<sub>ref</sub>], giving an indication of the confinement from those layers.)

The reduction of stiffness of the FDR material seen in the wheelpath is also consistent with the damage present at the site: the loss of stiffness of this material over time would lead to more accelerated accumulation of damage. Photos from the Caltrans Automated Pavement Condition Survey (APCS) reveal that surficial distresses in 2010 were less extreme (Figure 4.27) than present conditions (Figure 4.19). Because thorough monitoring of precipitation, traffic, and stiffness was not been performed at this site, the exact cause of the damage remains unknown, but it may be rooted in accelerated moisture ingress from cracked surface layers.



**Figure 4.27: Road condition on Sierra 89N PM 28.06 in 2010.**

#### *4.1.4 Plumas 70*

Testing and sampling at Plumas 70 (Plu 70) took place on July 21, 2015 (Round 1) and April 26, 2016 (Round 2). The surface wearing course was in good shape but road had poor drainage with little slope to dissipate water from the main road surface. Drainage ditches were located about five feet from the edges of the traveled way and were filled with vegetation. During July 2015, it was notable how dry the surrounding vegetation was compared to how lush and green it was during April 2016 (Figure 4.28a and b, respectively).



(a)



(b)

**Figure 4.28: Plumas 70 surrounding area road conditions in (a) July 2015 (b) and April 2016.**

#### 4.1.4.1 Structure

The structure and construction history of the test site as indicated from various Caltrans plans and documents are listed in Table 4.13, and the structure observed from coring, sampling, and DCP testing can be seen in Table 4.14. The pulverized asphalt base (PAB) material is unstabilized, and the thickness was inferred from DCP testing. The observed structure matches well with the information provided in the Caltrans plans; for the 135 mm asphalt layer, two distinct lifts were observed. The pulverized base material appeared to have inconsistent thickness, as revealed from DCP testing as well as iGPR information indicating variable thicknesses of base material between 200 and 380 mm.

**Table 4.13: Structure from Caltrans Plans for Plumas 70**

EA Number	Construction Began	Construction Completed	Material	Thickness (mm)
02-1E8704	10/13/2010	7/19/2011	HMA	30.5
02-263364	n/a	11/7/2003	AC	135
			PAB	210

**Table 4.14: Observed Structure for Plumas 70 (mm)**

Material	PM 83+50ft			PM 82-50ft			Source
	July 21, 2015	April 26, 2016	Average	July 21, 2015	April 26, 2016	Average	
AC	n/a	36	36	25.5	22	24	Core
AC		147	147	54	54	54	
AC				66	69	68	
PAB		198	198	325	337	331	DCP
Unbound		219	219	209	240	225	
Unbound		Subgrade	Subgrade	Subgrade	Subgrade		



**Figure 4.29: Cores from Plumas 70.**  
(Note: all cores are upside down in the figures.)

#### 4.1.4.2 Unbound Material Properties

Unbound testing and sampling took place at PM82-50ft in July 2015, and at both locations in April 2016. No visual or USCS analyses could be performed on PM83+50ft due to miscommunication and premature disposal of the materials. Results from DCP testing, moisture content testing, and soils characterization can be seen in Figure 4.30. Median DCP values can be found in Table 4.15.

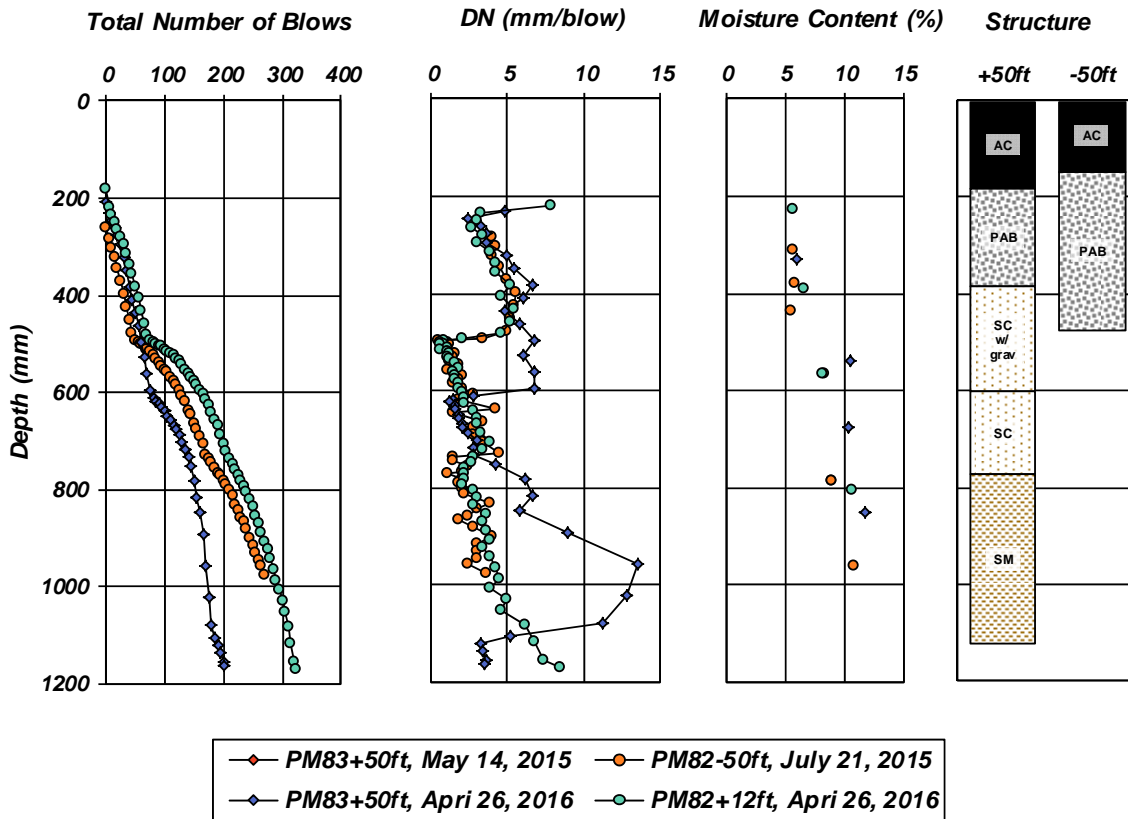


Figure 4.30: Unbound materials testing and sampling results for Plumas 70.

Table 4.15: Median DN (mm/blow) for Plumas 70

Material	DN PM 83+50ft		DN PM 82-50ft	
	July 21, 2015	April 26, 2016	July 21, 2015	April 26, 2016
PAB	n/a	4.8	4.7	4.2
Unbound	n/a	3.5	2.0	2.7

The material at the site consisted of clayey sands with gravel overlying low-plasticity clayey and silty sand. The material properties were fairly consistent across the site and during the two rounds of testing; little change in moisture content was observed, and penetration resistance also remained consistent. The moisture content increased with depth, and was lower in the PAB material than in the finer sands. The penetration resistance at

PM 82 was higher than PM 83, which could have been caused by differing soil properties or from the slightly higher moisture content; however, because soils characterization was not performed on PM 83 material, this remains unknown. Based on the alluvial and lacustrine environment, there may be thin clay or silt seams in the valley, which could explain a thin region of decreased penetration resistance as seen at PM 83.

4.1.4.3 Falling Weight Deflectometer

Backcalculated layer stiffnesses can be seen in Figure 4.31 to Figure 4.34. Station 0 corresponds to PM 82 and Station 1 corresponds to PM 83. A summary of the backcalculation results can be seen in Table 4.16.

**Table 4.16: Backcalculated Stiffnesses for Plumas 70 (in MPa)**

Material	Thickness Used (mm)	Between Wheelpaths				Wheelpath			
		July 21, 2015		April 26, 2016		July 21, 2015		April 26, 2016	
		Average	Std. Dev.	Average	Std. Dev.	Average	Std. Dev.	Average	Std. Dev.
Asphalt-bound	150	2,986	613	6,807	1,701	4,437	787	7,921	2,245
PAB	320	238	89	206	75	153	44	153	60
Subgrade	0	197	28	218	31	198	24	216	30
Average Asphalt Temp (°C)		35.2		23.3		29.9		20.9	

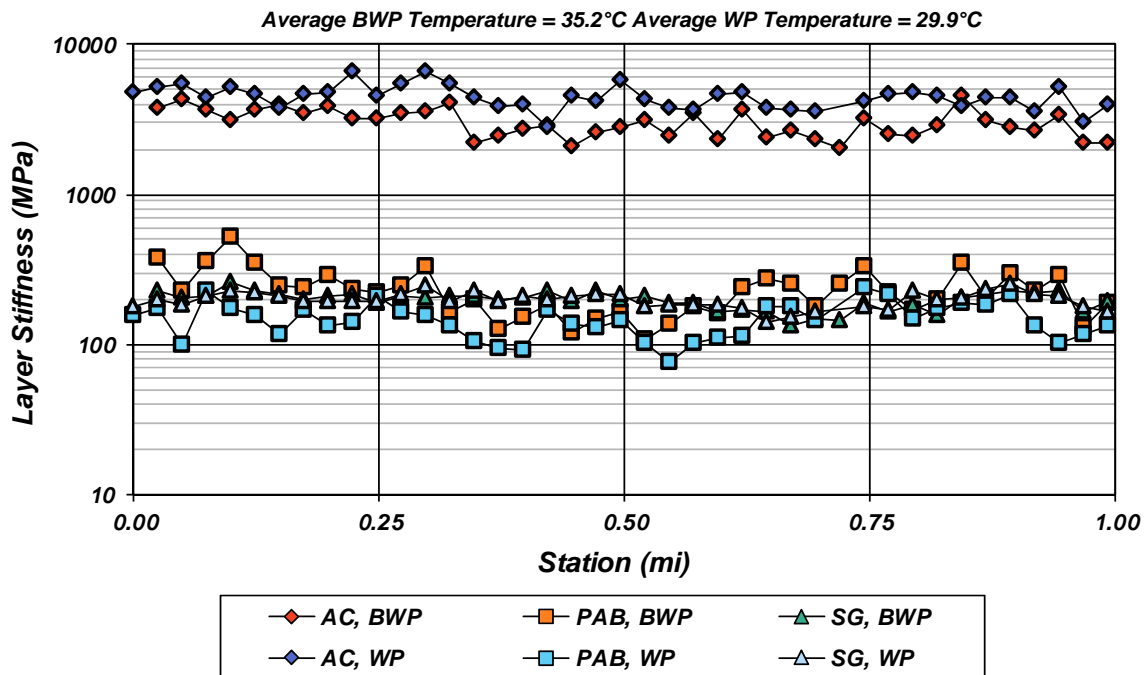


**Figure 4.31: Plumas 70 backcalculated stiffnesses, July 21, 2015.**

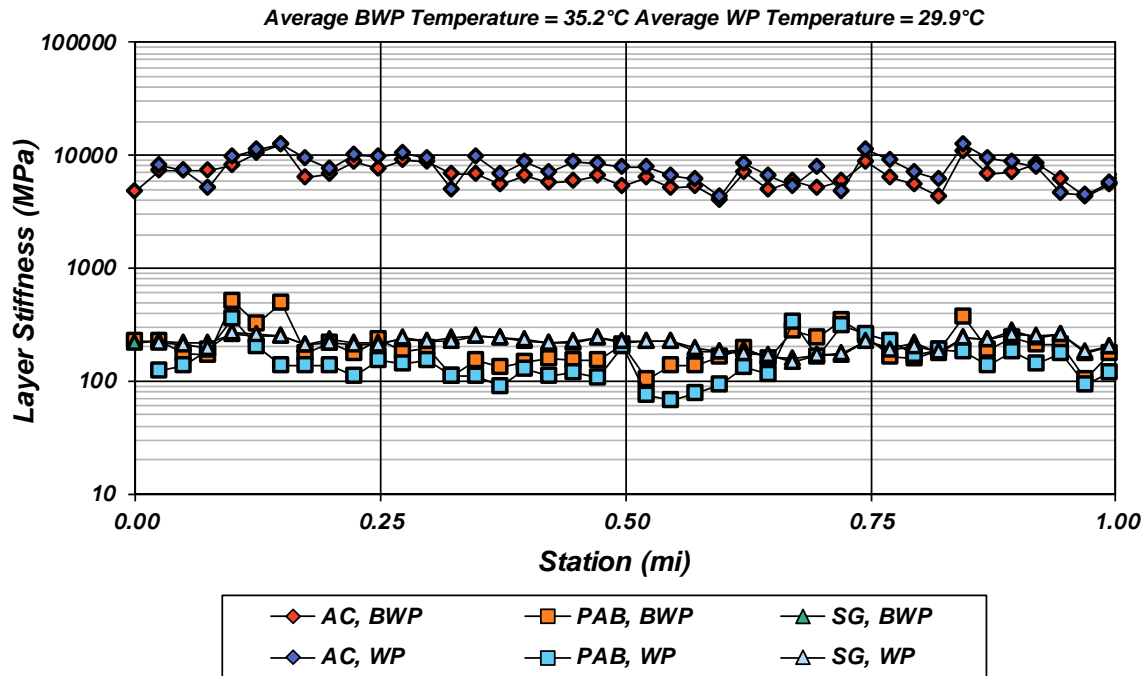


Figure 4.32: Plumas 70 backcalculated stiffnesses, April 26, 2016.

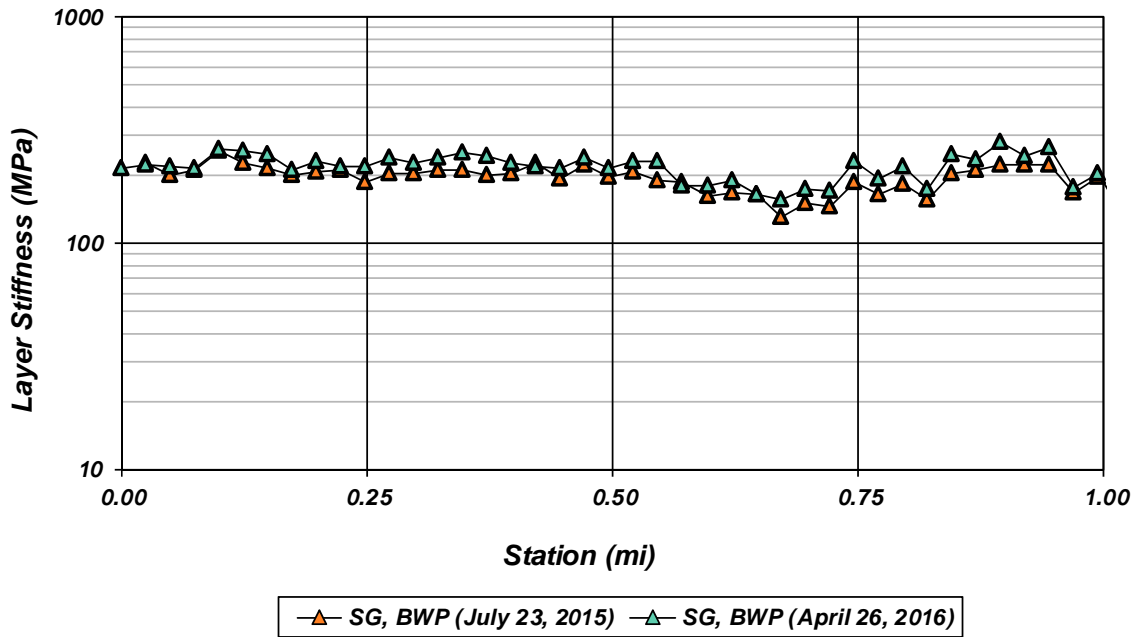


Figure 4.33: Plumas 70 unbound layer stiffnesses between the wheelpaths.

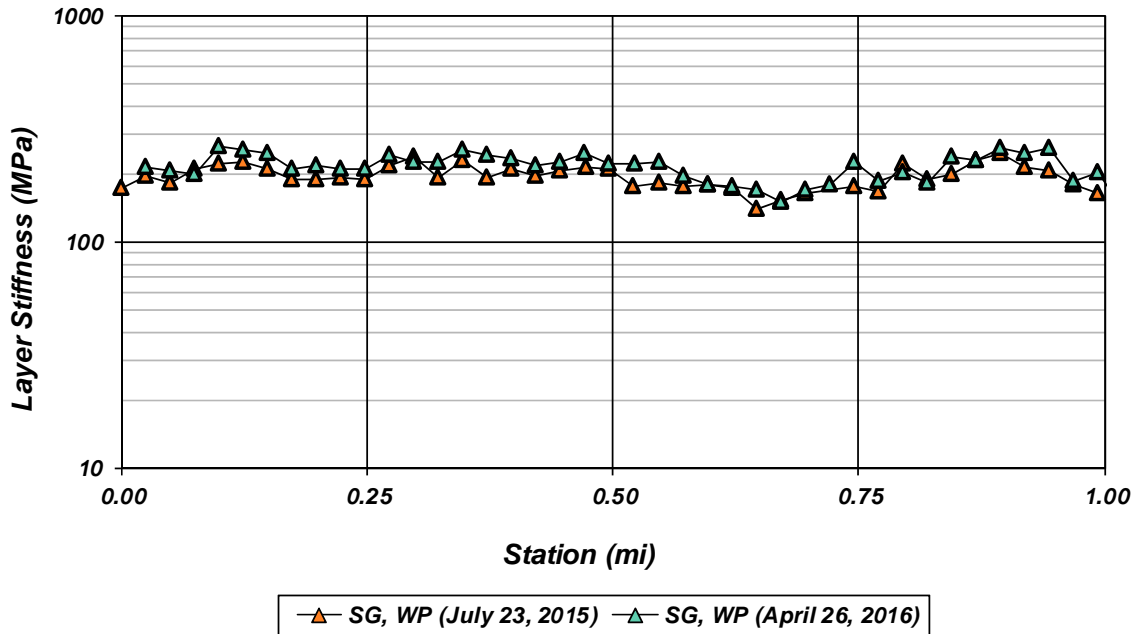


Figure 4.34: Plumas 70 unbound layer stiffnesses in the wheelpath.

The backcalculation results reveal fairly consistent material properties over the length of the section, with a slight increase in stiffness of the subgrade near the end of the section. The backcalculated stiffness of the PAB in general was less than that of the subgrade, which may either be a result of the gradual densification and permanent deformation of the PAB over time, or possibly a result of the variable thickness of the PAB material in the backcalculation procedure. However, the finding of less stiff PAB agrees with all the DCP tests performed at the site, which indicate stiffer material underlying the PAB.

PAB stiffness changed slightly from July 2015 to April 2016, and decreased between the wheelpaths but increased slightly in the wheelpath. The PAB stiffness was consistently less in the wheelpath. The stiffness of the subgrade at the site is almost identical between the wheelpaths and in the wheelpath, and was slightly higher in April 2016 than July 2015, which is consistent with the deflection data. Calculation of the stiffness ratio (Figure 4.35) reveals a slight relationship between the stiffness of the subgrade and the stiffness of the overlying layers, which would explain why the subgrade was consistently higher when the asphalt was colder and stiffer in April 2016.



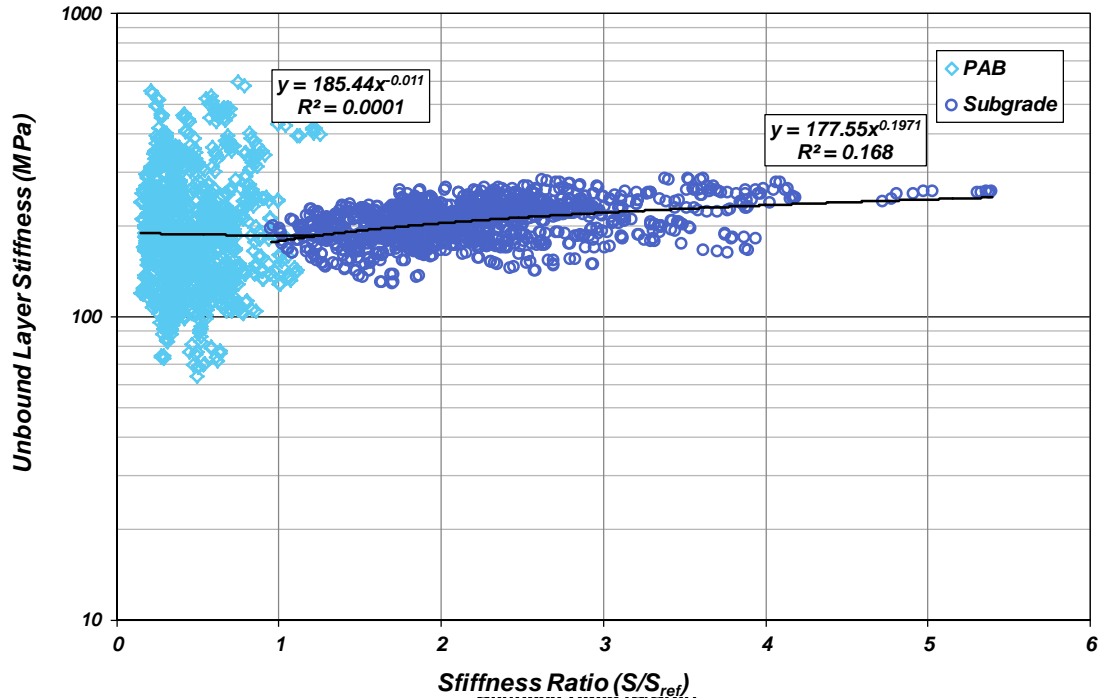


Figure 4.35: Plumas 70 overlying layer effect.

(Note: *stiffness ratio* is the ratio of the bending stiffness of the layers above the unbound layer relative [S] to a reference stiffness [S<sub>ref</sub>], giving an indication of the confinement from those layers.)

#### 4.1.5 Ventura 33

Testing and sampling on Ventura 33 (Ven 33) took place on July 28, 2015 (Round 1) and June 9, 2016 (Round 2). The test route is located in a valley area near Corral Canyon. Both tests took place in the summer months, spaced almost a year apart. The road has a small shoulder (~300 mm wide) with no adjacent drainage ditches. The first 900 m of testing were on a relatively smooth, flat part of the road, and the last 500 m were located near toe slope cuts (Figure 4.36a and b, respectively).



(a)



(b)

Figure 4.36: Road conditions near Ventura 33 (a) PM 51.5 and (b) PM 52.2 in June 2016.



#### 4.1.5.1 Structure

The structure and construction history of the test site as indicated from various Caltrans plans and documents are seen in Table 4.17, and the observed structure from coring and testing can be seen in Table 4.18. After the first round of field testing, a new overlay was placed on the site, which was consistent with Caltrans plans. Intact cores of FDR material were not obtained, and thickness was inferred from DCP testing. In general, the observed structure was consistent with the structure provided by Caltrans. The “unbound” materials listed in Table 4.18 are denser materials that were observed overlying softer material, indicating some sort of layer transition between the unbound materials.

**Table 4.17: Structure from Caltrans Plans Ventura 33**

EA Number	Construction Began	Construction Completed	Material	Thickness (mm)
07-2W8704	5/26/2016	7/30/2016 (est.)	HMA (Type A)	30.5
07-249304	4/1/2006	6/22/2006	AC (Type B)	45
			FDR (Cold Foam in-Place Recycling, 2% paving asph, 2% fly ash)	205

**Table 4.18: Observed Structure for Ventura 33 (in mm)**

Material	PM 52.5+50ft			PM 51.5-50ft			Source
	July 28, 2015	June 9, 2016	Average	July 28, 2015	June 9, 2016	Average	
AC	n/a	29	-	-	36	-	Core
AC	47	52	42	45	37	49	
FDR-FA	204	219	212	205	212	209	DCP
Unbound	702	537	620	200	163	182	
Unbound	Subgrade	Subgrade	-	Subgrade	Subgrade	-	

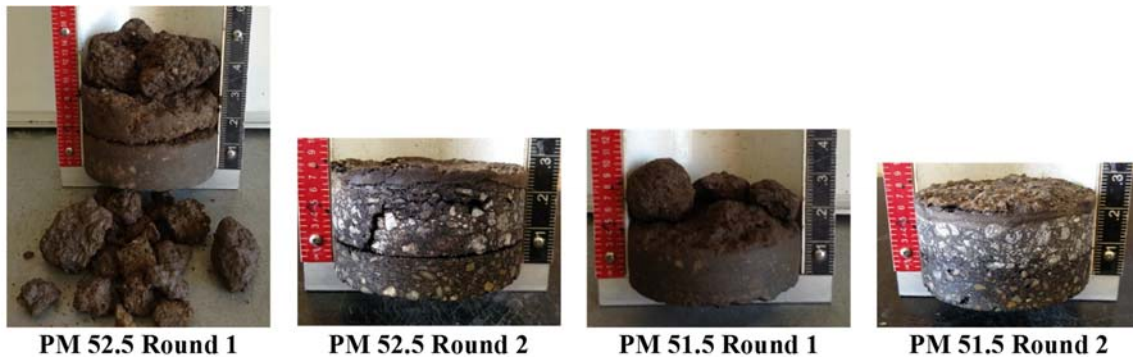


**Figure 4.37: Cores from Ventura 33.**  
(Note: all cores are upside down in the figures.)

#### 4.1.5.2 Unbound Material Properties

Unbound testing and sampling took place at PM 51.5 for both rounds of field testing and at PM 52.5 in June 2016. Material at PM 52.5 was only visually classified per ASTM D2488. Results from DCP testing, moisture content testing, and soils characterization can be seen in Figure 4.38. Median DCP values are summarized in Table 4.19.

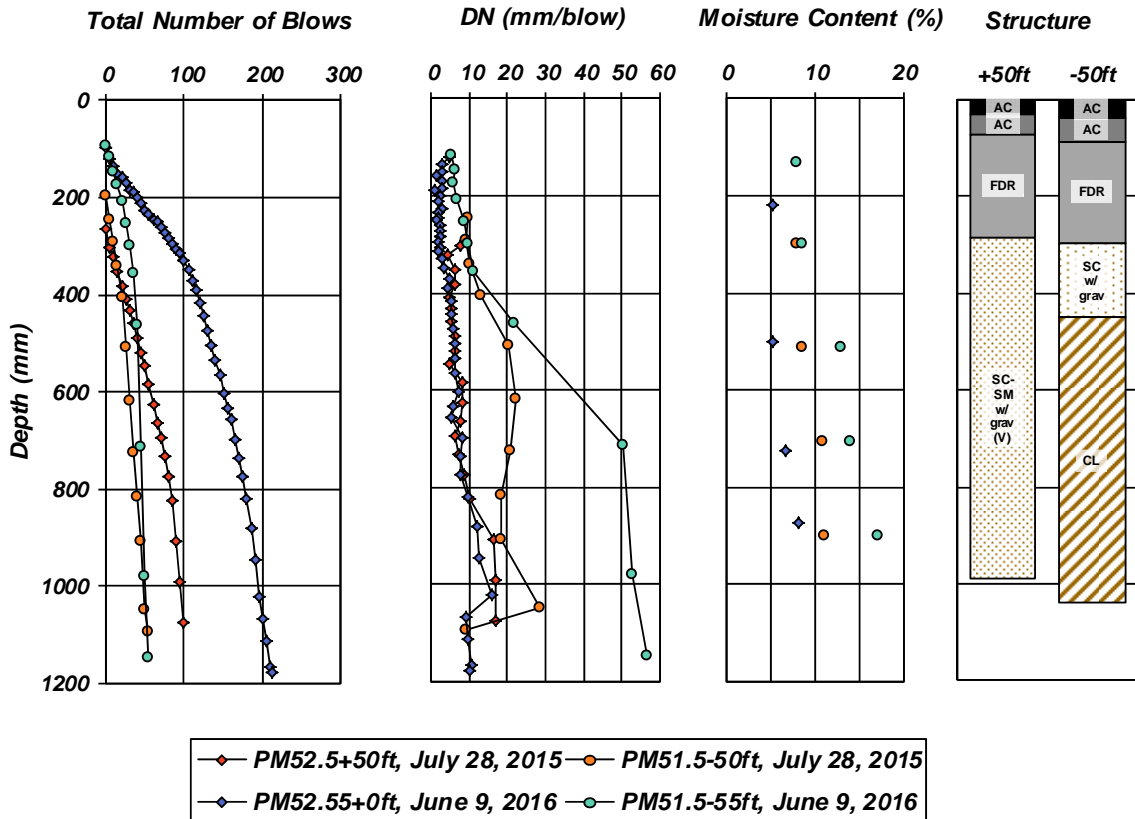


Figure 4.38: Unbound materials testing and sampling results for Ventura 33.

Table 4.19: Median DN (mm/blow) for Ventura 33

Material	DN PM 52.5+50ft		DN PM 51.5-50ft	
	July 28, 2015	June 9, 2016	July 28, 2015	June 9, 2016
FDR-FA	n/a	2.4	n/a	n/a
Unbound	6.7	6.0	15.8	21.6

The unbound material at the site consisted of low-medium plasticity clayey sands with gravel overlying finer sandy clay. While PM 52.5 was not classified per ASTM D2487, the material looked like non-low plasticity silty-clayey sand. The natural soil is a mixture of alluvial deposits and fluvial deposits, which is consistent with the

observed soil classifications. The material at PM 52.5 is coarser because it is on a cut portion near the toe slopes while PM 51.5 is more reminiscent of valley alluvial deposits and outwash plains.

The moisture content at PM 51.5 was higher in June 2016, which seems to have resulted in lower resistance to penetration from DCP tests. PM 52.5 had fairly consistent penetration resistance for both rounds, and lower moisture contents than PM 51.5. The moisture content tended to increase slightly with depth, and had little change near the surface.

#### 4.1.5.3 Falling Weight Deflectometer

Backcalculated stiffnesses can be seen in Figure 4.39 to Figure 4.42. Station 0 corresponds to PM51.5 and Station 1 corresponds to PM52.5. A summary of backcalculation results can be seen in Table 4.20.

**Table 4.20: Backcalculated Stiffnesses for Ventura 33 (in MPa)**

Material	Thickness Used (mm)	Between Wheelpaths				Wheelpath			
		July 28, 2015		June 9, 2016		July 28, 2015		June 9, 2016	
		Average	Std. Dev.	Average	Std. Dev.	Average	Std. Dev.	Average	Std. Dev.
AC	50	6,971	6,695	3,423	1,834	7,944	5,770	6,481	3,351
FDR-FA	205	351	327	456	501	528	477	369	373
Subgrade	0	147	93	154	81	189	114	170	80
Average Asphalt Temp (°C)		42.0		39.5		37.6		39.5	

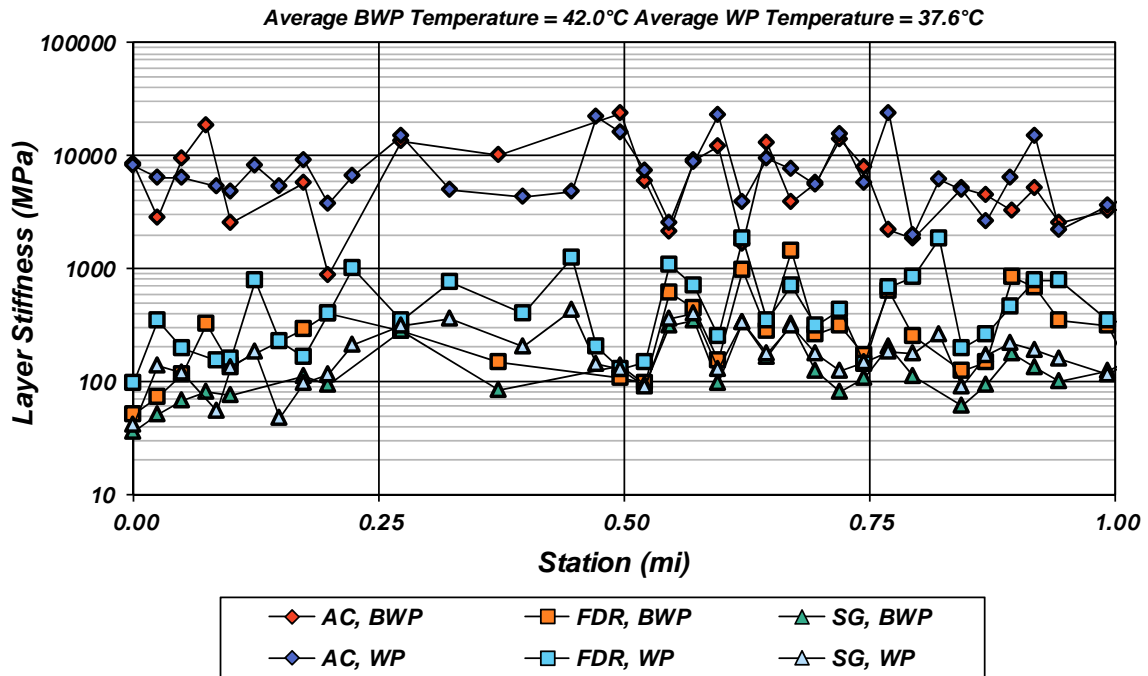


Figure 4.39: Ventura 33 backcalculated stiffnesses, July 28, 2015.

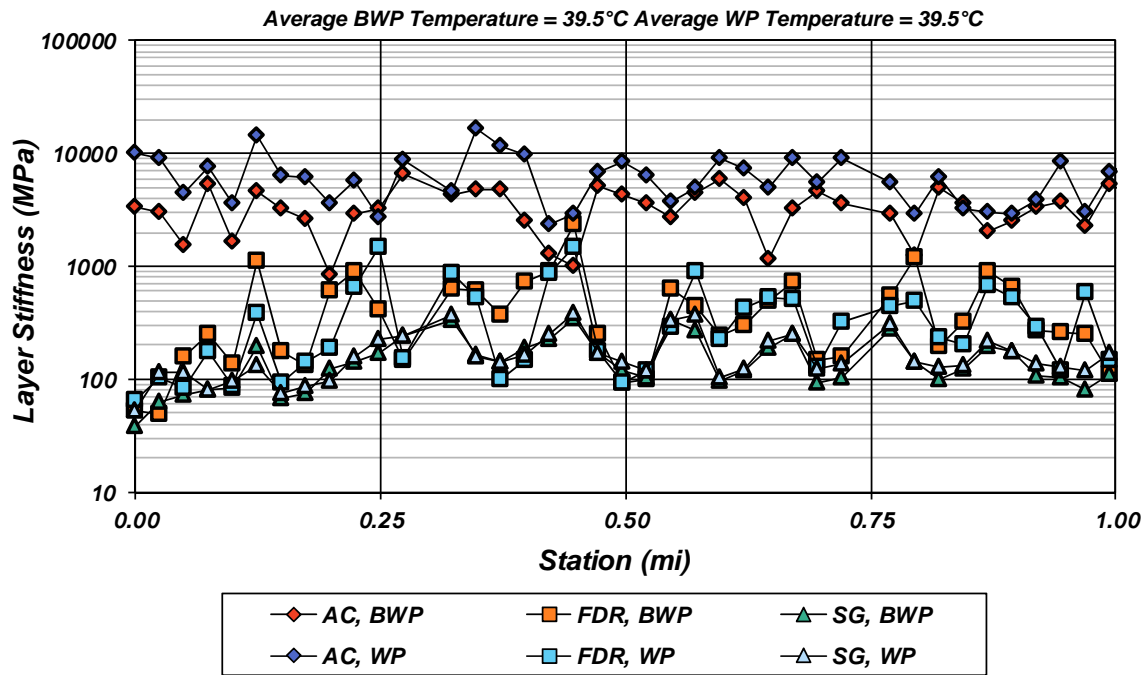


Figure 4.40: Ventura 33 backcalculated stiffnesses, June 9, 2016.

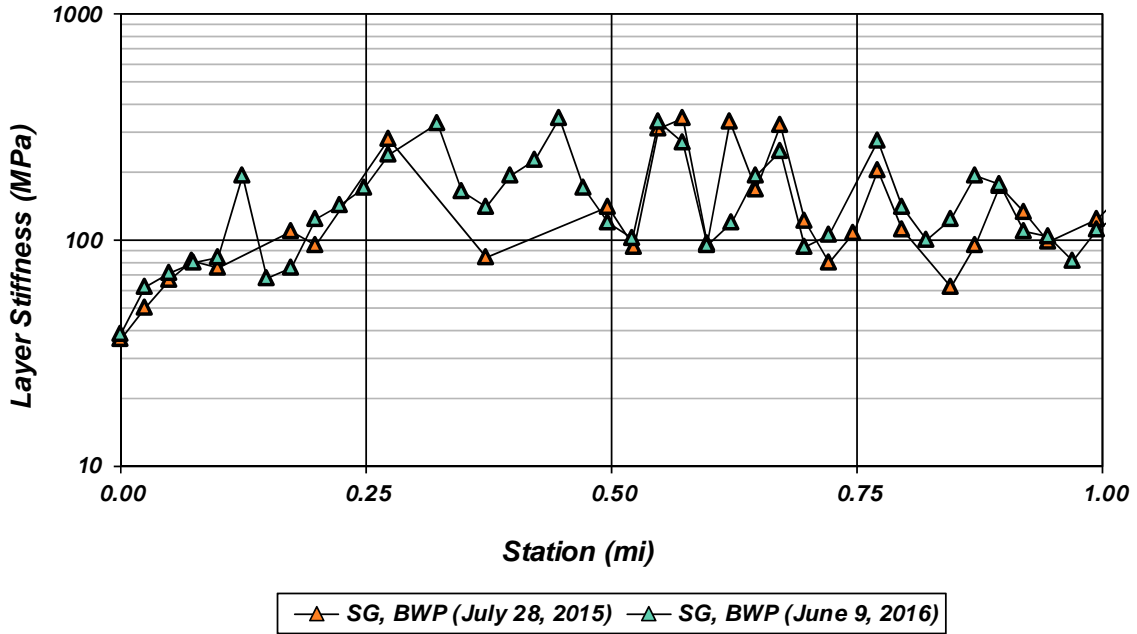


Figure 4.41: Ventura 33 unbound layer stiffnesses between the wheelpaths.

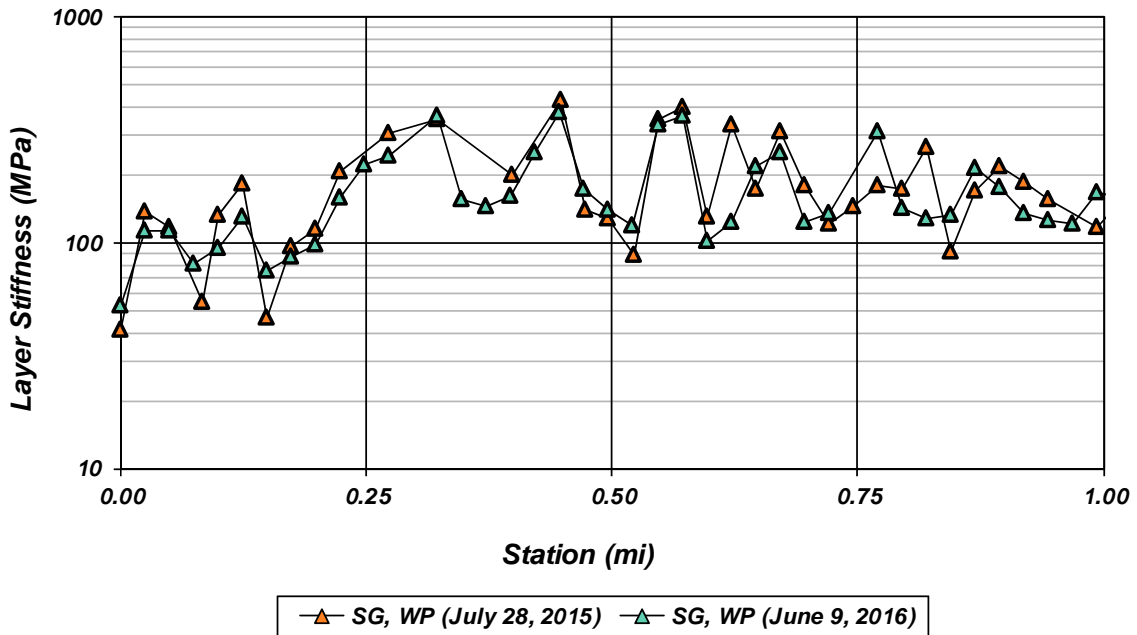
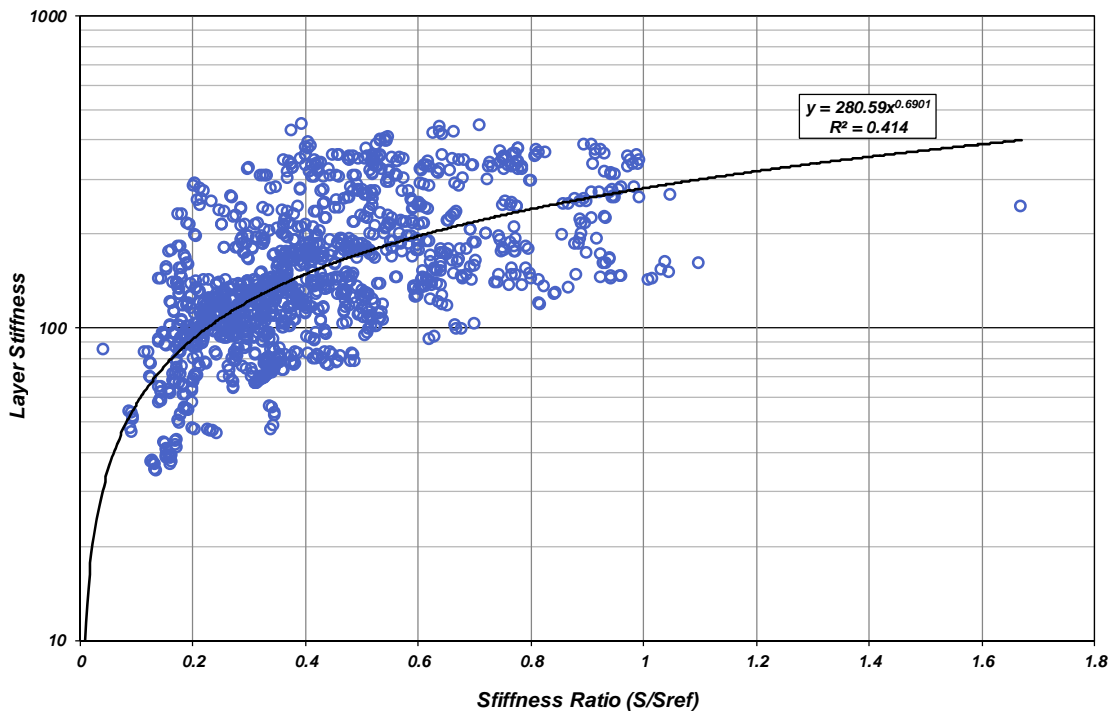


Figure 4.42: Ventura 33 unbound layer stiffnesses in the wheelpath.

The results obtained show more scatter than the other sites; however, this is consistent with the deflection data obtained during both rounds of field testing, which show a wide range of scatter for all geophones. This spatial variability could be a result of the geologic setting or the variability of construction of the FDR or AC material.

In general, the subgrade and FDR are less stiff the first 0.25 miles of the site, which is consistent with the clayey nature of the material observed. The FDR material in the wheelpath was generally stiffer than that in the center lane and the subgrade tended to be stiffer in July 2015 than in June 2016 for material near the wheelpath. The remaining 0.75 miles of the site contained significant variability, but in general the wheelpath material was stiffer in July 2015 than in June 2016 and the material between the wheelpaths was slightly stiffer in June 2016 than July 2015. This stiffness behavior of the subgrade also appears to be related to the stiffness of the overlying layers (Figure 4.43), which may explain why the wheelpath stiffness was greater than between the wheelpaths, because the stiffer overlying materials at cooler temperatures contributed to additional confinement.



**Figure 4.43: Ventura 33 overlying layer effect.**

(Note: *stiffness ratio* is the ratio of the bending stiffness of the layers above the unbound layer relative [S] to a reference stiffness [S<sub>ref</sub>], giving an indication of the confinement from those layers.)

#### 4.1.6 San Luis Obispo 166

Testing on San Luis Obispo 166 (SLO 166) took place on July 30, 2015 (Round 1) and May 4, 2016 (Round 2). The test site was a fairly straight road along the hillslopes running adjacent to the Cuyama River. Some portions of the road appeared to be fill across depressions carved by tributaries while other portions appeared to be cuts through toe slopes and hillsides. The surface wearing course was in good shape, with little damage observed. No engineered drainage ditches were observed at the site, although cross slopes appeared to allow for adequate drainage of water. The road had a small shoulder and was bounded on both sides by golden fields with sparse trees.



(a)



(b)

**Figure 4.44: Road conditions on San Luis Obispo 166 near (a) PM 41.5 and (b) PM 42.5 in May 2016.**

#### 4.1.6.1 Structure

The structure and construction history from Caltrans plans and documents are listed in Table 4.21 and the layer thicknesses found and evaluated in the observed structure can be seen in Table 4.22. Testing and sampling was performed at PM 42.5 for both rounds of field testing in July 2015 and May 2016, and at PM 41.5 in July 2015. Cores revealed that the remaining asphalt thicknesses are not consistent across the site.

**Table 4.21: Structure from Caltrans Plans for San Luis Obispo 166**

EA Number	Construction Began	Construction Completed	Material	Thickness (mm)
05-1F0104	8/19/2013	11/7/2013	AC	60
			CIR	60
Existing	n/a	n/a	Remaining AC	0-120
			AB	150
			AS	230

**Table 4.22: Observed Structure for SLO 166 (in mm)**

Material	PM 42.5+50ft			PM 41.5-50ft			Source
	July 30, 2015	May 4, 2016	Average	July 30, 2015	May 4, 2016	Average	
AC	75	63	69	85	65	75	Core
CIR	45	56	51	n/a	88	88	
AC	110	109	110		61	61	
					84	84	
					105	105	
	-	60	-		134	134	
Unbound	108	185	147	162	-	-	DCP
Unbound	n/a	Subgrade	-	n/a	Subgrade	-	

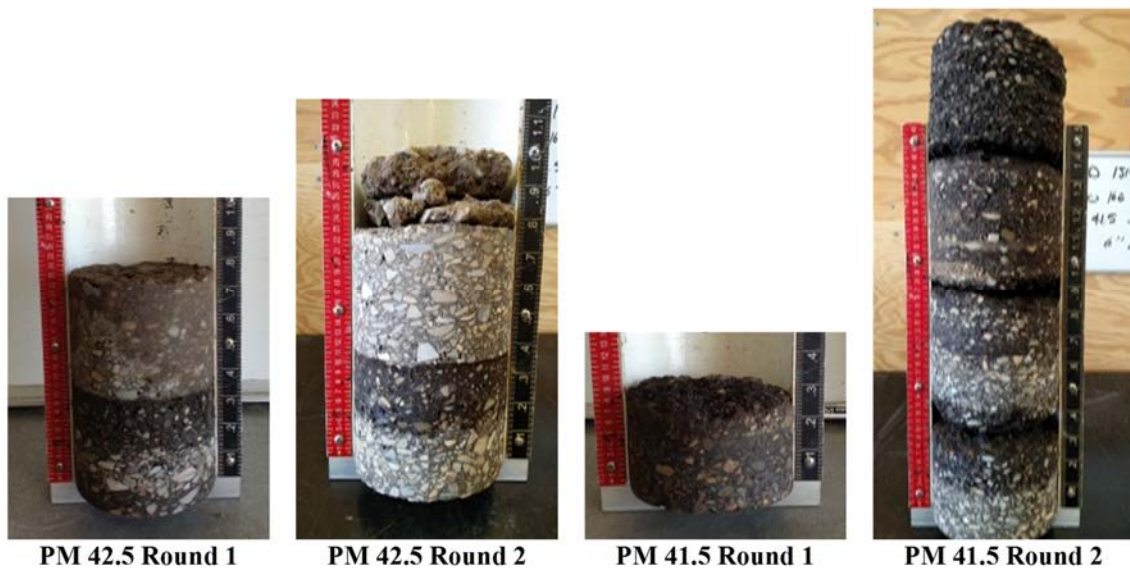


**Figure 4.45: Cores from San Luis Obispo 166.**  
*(Note: all cores are upside down in the figures.)*

#### 4.1.6.2 Unbound Material Properties

The unbound material at the site consisted of light-brown to reddish-brown well-graded sandy clay/clayey sand of medium plasticity. After the second round of field testing, it was determined that the difficulty in obtaining DCP test data and samples was due to a 500 mm thick layer of various lifts of asphalt concrete. From visual classification, the material at PM 41.5 appeared to have higher fines content than the material at PM 42.5, which would explain its decreased resistance to penetration. Given the lack of information obtained from DCP testing during the first round of field testing, as can be seen in Figure 4.46, it is likely that the penetration rod encountered a large piece of gravel at PM 42.5 and could not penetrate further. Median DCP values are summarized in Table 4.23.



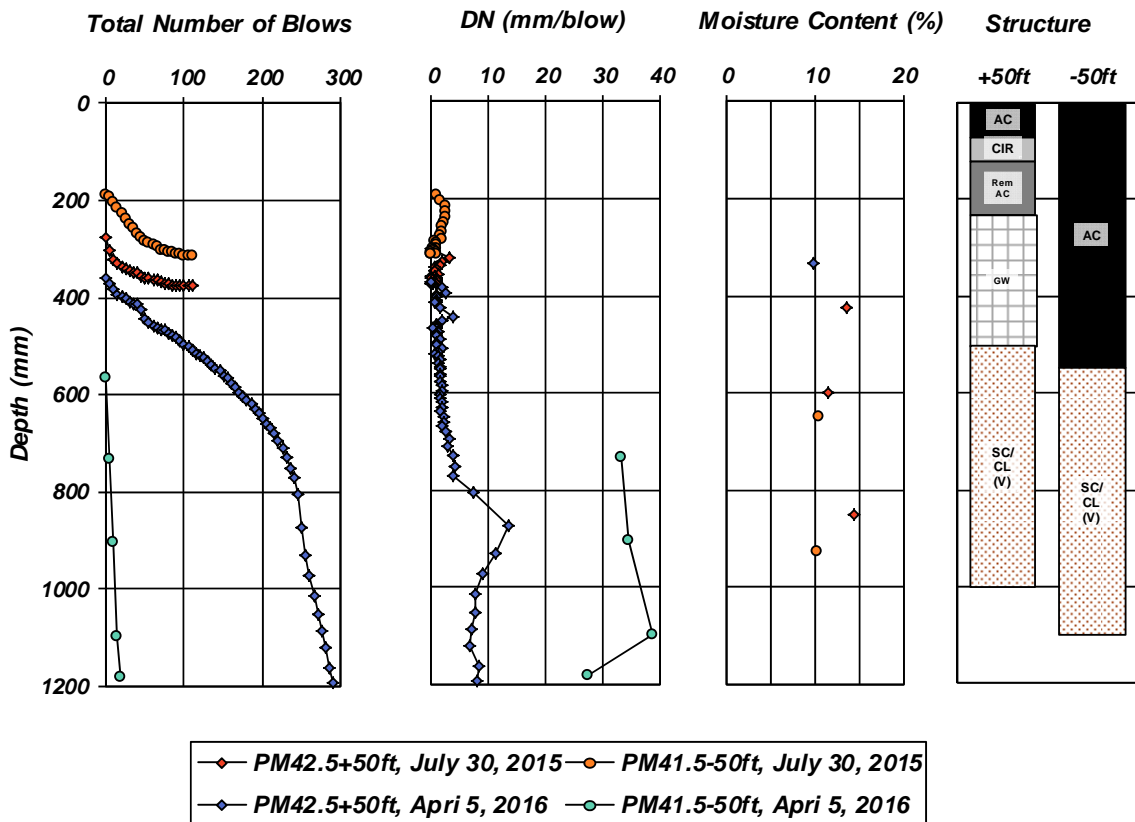


Figure 4.46: Unbound materials testing and sampling results for San Luis Obispo 166.

Table 4.23: Median DN (mm/blow) for San Luis Obispo 166

Material	DN PM 42.5+50ft		DN PM 41.5-50ft	
	July 30, 2015	May 4, 2016	July 30, 2015	May 4, 2016
Unbound	n/a	1.6	n/a	33.9

PM 41.5 is located in a cut portion of the road, while PM 42.5 is on a much flatter portion. Unfortunately, DCP data obtained at the site are such that they provide little to compare the two rounds of field testing. Moisture contents ranged from 9 to 15 percent for all the materials tested, and appeared to be fairly steady with depth for the six samples tested at PM 42.5. The first 600 mm underlying the asphalt material had high resistance to penetration, which decreased slightly at a depth of approximately 800 mm, where the materials tended to increase in plasticity.

#### 4.1.6.3 Falling Weight Deflectometer

Deflections along the length were variable and low across all geophones. Surface deflections under the load were a minimum of 95  $\mu\text{m}$  and a maximum of 615  $\mu\text{m}$ , while geophone 6 experienced a minimum of 21 $\mu\text{m}$  and a maximum of 131 $\mu\text{m}$ . Reasonable backcalculation results proved difficult to obtain, and no iterations produced results that made sense based on expected materials and DCP testing. Use of a 3-layer system within both backcalculation programs (*CalBack* and *KalmanBack*) resulted in a soft layer between the asphalt-bound material and subgrade, while a 2-layer system produced RMS errors in the range of 10 to 20 percent. Four-layer systems also resulted in soft layers underneath the asphalt-bound material, which is not consistent with the presence of aggregate base, subbase, or the granular material encountered at the site, nor the high resistance to penetration encountered.

Because coring and DCP testing at the site did not go as well as anticipated, insufficient information pertaining to the as-constructed structure was obtained. It was thus determined that more information about the site structure would be needed for a proper backcalculation analysis to be performed.

#### 4.1.7 *Santa Barbara 166*

Testing and sampling at Santa Barbara 166 (SB 166) took place on July 29, 2015 (Round 1) and May 5, 2016 (Round 2). The test site was located in alluvial and flood plains adjacent to the Cuyama River on the border of San Luis Obispo and Santa Barbara Counties. The site had a new overlay that evidently began at PM 55.1 and had a new drainage shoulder with various outlets (Figure 4.47a and b, respectively); the new overlay appeared to have undergone some wheelpath compaction over the year. The route was fairly flat on the plains (Figure 4.47c), crossed over an abandoned river channel from PM 55.6 to PM 55.7, and was on a cut portion for the remainder of the length (Figure 4.47d).



(a)



(b)



(c)



(d)

**Figure 4.47: Site conditions at Santa Barbara 166 in May 2016.**

#### 4.1.7.1 Structure

The structure and construction history of the test site as indicated from various Caltrans plans and documents are shown in Table 4.24, and the observed structure from coring, sampling and DCP testing can be seen in Table 4.25. It was determined that two different structures were present at the site. Although project records indicated that the FDR-FA rehabilitation extended from PM 55.1 to PM 70.6 it was apparent that the asphalt thicknesses were very different at the two ends of the test section, with much thicker asphalt at the PM 55-50 location than at the PM 56+50 location.

**Table 4.24: Structure from Caltrans Plans for Santa Barbara 166**

EA Number	Construction Began	Construction Completed	Material	Thickness (mm)
05-1A3304	6/3/2015	12/9/2015	RHMA	24
05-0A4904	3/3/2008	4/22/2009	AC	105
			FDR-FA	280

**Table 4.25: Observed Structure for Santa Barbara 166 (in mm)**

Material	PM 56+50ft			PM 55-50ft			Source
	July 29, 2015	May 5, 2016	Average	July 29, 2015	May 5, 2016	Average	
AC	20	30	25	-	-	-	Core
AC	105	85	109	106	104	105	
				24	37	31	
				30	26	28	
				25	36	31	
				32	33	33	
50	60	55					
FDR-FA	305	246	276	273	232	253	Core/DCP
Unbound	n/a	Subgrade	Subgrade	-	Subgrade	Subgrade	DCP

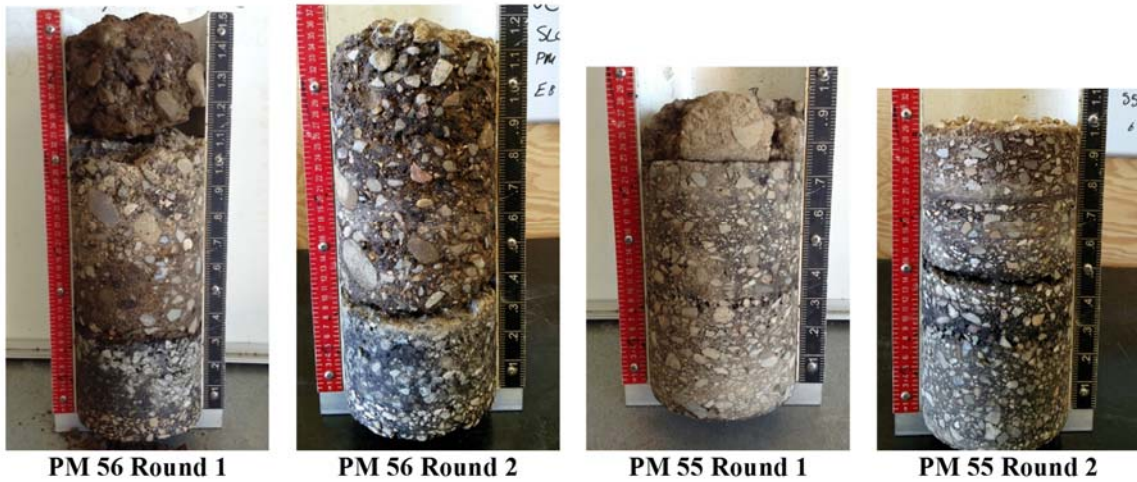


**Figure 4.48: Cores from Santa Barbara 166.**  
*(Note: all cores are upside down in the figures.)*

#### 4.1.7.2 Unbound Material Properties

Unbound testing and sampling took place at PM 55 for both rounds of field testing and at PM 56 for the second round. Unbound material at PM 56 could only be classified visually according to ASTM D2488. Intact FDR cores were obtained and revealed very competent bound material. Results from DCP testing, moisture content testing, and USCS classification can be found in Figure 4.49. Median DCP values are summarized in Table 4.26.

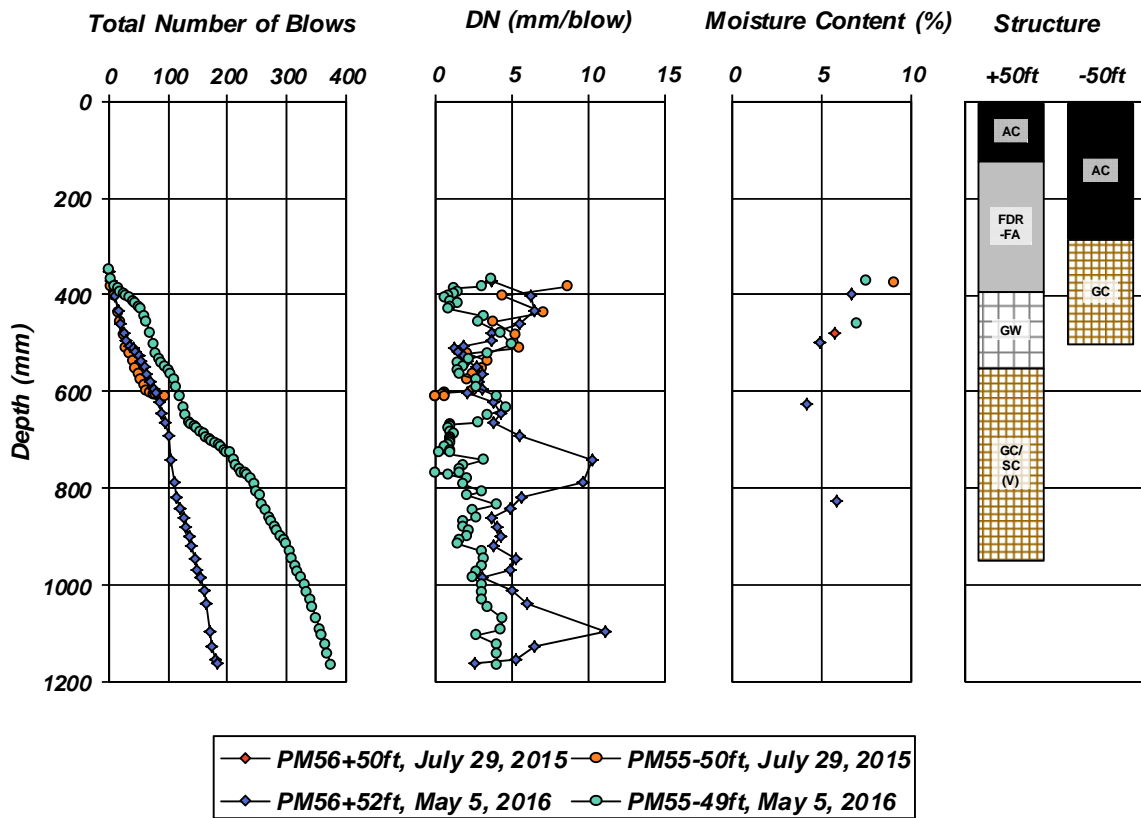


Figure 4.49: Unbound materials testing and sampling results for Santa Barbara 166.

Table 4.26: Median DN (mm/blow) for Santa Barbara 166

Material	DN PM 56+50ft		DN PM 55-50ft	
	July 29, 2015	May 5, 2016	July 29, 2015	May 5, 2016
FDR-FA	n/a	n/a	n/a	n/a
Unbound	n/a	3.8	2.4	2.0

The unbound material at the site generally consisted of fine gravelly soils with nonplastic to low-plasticity fines. Soils could not be fully classified according to USCS specifications, however the material directly underlying the FDR at PM 56 was well-graded gravel with few fines (<7 percent), and is likely to be aggregate base material. The gravelly material at PM 55 contained about 24 percent fines that had similar color to the surrounding material. This could be indicative of pumping of fines or due to the alluvial/fluvial depositional environment; gravelly material with fines would be expected to be present naturally.

The moisture content tended to increase with increased depth, and was higher at PM 55 than PM 56. The penetration resistance was also slightly higher at PM 55 than PM 56, which may be a result of the moisture

conditions, although since no DCP testing was conducted at PM 55 in July 2015 there is little basis for comparison between the two rounds and holes.

#### 4.1.7.3 Falling Weight Deflectometer

Results from backcalculation analyses can be found in Figure 4.50 to Figure 4.53; a summary is provided in Table 4.27. Station 0 corresponds to PM 55 and Station 1 corresponds to PM 56. Backcalculation results are summarized in Table 4.27.

**Table 4.27: Backcalculated Stiffnesses for Santa Barbara 166 (in MPa)**

Material	Thickness Used (mm)	Between Wheelpaths				Wheelpath			
		July 29, 2015		May 5, 2016		July 29, 2015		May 5, 2016	
		Average	Std. Dev.	Average	Std. Dev.	Average	Std. Dev.	Average	Std. Dev.
Asphalt-bound	110	24,387	23,645	61,068	42,560	23,644	25,278	45,624	28,197
FDR-FA	275	2,679	3,639	1,522	2,128	3,481	5,325	2,739	3,492
Unbound	0	291	81	296	86	307	96	311	96
Average Asphalt Temp (°C)		44.5		28.6		38.5		27.8	

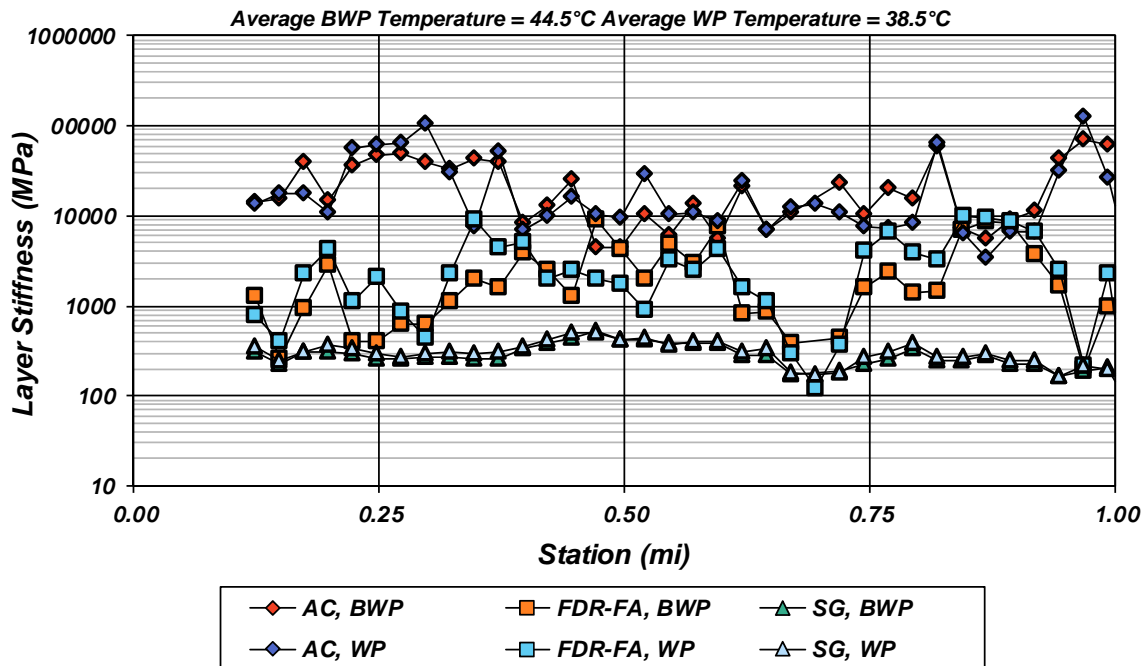


**Figure 4.50: Santa Barbara 166 backcalculated stiffnesses, July 29, 2015.**

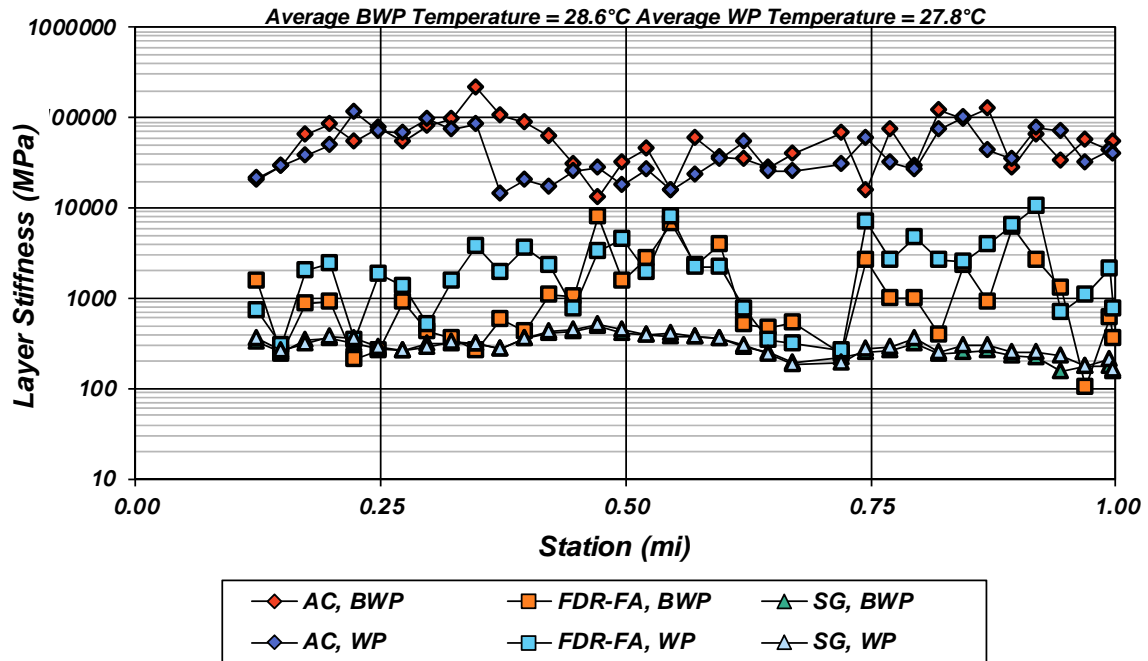


Figure 4.51: Santa Barbara 166 backcalculated stiffnesses, May 5, 2016.

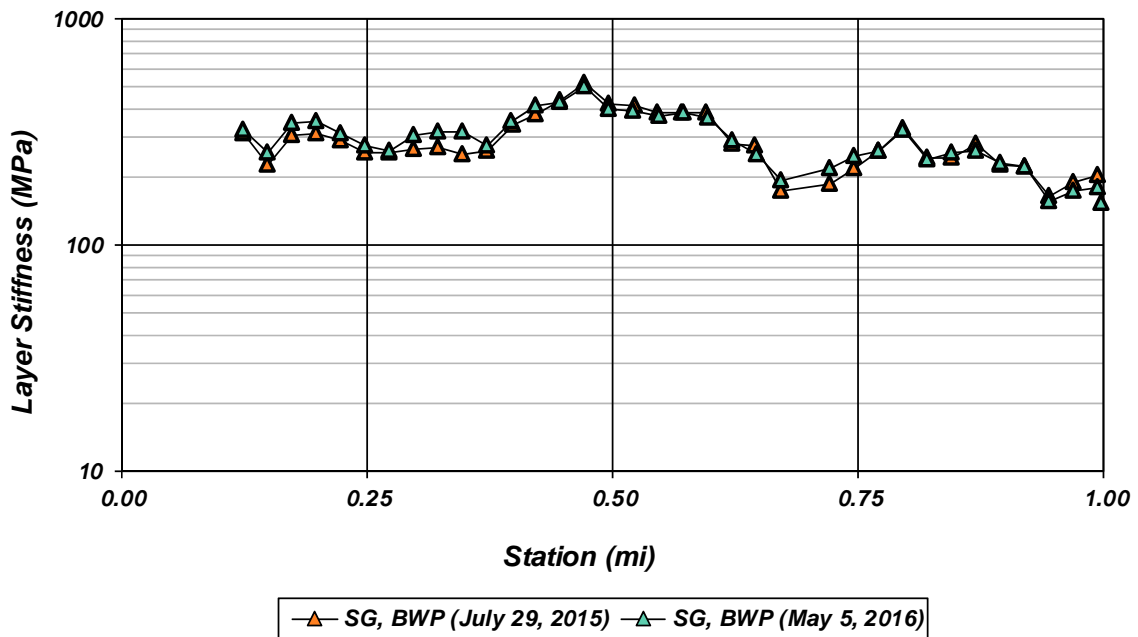


Figure 4.52: Santa Barbara 166 unbound layer stiffness between the wheelpaths.



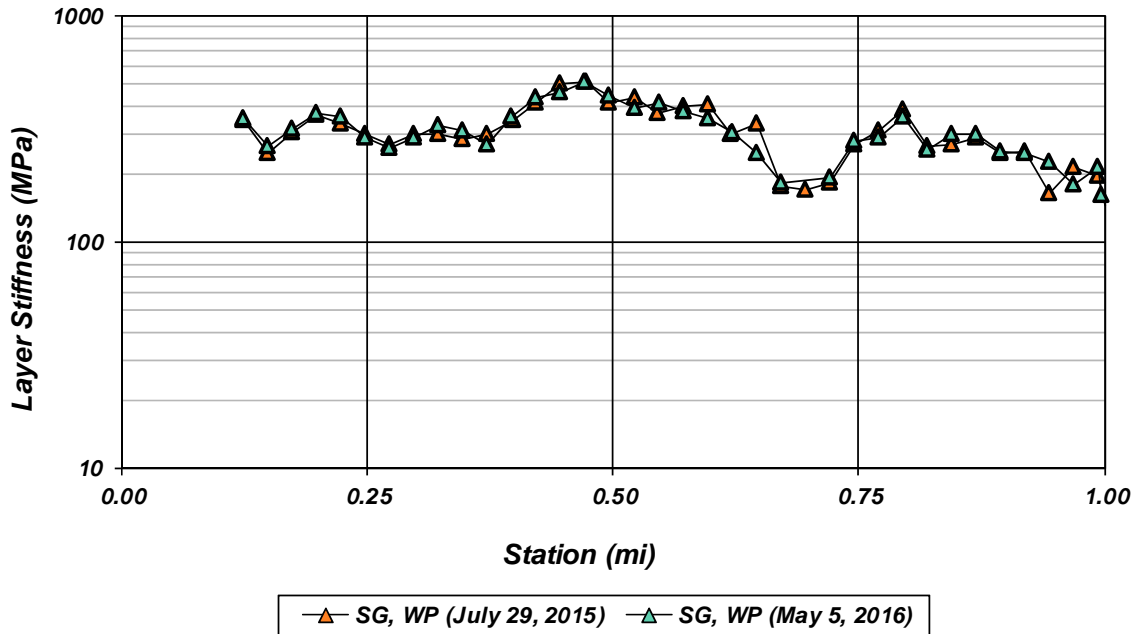


Figure 4.53: Santa Barbara 166 unbound layer stiffness in the wheelpath.

The backcalculation results indicate much stiffer FDR material than was typically seen at the rest of the sites; this finding is consistent with the intact cores obtained, which indicate intact and competent material that should have been stiffer than the more crumbled material at other sites. The material was generally stiffer in the wheelpath than between the wheelpaths; however this did not appear to be caused by the influence of overlying layers (Figure 4.54).

The stiffness of the unbound material was also high, which is consistent with the gravelly material encountered, and it shows slight variability along the length of the structure. Deflections were fairly constant in both the wheelpath and between the wheelpaths, indicative of consistent substructure conditions.

The fluctuations in the stiffness of the unbound material and FDR seem to correlate well with the surrounding environment; the stronger portions were located on the straight stretches where the road is in a cut portion while the weaker portions seemed to be confined to the stretch where the road crosses an abandoned river channel, which is likely comprised of fill material from the cut portions of the road.



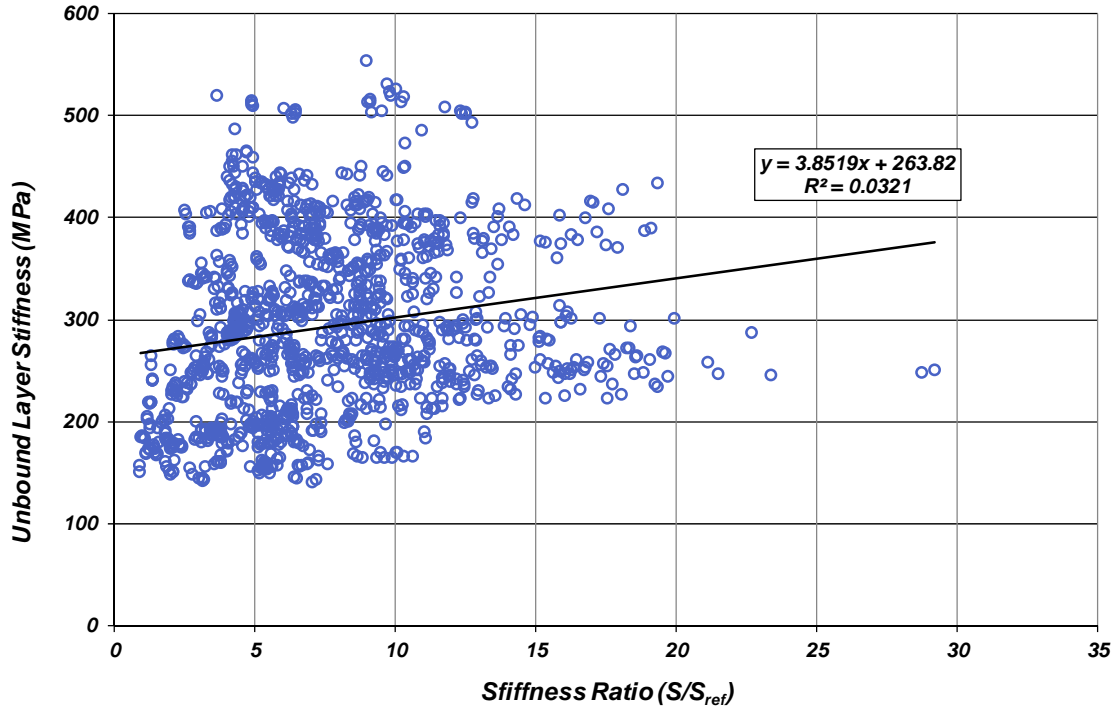


**Figure 4.54: Santa Barbara 166 overlying layer effect.**

(Note: *stiffness ratio* is the ratio of the bending stiffness of the layers above the unbound layer relative [S] to a reference stiffness [S<sub>ref</sub>], giving an indication of the confinement from those layers.)

#### 4.1.8 San Luis Obispo 46

Testing on San Luis Obispo 46 (SLO 46) took place on July 31, 2015 (Round 1) and May 3, 2016 (Round 2). The route is a heavily trafficked two-lane highway that serves as a connector road between US 101 at Paso Robles and Interstate 5 at Kettleman City. The center and outside lanes appeared to be milled and repainted, and the median and shoulders contained yellow grass that had slightly more green during the May 2016 testing than the July 2015 testing. Good drainage conditions existed at the site, with many drainage gates, pipes, and channels to remove water from the roadway to the shoulder. The land off to the sides of the highway contained several vineyards and side roads.



**Figure 4.55: Site and drainage conditions at San Luis Obispo 46 in May 2016.**

#### 4.1.8.1 Structure

The structure and construction history of the test site as indicated from various Caltrans plans and documents can be seen in Table 4.28 and the structure observed from coring and testing can be seen in Table 4.29. Coring results from PM 36.6 indicate a different structure than was anticipated from the plans; this is because Project 05-330724 extended from PM 36.6 to PM 41.2, which means that PM36.6-50ft would have a different structure. Overall, the structure observed from PM 37.6 was consistent with that listed in the Caltrans plans: two lifts of the HMA layer were distinguished and DCP testing revealed stiffer unbound material overlying the subgrade.

**Table 4.28: Structure from Caltrans Plans for San Luis Obispo 46**

EA Number	Construction Began	Construction Completed	Material	Thickness (mm)
05-330724	12/30/2010	10/9/2014	RHMA	45
			HMA (Type A)	183
			LCB	168
			Class 1 AS	320-630

**Table 4.29: Observed Structure for San Luis Obispo 46 (in mm)**

Material	PM 37.6+50ft			PM 36.6-50ft			Source
	July 31, 2015	May 3, 2016	Average	July 31, 2015	May 3, 2016	Average	
AC	53	53	53	45	45	45	Core
AC	132	99	116	86	83	85	
AC	58	92	75	105	114	110	
LCB	n/a	172	172	-	-	-	
Unbound	n/a	511	511	306	322	314	DCP
Unbound	n/a	Subgrade	-	n/a	Subgrade	-	



**Figure 4.56: Cores from San Luis Obispo 46.**  
(Note: all cores are upside down in the figures.)

#### 4.1.8.2 Unbound Material Properties

Unbound testing and sampling took place at PM 36.6 for both rounds of field testing while only DCPs were performed at PM 37.7. Partially intact lean concrete base (LCB) material could be obtained at PM 37.6, and as mentioned previously PM 36.6 had a different structure than the rest of the section. Results from DCP testing, moisture content testing, and USCS classification can be found in Figure 4.57. Median DCP values are summarized in Table 4.30.

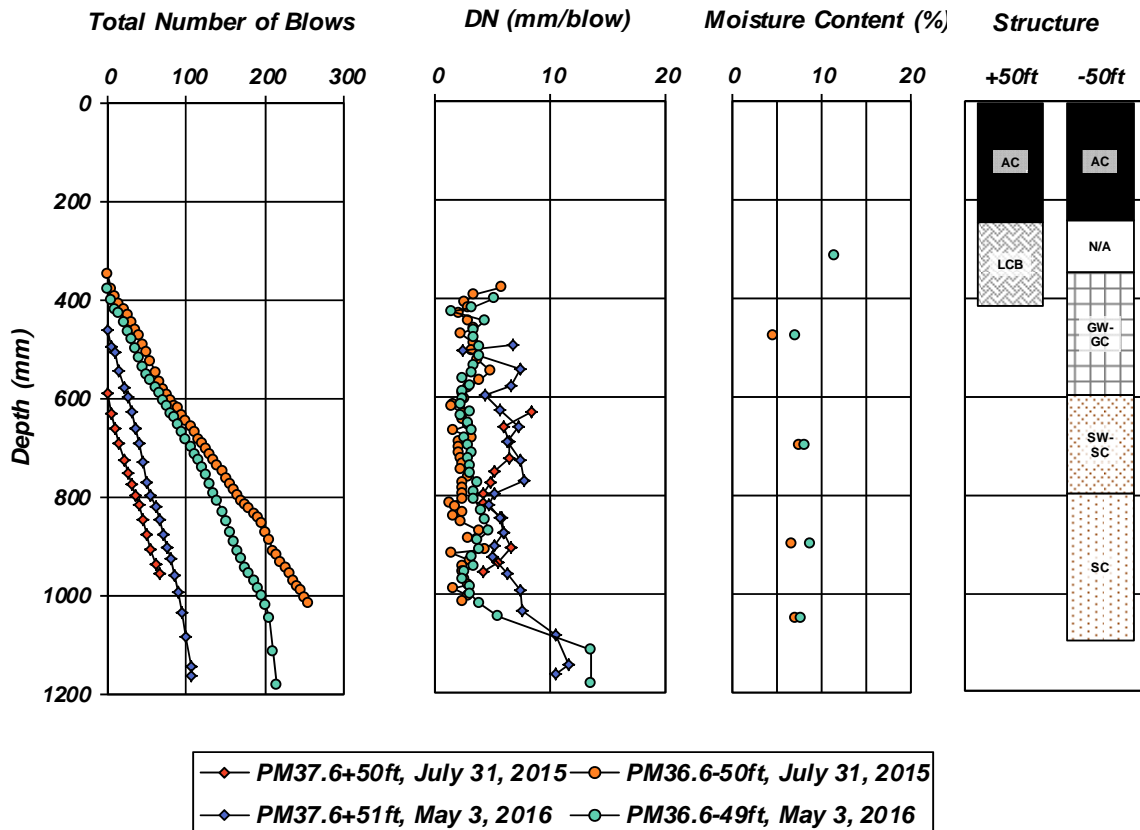


Figure 4.57: Unbound materials testing and sampling results for San Luis Obispo 46.

Table 4.30: Median DN (mm/blow) for San Luis Obispo 46

Material	DN PM 37.5+50ft		DN PM 36.5-50ft	
	July 31, 2015	May 3, 2016	July 31, 2015	May 3, 2016
LCB	n/a	n/a	n/a	n/a
Class 1 AS + Subgrade	5.8	6.0	2.4	3.2

The unbound material consisted of well-graded gravelly clay overlying orange-brown low-plasticity silty and clayey sand. The gravel material is most likely the subbase, as indicated by Caltrans plans and the silty and clayey sand is likely compacted natural material, since softer material is encountered at depths below 1,100 mm. Interestingly enough, *iVision* images from the Caltrans Automated Pavement Condition Survey (APCS) taken at the time were also taken while the section was being constructed, and they agree with this assumption. The moisture contents did not change substantially between the two rounds of testing, and penetration resistance decreased slightly.

#### 4.1.8.3 Falling Weight Deflectometer

Results from backcalculation analysis can be found in Figure 4.58 to Figure 4.61. Station 0 corresponds to PM 36.5 and Station 1 corresponds to PM 37.5. A summary of the results is found in Table 4.31. Caltrans plans indicate that while Project 05-330724 begins at PM 36.6, the LCB structure does not begin until PM 36.8. The backcalculated structure is representative of the LCB structure and PM 36.6 to 36.8 results have been omitted.

**Table 4.31: Backcalculated Stiffnesses for San Luis Obispo 46 (in MPa)**

Material	Thickness Used (mm)	Between Wheelpaths				Wheelpath			
		July 31, 2015		May 3, 2016		July 31, 2015		May 3, 2016	
		Average	Std. Dev.	Average	Std. Dev.	Average	Std. Dev.	Average	Std. Dev.
Asphalt-bound	240	7,889	2,743	11,185	3,927	5,989	1,070	10,422	3,024
LCB	170	7,826	3,150	9,044	3,888	6,841	3,563	8,083	5,326
Class 1 AS + Subgrade	0	222	36	228	36	217	32	238	36
Average Asphalt Temp (°C)		31.1		26.4		33.3		25.3	

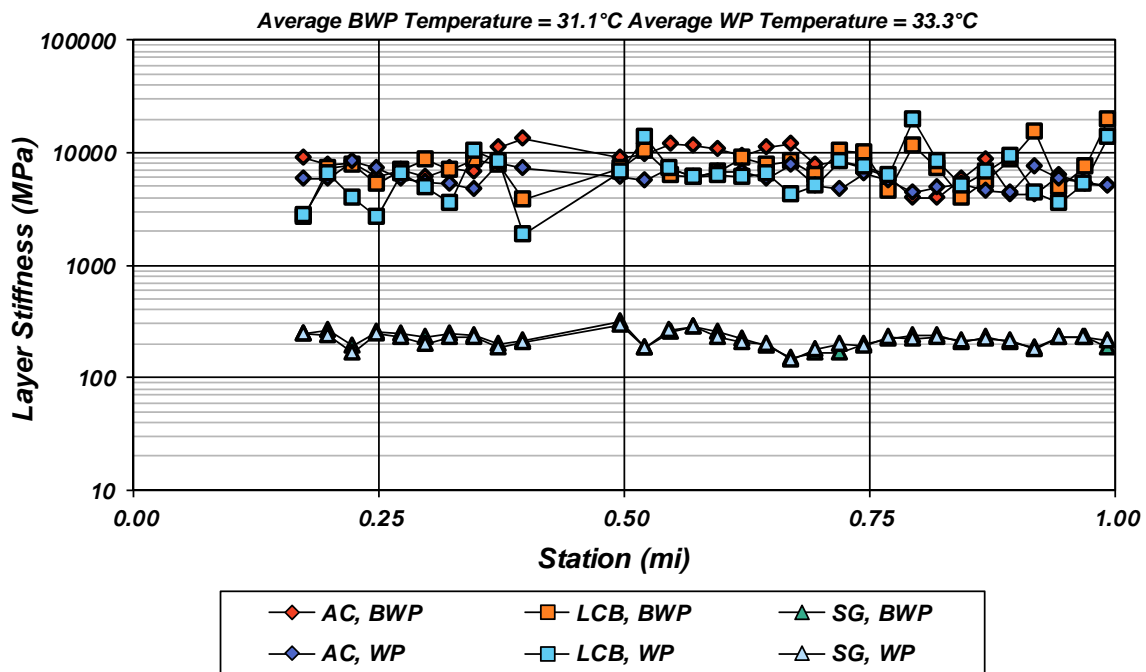


**Figure 4.58: San Luis Obispo 46 backcalculated stiffnesses, July 31, 2015.**

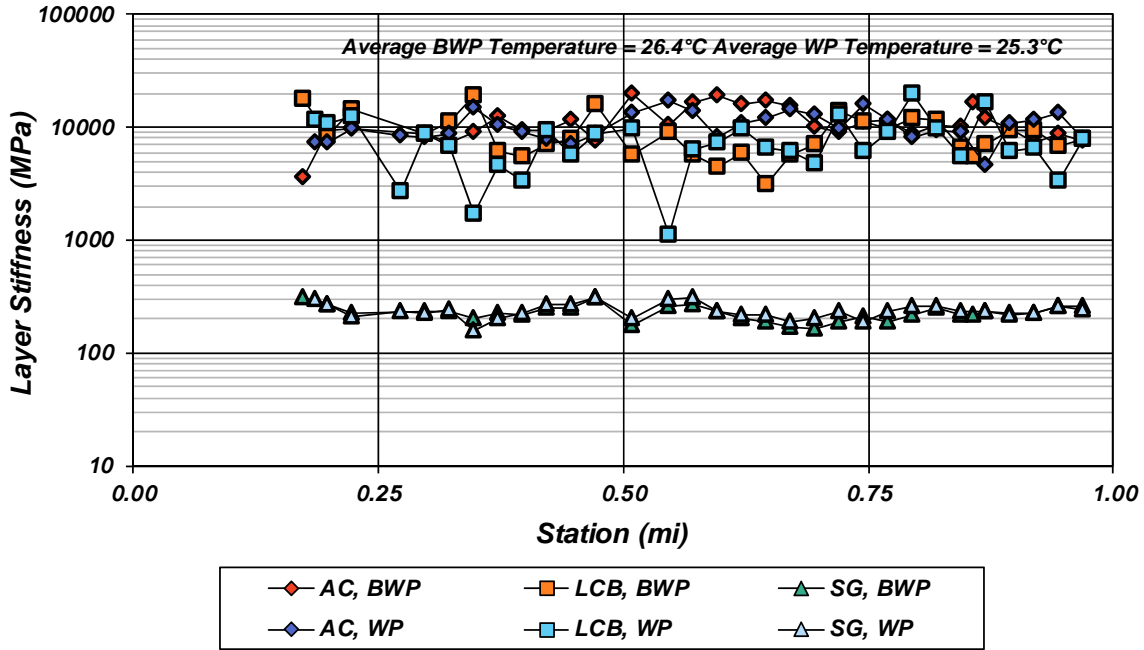


Figure 4.59: San Luis Obispo 46 backcalculated stiffnesses, May 3, 2015.

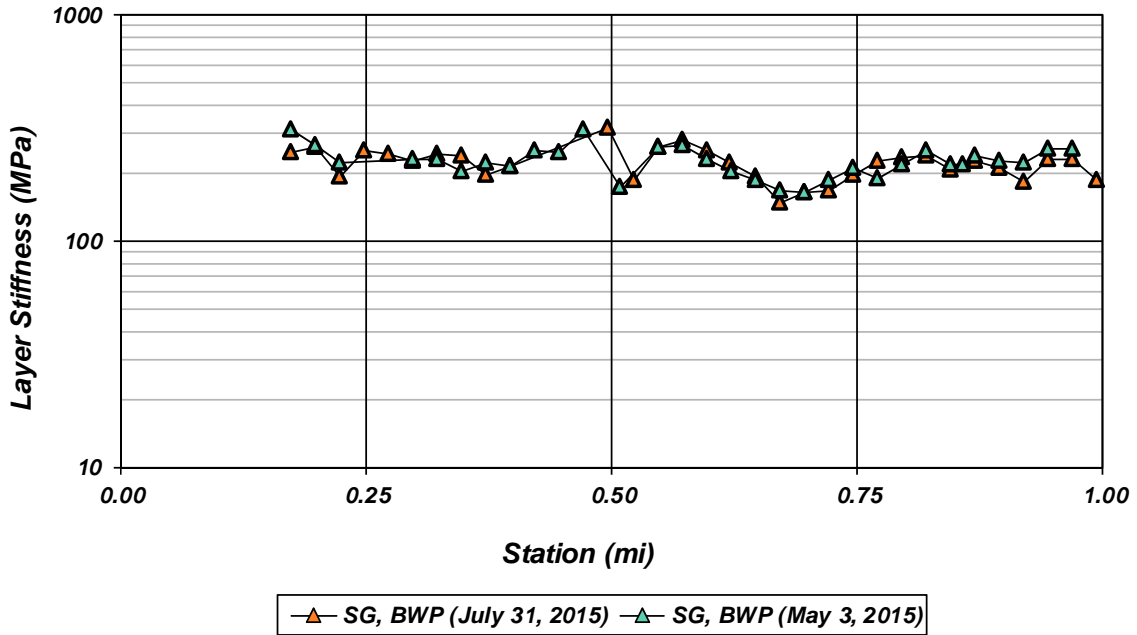
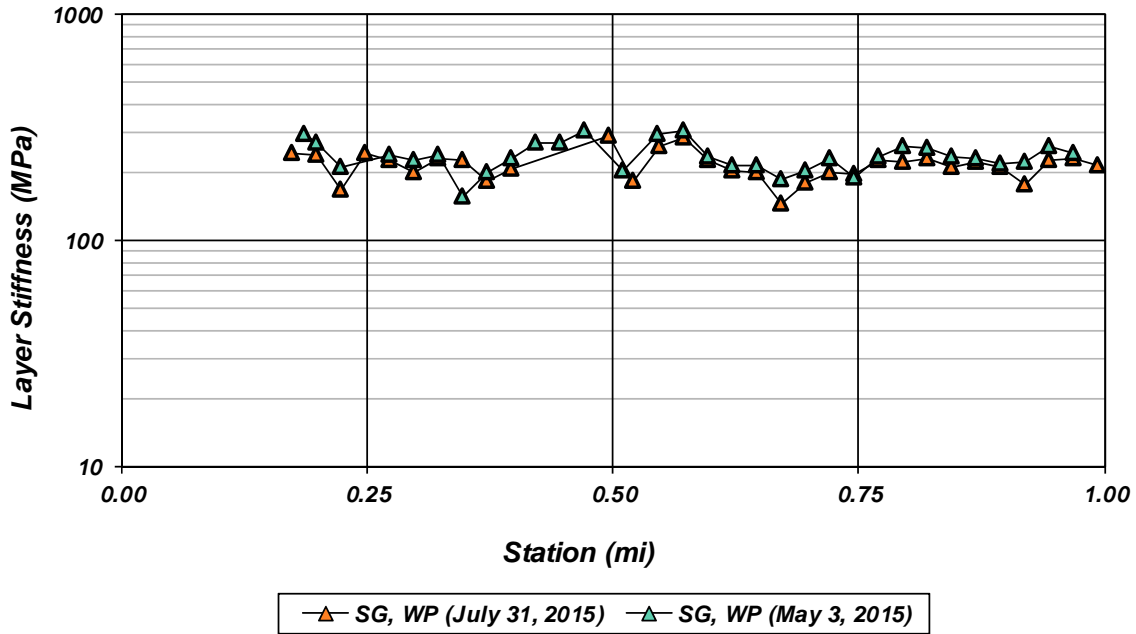
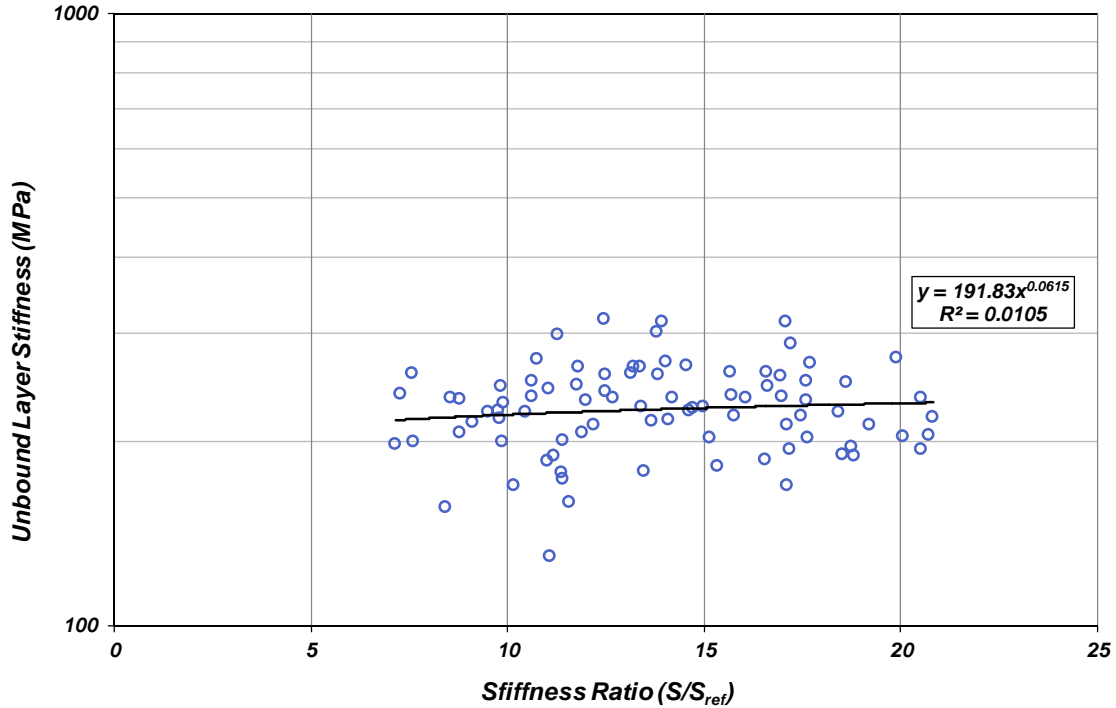


Figure 4.60: San Luis Obispo 46 unbound layer stiffnesses between the wheelpaths.



**Figure 4.61: San Luis Obispo 46 unbound layer stiffnesses in the wheelpath.**

The backcalculated stiffnesses reveal consistent results in both lateral locations as well as between testing rounds. The LCB stiffness is generally less in the wheelpath than between the wheelpaths and may indicate damage or could be a result of spatial variability. The unbound material stiffness fluctuated slightly along the length, most likely because the stretch of road consists of some cut portions and some fill portions where the thickness of subbase might vary. Seasonally there is hardly any difference in the stiffness of the unbound material between the wheelpaths and the slightly higher stiffnesses during the May 2016 testing of the material in the wheelpath. The material shows no relationship to the stiffness of the overlying layers (Figure 4.62), and it does not appear to be a significant enough difference to warrant further investigation.



**Figure 4.62: San Luis Obispo overlying layer effect.**

(Note: *stiffness ratio* is the ratio of the bending stiffness of the layers above the unbound layer relative [S] to a reference stiffness [S<sub>ref</sub>], giving an indication of the confinement from those layers.)

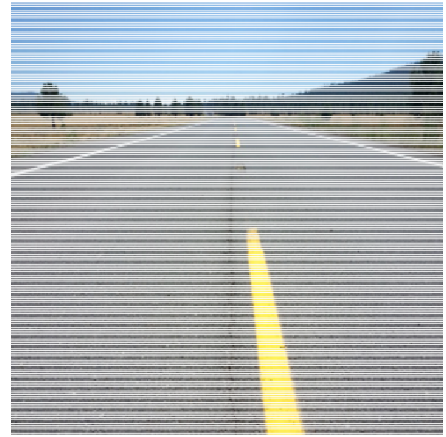
#### 4.1.9 Lassen 44

Testing and sampling at Lassen 44 (Las 44) took place on August 3, 2015 (Round 1) and April 21, 2016 (Round 2). The test road was located along a straight and flat portion of the highway, with sparse trees surrounding the area. The asphalt surface looked to be in fair condition; transverse cracks were observed in the shoulder and lanes, and lateral cracking was observed in the centerline; slight raveling was also observed (Figure 4.63). The road shifts from being slightly embanked to being even with the surrounding ground, with varying drainage conditions ranging from being distinct ditches to runoff slopes along the length. Drainage conditions were dry during the August 2015 testing and some standing water was observed along both the eastbound and westbound sides during the April 2016 testing (Figure 4.64).





(a)



(b)

**Figure 4.63: Surface conditions at Lassen 44 in August 2015.**



(a)



(b)

**Figure 4.64: Drainage conditions at Lassen 44 in (a) August 2015 and (b) April 2016.**

#### 4.1.9.1 Structure

The structure and construction history of the test site as indicated from various Caltrans plans and documents can be seen in Table 4.32 and the observed structure from coring and DCP testing can be found in Table 4.33. The observed structure matches well with that listed in the Caltrans plans, except no AB was observed over the pulverized material. The PAB seems to have variable thickness over the length, which is consistent with findings from Jeon (15).

**Table 4.32: Structure from Caltrans Plans for Lassen 44**

EA Number	Construction Began	Construction Completed	Material	Thickness (mm)
02-3E0204	2/22/2011	8/19/2011	AC (Overlay)	30
02-325804	12/31/2003	9/2/2005	AC	135
			AB (Class 2)	0-770
			PAB	270

**Table 4.33: Observed Structure for Lassen 44 (in mm)**

Material	PM 10.5+50ft			PM 9.5-50ft			Source
	August 3, 2015	April 21, 2016	Average	August 3, 2015	April 21, 2016	Average	
AC	20	21	21	25	24	25	Core
	47	45	46	40	44	42	
	40	41	41	45	44	45	
	48	50	49	55	54	55	
PAB	237	190	214	215	237	226	DCP
Unbound	191	156	174	240	246	243	
	325	336	331	305	383	344	
	Subgrade	Subgrade	-	Stiff	Stiff	-	

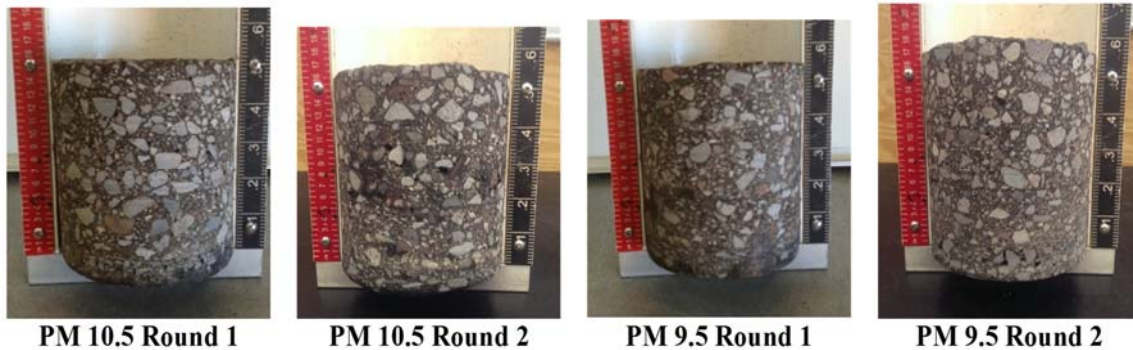


**Figure 4.65: Cores from Lassen 44.**  
 (Note: all cores are upside down in the figures).

**4.1.9.2 Unbound Material Properties**

Unbound testing and sampling was performed at both coring locations during both rounds of testing. While sufficient material was obtained to perform all soils tests, the material passing the #40 sieve slipped in the Casagrande device while testing and the liquid limit could not be determined. Results from DCP testing, moisture content testing, and USCS classification can be found in Figure 4.66. Median DCP values are summarized in Table 4.34.

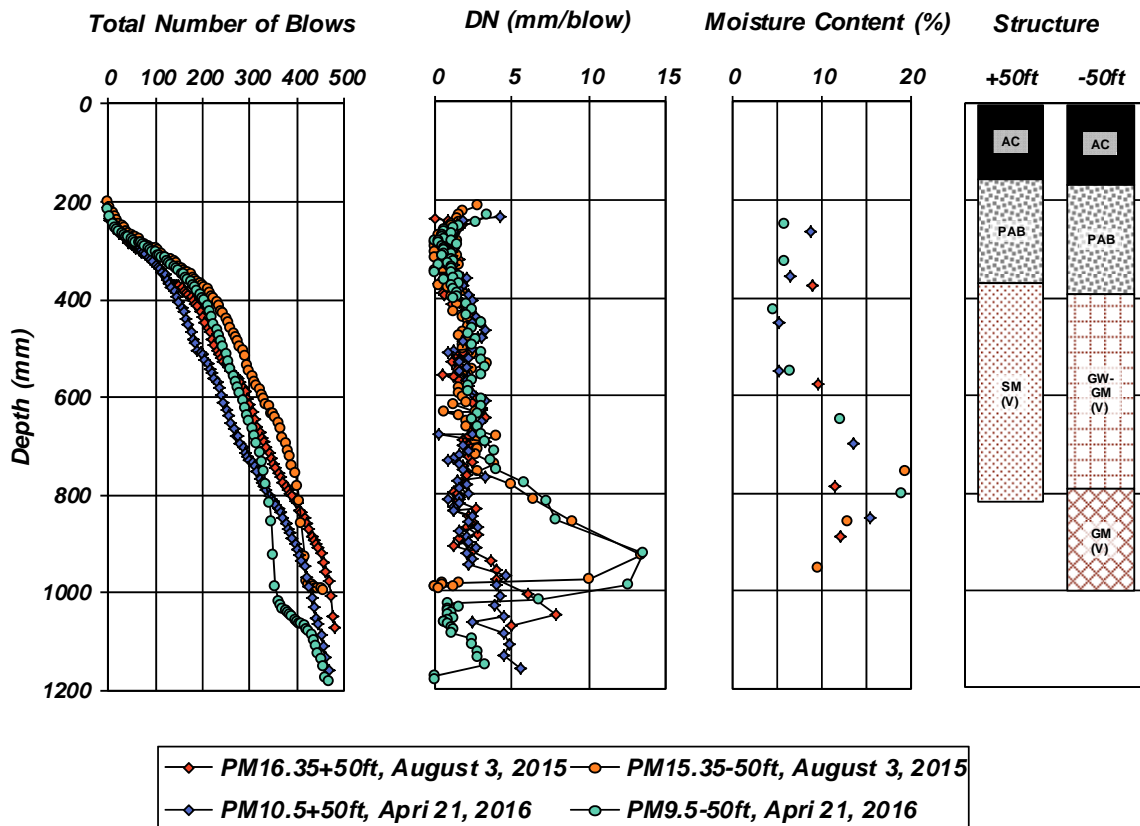


Figure 4.66: Unbound materials testing and sampling results for Lassen 44.

Table 4.34: Median DN (mm/blow) for Lassen 44

Material	DN PM 10.5+50ft		DN PM 9.5-50ft	
	August 3, 2015	April 21, 2016	August 3, 2015	April 21, 2016
PAB	0.8	1.0	0.8	0.7
Unbound	2.0	2.2	2.0	2.4

The unbound materials at the site consisted of pulverized asphalt base overlying well-graded silty gravels and silty sands. The silty sand and gravel were volcanic in nature, and at the specific sampling locations were most likely compacted in situ material. Resistance to penetration was fairly consistent with depth for both locations, and showed minor changes seasonally. Penetration resistance decreased in the silty gravel material encountered at PM 9.5 and then increased as much stiffer material was encountered. This silty gravel also had consistently higher moisture contents than the shallower materials. Moisture contents were slightly higher during Round 2 of testing for both locations.

### 4.1.9.3 Falling Weight Deflectometer

Results from backcalculation can be found in Figure 4.67 to Figure 4.70. Station 0 corresponds with PM 10.5 while Station 1 corresponds to PM 9.5. A summary of the results can be found in Table 4.35.

**Table 4.35: Backcalculated Stiffnesses for Lassen 44 (in MPa)**

Material	Thickness Used (mm)	Between Wheelpaths				Wheelpath			
		August 3, 2015		April 21, 2016		August 3, 2015		April 21, 2016	
		Average	Std. Dev.	Average	Std. Dev.	Average	Std. Dev.	Average	Std. Dev.
AC	160	1,867	390	3,042	688	2,810	519	4,387	842
PAB	225	396	124	345	118	256	98	225	108
Unbound	0	278	52	261	49	257	45	245	42
Average Asphalt Temp (°C)		37.5		22.7		34.0		19.5	

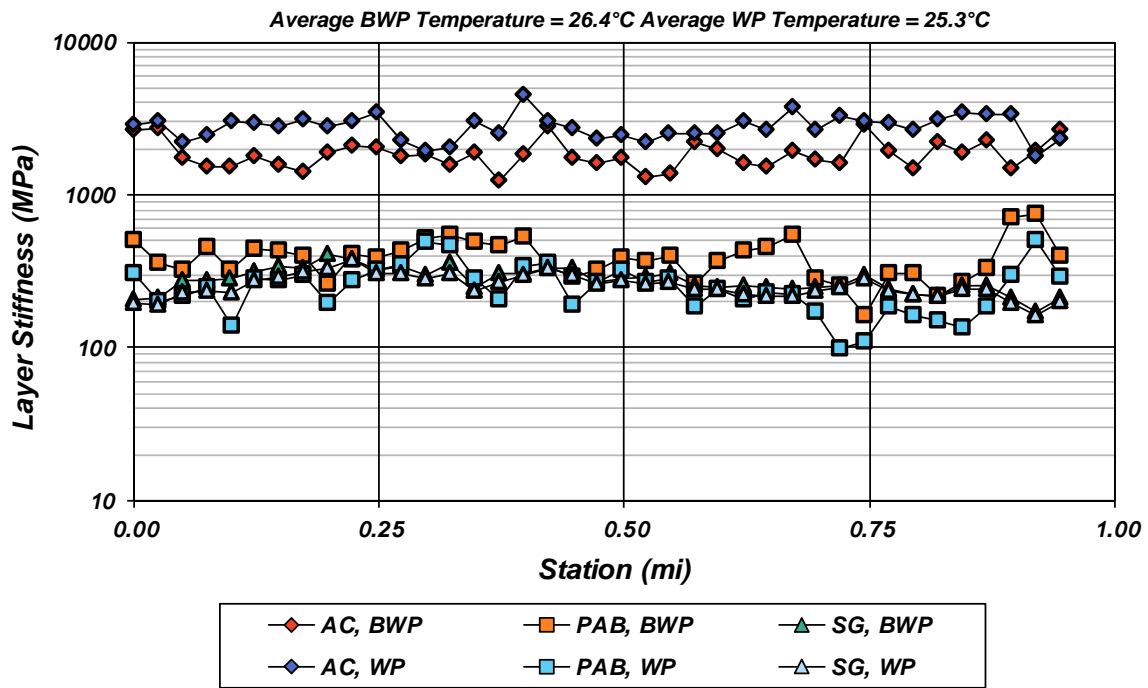


**Figure 4.67: Lassen 44 backcalculated stiffnesses, August 3, 2015.**

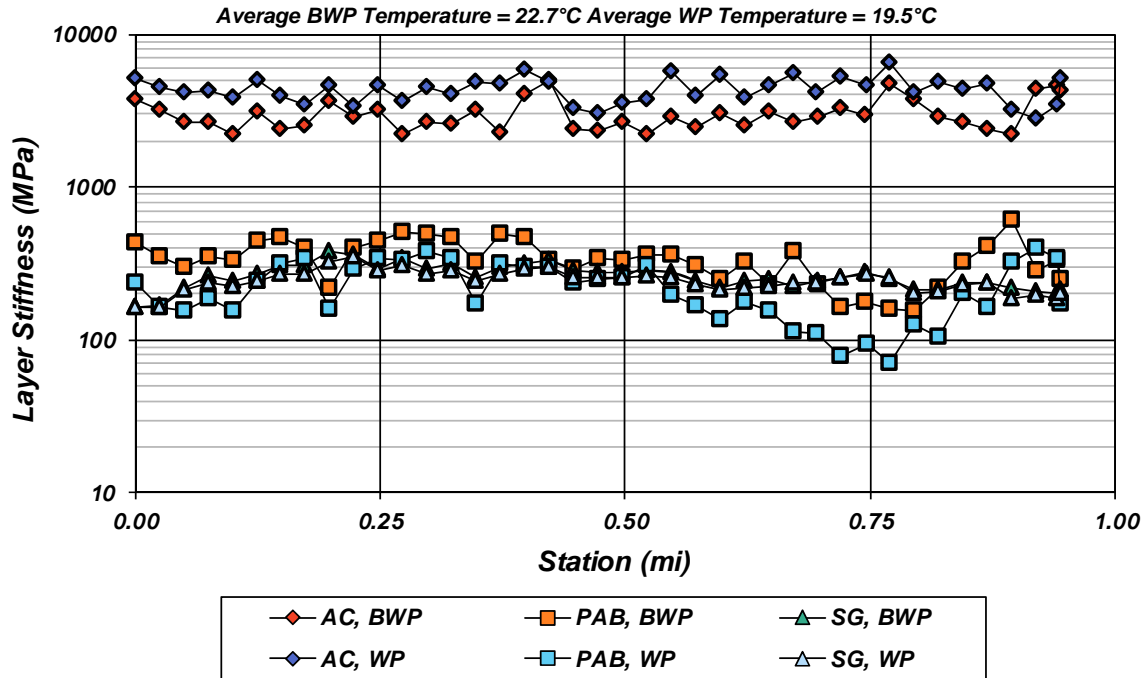


Figure 4.68: Lassen 44 backcalculated stiffnesses, April 21, 2016.

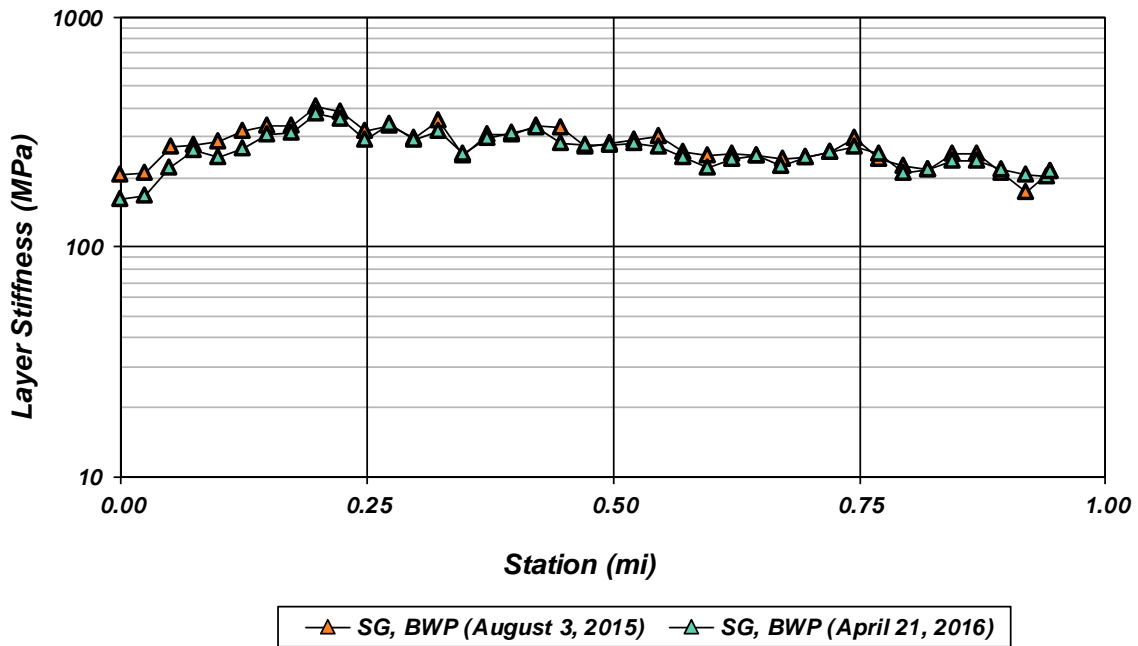


Figure 4.69: Lassen 44 unbound layer stiffness between the wheelpaths.

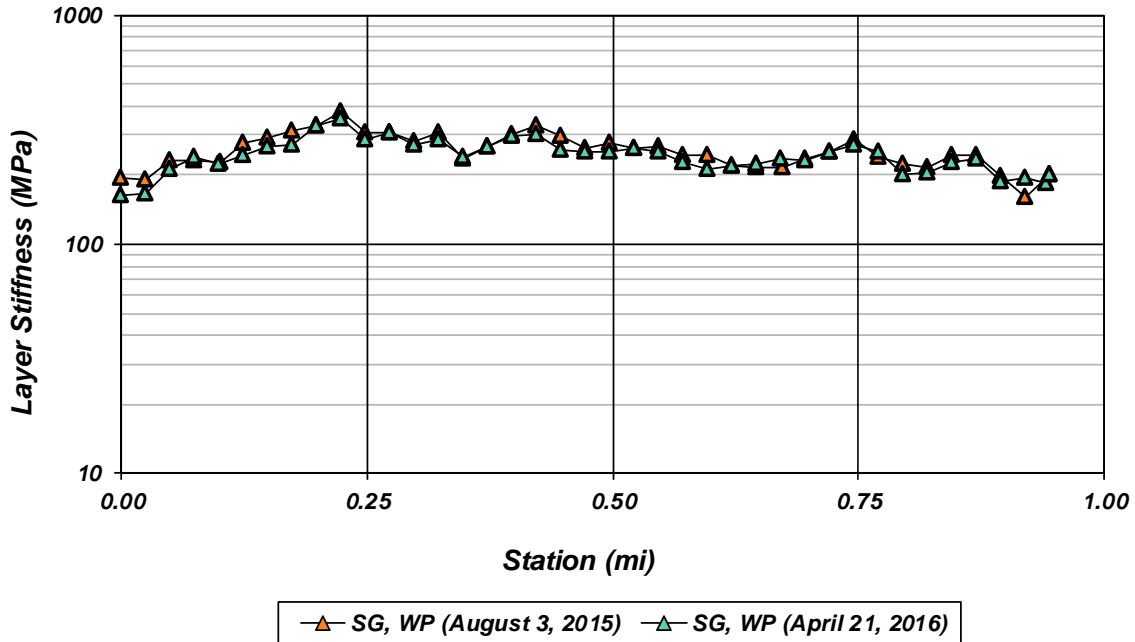
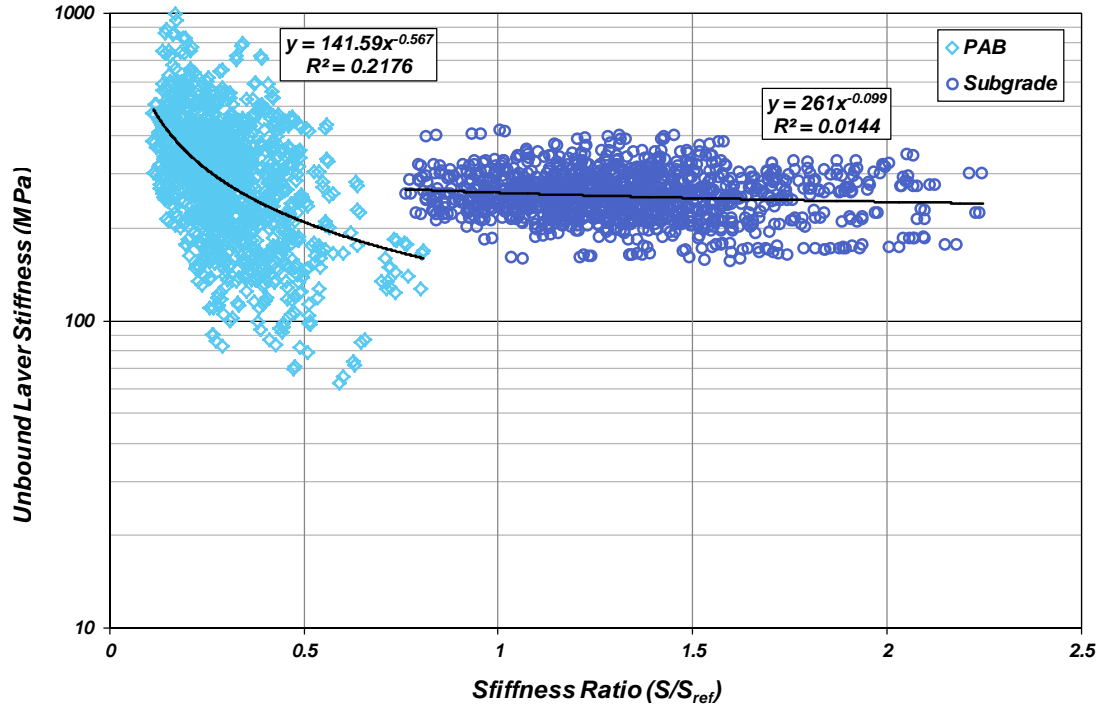


Figure 4.70: Lassen 44 unbound layer stiffnesses in the wheelpath.

Subgrade material stiffnesses were consistently less in the wheelpath than between the wheelpaths and were slightly lower in April 2016. Subgrade material stiffness showed no relationship to overlying layer stiffness (Figure 4.71) and given the drainage conditions observed, this decrease in stiffness between the rounds is likely a result of increased saturation of the material; the largest disparities in stiffness between the two rounds occurred closer to PM 10.5 where standing water was observed. The PAB stiffness followed a similar trend and is substantially lower in the wheelpath than between the wheelpaths regardless of the asphalt temperatures, which were substantially different in 2015 and 2016, and it is not certain why this occurred. Regression analyses revealed that the PAB stiffness may decrease as overlying stiffness increases, which might explain why the material was somewhat less stiff when colder temperatures increased asphalt stiffness in 2016 compared with 2015. The effects of the stiffness of the overlying layers on the PAB stiffness were much less than the difference between the wheelpath and between the wheelpath PAB stiffnesses.



**Figure 4.71: Lassen 44 overlying layer effect.**

(Note: *stiffness ratio* is the ratio of the bending stiffness of the layers above the unbound layer relative [S] to a reference stiffness [S<sub>ref</sub>], giving an indication of the confinement from those layers.)

#### 4.1.10 Modoc 395

Testing and sampling at Modoc 395 (Mod 395) took place on August 4, 2015 (Round 1) and April 20, 2016 (Round 2). The specific section of US Route 395 is on a fairly straight stretch with minor curves that was situated above marshland. The route is generally on the cut portion of the road and winds through a few portions where the entire road is located in a slope cut. The surface appeared to be in fair condition (Figure 4.72a), although raveling and smaller transverse cracks were observed in the wheelpaths (Figure 4.72b). The road has a moderately high shoulder with minor or no drainage ditches on either side; sparse vegetation and desert shrubs are scattered along the road and surround area that were notably greener in April 2016.





(a)



(b)

**Figure 4.72: Site conditions at Modoc 395.**

#### 4.1.10.1 Structure

The structure and construction history of the test site as indicated from various Caltrans plans and documents are shown in Table 4.36, and the observed structure from coring and DCP testing can be found in Table 4.37. The observed structure matches well with that provided in the Caltrans plans. The PAB thickness fluctuates slightly over the course of the section.

**Table 4.36: Structure from Caltrans Plans for Modoc 395**

EA Number	Construction Began	Construction Completed	Material	Thickness (mm)
02-1E3204	8/17/09	12/29/2010	Chip Seal	n/a
02-360314	n/a	10/10/2001	AC	150
			PAB	200
			AB	0-100



**Table 4.37: Observed Structure for Modoc 395 (in mm)**

Material	PM 14.5+50ft			PM 13.5-50ft			Source
	August 4, 2015	April 20, 2016	Average	August 4, 2015	April 20, 2016	Average	
Chip Seal	4.25	10	7	5	10	8	Core
AC	160	162	161	180	135	158	
PAB	Inconclusive	172	172	Inconclusive	197	197	DCP
Unbound	-	-	-	56	51	54	
Unbound	204	203	204	202	205	204	
Unbound	Subgrade	Subgrade	-	Subgrade	Subgrade	-	



**Figure 4.73: Cores for Modoc 395.**  
*(Note: all cores are upside down in the figures.)*

#### 4.1.10.2 Unbound Material Properties

Unbound materials testing and sampling occurred at both locations, PM 13.5 and PM 14.5, for both rounds of testing. In August 2015, DCPs were started deeper, after excavating the PAB, which made evaluation of the pavement structure difficult to infer; fortunately full-depth DCPs were performed in April 2016 to bridge this gap. Results from DCP testing, moisture content testing, and USCS classification can be seen in Figure 4.74. Median DCP values are summarized in Table 4.38.

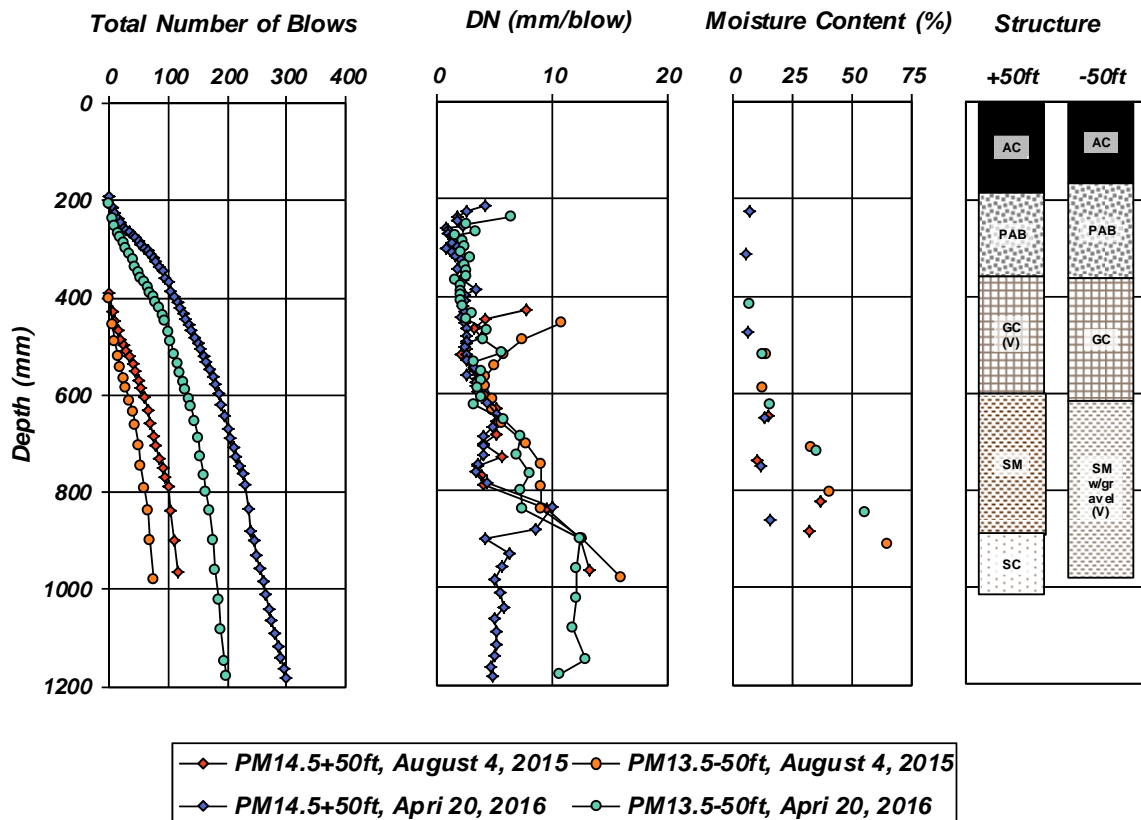


Figure 4.74: Unbound materials testing and sampling results for Modoc 395.

Table 4.38: Median DN (mm/blow) for Modoc 395

Material	DN PM 14.5+50ft		DN PM 13.5-50ft	
	August 4, 2015	April 20, 2016	August 4, 2015	April 20, 2016
PAB	n/a	1.8	n/a	2.5
Unbound	4.0	3.4	7.4	3.8

The unbound material consisted of clayey gravel underlain by silt. The silt proved to be the most unusual soil encountered during testing as it had seemingly normal resistance to penetration but astoundingly high moisture contents. The material at the shoulder was dry and desiccated, and when handled it was found to be very soft and light. Further investigation revealed that the surrounding soil is derived from igneous rocks, tuff, and pyroclastic material that formed in an ancient lake bed, and that these materials can often hold substantial amounts of water. The clayey gravel encountered had low plasticity and is most likely aggregate subbase.

The penetration resistance was fairly consistent for both locations, and penetration resistance decreased slightly from August 2015 to April 2016. At PM 13.5, a softer layer was encountered at about 900 mm whereas at PM 14.5, a soft seam appeared to have been encountered before returning to stiffer material. The moisture contents

tended to increase with depth: it did not change much at PM 13.5 between the two rounds of testing and at PM 14.5 was slightly higher in August 2015 than April 2016.

#### 4.1.10.3 Falling Weight Deflectometer

Results from backcalculation analysis can be found in Figure 4.75 to Figure 4.78. Station 0 corresponds to PM 36.5 and Station 1 corresponds to PM 37.5. A summary of the results is found in Table 4.39.

**Table 4.39: Backcalculated Stiffnesses (MPa) for Modoc 395 (in MPa)**

Material	Thickness Used (mm)	Between Wheelpaths				Wheelpath			
		August 4, 2015		April 20, 2016		August 4, 2015		April 20, 2016	
		Average	Std. Dev.	Average	Std. Dev.	Average	Std. Dev.	Average	Std. Dev.
AC	160	6,239	1,735	10,407	2,535	6,507	2,746	9,991	4,585
PAB	200	410	344	364	357	277	240	236	213
Unbound	0	129	15	133	20	123	14	126	17
Average Asphalt Temp (°C)		33.8		23.1		26.8		19.2	

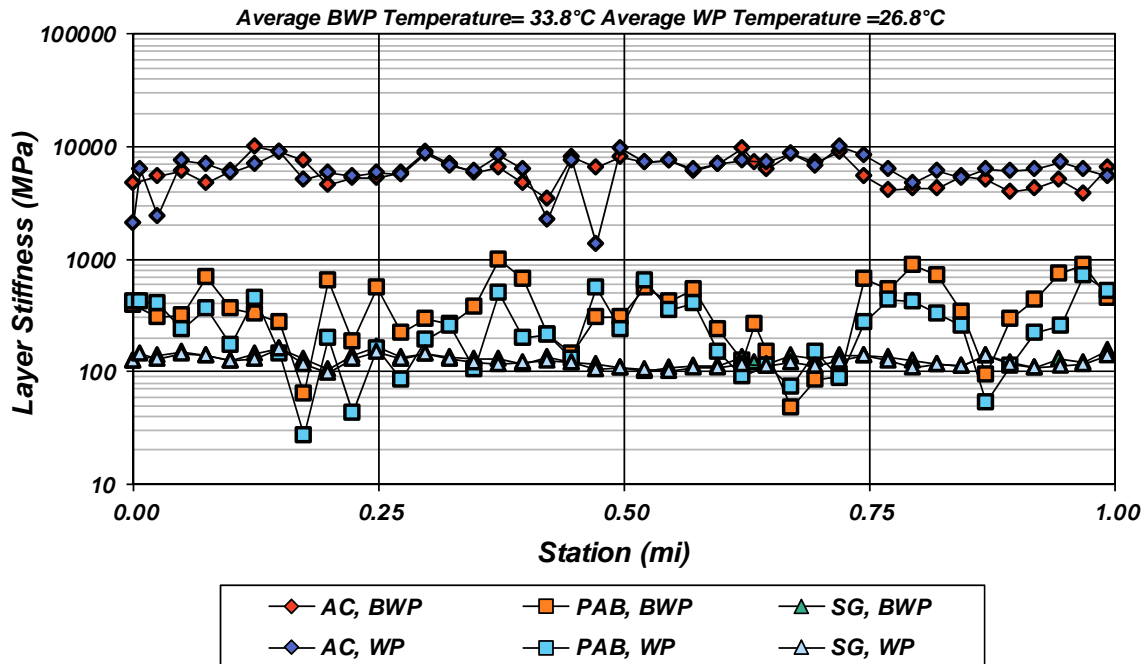


**Figure 4.75: Modoc 395 backcalculated stiffnesses, August 4, 2015.**

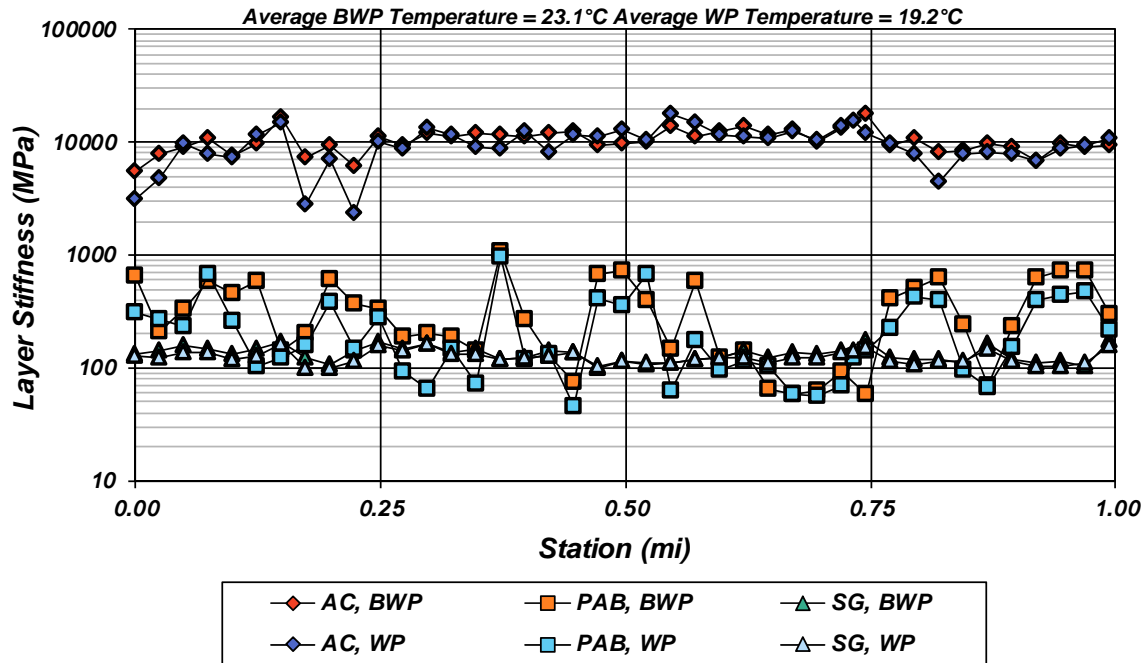


Figure 4.76: Modoc 395 backcalculated stiffnesses, April 20, 2016.

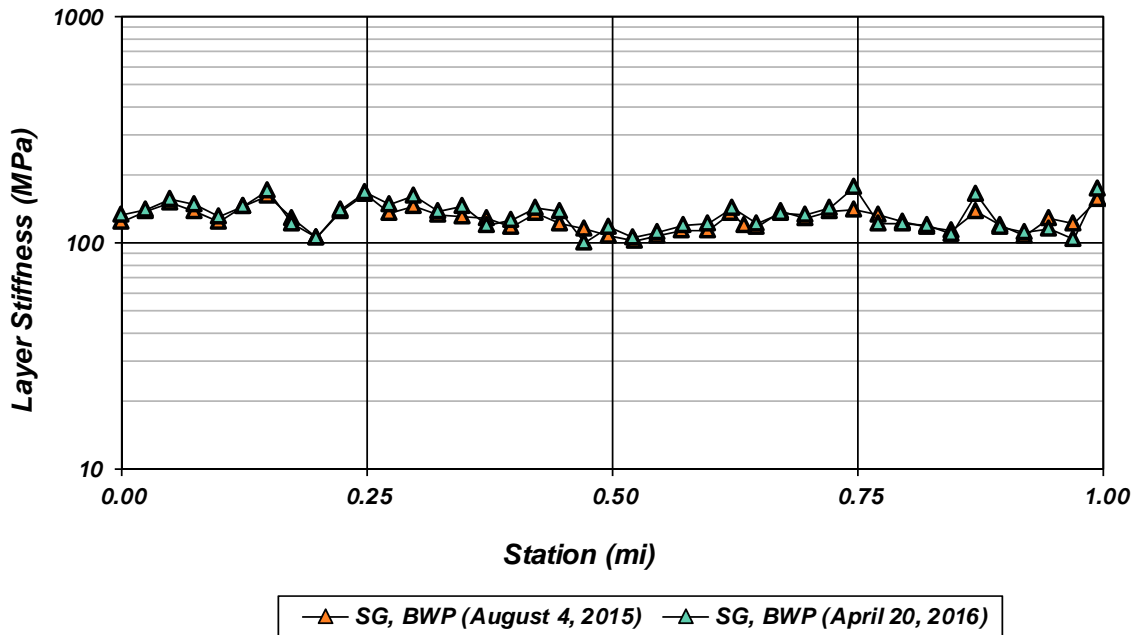
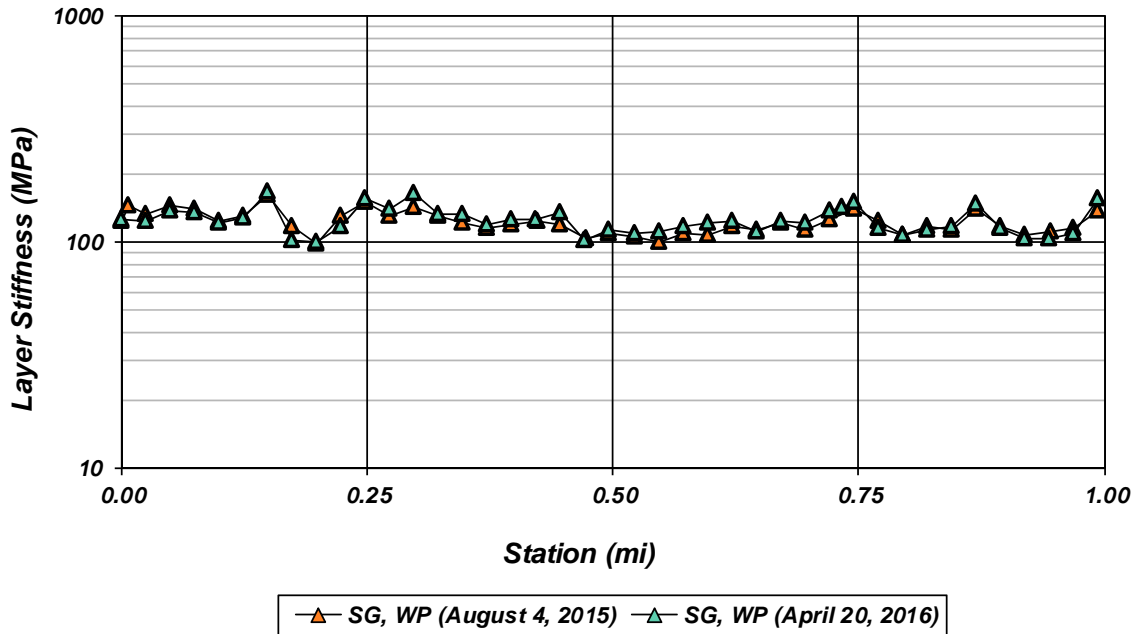


Figure 4.77: Modoc 395 unbound layer stiffnesses between the wheelpaths.



**Figure 4.78: Modoc 395 unbound layer stiffnesses in the wheelpath.**

The stiffness of the PAB material fluctuated along the length, and was consistently lower in the wheelpath and in April 2016. Similar to Lassen 44, the PAB material stiffness likely decreased in April 2016 due to environmental influences and increased rainfall, while the wheelpath material is likely weaker because of densification and fatigue decreasing the resistance to deformation.

The subgrade material stiffness and deflections changed little between the two rounds of testing and were very consistent along the length of the section. There appeared to be no relationship between either of the unbound materials and the overlying layer stiffness (Figure 4.79), and hence changes in stiffness are likely to have been caused by traffic-induced loading, the environment, and spatial variability.

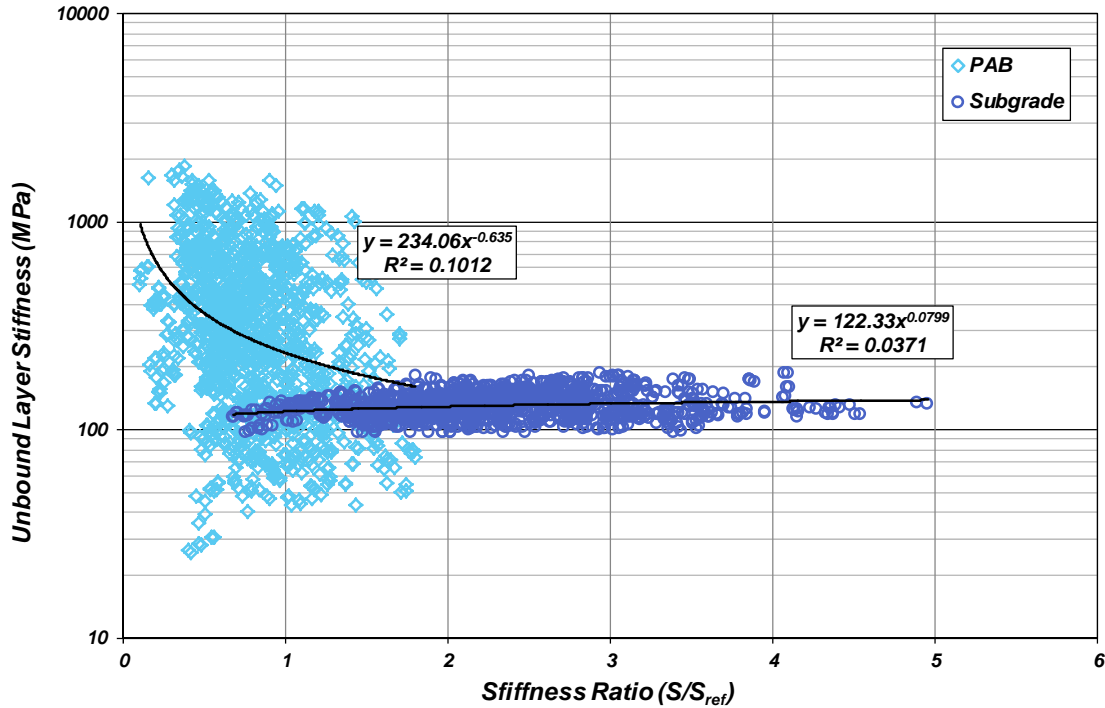


**Figure 4.79: Modoc 395 overlying layer effect.**

(Note: *stiffness ratio* is the ratio of the bending stiffness of the layers above the unbound layer relative [S] to a reference stiffness [S<sub>ref</sub>], giving an indication of the confinement from those layers.)

#### 4.1.11 Modoc 299

Testing and sampling at Modoc 299 (Mod 299) took place on August 8, 2015 (Round 1) and April 4, 2016 (Round 2). The road is an embankment road that serves as a causeway over Middle Alkali Lake near Cedarville and the California–Nevada border. In August 2015, the lake was completely dry and desiccated, and in April 2016 water was present on both sides of the road in the morning and evaporated as the day progressed (Figure 4.80). The surface conditions of the road were fairly good, with minor cracking observed. The road has hardly any asphalt shoulder, and the embankment material is widely variable with some vegetation along the slope and at the base.



(a)



(b)

**Figure 4.80: Middle Alkali Lake next to Modoc 299 during testing in August 2015 (a) and April 2016 (b).**

#### 4.1.11.1 Structure

The structure and construction history of the test site as indicated from various Caltrans plans and documents can be seen in Table 4.40, and the observed structure from coring and DCP testing can be seen in Table 4.41. The observed structure matches well with that provided by Caltrans Figure 4.81.

**Table 4.40: Structure from Caltrans Plans for Modoc 299**

EA Number	Construction Began	Construction Completed	Material	Thickness (mm)
02-4E2404	9/6/2011	10/31/2011	AC	91
			FDR-PC	183

*Note:* FDR-PC is full-depth reclamation with cement stabilization, in this case 1% cement.

**Table 4.41: Observed Structure for Modoc 299 (in mm)**

Material	PM 60.5+50ft			PM 59.5-50ft			Source
	August 5, 2015	April 19, 2016	Average	August 5, 2015	April 19, 2016	Average	
AC	101	100	101	93	90.5	92	Core
FDR-PC	180	182	181	169	163	166	DCP
Unbound	142	142	142	582	325	454	
Unbound	300	331	316	-	432	432	
Unbound	307	319	313	-	-	-	
Unbound	Subgrade	Subgrade	-	Subgrade	Subgrade	Subgrade	



**Figure 4.81: Cores for Modoc 299.**  
(Note: all cores are upside down in the figures.)

#### 4.1.11.2 Unbound Material Properties

DCP testing, moisture content evaluation, and USCS classification were performed at the two coring locations, PM 60.5 and PM 59.5, for both rounds of testing. Results from unbound material testing and sampling can be found in Figure 4.82. Median DCP values are summarized in Table 4.42.

The unbound materials encountered at the site consisted of clayey gravel and clayey sands with gravel, and were assumed to be imported base and/or subbase material that were used to construct the embankment. The moisture content increased slightly with depth and was slightly lower in April 2016 than August 2015, despite the presence of the lake. In August 2015, the deeper material was notably warm, which is likely a result of geothermal activity in the area. Material penetration resistance was variable with depth, which would be expected of imported granular material. Penetration resistance was slightly lower in April 2016 than August 2015, and was generally greater at PM 59.5 than at PM 60.5.



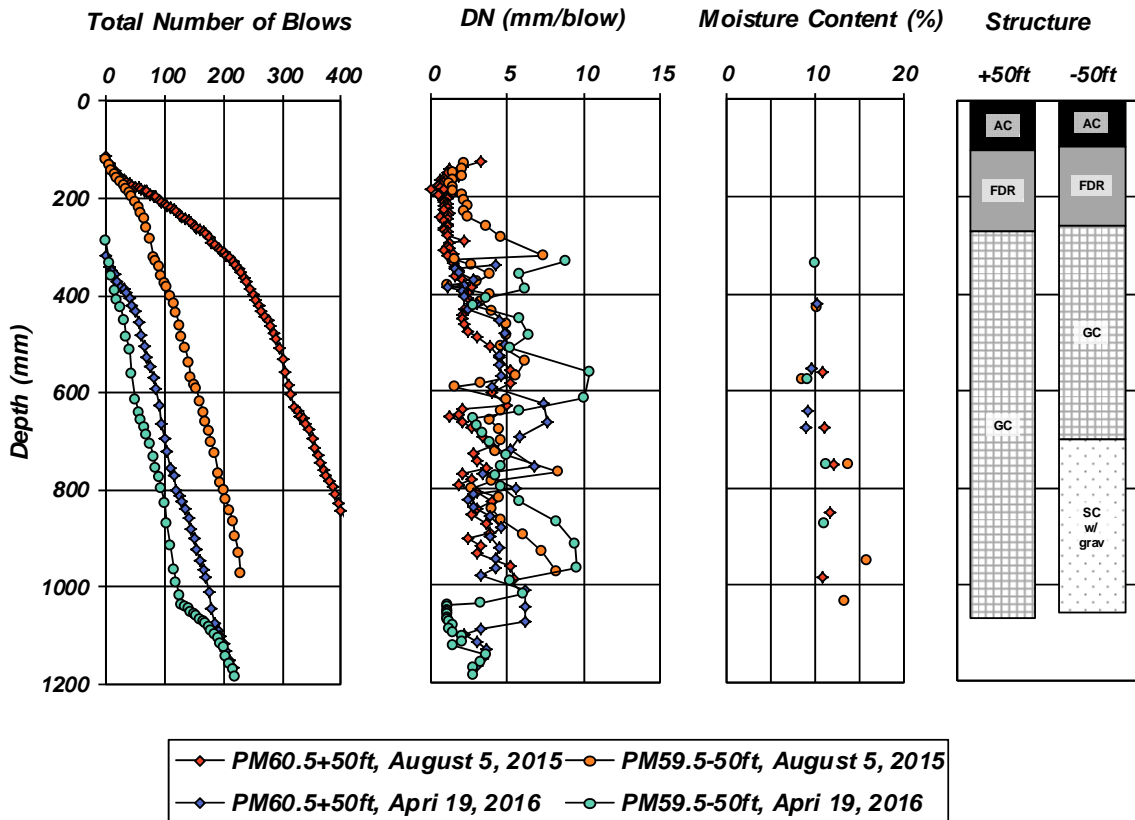


Figure 4.82: Unbound materials testing and sampling results for Modoc 299.

Table 4.42: Median DN (mm/blow) for Modoc 299

Material	DN PM 60.5+50ft		DN PM 59.5-50ft	
	August 5, 2015	April 19, 2016	August 5, 2015	April 19, 2016
FDR-PC	1.0	n/a	1.7	n/a
Unbound	1.7	3.9	3.9	5.2

### 4.1.11.3 Falling Weight Deflectometer

Results from the backcalculation analysis can be seen in Figure 4.83 to Figure 4.86. Station 0 corresponds to PM 59.5 and Station 1 corresponds to PM 60.5. A summary table is shown below in Table 4.43.

**Table 4.43: Backcalculated Stiffnesses (MPa) for Modoc 299 (in MPa)**

Material	Thickness Used	Between Wheelpaths				Wheelpath			
		August 5, 2015		April 19, 2016		August 5, 2015		April 19, 2016	
	mm	Average	Std. Dev.	Average	Std. Dev.	Average	Std. Dev.	Average	Std. Dev.
AC	100	6,146	2,375	7,896	3,171	7,840	2,566	10,957	4,373
FDR-PC	175	351	335	238	280	436	737	183	246
Unbound	0	200	32	190	21	191	23	191	21
Average Asphalt Temp (°C)		27.2		27.4		26.8		22.3	

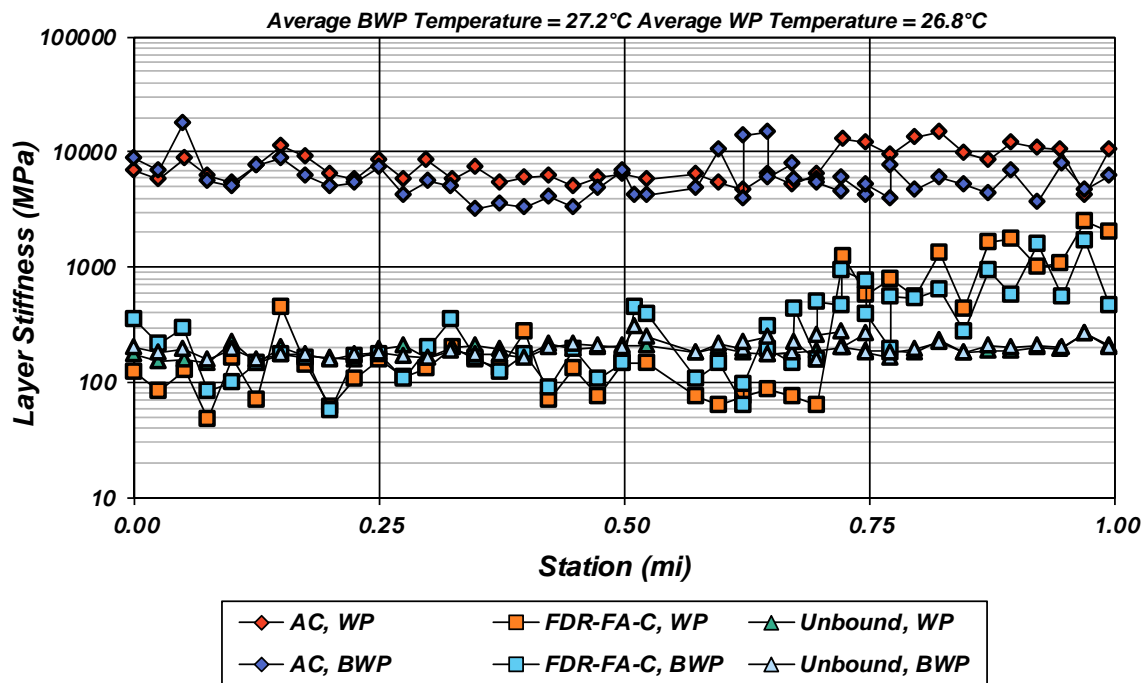


**Figure 4.83: Modoc 299 backcalculated stiffnesses, August 5, 2015.**

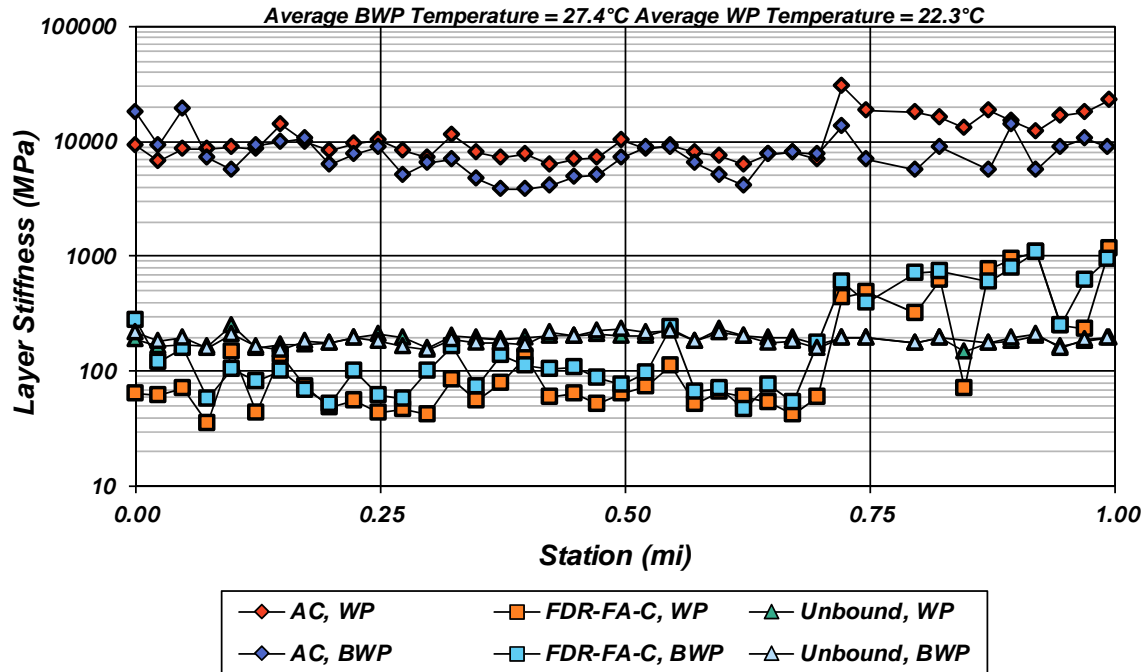


Figure 4.84: Modoc 299 backcalculated stiffnesses, April 19, 2016.

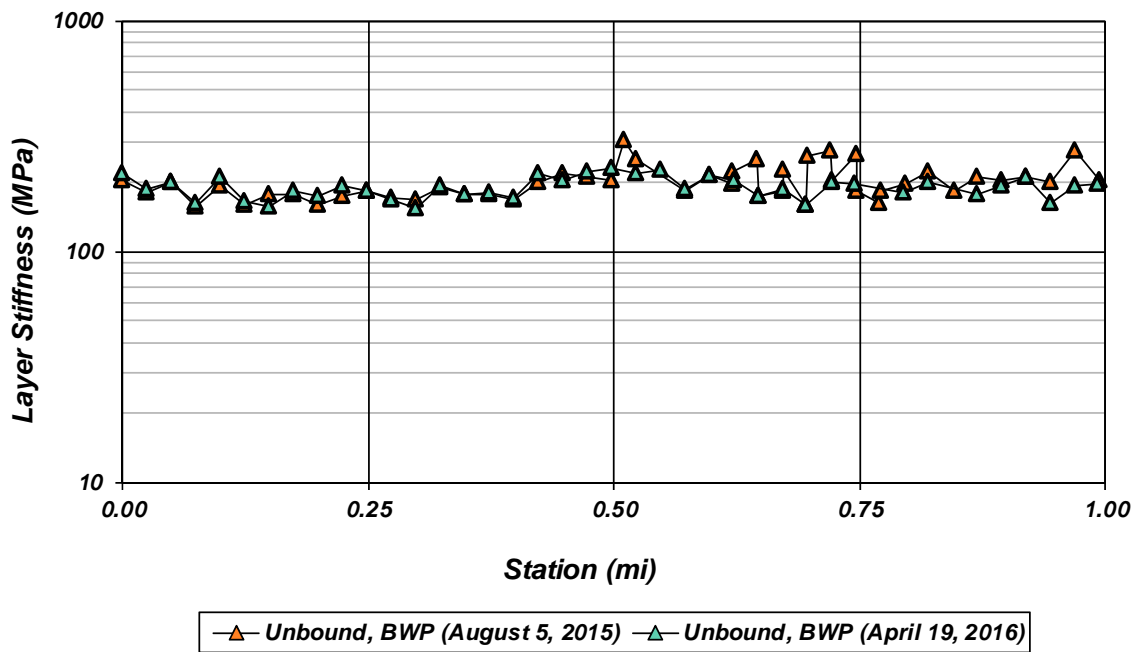
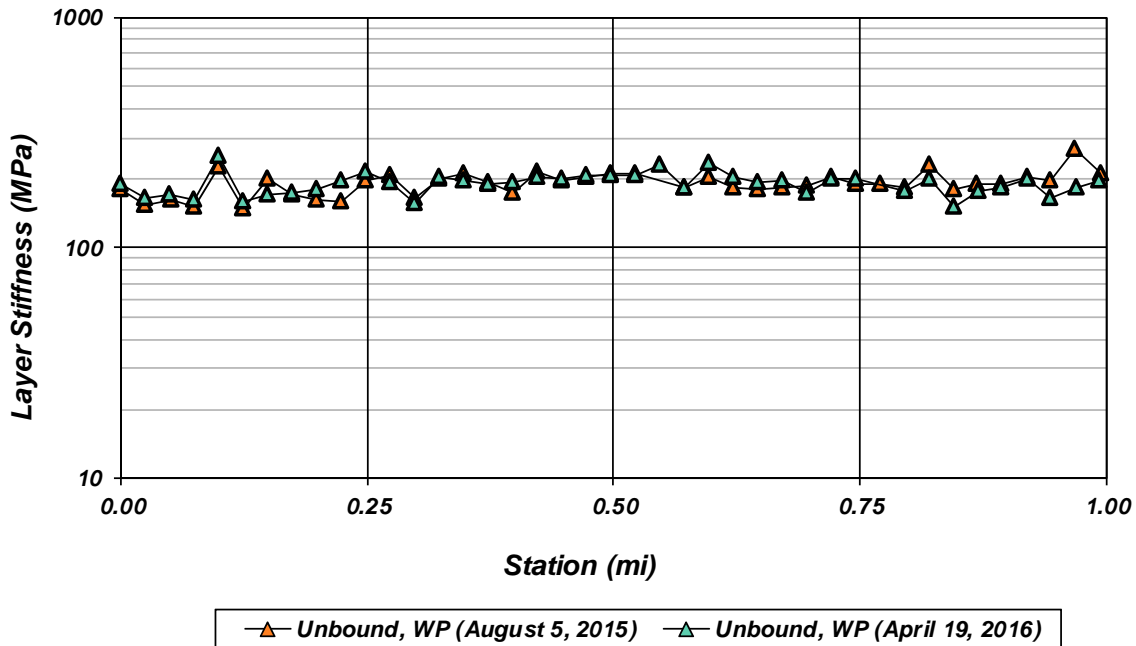


Figure 4.85: Modoc 299 unbound layer stiffness between the wheelpaths.



**Figure 4.86: Modoc 299 unbound layer stiffnesses in the wheelpath.**

The backcalculation results reveal consistent “subgrade” stiffness along the length and minor, if any, fluctuation in the observed stiffness of the embankment material. The FDR stiffness was much lower between PM 59.5 and 60.2 and increased substantially from PM 60.2 to 60.5. The stiffnesses of the FDR are similar to those of PAB from PM 59.5 to 60.2, while those from PM 60.2 to 60.5 are similar to FDR-PC (including a small amount of cement with the foamed asphalt). This indicates that in the low stiffness areas the stabilization may not have occurred, or else the small amount of stabilizer (the design called for one percent cement) was not effective.

The stiffness of the FDR material in the wheelpath decreased substantially from the dry season to the wet season. While these results may appear surprising, given the presence of the lake and snowmelt runoff during April 2016, observed deflections in the respective materials agreed that only minor changes occurred at depths relevant to the subgrade material (an average of 6 $\mu$ m difference) while the deflections in the FDR material were substantially greater in April 2016 (an average of 35 $\mu$ m difference), leading to the more severe decrease in stiffness in the FDR. A much smaller seasonal decrease was seen in the stiffness of the FDR material from PM 60.2 to 60.5 than in the material from PM 59.5 to 60.2. This again suggests that the material from PM 59.5 to 60.2 may not have been stabilized or the stabilization may not have been effective.

There appears to be no relationship between the unbound material stiffness and the stiffness of the overlying layers (Figure 4.87).

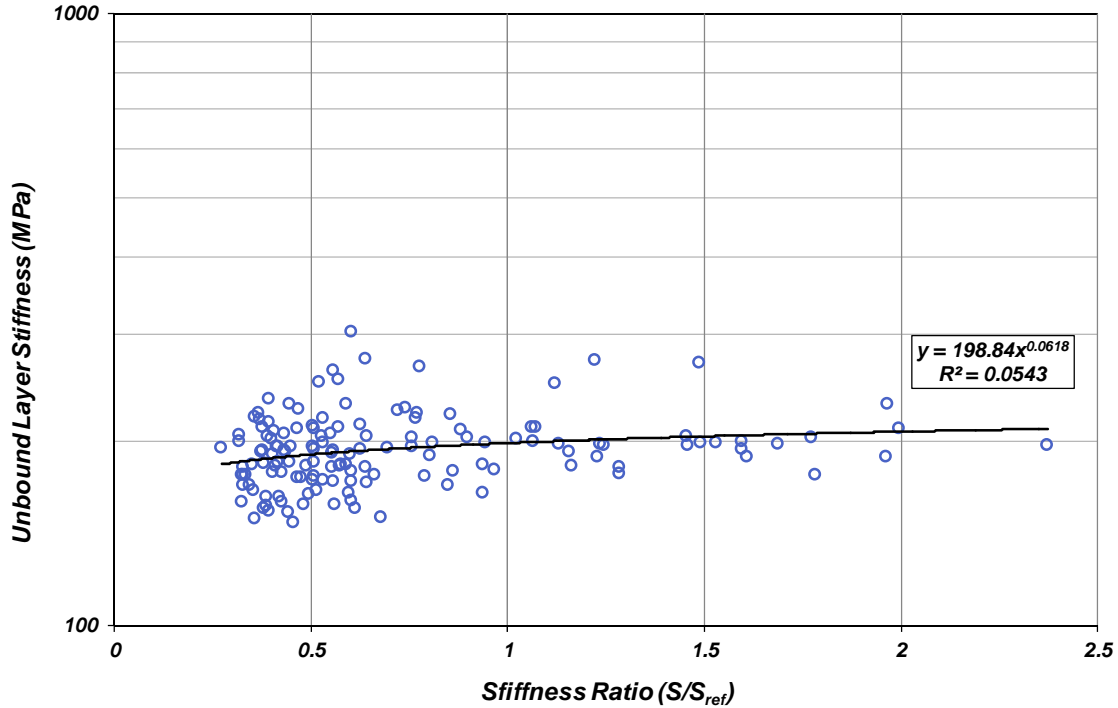


**Figure 4.87: Modoc 299 overlying layer effect.**  
 (Note: *stiffness ratio* is the ratio of the bending stiffness of the layers above the unbound layer relative [S] to a reference stiffness [S<sub>ref</sub>], giving an indication of the confinement from those layers.)

#### 4.2 Short-Term Seasonal Behavior Measured at ATIRC Test Track

Figure 4.88 illustrates the change in daily average backcalculated stiffness over time for the three unbound materials in the test track at ATIRC.

The backcalculation analysis revealed a wide range of values for the aggregate base stiffness. Further analysis revealed a consistent relationship between the stiffness of the asphalt and that of the aggregate base (Figure 4.89), indicating that as the stiffness of the asphalt increased, the aggregate base stiffness tended to increase with the increase in confinement.

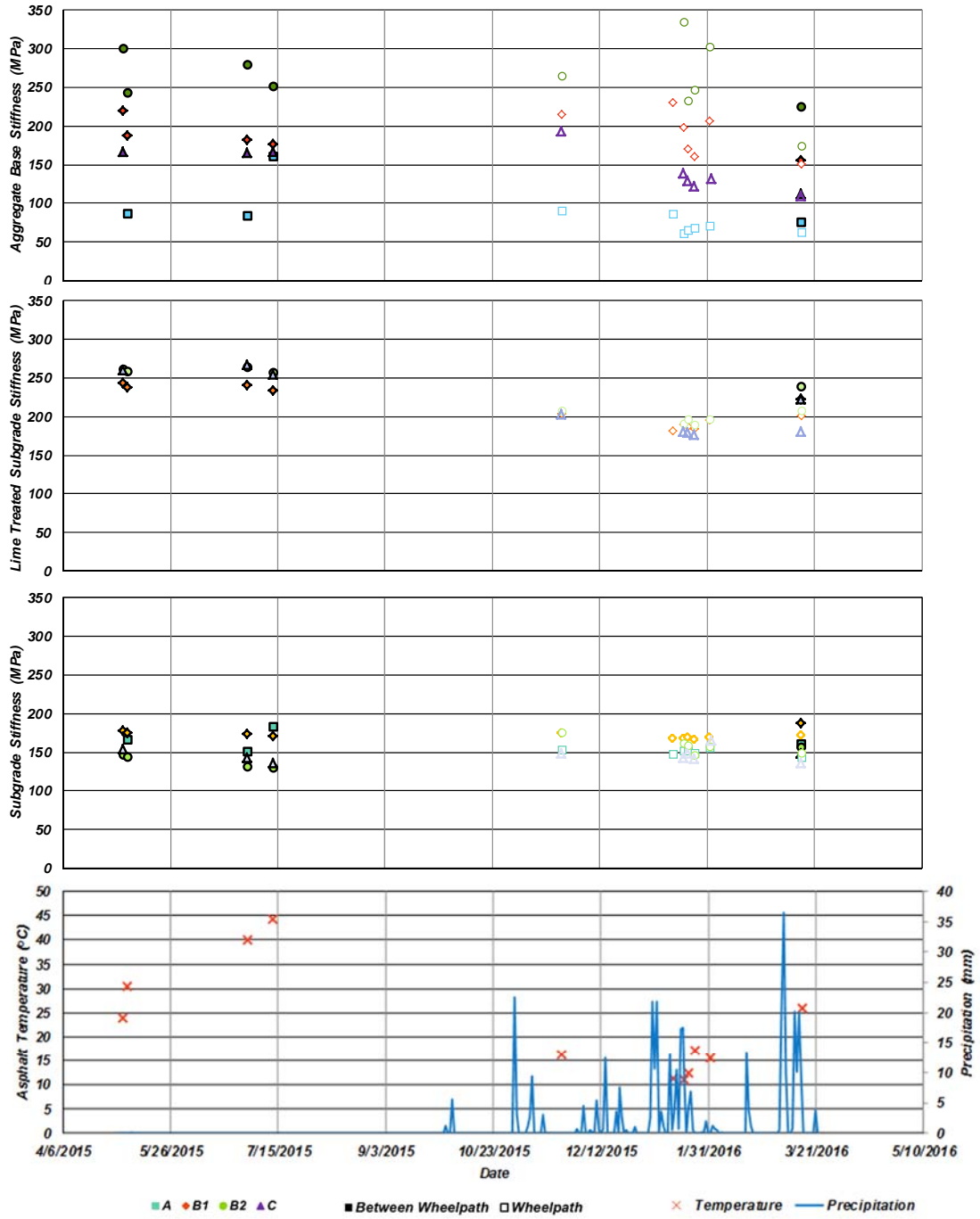
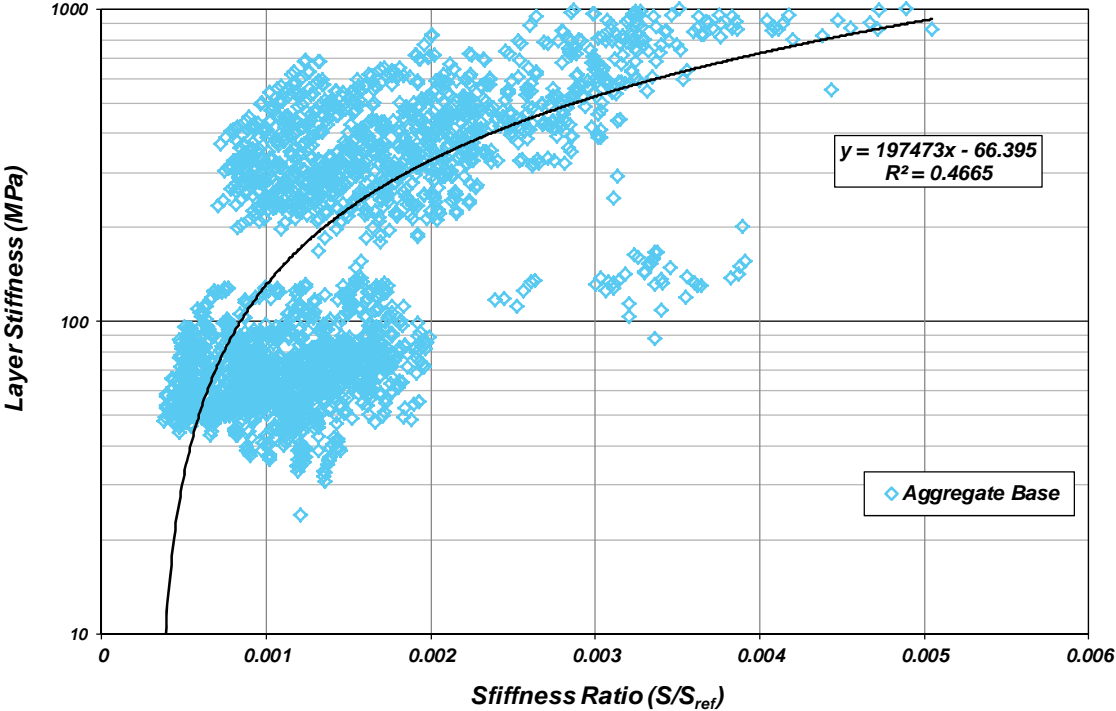


Figure 4.88: ATIRC stiffness time history.

Referring to Figure 3.9 for the locations on the ATIRC outside test track, the stiffness values for the aggregate base in Sections A and C tended to be lower than those in Sections B1 and B2, and this may have been due to drainage differences: Sections A and C had no shoulder drainage whereas Sections B1 and B2 had some engineered drainage (Figure 4.90). It is suspected that the lack of drainage in Sections A and C likely inhibited the ability of excess water under the pavement to drain or to reach more permeable layers, thus increasing the saturation of the base. However, without moisture measurements, it is difficult to say if this is exactly the case.



**Figure 4.89: ATIRC AB overlying layer effect.**

(Note: *stiffness ratio* is the ratio of the bending stiffness of the layers above the unbound layer relative [S] to a reference stiffness [S<sub>ref</sub>], giving an indication of the confinement from those layers.)



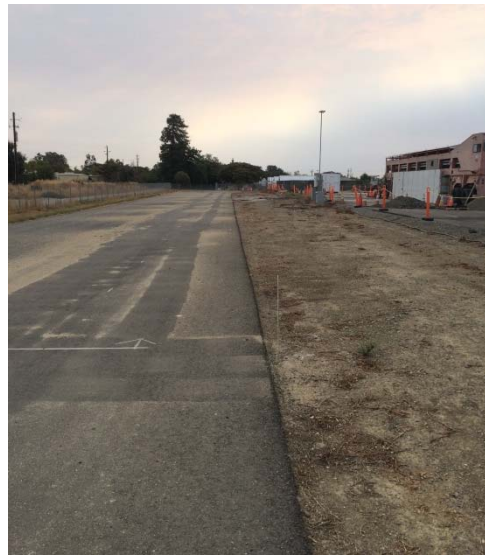
**Section A**



**Section B1**



**Section B2**



**Section C**

**Figure 4.90: ATIRC outside tracks drainage conditions.**

As can be seen in Figure 4.88, the subgrade and lime-treated subgrade showed a more narrow range in stiffness over time than that of the aggregate base. There appears to be no relationship between the stiffness of the lime-treated subgrade and the overlying layer stiffness, and there may only be a weak relationship (if any) between the untreated subgrade stiffness and the overlying layer stiffness (Figure 4.91). The backcalculated values indicate that both the lime-treated and untreated subgrade stiffnesses appeared to be fairly consistent over time, and data indicate little change over time.



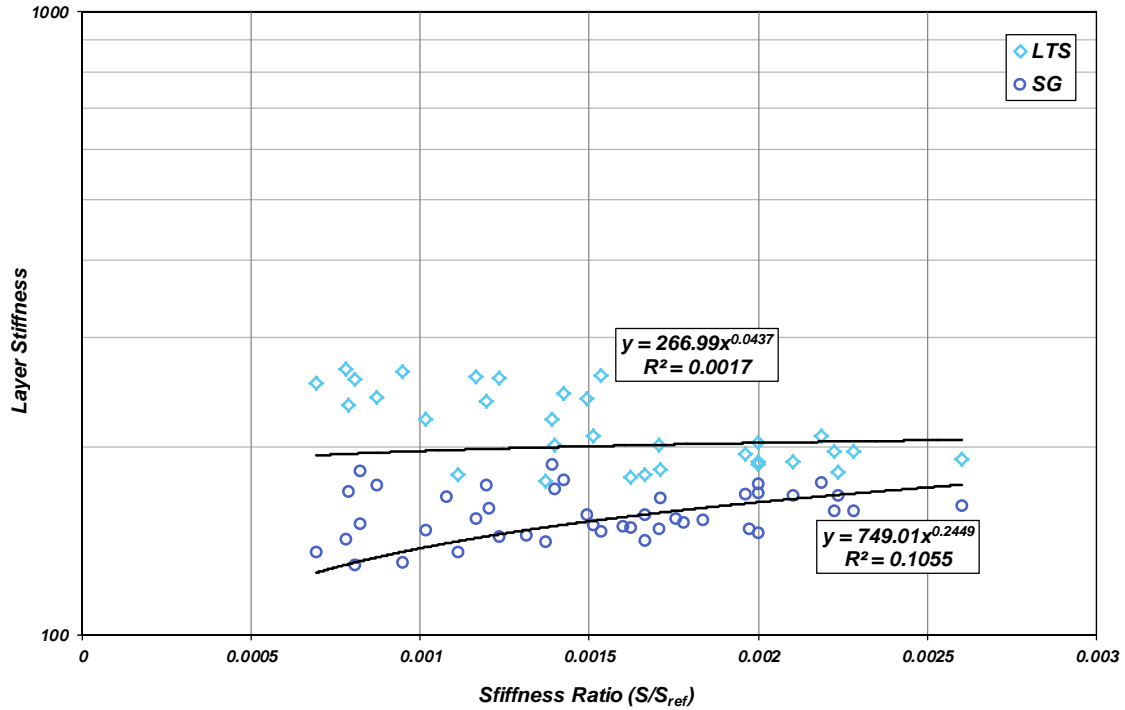


**Figure 4.91: Lime-treated subgrade and subgrade overlying layer effect.**  
 (Note: *stiffness ratio* is the ratio of the bending stiffness of the layers above the unbound layer relative [S] to a reference stiffness [S<sub>ref</sub>], giving an indication of the confinement from those layers.)

The range of the stiffnesses observed over time can be found in Table 4.44. The aggregate base stiffness ranges were greater than those observed for the subgrades, and the seasonal fluctuation in stiffness of the aggregate base appears to be dependent on the overlying asphalt stiffness, drainage conditions, and precipitation—although without instrumentation it is difficult to identify which condition dominates the change in behavior. Lime-treated subgrade and untreated subgrade stiffnesses had a smaller range seasonally, and their properties fluctuated both along the length and laterally across the lane.

**Table 4.44: Range of Stiffnesses for Outside Track (MPa)**

	Between Wheelpaths			Wheelpath		
	AB	LS	SG	AB	LS	SG
A	75 – 161	n/a	151 – 183	61 – 91	n/a	144 – 156
B1	156 – 220	221 – 243	170 – 187	151 – 230	182 – 204	166 – 175
B2	224 – 300	239 – 264	130 – 156	175 – 335	189 – 208	146 – 179
C	112 – 167	221 – 266	136 – 154	109 – 193	176 – 202	136 – 164

### 4.3 DCP Correlated Stiffness Evaluation

In assessing the relationships between DN and stiffness in the literature (Section 3.2.2), the median DCP values representative of the unbound material at each site were used to calculate the DN-correlated stiffness.

Regression analyses performed correlating backcalculated stiffnesses with the median DN between the two backcalculated values (stiffness between the wheelpaths [EBWP] and stiffness in the wheelpaths [EWP]) also agree with this finding (Figure 4.92 and Figure 4.93).

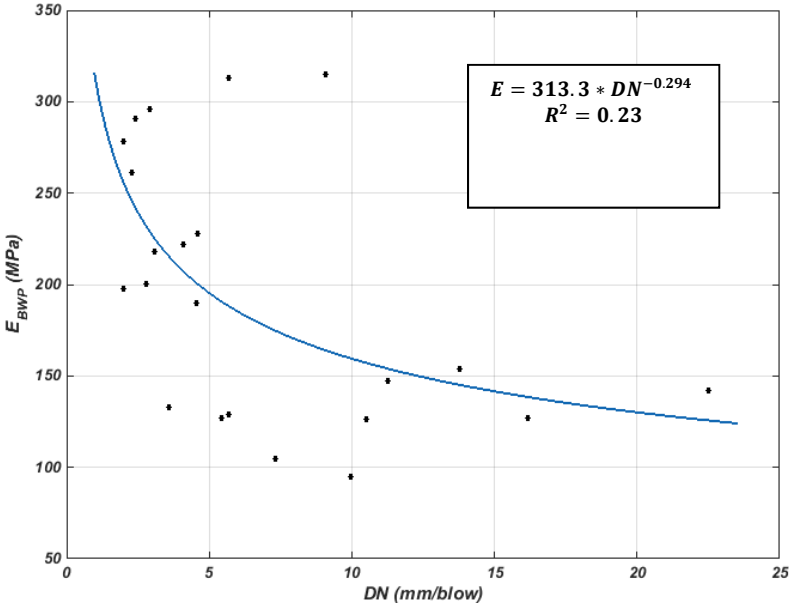


Figure 4.92: DN median versus backcalculated stiffness between the wheelpaths (EBWP).

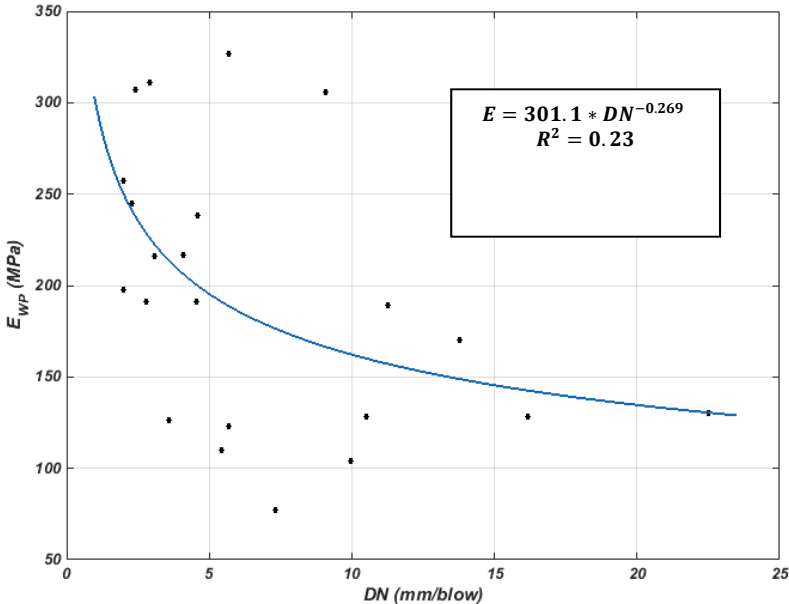


Figure 4.93: DN median versus backcalculated stiffness in the wheelpath (EWP).

From the regression analysis, the relationships described by CSIR (44), Chai and Roslie (45), and Chen et al. (46, 47) provide the best fit to the data obtained in the field. The CSIR (44) and Chai and Roslie (45) relationships, while providing seemingly good linear fit to the data obtained in the field, tend to overestimate the stiffness slightly, while the relationships presented by Chen et al. (46, 47) tended to be closer to the 1:1 line, as seen in Figure 4.94.

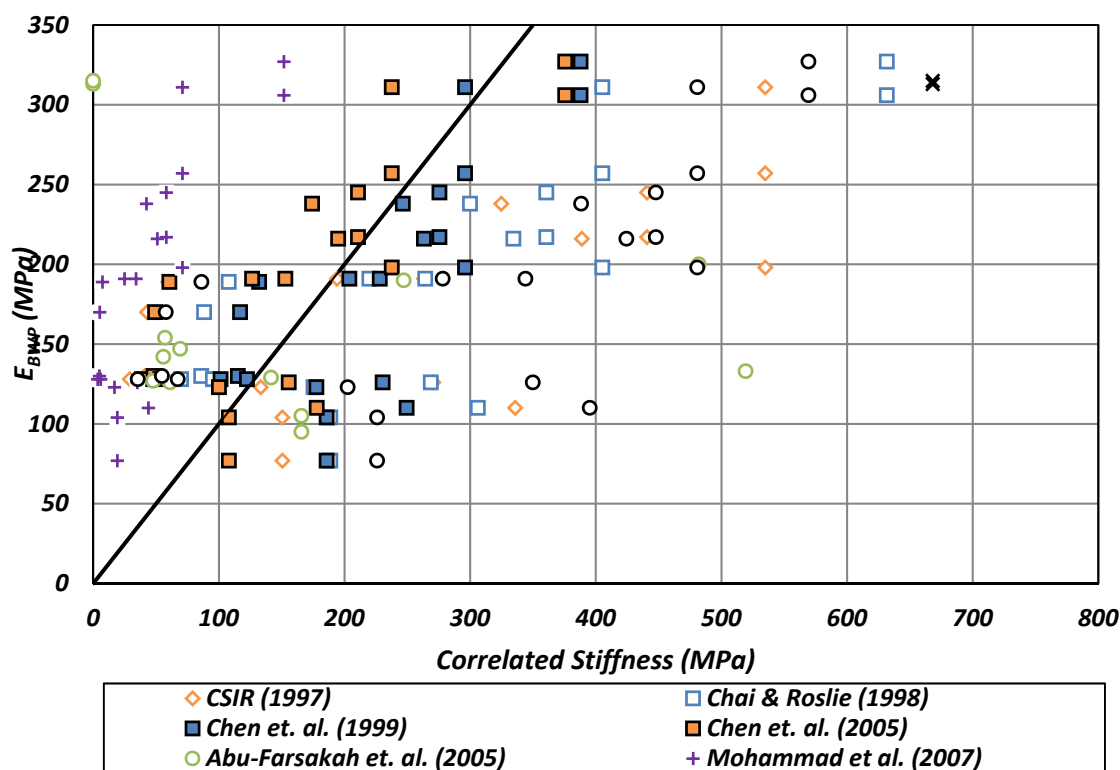


Figure 4.94: Comparison of backcalculated modulus with DCP-correlated stiffness.

#### 4.4 Asphalt-Bound Materials

Given the amount of data obtained in testing, it was of interest to evaluate whether the data could be used to evaluate the temperature susceptibility of the asphalt-bound and stabilized materials and the presence of damage at the test sites. The next three sections describe the methods used for evaluating the damage of surface layers and the temperature susceptibility of the asphalt-bound materials.

##### 4.4.1 Damage in Hot Mix Asphalt

The damage to hot mix asphalt (HMA) was assessed by comparing the backcalculated stiffnesses in the wheelpath (where damage is expected) with the stiffnesses between the wheelpaths. Because asphalt stiffness is temperature dependent, the backcalculated stiffnesses at the time of testing do not reveal if damage has occurred in the

wheelpath because the asphalt layer is tested at different times of the day and the temperatures are therefore different. To assess whether damage had occurred at the sites, the backcalculated asphalt stiffness for each site was plotted against the BELLS-calculated temperature at 1/3 depth of the asphalt layer and a best-fit relationship was found. Since the stiffnesses followed a lognormal distribution, a power relationship was fit to the data to obtain an approximate slope of the field master curve for the range of temperatures observed during testing (found in Appendix B). While the relationships between asphalt stiffness and temperature indicate a wide degree of variability, the slope was calculated in order to obtain a rough measure of the change in stiffness that might correspond to temperature changes. Using the slope, an “equivalent” average stiffness at the average asphalt temperature from both rounds of testing was calculated using the power function relationships as follows:

$$m = \frac{\Delta \log E}{\Delta \log T}$$

$$E_{equivalent} = 10^{[\log(E_{actual}) + m \times (\log(T_{average}) - \log(T_{actual}))]}$$

where:

$E_{equivalent}$  is the equivalent average stiffness at a given average temperature,

$E_{actual}$  is the actual backcalculated stiffness,

$m$  is the slope of the power function,

$T_{average}$  is the average asphalt temperature from all the tests, and

$T_{actual}$  is the actual asphalt temperature during testing.

Using these transformations, the “equivalent” asphalt stiffnesses at the sites were calculated, and are tabulated below in Table 4.45.

**Table 4.45: Equivalent Asphalt Stiffness and Damage Assessment**

	Average Asphalt Temperature (°C)	Round 1			Round 2		
		Between Wheelpaths	Wheelpath	Percent Difference (%)	Between Wheelpaths	Wheelpath	Percent Difference (%)
Col 20	30.4	10,425	12,108	-15	13,313	12,439	7
ED 193	22.0	3,665	3,096	17	5,713	4,949	14
Sie 89	29.9	13,600	17,130	-23	19,224	12,250	44
Plu 70	25.6	4,844	5,651	-15	5,927	5,879	1
Ven 33	39.8	8,474	6,463	27	3,330	6,306	-62
SB 166	33.3	46,688	32,725	35	43,431	30,449	35
SLO 46	29.8	8,581	7,454	14	8,810	7,549	15
Las 44	27.6	2,490	3,419	-31	2,531	3,165	-22
Mod 395	24.0	8,261	7,123	15	10,086	8,320	19
Mod 299	26.0	6,424	8,076	-23	8,312	9,427	-13

The purpose of calculating the equivalent stiffness was to assess whether damage can be observed through the manipulation of backcalculation data and field testing data. The results in Table 4.45 indicate that some of the sites consistently had lower stiffness in the wheelpaths than between the wheelpaths (ED 193, SB 166, SLO 46, and Mod 395), some of the sites had consistently higher asphalt stiffness in the wheelpaths (Las 44, Mod 299), and the remaining sites had no consistent trends.

#### 4.4.2 Temperature Susceptibility of Hot Mix Asphalt

In addition to evaluating damage, the temperature data could also be used to evaluate temperature susceptibility and aging effects on the asphalt surface layer. Table 4.46 includes a summary of the different test sites, the year of last surface layer construction, slope of the master curve (m) for both lateral locations, and the age in years. Figure 4.95 shows the field master curves for all the sites while Figure 4.96 shows the regression of the asphalt age and slope of master curve. A strong relationship was found between the asphalt age and the slope of the field master curve, revealing that newer asphalt concrete layers are more susceptible to temperature changes and that effects of aging can readily be seen in the field.

**Table 4.46: Asphalt Age and Temperature Susceptibility**

Site	Last Surface Construction Year	Slope of Master Curve	Age (years)
Col 20	2012	-1.249	4
ED 193	2014	-0.68	2
Sie 89	2002	-0.6	14
Plu 70	2011	-1.47	5
Ven 33	2016	-3.63	0
SB 166	2015	-2.24	1
SLO 46	2014	-1.97	2
Las 44	2011	-0.94	5
Mod 395	2010	-0.82	6
Mod 299	2011	-0.98	5

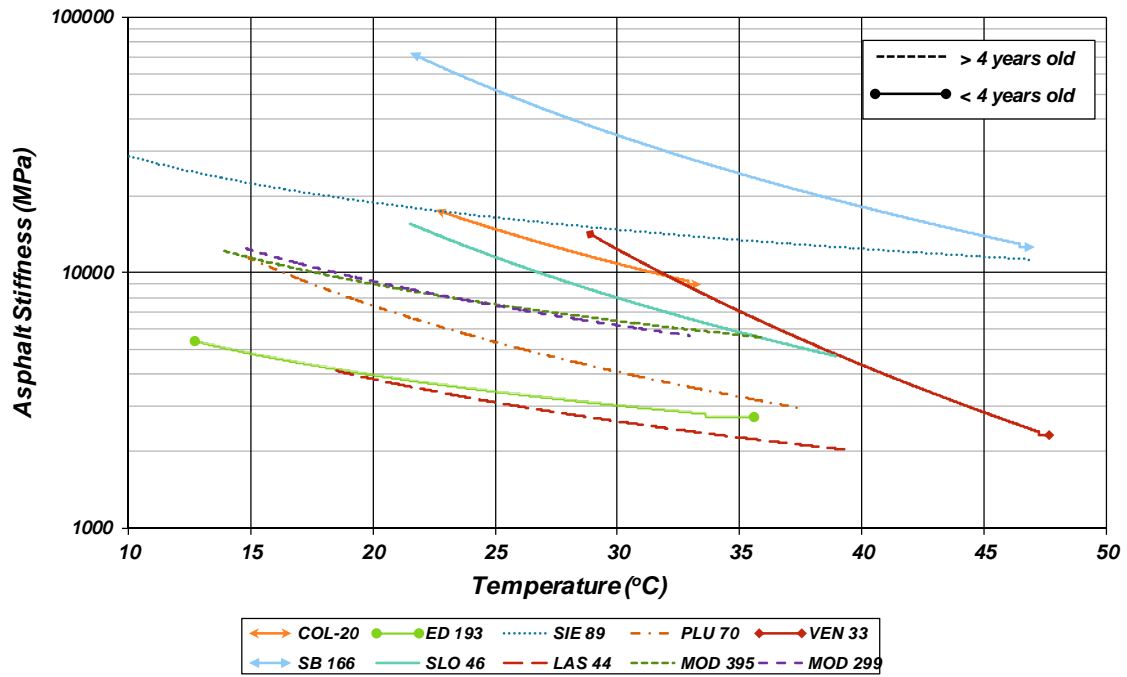


Figure 4.95: Temperature susceptibility of HMA from backcalculated master curves.

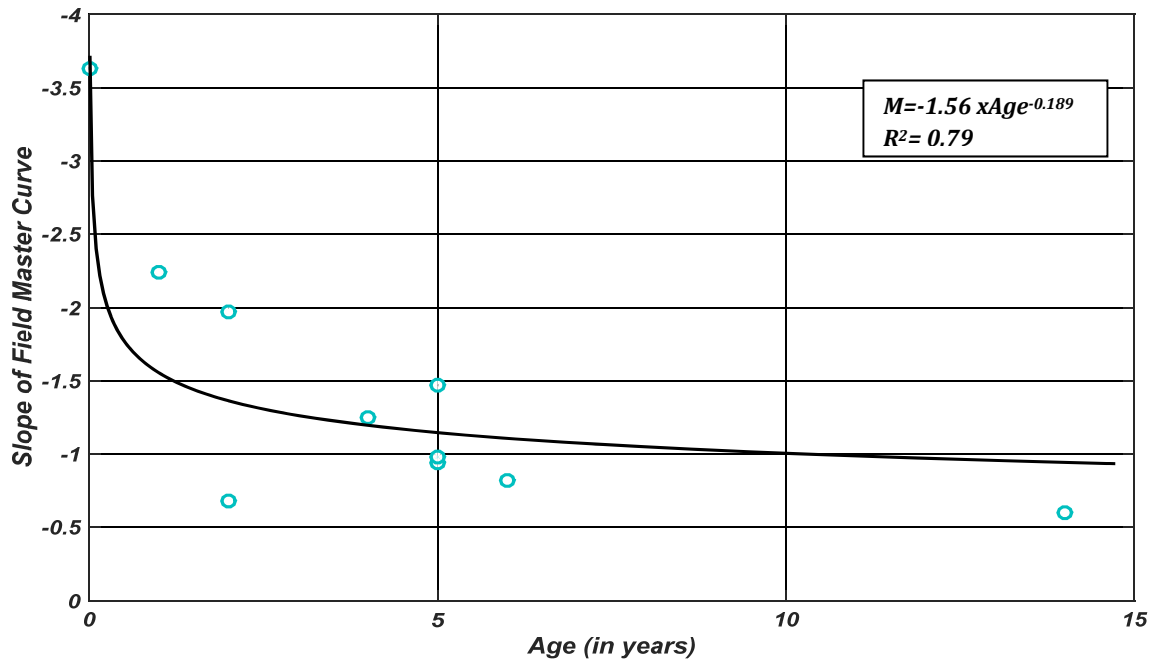


Figure 4.96: Asphalt aging and temperature susceptibility from backcalculated master curves.

#### 4.4.3 Temperature Susceptibility of Full-Depth Reclamation with Foamed Asphalt

Similar to the way that temperature susceptibility of asphalt surface layers were evaluated, the backcalculated stiffnesses of the FDR-FA were plotted against the temperature at 1/3 depth in the base layer. The individual plots for each site can be found in Figure B.12 through Figure B.15 in Appendix B, while a summary plot of these relationships is shown in Figure 4.97. The summary plot seems to indicate that generally the base stiffness increases with increases in temperature for three of the four projects with this type of base. In evaluating the individual plots, it is clear that there seems to be little, if any, relationship between the asphalt-stabilized base material and temperature. It must be remembered that the stiffness of the asphalt concrete surface was changing also, changing the confinement and shear stresses in the base. Jones et al. found that the stress state was at least as important as the temperature for FDR-FA layers in California (57).

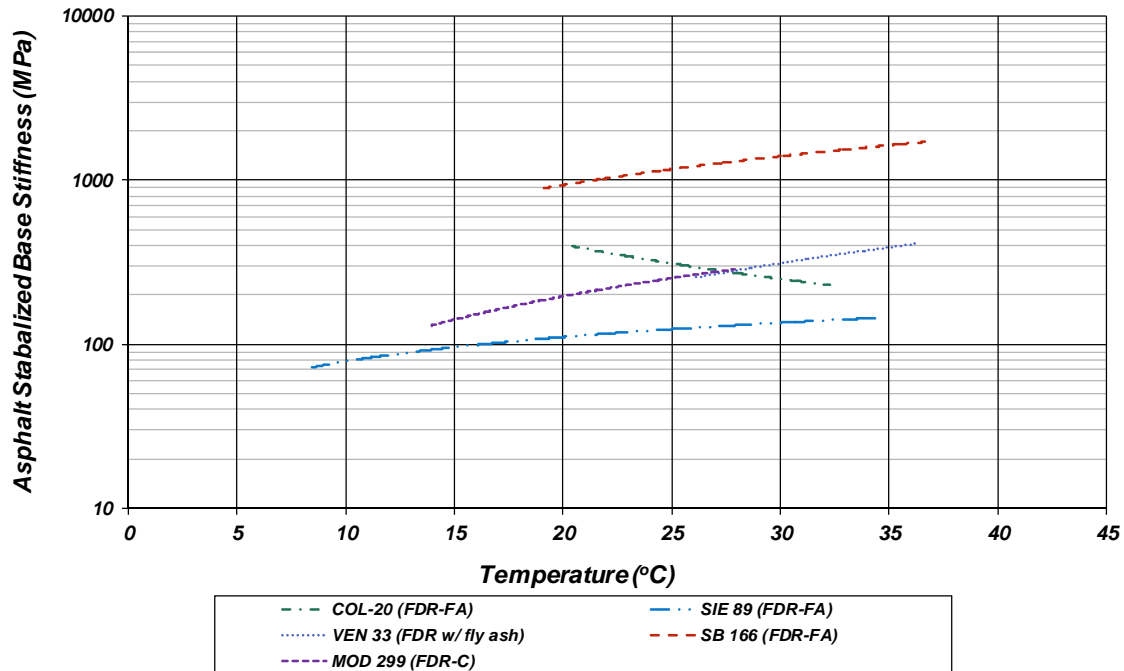


Figure 4.97: Temperature susceptibility of asphalt-stabilized base (full-depth reclamation with foamed asphalt).

#### 4.5 Summary of Results

Figure 4.98 through Figure 4.101 provide summaries of the stabilized base stiffnesses and unbound material stiffnesses categorized by type and by climate region. Because soil classification varied with depth in most of the testing locations, the predominant material type found at the site was used for categorization.

All base materials except for lean concrete base (LCB) experienced a decrease in stiffness between the two rounds of testing, whereas the underlying unbound materials did not seem to show any trends in variability based purely on soil type. When assessing the sites based off climate regions, it becomes clear that the sites in the High Mountain climate region experienced reductions in both base and unbound material stiffnesses after the wet season, while all other climate regions experienced consistent reductions in the base material stiffness in the wet season. The one site that does not appear to reveal any consistent trend in seasonal variation of stiffness is San Luis Obispo 46; this was the only two-lane highway tested and was the only site to have notable side drains present along the length of the section, which likely played a role in consistent behavior.

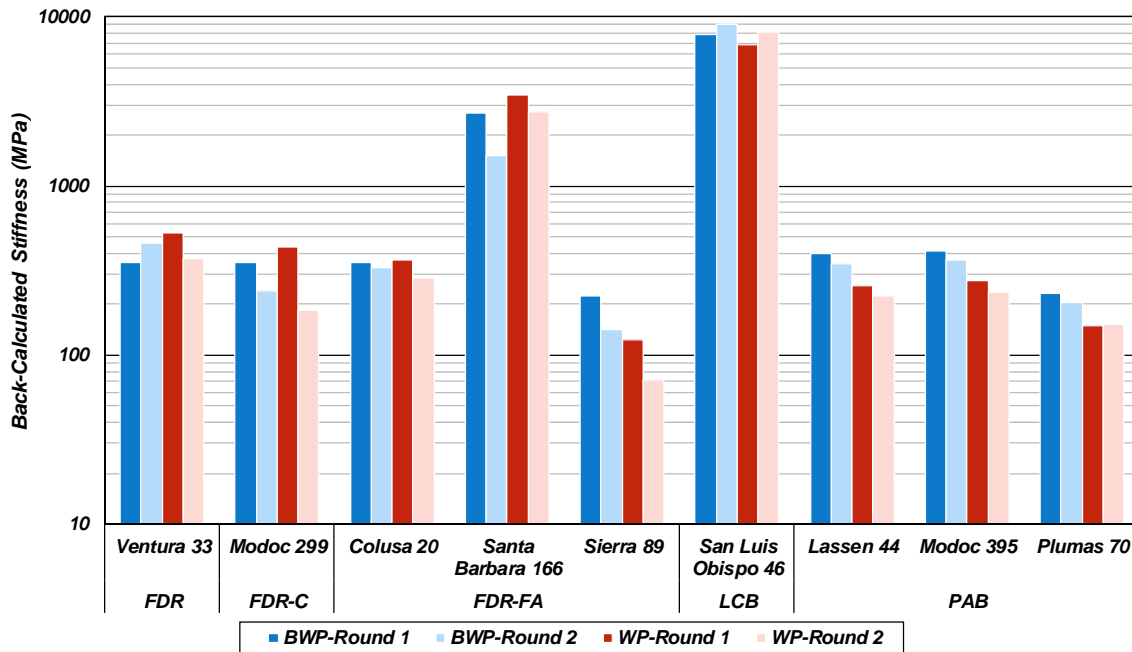


Figure 4.98: Summary of base stiffness by type (Round 1 at end of 2015 dry season, Round 2 at end of 2016 wet season).



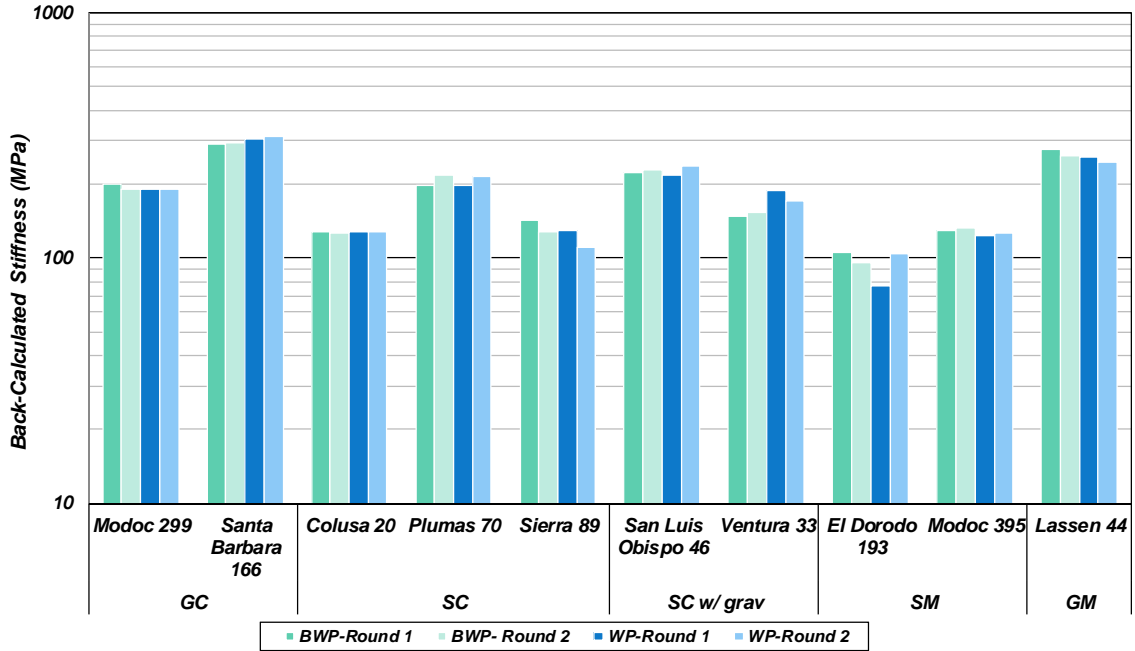


Figure 4.99: Summary of unbound material stiffness by type (Round 1 at end of 2015 dry season, Round 2 at end of 2016 wet season).

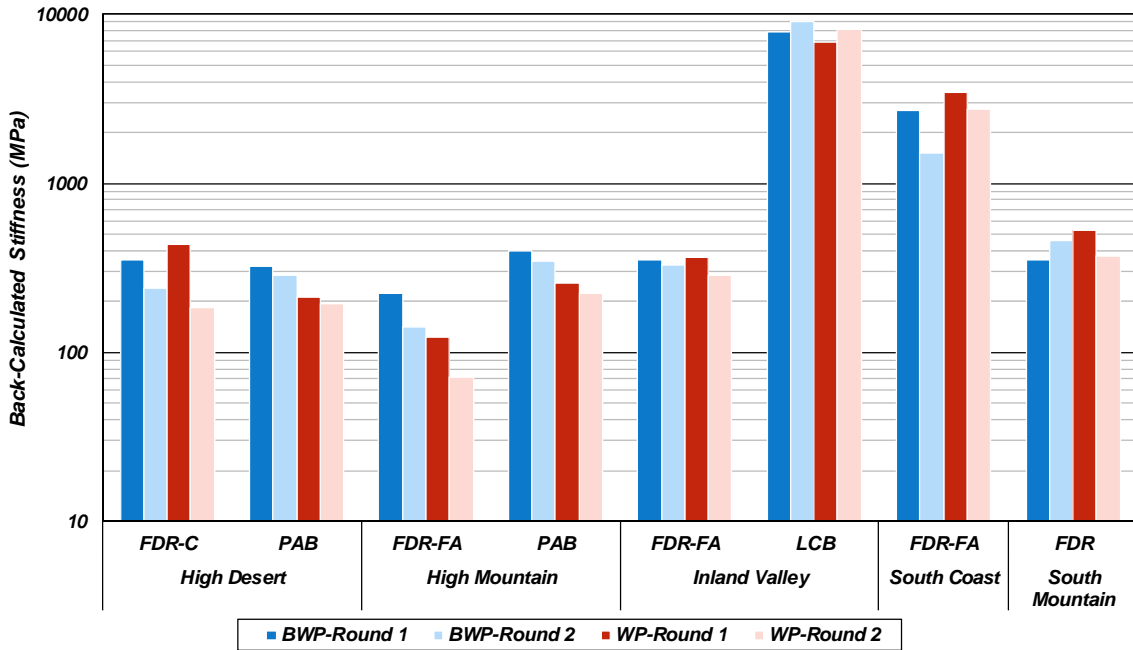
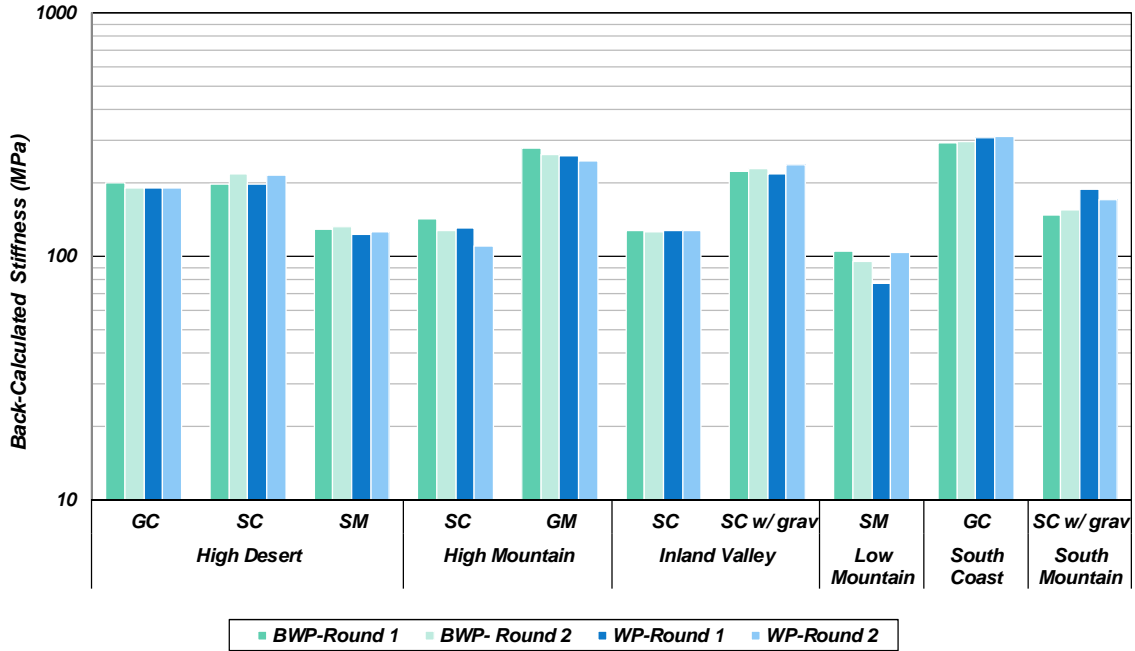


Figure 4.100: Summary of base stiffness by climate region (Round 1 at end of 2015 dry season, Round 2 at end of 2016 wet season).

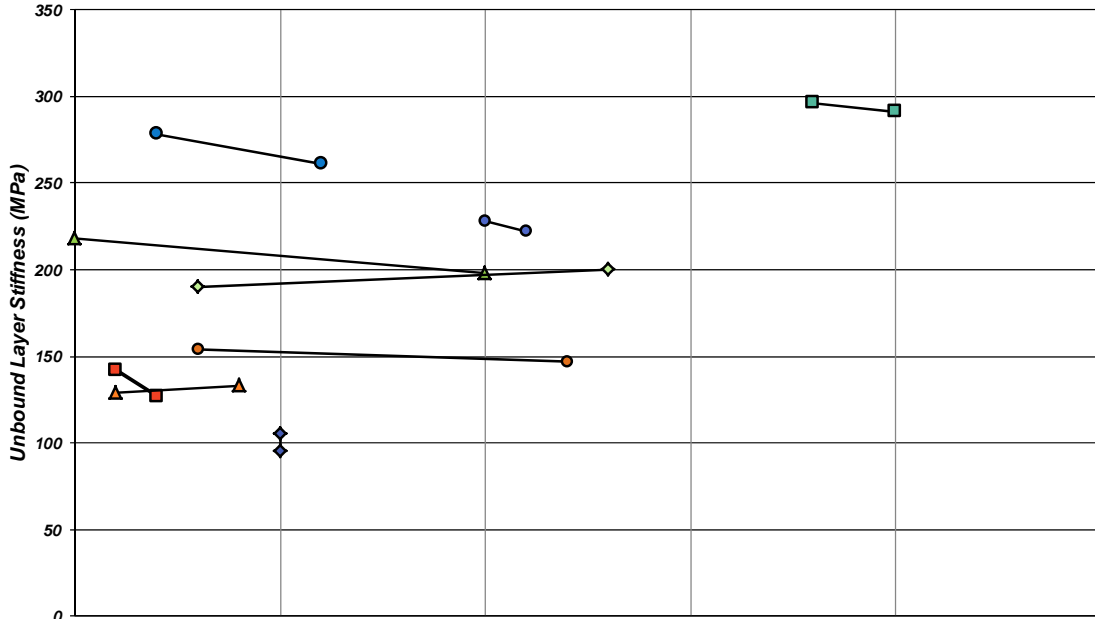


**Figure 4.101: Summary of soil stiffness by climate region (Round 1 at end of 2015 dry season, Round 2 at end of 2016 wet season).**

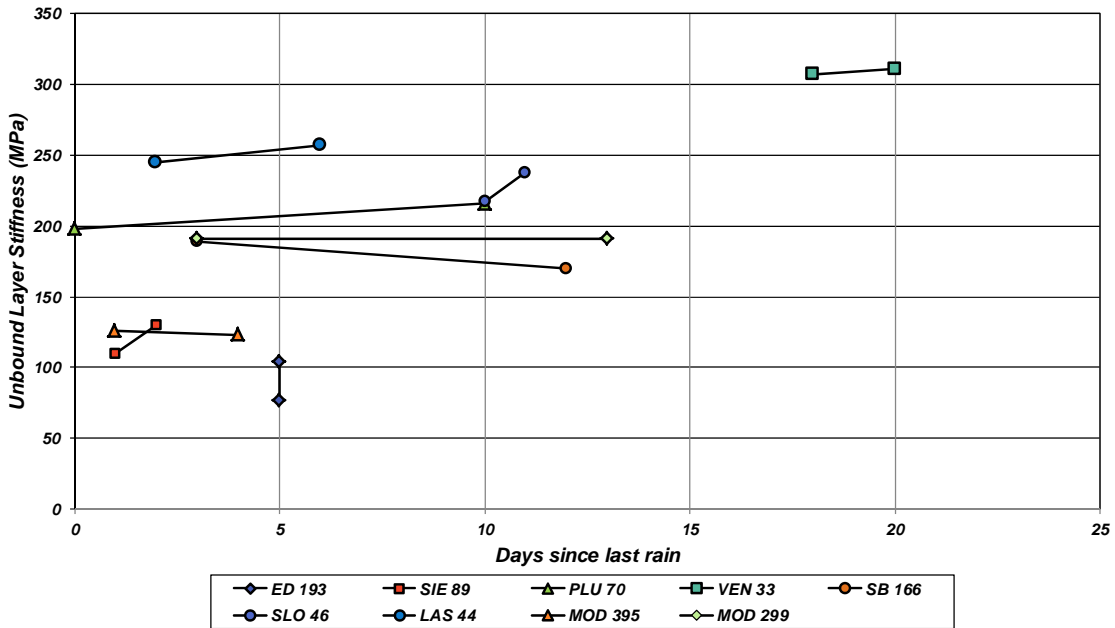
Figure 4.102 depicts the unbound layer stiffness versus days since last rainfall (from the day of testing).

By assessing the influence of specific rainfall events on the stiffness of the material, it was found that the stiffness of unbound material between the wheelpaths generally tended to decrease with time after rainfall, while the opposite was true for the stiffness of material in the wheelpath, which increased with time after rainfall. Figure 4.103 shows the change in unbound layer stiffness versus the distance to the unpaved portion of the road (negative denotes a decrease in stiffness from the first round of testing to the second round). Generally the material between the wheelpaths did not show a clear relationship between the distance to the unpaved portion of the road and changes in stiffness, while the wheelpath material tended to be softer in the wet season when the site had narrower shoulders.

Figure 4.102 and Figure 4.103 indicate that roadway conditions and rainfall events tended to influence the patterns of stiffness of the material; for the wheelpaths (where most pavement distresses are typically observed), the variability of the unbound layers seemed to be heavily influenced by the width of the shoulder as well as the climate and precipitation. Materials in the wheelpath tended to be softer shortly after rainfall and increased in stiffness as time elapsed after the rainfall, while material between the wheelpaths did not follow any specific pattern, seemingly validating the inherent complexities of water flow beneath pavement structures noted in the literature.



(a)



(b)

Figure 4.102: Unbound layer stiffness versus days since last rainfall event (a) between the wheelpaths and (b) in the wheelpath. (Note: data from NOAA) (55)

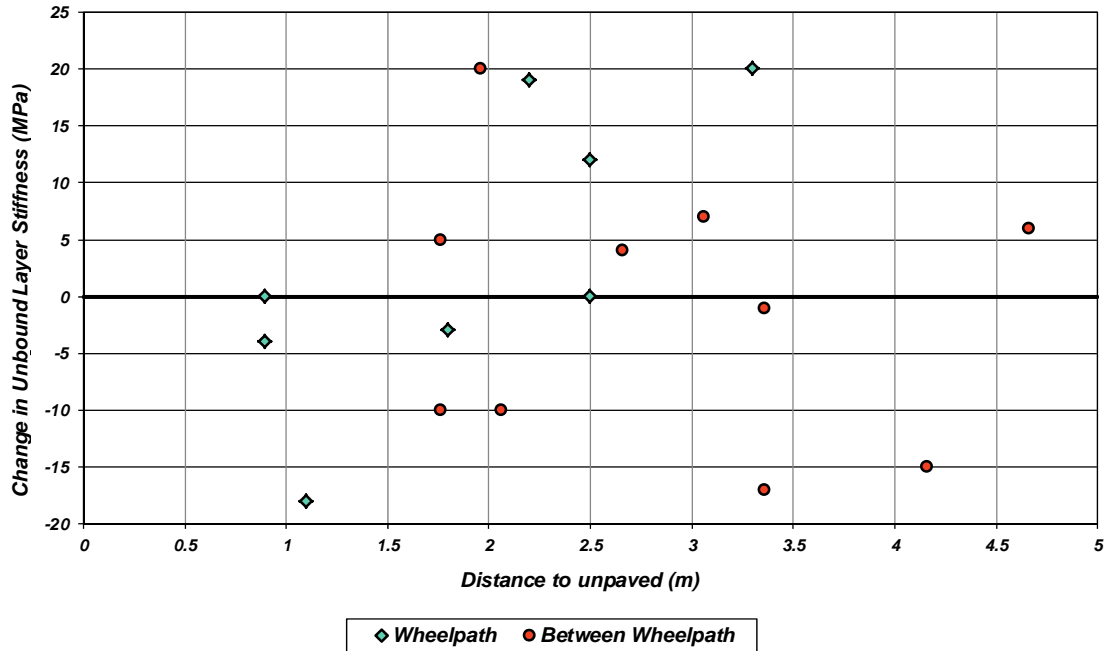


**Figure 4.103: Influence of shoulder distance on stiffness.**  
 (Note: negative denotes decrease in stiffness.)

Figure 4.104 illustrates the unbound material stiffnesses obtained through backcalculation compared to the average and range typically attributed to the specific soil type in *MEPDG*. From this comparison, it is apparent that the backcalculated values were consistently higher than those in *MEPDG*, with the exception of the silty sand material. The resilient modulus ranges provided in *MEPDG* correspond to CBR-correlated stiffnesses and are calibrated from soil index testing and laboratory testing. It is noted in the *MEPDG* design guide document that the correlations were originally intended to obtain realistic  $M_R$ , including consideration of frozen material using a limited database of triaxial test data, and that caution should be exercised when extrapolating these values for non-frozen soils (12, Appendix DD). While oftentimes the moduli values listed in these tables are used for design, there seems to be relatively little relation to the values that were observed during field testing.

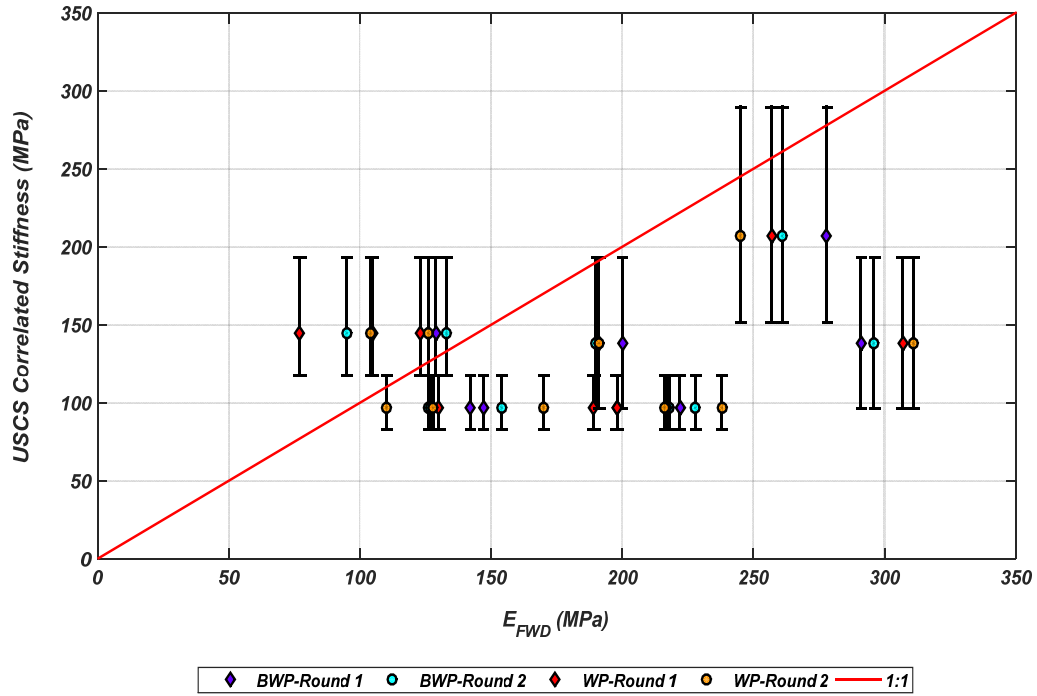


Figure 4.104: Unbound material stiffness compared with MEPDG-correlated values (Round 1 at end of 2015 dry season, Round 2 at end of 2016 wet season).

*(This page intentionally blank)*

## 5 CONCLUSIONS AND RECOMMENDATIONS

---

The goal of this research is to provide guidance regarding the selection of materials from the standard materials library in the *CalME* design software. The work presented in this report investigated how the stiffness of unbound materials varies seasonally, identified which factors might be most influential in causing seasonal changes, and provides guidance for future research and characterization.

### 5.1 Summary and Conclusions

The literature reveals that moisture conditions and suction have strong influences on the resilient behavior of unsaturated soils, as modeled and observed in numerous and extensive laboratory tests by many researchers and practitioners. However, while the past fifty-some years of soil mechanics research has vastly improved the knowledge of and explanations for soil behavior, the current literature seems to be particularly lacking in knowledge or experiments pertaining to how these well-established properties and behavior extrapolate to conditions typically seen in the field.

To help bridge that gap by having a better understanding of the effects that moisture conditions, environmental factors, and climate can have on seasonal changes to the in situ properties of pavement materials assumed for design, an experiment was performed to evaluate whether noticeable changes in subgrade stiffness could be measured in the field based on backcalculation. The experiment involved testing at the end of a dry period and a wet period on 11 field sites across California. The flexible pavement structures included aggregate, full-depth reclamation (FDR), and lean concrete bases (LCBs), and a range of subgrade types. Laboratory testing was performed to classify the materials found in the field.

The main results of the study and answers to the questions posed from the literature can be summarized as follows:

#### *5.1.1 Seasonal Changes in Unbound Material Properties*

Questions were posed pertaining to what kinds of seasonal changes in unbound materials properties could be observed and whether or not they corresponded to significant changes in stiffness observed in the field. The data indicate that changes in both moisture content and penetration resistance were readily observed, indicative of seasonal fluctuation of moisture conditions and shear strength that would be expected for soils. However, these small-scale changes did not necessarily correspond to significant fluctuations or noticeable trends in measured deflections or backcalculated stiffness of the unbound materials; rather, spatial variability, observed drainage and site conditions, and soil type tended to have a much larger influence on the resilient response of the materials tested than did observed changes in moisture or penetration resistance.

In almost all cases, the stabilized and unstabilized base and subbase materials, not the subgrade, experienced the largest changes in stiffness between the two rounds of testing. This result may be rooted in the relative permeability of the materials: the more permeable granular materials were expected to experience quicker changes in moisture conditions (and therefore suction and stress state) and the less permeable subgrade materials were expected to not experience these changes as quickly. The data also suggest that in some cases, the stiffness of, and additional confinement from, the overlying layers may play an important role in the resulting resilient response of the unbound material.

While the literature consistently indicates that significant changes in resilient modulus can occur with changing moisture regime, the field testing results presented in this report indicated that changes in stiffness at different moisture conditions did not seem to be as large as those evaluated in laboratory testing found in the literature. This could be due to the nature of the in situ testing performed: FWD testing takes place on a larger scale than resilient modulus testing and therefore the averaging of material properties, the specific stress state conditions (particularly lateral and overburden confining stresses), and the greater chances of nonhomogeneity in materials may each be a part of the reason why stark changes in subgrade stiffness magnitude were not seen from field testing. While it was outside the scope of this project to perform resilient modulus tests on these materials, this finding may help shed some light on some of the discrepancies between field and laboratory testing conditions, results, and appropriate design applications.

Regarding the range of materials properties observed for different soil types, spatial variability and geologic conditions appeared to contribute the most to the range of subgrade stiffnesses seen within each test site. Sites constructed using cut/fill methods tended to exhibit a much wider degree of variability in backcalculated stiffnesses, while sites situated in more level or alluvial plains had much lower standard deviations for unbound material stiffness. Gravelly materials and pulverized asphalt base (PAB) consistently exhibited the highest stiffnesses of the unbound materials. Stiffness tended to decrease with increasing fines, and the unbound material stiffness values obtained from backcalculation did not show a strong relationship to the  $M_R$  values typically assumed in the MEPDG design method.

### *5.1.2 DCP-Correlated Stiffness*

This research did not aim to provide additional relationships between DCP penetration index and backcalculated stiffness, but rather evaluated the effectiveness and reliability of some of the DCP-stiffness relationships expressed in the literature. Backcalculated stiffnesses of the unbound material tested seemed to correlate well with DCP penetration resistance (DN). Of the relationships proposed in the literature, those developed by Chen et al. (47) and Chen et al. (46) produced the estimated stiffnesses most consistent with the data obtained in this study. The



relationships proposed by CSIR (44) and Chai and Roslie (45) also fit well with the data, but tended to overestimate stiffness.

### 5.1.3 Asphalt-Bound and Lightly Stabilized Materials

Because of the quantity of information obtained, it was of interest to assess whether field data could be useful for evaluating the damage, aging, and temperature susceptibility of asphalt-bound and lightly stabilized materials. The field data revealed that FWD test data can be used to roughly estimate a field asphalt concrete (AC) master curve that can then be used to evaluate the effects of aging and damage. Evaluating the effects of aging revealed a strong relationship between asphalt age and temperature susceptibility for asphalt concrete. Calculation of “equivalent” asphalt stiffness also showed that damage was observed in the asphalt concrete at about one-third of the sites tested. Little to no relation to temperature was observed for full-depth reclamation materials stabilized with foamed asphalt, which have shown as much sensitivity to stress state as temperature in previous research. This research does not necessarily intend to propose new methods or models for evaluating these phenomena, but rather sheds light on the potential usefulness of field data for investigating them.

## 5.2 Recommendations

While knowing the expected behavior of unbound pavement soils is necessary for any design application, the actual conditions and various environmental factors that can influence behavior must be taken into account to produce a more holistic and complete evaluation of expected pavement performance. The results of this study represent a small sample of conditions on asphalt concrete-surfaced state highways that exist in the field.

The results revealed that many of the unbound materials tested experienced minor, if any, changes in stiffness between the two rounds of testing in the “dry” and “wet” conditions. This indicates that the current assumption within *CalME*, that unbound material stiffness does not change seasonally, is evidently not far off from the behavior that was observed in the finer subgrade materials evaluated during field testing, despite noted changes in moisture content and penetration resistance. The results indicate that this assumption does not necessarily hold true for the shallower granular base and subbase materials, and it is recommended that further assessment of the causes and degrees of variability in modulus of these coarser materials be evaluated. *CalME*'s model for the effects of overlying layer stiffness tended to be more applicable to these granular materials as well; however, material stiffening from increased confinement did appear to occur in some of deeper materials tested, and this phenomenon may be worth investigating further depending on the importance of the proposed structure. It is therefore recommended that *CalME*'s current assumption of constant stiffness for unbound layers continue to be used, except in cases where the designer identifies issues with drainage, irrigation, or other likely causes of seasonal variation of stiffness. Performing FWD testing for backcalculation of unbound layer stiffnesses after the

rainy season, or other times of highest moisture contents where rainfall is not the main source of moisture, will impart some conservatism into designs.

While the results of the field investigations revealed that the subgrade backcalculated stiffness experienced minor changes between the two rounds of testing, DCP testing consistently revealed patterns of decreased penetration resistance when material had higher moisture contents and when material had greater fines content. Though the objectives of the research did not involve evaluating the change in the shear strength of the materials, data reveal that seasonal fluctuation of in situ shear strength of both granular and subgrade materials was observed based on the DCP results.

The results of this research provide field data characterizing the stiffnesses of subgrades, granular material, FDR-FA, and lean concrete bases that should be used to update options for designers in the *CalME* Standard Materials Library.

## REFERENCES

---

1. Basheer, I., Harvey, J.T., Hogan, R., Signore, J., Jones, D., and Holland, T.J. (2010). Transition to Mechanistic Empirical Pavement Design in California. 11th International Conference on Asphalt Pavements, Nagoya, Japan, 81-90.
2. California Department of Transportation. 2016. Highway Design Manual. Sacramento, CA [www.dot.ca.gov/design/manuals/hdm.html](http://www.dot.ca.gov/design/manuals/hdm.html). (Accessed September 6, 2017)
3. Thom, N. (2014). Principles of Pavement Engineering (2nd ed.). Westminster, London: ICE Publishing.
4. Brown, S.F. (2004). Application of Soil Mechanics Principles to Design and Testing of Pavement Foundations. Paper presented at the Proceedings of the 8th Conference on Asphalt Pavements for Southern Africa (CAPSA'04). (12). 16.
5. Brown, S.F. (1996). Soil Mechanics in Pavement Engineering. *Géotechnique*, 46(3), 383-426.
6. van Aswegen, E. (2013). Effect of Density and Moisture Content on the Resilient Response of Unbound Granular Material. PhD thesis, University of Pretoria, Pretoria, South Africa.
7. Ullidtz, P. (1998). Modeling Flexible Pavement Response and Performance. Gylling, Denmark: Narayana Press.
8. Powrie, W. (2013). Soil Mechanics: Concepts and Applications (3rd ed.). Boca Raton, FL: CRC Press. 177-178.
9. Seed, H. B., Chan, C.K., and Lee, C.E. (1962). Resilience Characteristics of Subgrade Soils and Their Relation to Fatigue Failures in Asphalt Pavements. In International Conference on the Structural Design of Asphalt Pavements. Supplement.
10. Monismith, C.L. (1992). Analytically Based Asphalt Pavement Design and Rehabilitation: Theory to Practice, 1962-1992. Transportation Research Record: Journal of the Transportation Research Board (1354), 5-26.
11. Ullidtz, P., J.T. Harvey, B.-W. Tsai, and C.L. Monismith. (2005) Calibration of Incremental-Recursive Flexible Damage Models in CalME Using HVS Experiments. Report prepared for the California Department of Transportation (Caltrans) Division of Research and Innovation by the University of California Pavement Research Center, Davis and Berkeley. UCPRC-RR-2005-06.
12. ARA, Inc. ERES Consultants Division (2004) Guide for Mechanistic-Empirical Design of New and Rehabilitated Pavement Structures. Final Report, NCHRP Project 1-37A. Transportation Research Board of the National Academies, Washington, D.C.
13. Kramer, S.L. (1996). Geotechnical Earthquake Engineering. Prentice Hall Civil Engineering and Engineering Mechanics Series, Upper Saddle River, NJ: Prentice Hall. 191-206.
14. Choi, J.W., Wu, R., Pestana, J.M., and Harvey, J.T. (2009). New Layer-moduli Back-calculation Method Based on the Constrained Extended Kalman Filter. *Journal of Transportation Engineering*, 136(1), 20-30.

15. Jeon, E.J. (2009). Comprehensive Performance Evaluation of In-place Recycled Hot Mix Asphalt as Unbound Granular Material. PhD Dissertation, University of California, Davis.
16. Lekarp, F., Isacsson, U., and Dawson, A. (2000). State of the Art. I: Resilient Response of Unbound Aggregates. *Journal of Transportation Engineering*, 126(1), 66-75.
17. Richards, B.G. (1967). Moisture Flow and Equilibria in Unsaturated Soils for Shallow Foundations. In A. Johnson (Ed.), *Permeability and Capillarity of Soils*. 4-34.
18. Lu, N., and Likos, W.J. (2004). *Unsaturated Soil Mechanics*: Hoboken, New Jersey: John Wiley and Sons, Inc.
19. Mitchell, J., and Soga, K. (2005). *Fundamentals of Soil Behavior* (3rd ed.). India: Wiley-India.
20. Holtz, R. D. K., William D., Sheahan, Thomas C. (2011). *An Introduction to Geotechnical Engineering* (2<sup>nd</sup> ed.). Upper Saddle River, NJ: Pearson Education, Inc.
21. Kannemeyer, L, Theyse, H.L., Verhaeghe, B., and Van As, S.A. 2015. Revision of South African Pavement Design Method. In: 11th Conference on Asphalt Pavements for Southern Africa (CAPSA) 2015, Sun City, South Africa, 16-19 August 24, 2015.
22. Fredlund, D.G., and Rahardjo, H. (1993). *Soil Mechanics for Unsaturated Soils*. John Wiley and Sons Inc., New York.
23. Mitchell, J. (1962). Components of Pore Water Pressure and Their Engineering Significance. *Clays and Clay Minerals*, 9, 162-184.
24. Hilf, J.W. (1991). Compacted Fill. *Foundation Engineering Handbook*. New York: Springer. 249-316.
25. Monismith, C.L. 2004. Evolution of Long-Lasting Asphalt Pavement Design Methodology: A Perspective. Distinguished Lecture, International Society for Asphalt Pavements, International Symposium on Design and Construction of Long Lasting Asphalt Pavements, June 7-9, Auburn, AL.
26. Bishop, A.W. (1959). The Principle of Effective Stress. Lecture delivered in Oslo, Norway in 1955; published in *Teknisk Ukebla* 106 (39). 859-863.
27. Khoury, C., Khoury, N., and Miller, G. (2011). Effect of Cyclic Suction History (Hydraulic Hysteresis) on Resilient Modulus of Unsaturated Fine-Grained Soil. *Transportation Research Record: Journal of the Transportation Research Board*, 2232(-1), 68-75. *doi: 10.3141/2232-07*
28. Yang, S.R., Huang, W.H., and Tai, Y.T. (2005). Variation of Resilient Modulus with Soil Suction for Compacted Subgrade Soils. *Transportation Research Record: Journal of the Transportation Research Board*, (1913), 99-106.
29. Sawangsuriya, A., Edil, T.B., and Bosscher, P.J. (2009). Modulus-suction-moisture Relationship for Compacted Soils in Postcompaction State. *Journal of Geotechnical and Geoenvironmental Engineering*, 135(10), 1390-1403.

30. Mazari, M., Garibay, J., Abdallah, I., and Nazarian, S. (2015). Effects of Moisture Variation on Resilient and Seismic Moduli of Unbound Fine-Grained Materials. In *Airfield and Highway Pavements 2015*. 885-895.
31. Zapata, C., and C. Cary. (2012). Development of a National Catalog of Subgrade Soil-Water Characteristic Curves (SWCC) Default Inputs to Use in the Mechanistic-Empirical Pavement Design Guide (MEPDG), Preliminary Draft Final Report, National Cooperative Highway Research Program project 9-23A, National Academy of Science, Transportation Research Board.
32. Zapata, C., and C. Cary. (2013). Integrating National Database of Subgrade Soil–Water Characteristic Curves and Soil Index Properties with Mechanistic–Empirical Pavement Design Guide. *Transportation Research Record: Journal of the Transportation Research Board*, (2349), 41-51. *doi:10.3141/2349-06*.
33. Witczak, M., Andrei, D., and Houston, W. (2000). Resilient Modulus as Function of Soil Moisture–Summary of Predictive Models. *Development of the 2002 Guide for the Development of New and Rehabilitated Pavement Structures*, NCHRP, 1-37A.
34. Cary, C., and Zapata, C. (2010). Enhanced Model for Resilient Response of Soils Resulting from Seasonal Changes as Implemented in Mechanistic-Empirical Pavement Design Guide. *Transportation Research Record: Journal of the Transportation Research Board*, (2170), 36-44. *doi:10.3141/2170-05*
35. Monismith, C. L., Deacon, J. A., and Harvey, J. T. (2000). *WesTrack: Performance Models for Permanent Deformation and Fatigue*. Pavement Research Center, University of California, Berkeley.
36. Monismith, C.L. (2016) Personal communication with the H. M. Curran, July, 2016.
37. R.W. Boulanger, personal communication with H. M. Curran, August 10, 2016.
38. Lea, J. D., and Harvey, J. T. (2015a). A Spatial Analysis of Pavement Variability. *International Journal of Pavement Engineering*, 16(3), 256-267.
39. Lea, J. D., and Harvey, J. T. (2015b). Using Spatial Statistics to Characterise Pavement Properties. *International Journal of Pavement Engineering*, 16(3), 239-255.
40. Salour, F., and Erlingsson, S. (2013). Moisture-Sensitive and Stress-Dependent Behavior of Unbound Pavement Materials from In Situ Falling Weight Deflectometer Tests. *Transportation Research Record: Journal of the Transportation Research Board*, 2335, 121-129. *doi:10.3141/2335-13*.
41. Sauer, E. K., and Monismith, C. L. (1968). Influence of Soil Suction on Behavior of a Glacial Till Subjected to Repeated Loading. *Highway Research Record 215*, Highway Research Board, National Academy of Sciences, Washington DC.
42. Lukanen, E. O., Stubstad, R., and Briggs, R. (2000). *Temperature Predictions and Adjustment Factors for Asphalt Pavement* (No. FHWA-RD-98-085).
43. Paige-Green, P., and Du Plessis, L. (2009). *Use and Interpretation of the Dynamic Cone Penetrometer (DCP) Test*. CSIR Built Environment, Pretoria.

44. Council for Science and Industrial Research (1997). Short Courses on Design of Flexible Pavements in South Africa. Volumes 1 and 2. 24 to 28, Roads and Transport Technology, Pretoria, South Africa, 5-1 to 6-35.
45. Chai, G., and Roslie, N., 1998. The Structural Response and Behavior Prediction of Subgrade Soils using Falling Weight Deflectometer in Pavement Construction. In: Proceedings of the 3rd International Conference on Road and Airfield Pavement Technology.
46. Chen, J., Hossain, M., and Latorella, T. (1999). Use of Falling Weight Deflectometer and Dynamic Cone Penetrometer in Pavement Evaluation. Transportation Research Record: Journal of the Transportation Research Board, (1655), 145-151. *doi:10.3141/1655-19*.
47. Chen, D., Lin, D., Liau, P., and Bilyeu, J. (2005). A Correlation between Dynamic Cone Penetrometer Values and Pavement Layer Moduli. Geotechnical Testing Journal, 28 (1), 1-8. Retrieved from <http://dx.doi.org/10.1520/GTJ12312>.
48. Abu-Farsakh, M., Nazzal, M., Alshibli, K., and Seyman, E. (2005). Application of Dynamic Cone Penetrometer in Pavement Construction Control. Transportation Research Record: Journal of the Transportation Research Board (1913), 52-61. *doi: 10.3141/1913-06*.
49. Mohammad, L. N., Herath, A., Abu-Farsakh, M. Y., Gaspard, K., and Gudishala, R. (2007). Prediction of Resilient Modulus of Cohesive Subgrade Soils from Dynamic Cone Penetrometer Test Parameters. Journal of Materials in Civil Engineering, 19 (11), 986–992.
50. Nazzal, M., Abu-Farsakh, M., Alshibli, K., and Mohammad, L. (2007). Evaluating the Light Falling Weight Deflectometer Device for In Situ Measurement of Elastic Modulus of Pavement Layers. Transportation Research Record: Journal of the Transportation Research Board, (2016), 13-22. *doi:10.3141/2016-02*.
51. Mejías-Santiago, M., García, L., and Edwards, L. (2015). Assessment of Material Strength Using Dynamic Cone Penetrometer Test for Pavement Applications. In Airfield and Highway Pavements 2015. 837-848.
52. Tseng, E. (2013) The Construction of Pavement Performance Models for Flexible Pavement Wheelpath Cracking and IRI for the California Department of Transportation New Pavement Management System. Masters Thesis, University of California, Davis.
53. Department of Transportation, Republic of South Africa (1979) Standard Test Methods for Highways TMH1, Method No. A4. The Determination of the Linear Shrinkage of Soils. Pretoria: National Institute for Road Research. 15-16.
54. Wu, R., Lea, J., Harvey, J., Reazei, A., and Holland, T. J. (2013). The Benefit of Ground Penetration Radar Thicknesses for Back-Calculation Using FWD Data. In Transportation Research Board 92nd Annual Meeting, Washington, D.C. (No. 13-5178).
55. NOAA (2016), Climate Data Online. Precipitation data obtained from [www.ncdc.noaa.gov/cdo-web/](http://www.ncdc.noaa.gov/cdo-web/). (Accessed July 20, 2016.)
56. Weather Underground, Calpine, CA. [www.wunderground.com/history](http://www.wunderground.com/history) (Accessed September 2016)

57. D. Jones, P. Fu, J. Harvey, and F. Halles. 2008. Full-Depth Pavement Reclamation with Foamed Asphalt: Final Report. UCPRC-RR-2008-07.

## **ADDITIONAL SOURCES**

---

Agus, S. S., and T. Schanz. (2005). Comparison of Four Methods for Measuring Total Suction. *Vadose Zone Journal*, 4(4), 1087-1095.

Andrei, D., M/ Witzak, C. Schwartz, and J. Uzan. (2004). Harmonized Resilient Modulus Test Method for Unbound Pavement Materials. *Transportation Research Record: Journal of the Transportation Research Board*, (1874), 29-37.

Ayithi, A., and D. Hiltunen. (2013). Characterization of Moisture-Dependent Changes in Stiffness of Unbound Aggregate Base Materials in Florida. *Transportation Research Record: Journal of the Transportation Research Board*, 2349(-1), 25-31. *doi:10.3141/2349-04*

Bartow, J.A. (1974). Sedimentology of the Simmler and Vaqueros Formations in the Caliente Range-Carrizo Plain area, California (2331-1258).

Burnham, T., and D. Johnson. (1993). In situ Foundation Characterization Using the Dynamic Cone Penetrometer. Minnesota Department of Transportation.

California Department of Transportation (2000). Method of Test for Determining “R” Value of Treated and Untreated Bases, Subbases, and Basement Soils by the Stabilometer. Test CTM-301, Caltrans Engineering Service Center, Transportation Laboratory, Sacramento, CA.

Christopher, B.R., C. Schwartz, and R. Boudreau. (2006). Geotechnical Aspects of Pavements: Reference Manual. US Department of Transportation, Federal Highway Administration. FHWA NHI-05-037

Dibblee, T.W., and J.A. Minch. (2006). Geologic Map of the Miranda Pine Mountain quadrangle, San Luis Obispo and Santa Barbara Counties, California: Dibblee Geological Foundation, Dibblee Foundation Map DF-265, scale 1:24,000

Drumm, E.C., J.S. Reeves, M.R. Madgett, and W.D. Trolinger. (1997). Subgrade Resilient Modulus Correction for Saturation Effects. *Journal of Geotechnical and Geoenvironmental Engineering*, 123(7), 663-670.



Fredlund, D., J.K. Gan, and P. Gallen. (1995). Suction Measurements on Compacted Till Specimens and Indirect Filter Paper Calibration Technique. *Transportation Research Record: Journal of the Transportation Research Board*, 1481, 3-9.

Gabr, M., K. Hopkins, J. Coonse, and T. Hearne. (2000). DCP Criteria for Performance Evaluation of Pavement Layers. *Journal of Performance of Constructed Facilities*, 14(4), 141-148.

George, K. (2003). *Falling Weight Deflectometer for Estimating Subgrade Resilient Moduli*: University of Mississippi.

Gupta, S., A. Ranaivoson, E. Edil, C. Benson, and A. Sawangsuriya. (2007). *Pavement Design Using Unsaturated Soil Technology*. Minnesota Department of Transportation, Research Services Section. Retrieved from the University of Minnesota Digital Conservancy. *hdl.handle.net/11299/5570*

Krahn, J., and D.G. Fredlund. (1972). On Total, Matric and Osmotic Suction. *The Emergence of Unsaturated Soil Mechanics*, 35.

Lekarp, F., I. Richardson, and A. Dawson. (1996). Influences on Permanent Deformation Behavior of Unbound Granular Materials. *Transportation Research Record: Journal of the Transportation Research Board*, (1547), 68-75. *doi: 10.3141/1547-10*

Liang, R.Y. (2006). Validation of Enhanced Integrated Climatic Model Prediction over Different Drainable Base Materials. In *Transportation Research Board 85th Annual Meeting* (No. 06-2529).

Likos, W.J., and N. Lu. (2003). Automated Humidity System for Measuring Total Suction Characteristics of Clay. *Geotechnical Testing Journal*, 26 (2), 1-12. *doi:10.1520/GTJ11321J*

McKeen, R.G. (1981). *Design of Airport Pavements for Expansive Soils* (No. NMERI-AP-37). New Mexico Engineering Research Inst. Albuquerque.

Pavement Interactive (2009). Resistance Value. Accessed from [www.pavementinteractive.org/article/resistance-value/](http://www.pavementinteractive.org/article/resistance-value/)

Papagiannakis, A.T., and E.A. Masad. (2008). *Pavement Design and Materials*. Hoboken, NJ: John Wiley and Sons, Inc.

Puppala, A.J., T. Manosuthkij, S. Nazarian, and L.R. Hoyos. (2011). Threshold Moisture Content and Matric Suction Potentials in Expansive Clays prior to Initiation of Cracking in Pavements. *Canadian Geotechnical Journal*, 48(4), 519-531.

Puppala, A.J., T. Manosuthkij, S. Nazarian, L.R. Hoyos, and B. Chittoori (2012). In Situ Matric Suction and Moisture Content Measurements in Expansive Clay during Seasonal Fluctuations. *Geotechnical Testing Journal*, 35(1), 1-9.

Rahardjo, H., and E.C. Leong. (2006). Suction Measurements. In *Unsaturated Soils 2006*, American Society of Civil Engineers. 81-104

Rosenbalm, D.C., and C.E. Zapata. (2012). Incorporating Stochastic Evaluation in the Estimation of Soil Resilient Modulus. In *Geotechnical Special Publication*. (225 GSP ed., pp. 1458-1467). *doi: 10.1061/9780784412121.150*

Salour F., S. Erlingsson, and C.E. Zapata. (2015). Evaluating a Model for Seasonal Variation of Silty Sand Subgrade Resilient Modulus with FWD Tests. Transportation Research Board 94th Annual Meeting, January 2015, Washington, D.C. (under publication for Transportation Research Record: Journal of the Transportation Research Board).

Seed, H.B., and C.E. Chan. (1960). *Structure and Strength Characteristics of Compacted Clays*: Institute of Transportation and Traffic Engineering, University of California.

Seed, H.B., J. Mitchell, and C. Chan. (1960). The Strength of Compacted Cohesive Soils. ASCE Research Conference on Shear Strength of Cohesive Soils. Boulder, Colorado, 877-964.

Soil Survey Staff, Natural Resources Conservation Service, United States Department of Agriculture. Official Soil Series Descriptions. Available online from [casoilresource.lawr.ucdavis.edu/gmap](http://casoilresource.lawr.ucdavis.edu/gmap).

Thom, N., and S.F. Brown. (1987). Effect of Moisture on the Structural Performance of a Crushed-limestone Road Base. *Transportation Research Record: Journal of the Transportation Research Board*, (1121), 50-56.

Van Aswegen, E., W. Steyn, and H. Theyse. (2015). Development of a Saturation and Stress-dependent Chord Modulus Model for Unbound Granular Material. *Journal of the South African Institution of Civil Engineering*, 57(2), 8-21.

Vanapalli, S., D. Fredlund, D. Pufahl, and A. Clifton. (1996). Model for the Prediction of Shear Strength with Respect to Soil Suction. *Canadian Geotechnical Journal*, 33(3), 379-392.

Wei, Y., and W. Hansen. (2011). Characterization of Moisture Transport and Its Effect on Deformations in Jointed Plain Concrete Pavement. *Transportation Research Record: Journal of the Transportation Research Board*, 2240(-1), 9-15. *doi:10.3141/2240-02*

Zapata, C., Y. Perera, and W. Houston. (2009). Matric Suction Prediction Model in New AASHTO Mechanistic-Empirical Pavement Design Guide. *Transportation Research Record: Journal of the Transportation Research Board*, (2101), 53-62. *doi:10.3141/2101-07*

## APPENDIX A: SITE DESCRIPTIONS

---

### *Colusa 20*

The test section on State Route 20 in Colusa County is located on the eastbound side between PMs 15.35 and 16.35, approximately six miles west of Interstate 5 near Williams. The structure of Col 20 consists of 90 mm of AC over approximately 230 mm of foamed asphalt-stabilized, full-depth reclaimed base (FDR-FA) constructed in 2002. The stretch of road lies just east of the Coast Ranges and is situated upon fan deposits (1, 2). Remote screening of the site from Google Earth™ indicated that agricultural fields were located along both sides of this specific stretch of road and geologic maps also indicated the presence of nearby streams. Surficial soil maps indicate soil is mostly fine-loamy soil (mix of sand, silt, and clay) originating from alluvium. The site lies within the Inland Valley climate region, has an average annual precipitation of approximately 460 mm (18 inches), and lies at an elevation of approximately 49 m.

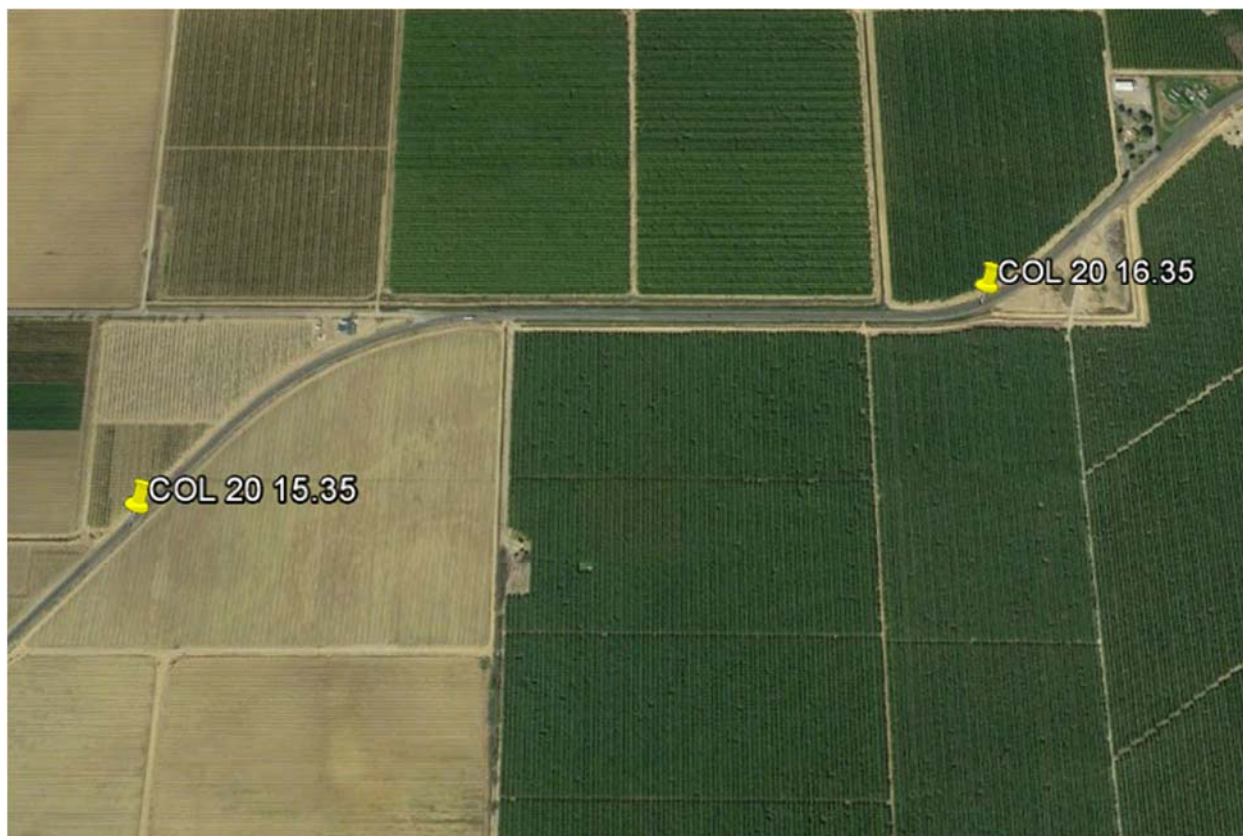


**Figure A.1: Test section on Colusa 20.**

### *El Dorado 193*

The test section on State Route 193 in El Dorado County is located on the eastbound side between PMs 10.4 and 11.4, south of the town of Georgetown. The pavement structure consists of approximately 50 mm of asphalt over approximately 75 mm of cold in-place recycled (CIR) base over the existing pavement structure, and this most

recent rehabilitation was completed in 2014. The site lies in the foothills of the Sierra Nevada; surficial soil maps indicate surficial deposits of weathered material originating from greenstone and/or schist parent rocks and that rock outcrops are often encountered. (2, 3). The site is located within the Low Mountain climate region and gets approximately 1,320 mm (52 inches) of rain per year and 431 mm (17 inches) of snowfall per year, lying at an approximate elevation of 700 m.

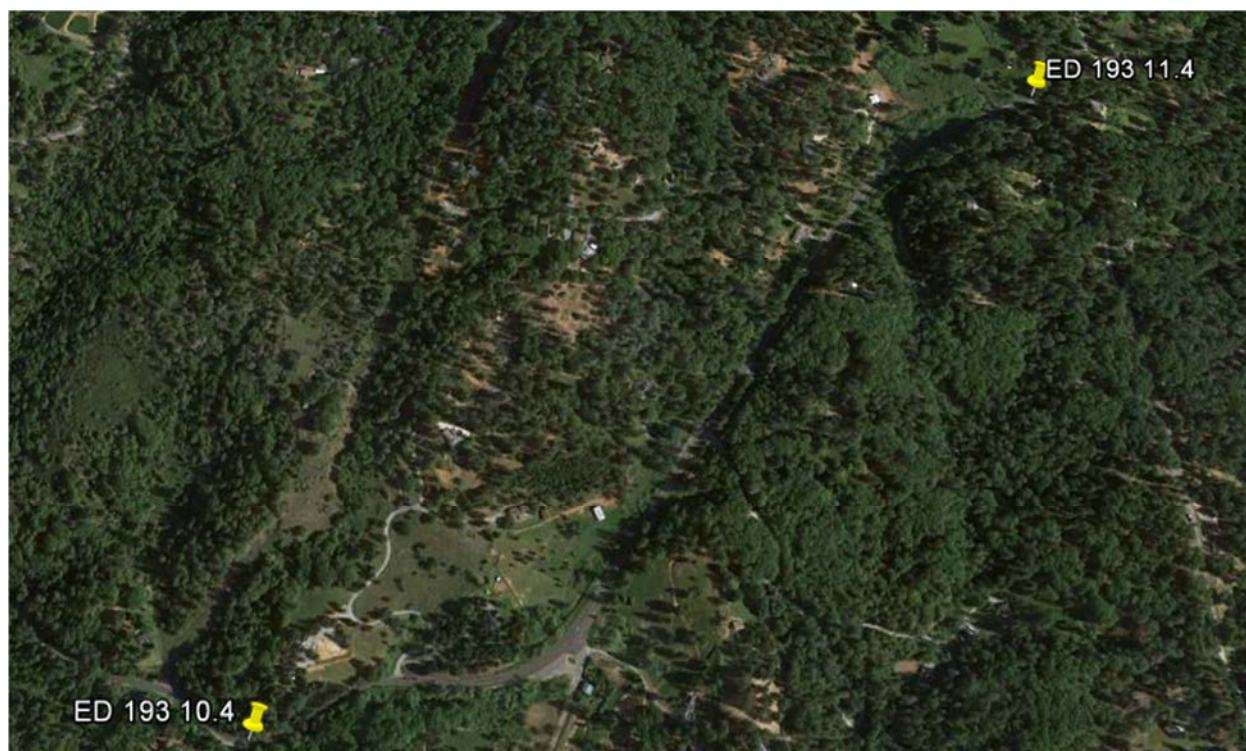


**Figure A.2: Test section on El Dorado 193.**

### *Sierra 89*

The test section on State Route 89 in Sierra County is in the northbound lane between PMs 28 and 29, and is located about 4.5 miles northwest of Calpine. The structure consists of 37 mm of asphalt over 200 mm of FDR-FA base material that was constructed in 2002. The road is north of Sulphur Creek and winds through Plumas National Forest; surficial soil maps indicate coarse to loamy residual soils derived from granodiorite from bedrock and surrounding hillslopes (4). Calpine is located in the High Mountain climate region, averages approximately 1,143 mm (45 inches) of rain and 1,092 mm (43 inches) of snowfall per year, and is located at an elevation of approximately 1,510 m.



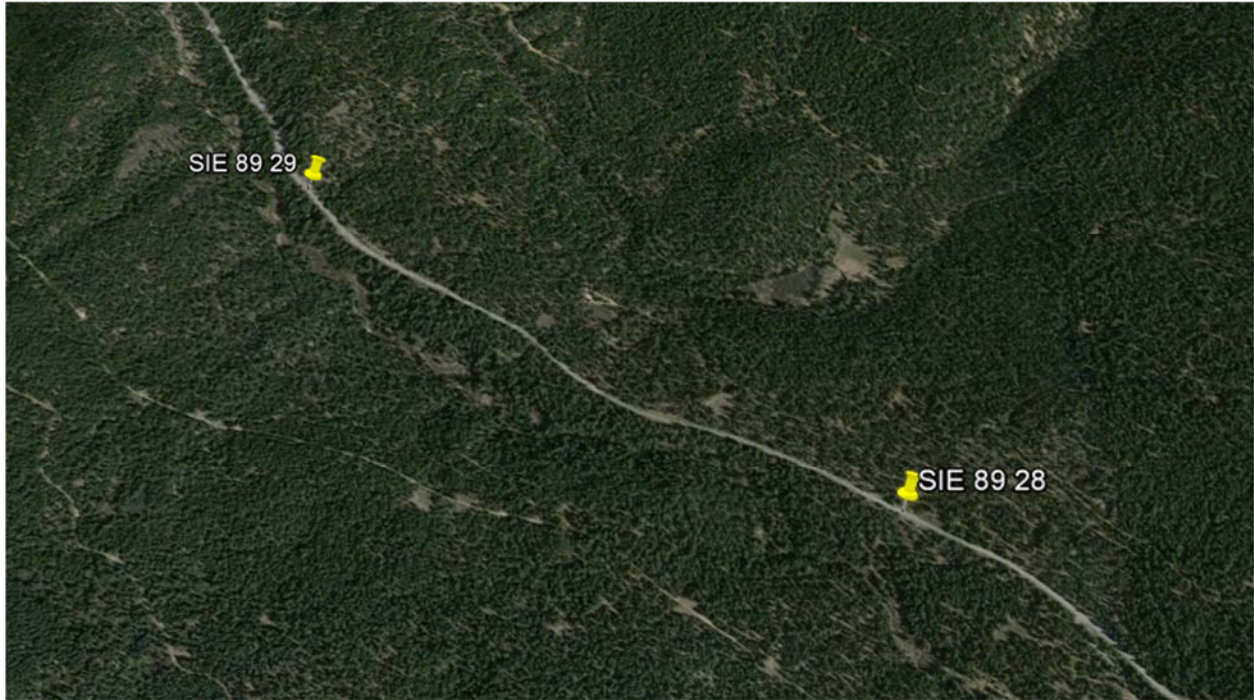


**Figure A.3: Test section on Sierra 89.**

#### *Plumas 70*

The test section on State Route 70 in Plumas County is in the eastbound lane between PM 82 and 83. The structure consists of 165 mm of asphalt overlying 210 mm of pulverized asphalt base (PAB) constructed in 2003, and was evaluated by the UCPRC in 2005. The site is situated approximately two miles east of the town of Beckwourth on the northern edge of the Sierra Valley; surficial soil maps indicate sandy to-silty to-clayey loams are the predominant soil type near the surface (4). Beckwourth is located in the High Desert climate region, averages 229 mm (22 inches) of rain and 1,244 mm (49 inches) of snowfall per year and is located at an elevation of approximately 1,490 m.



**Figure A.4: Test section on Plumas 70.**

### *Ventura 33*

The test section on State Route 33 in Ventura County is in the eastbound lane between PMs 51.5 and 52.5. The structure consists of 75 mm of asphalt material overlying 205 mm of FDR with fly ash and paving ash additives, which was constructed in 2006. The road runs through Los Padres National Forest and is situated approximately nine miles southeast of the town of Ventucopa. The road closely parallels the Cuyama River to the southwest, and surficial sediments indicate alluvial terrace deposits of gravel and sand (5). The site is located within the South Mountain climate region. The nearby town of Ventucopa averages 211 mm (8.3 inches) of rainfall a year and the town is seated at an elevation of approximately 1,030 m.



**Figure A.5: Test section on Ventura 33.**

#### *State Route 166*

Two test sites were located along State Route 166 (New Cuyama Highway) in San Luis Obispo and Santa Barbara Counties in the southern Coast Ranges, just northeast of the Cuyama Valley. This particular stretch of highway is considered a part of the South Coast climate region, typically experiences on average 212 mm (8.33 inches) of rainfall a year, and lies at approximate elevations of 450 to 550 m.

The test section at PM 41.5 in San Luis Obispo County is located approximately 24 miles northwest of the town of New Cuyama and has a structure of 60 mm of AC over 60 mm of CIR; the actual date of construction is unknown. This portion of the highway lies north of the Cuyama River channel, and at the base of a hillslopes comprised of sandstone and conglomerate; soil maps indicate sandy loam fan and terrace deposits derived from the surrounding hills comprise the surface layers. (6).





**Figure A.6: Test section on San Luis Obispo 166.**

The test section at PM 55, located in Santa Barbara County, lies approximately 13.5 miles east of the aforementioned test section on SLO 166. The structure of the highway at this point is comprised of approximately 115 mm of AC over 305 mm of FDR-FA, which was constructed in 2009. The test site lies just south of the Cuyama River channel, founded upon alluvial gravel and sands; soil maps indicate that terraced deposits and gravelly alluvium from abandoned stream channels comprise the surficial layers along this portion of the route (5).



**Figure A.7: Test section on Santa Barbara 166.**

*San Luis Obispo 46*

The test section on State Road 46 in San Luis Obispo County is located on the eastbound side between PMs 36.6 and 37.6, approximately five miles northeast of the city of Paso Robles and about seven miles east of Highway 101. The test site has a structure of approximately 230 mm of AC over 170 mm of LCB that was constructed in 2014. The site is founded upon valley sediments consisting mostly of pebbles, gravel, sand, and clay, as well as older alluvial terrace deposits; soil maps indicate a fine loamy surface material comprised of residual soils from the valley sediments (7). Historical satellite images and street views of the road indicate the presence of vineyards along both sides of the road, approximately 20 meters from either shoulder, that appear to be well watered in summer months. The route lies within the Inland Valley climate region, experiences an annual rainfall of about 330 mm (13 inches), and lies at an elevation of approximately 285 m above sea level.



**Figure A.8: Test section on San Luis Obispo 46.**

*Lassen 44*

The test section along State Route 44 (Feather Lake Highway) is located on the westbound site between PMs 9.5 and 10.5, and is situated within the Lassen National Forest in Grays Valley, approximately fourteen miles east of Old Station and six miles west of Crater Mountain. The structure consists of 165 mm of AC over 270 mm of PAB that was constructed in 2005. Geologic maps indicate that the road is founded upon a combination of basalt and poorly sorted stream-laid alluvium derived from surrounding volcanic rocks; soil maps indicate that surficial deposits are mostly comprised of residual soils derived from basalt and andesite (8). The route lies with the High Mountain climate region at an elevation of approximately 1,700 m.



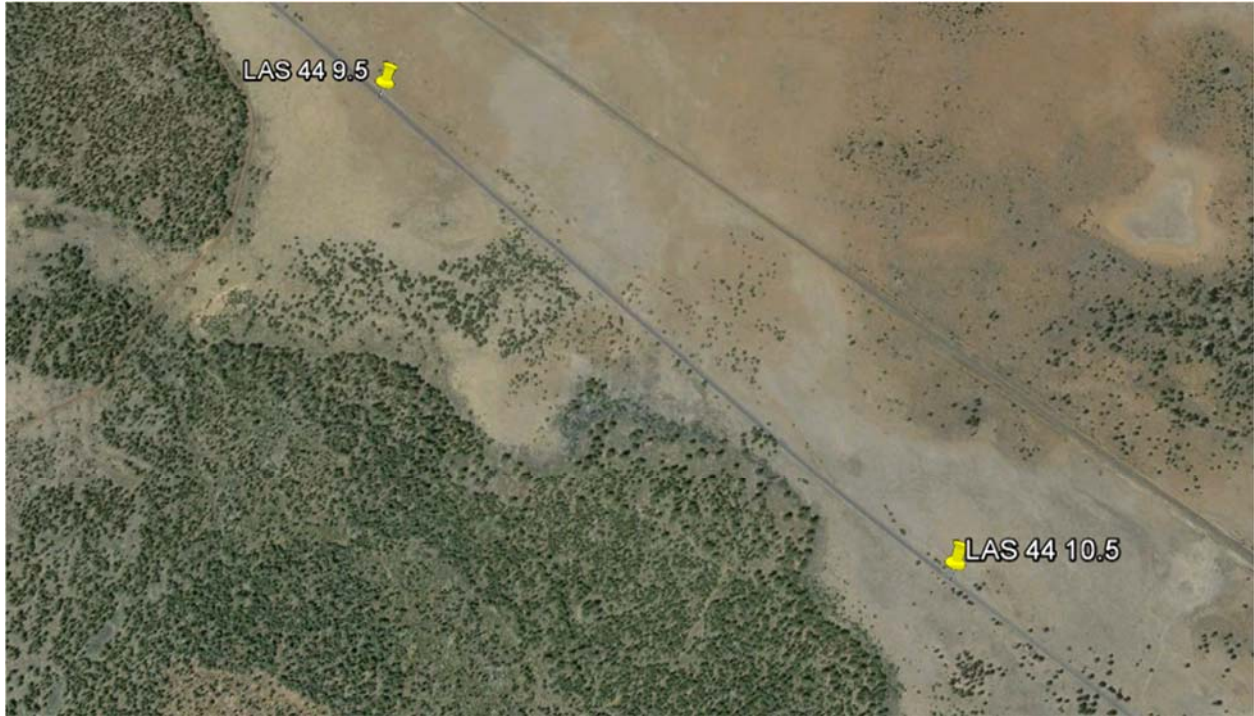


**Figure A.9: Test section on Lassen 44.**

*Modoc 395*

The test section on U.S. Route 395 is located on the northbound lane between PMs 13.5 and 14.5, approximately 10.5 miles south of the town of Alturas. The site structure consists of 150 mm of AC over 200 mm of PAB that was constructed in 2001. The road is situated to the east of the South Fork Pit River and lies within the geologic setting of the site the Modoc Plateau, which is comprised of assorted volcanic materials. Soil maps indicate that residual and lacustrine soils derived from igneous rock are the predominant surface material, although various ash or pyroclastic deposits may also be present (9). The site is a part of the High Desert climate region, experiences average rainfall of 12 inches and average snowfall of 762 mm (30 inches), and lies at an elevation of approximately 1,340 m.



**Figure A.10: Test section on Modoc 395.**

### *Modoc 299*

The test site on State Route 299 is located in the eastbound lane between PMs 59.5 and 60.5, approximately two miles east of the town of Cedarville in the Surprise Valley. The road is an embankment road with a known structure of 91 mm of AC over 183 mm of cement-stabilized, full-depth reclaimed base (FDR-C) constructed in 2011 that serves as a causeway over Middle Alkali Lake near the California-Nevada border. Similar to Route 395, the site is within the geologic region of the Modoc Plateau, and geologic and soil maps indicate lacustrine deposits are the predominant surficial material (9). In addition, notable geothermal activity occurs in the valley and appears to be related to residual volcanism (2). The site lies within the High Desert climate region, has average annual precipitation of approximately 381 mm (15 inches) of rainfall and 787 mm (31 inches) of snowfall per year, and lies at an elevation of approximately 1,370 m.



**Figure A.11: Test section on Modoc 299.**

### **Appendix A References**

1. Jennings, C., and Strand, R. (1960). Geologic Map of California: Ukiah Sheet. California Division of Mines and Geology, scale 1:250,000
2. Norris, R. M., and Webb, R. W. (1990). Geology of California (2nd ed.). United States of America: Somerset, New Jersey: John Wiley and Sons, Inc.
3. Wagner, D., Jennings, C., Bedrossian, T., and Bortugno, E. (1981). Geologic Map of the Sacramento Quadrangle: California Division of Mines and Geology Regional Geologic Map 1A, scale 1:250,000
4. Saucedo, G.J., and Wagner, D.L. (1992) Geologic Map of the Chico Quadrangle: California Division of Mines and Geology, Regional Geologic Map 7A, scale 1:250,000
5. Dibblee, T. W., and Minch, J. A. (2006). Geologic Map of the Rancho Nuevo Creek Quadrangle, Santa Barbara and Ventura Counties, California: Dibblee Geological Foundation, Dibblee Foundation Map DF-258, scale 1:24,000
6. Dibblee, T.W., and Minch, J.A. (ed.), 2005, Geologic Map of the Caliente Mountain Quadrangle, San Luis Obispo and Santa Barbara Counties, California: Dibblee Geological Foundation, Dibblee Foundation Map DF-178, scale 1:24,000.

7. Dibblee, T. W., and Minch, J. A. (2004). Geologic Map of the Estrella and Shandon Quadrangles, San Luis Obispo County, California: Dibblee Geological Foundation, Dibblee Foundation Map DF-138, scale 1:24,000
8. Macdonald, G. A. (1965). Geologic Map of the Harvey Mountain Quadrangle, Lassen County, California. U.S. Geological Survey, Geologic Quadrangle Map GQ-443, scale 1:62,500
9. Gay Jr, T. E., and Aune, Q. A. (1958). Geologic Map of California, Alturas Sheet: California Division of Mines and Geology Map Sheet, scale 1:250,000

## APPENDIX B: ASPHALT-BOUND MATERIAL

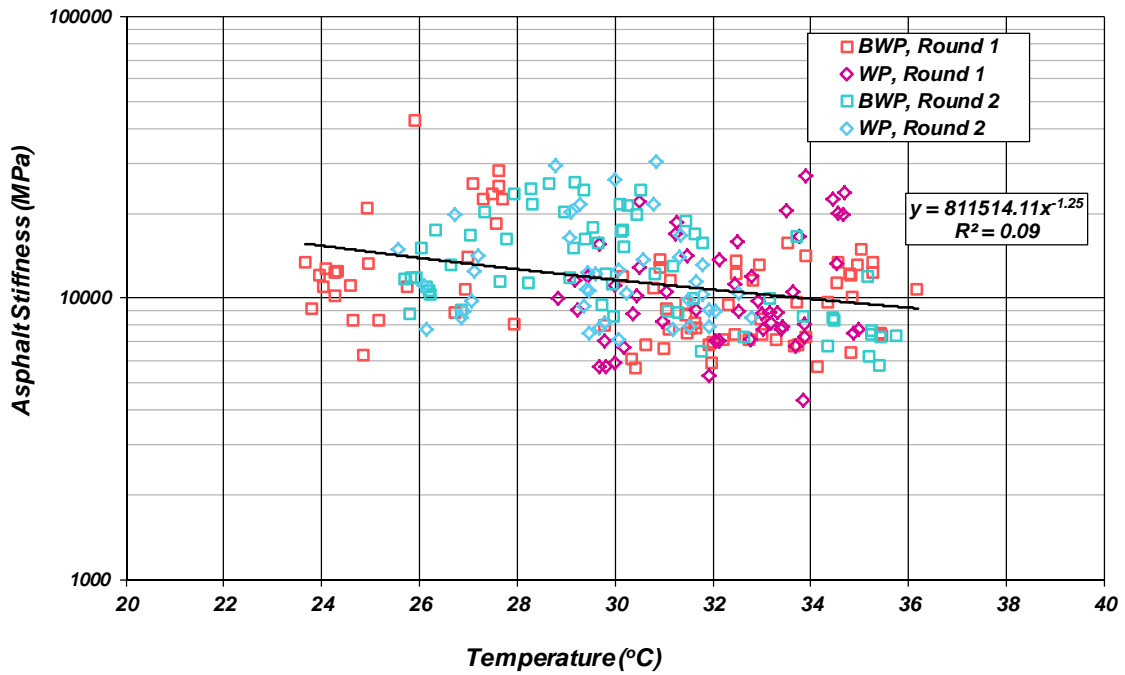


Figure B.1: Colusa 20 asphalt stiffness versus temperature.

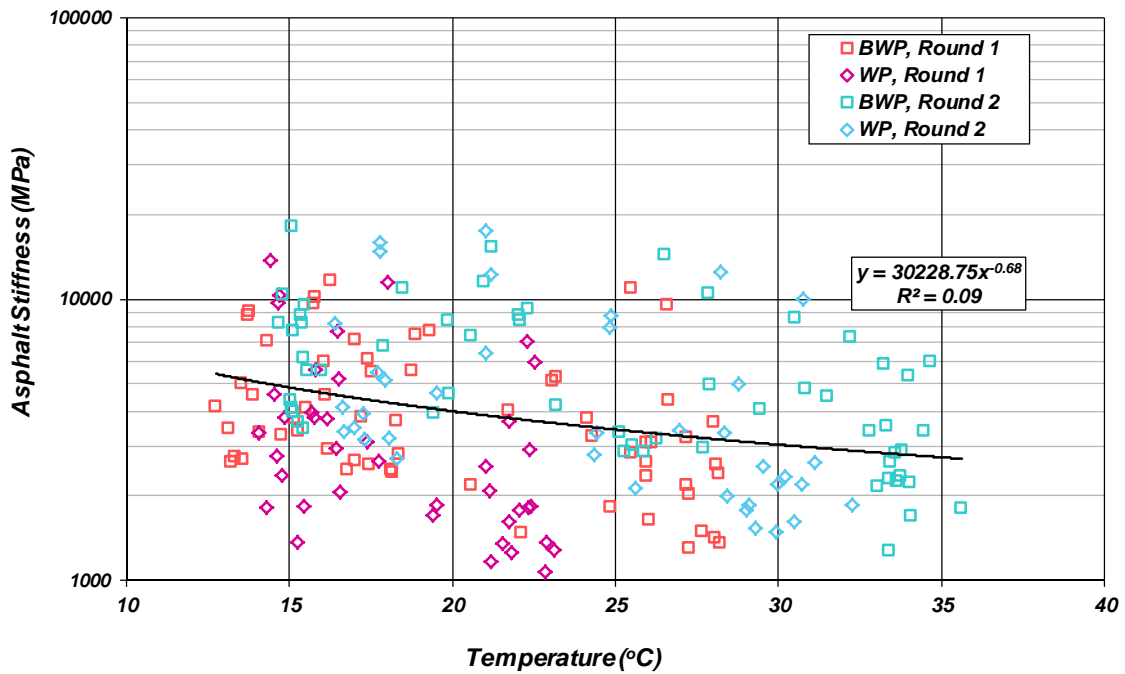


Figure B.2: El Dorado 193 asphalt stiffness versus temperature.



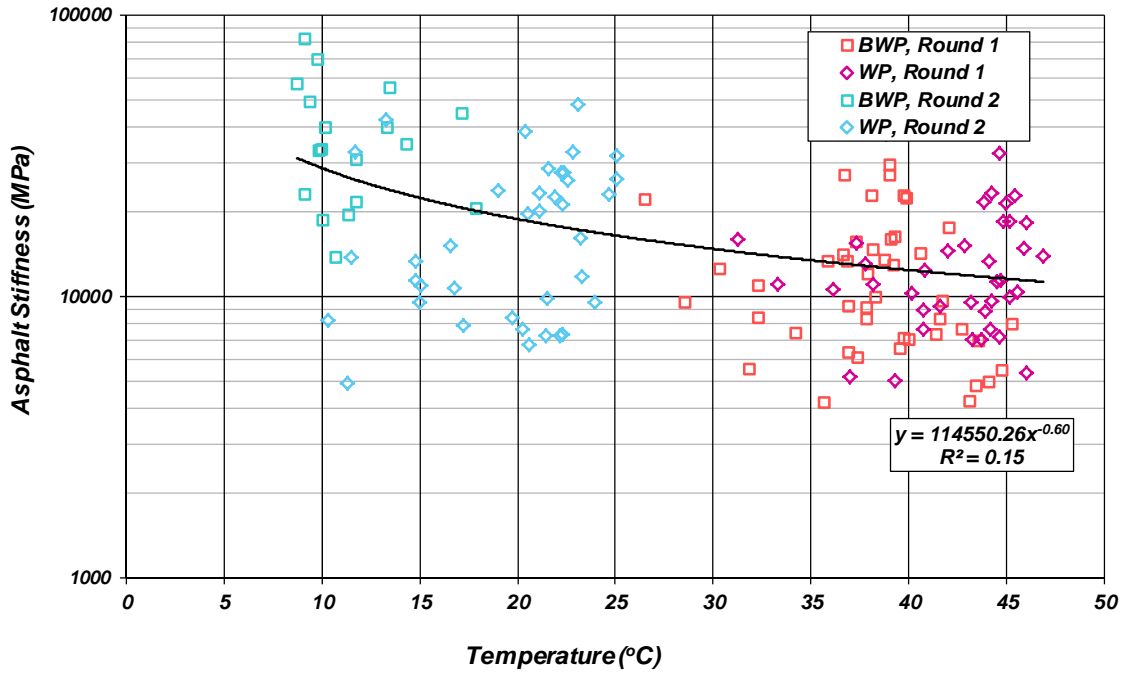


Figure B.3: Sierra 89 asphalt stiffness versus temperature.

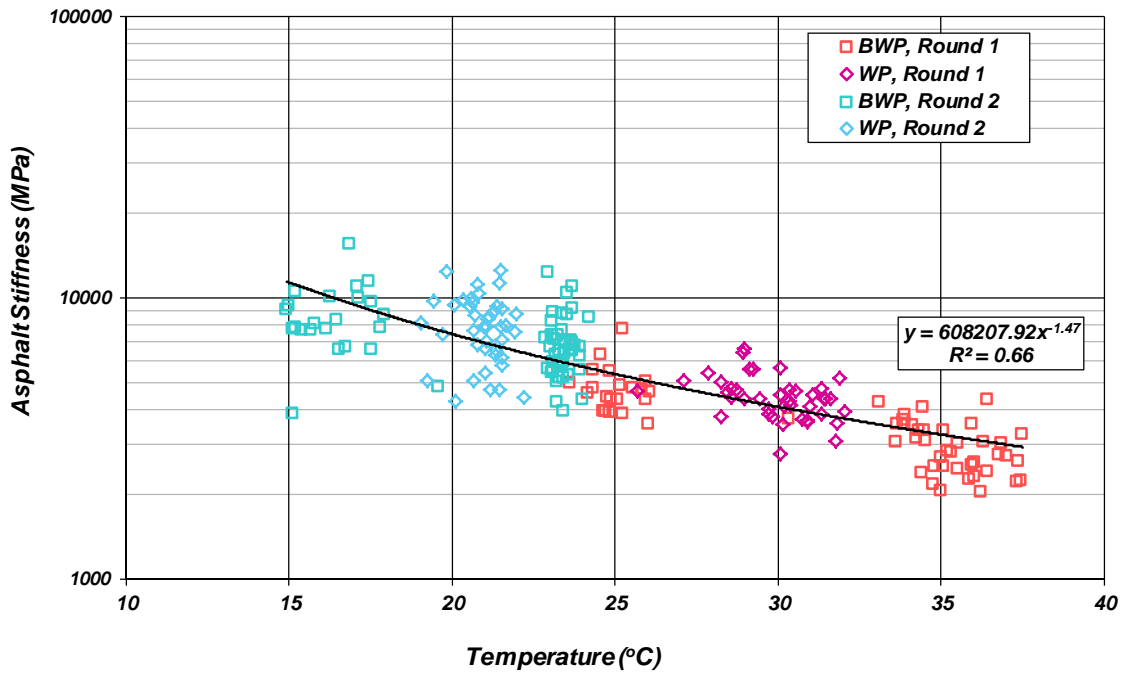


Figure B.4: Plumas 70 asphalt stiffness versus temperature.

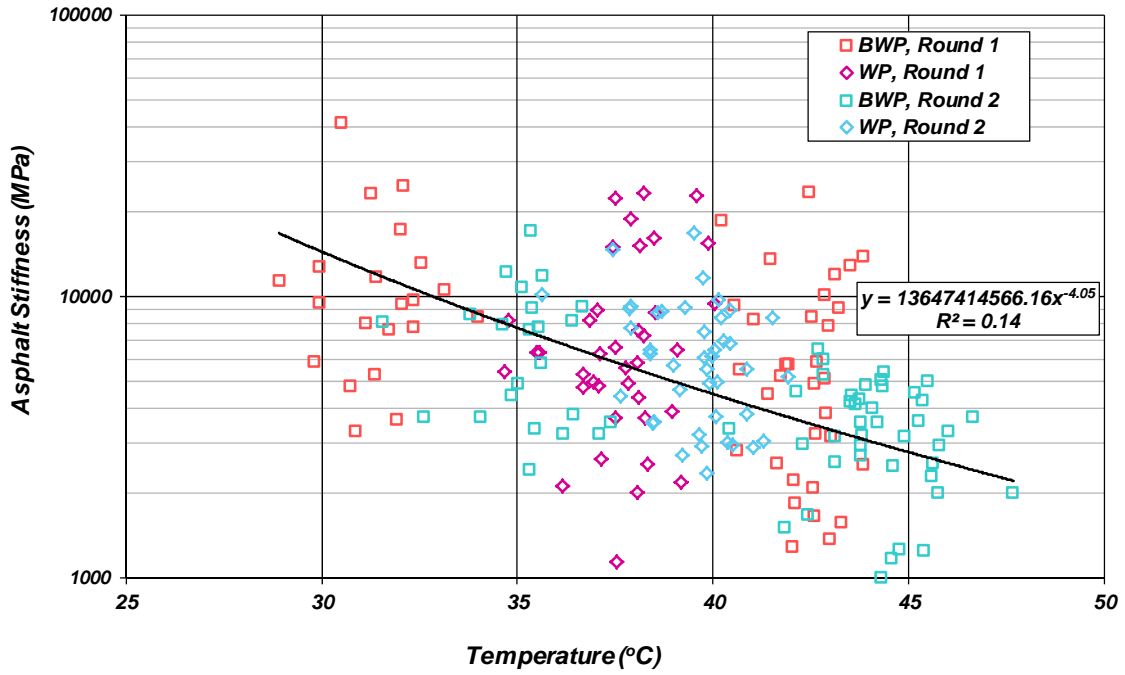


Figure B.5: Ventura 33 asphalt stiffness versus temperature.

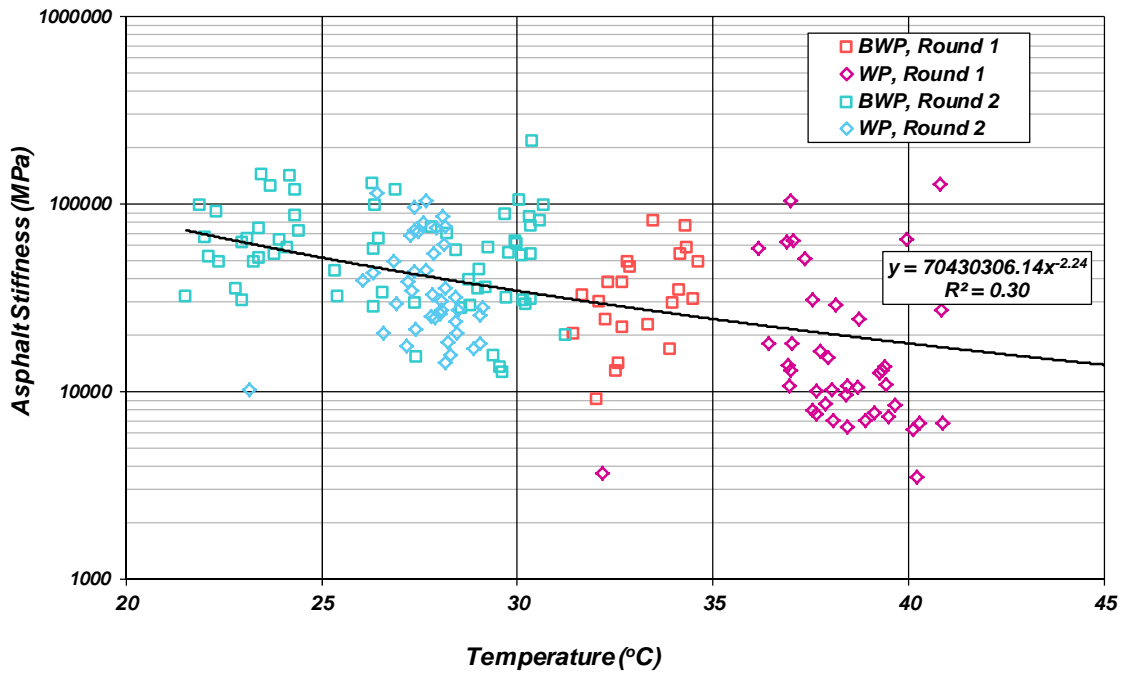


Figure B.6: Santa Barbara 166 asphalt stiffness versus temperature.

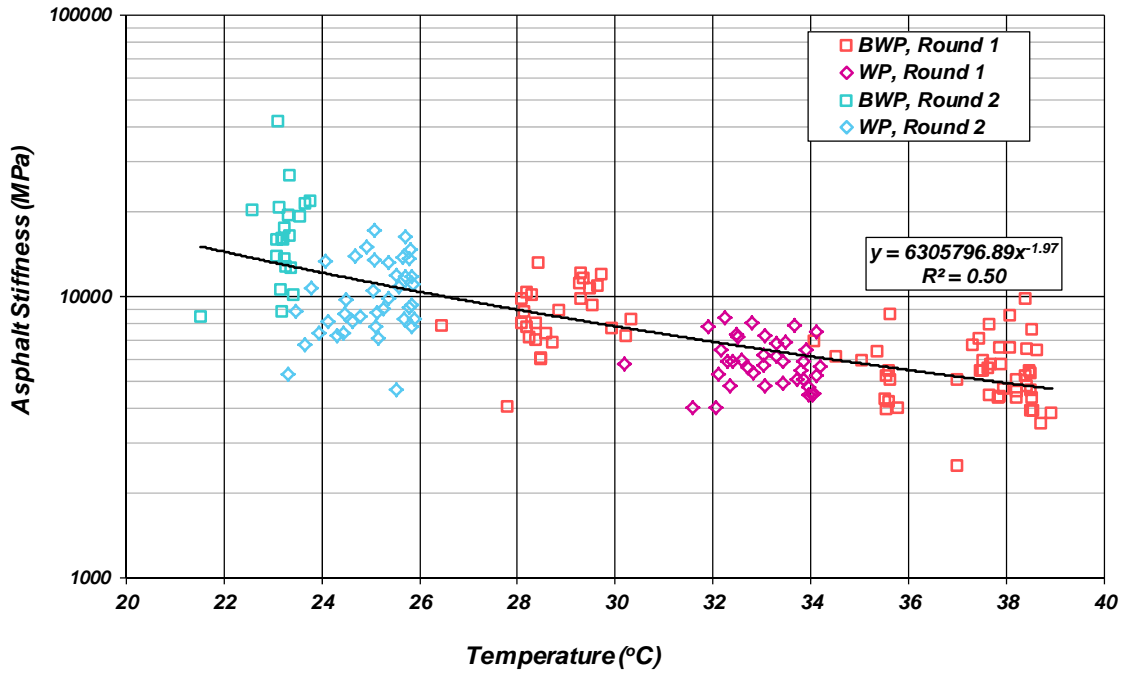


Figure B.7: San Luis Obispo 46 asphalt stiffness versus temperature.

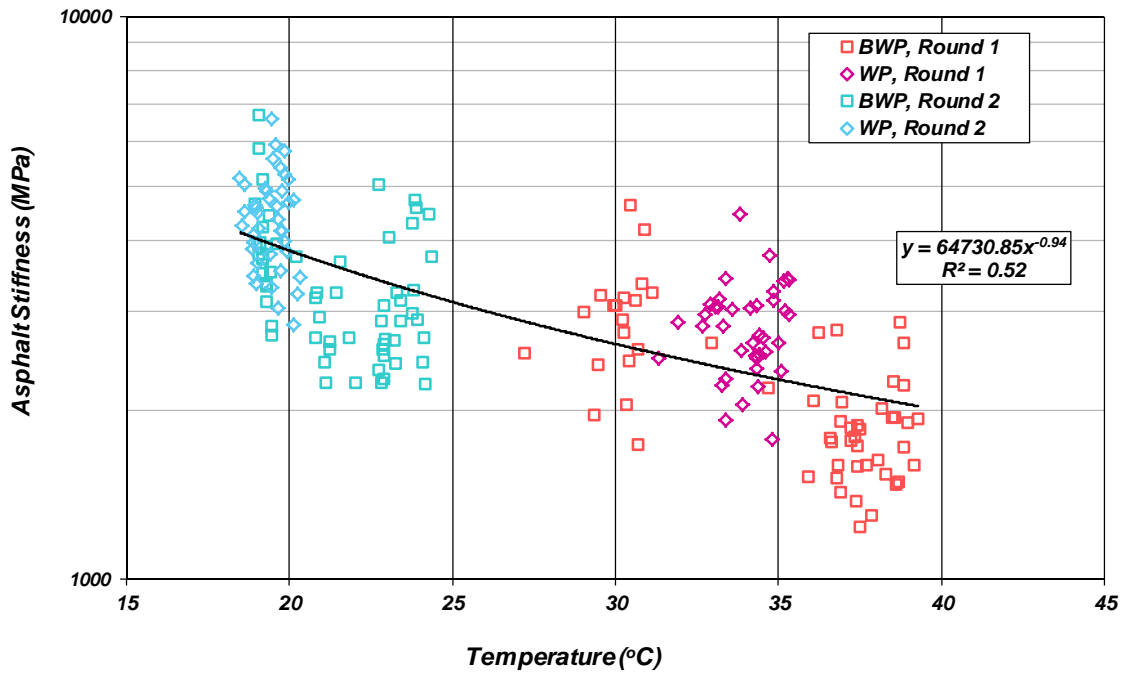


Figure B.8: Lassen 44 asphalt stiffness versus temperature.

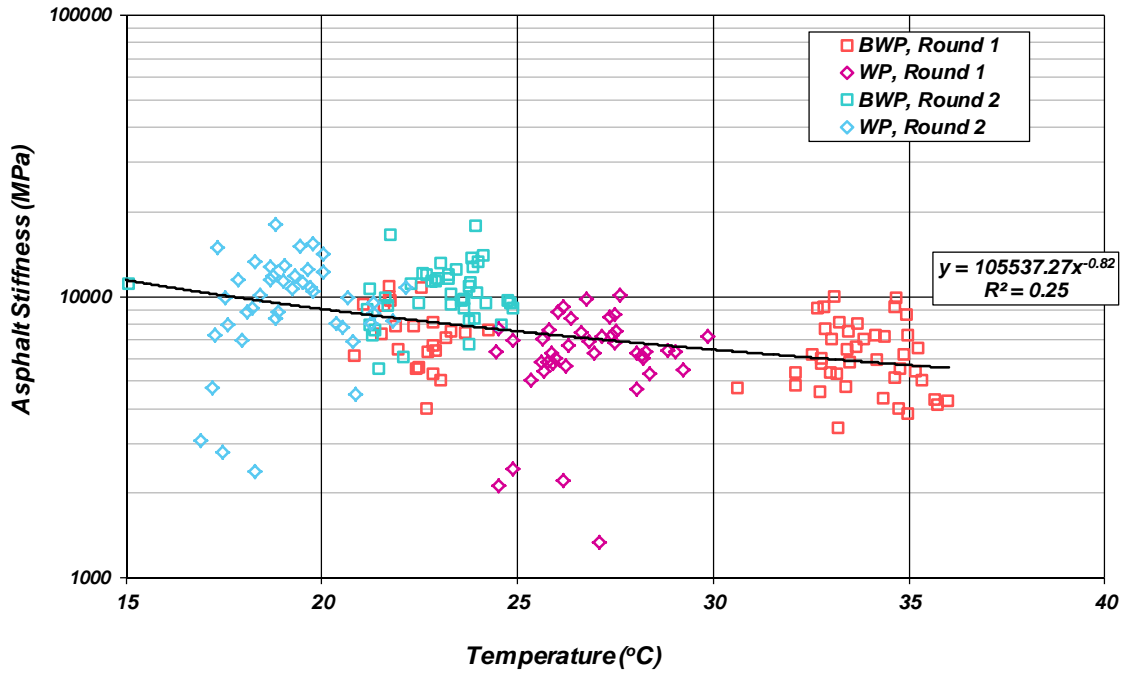


Figure B.9: Modoc 395 asphalt stiffness versus temperature.

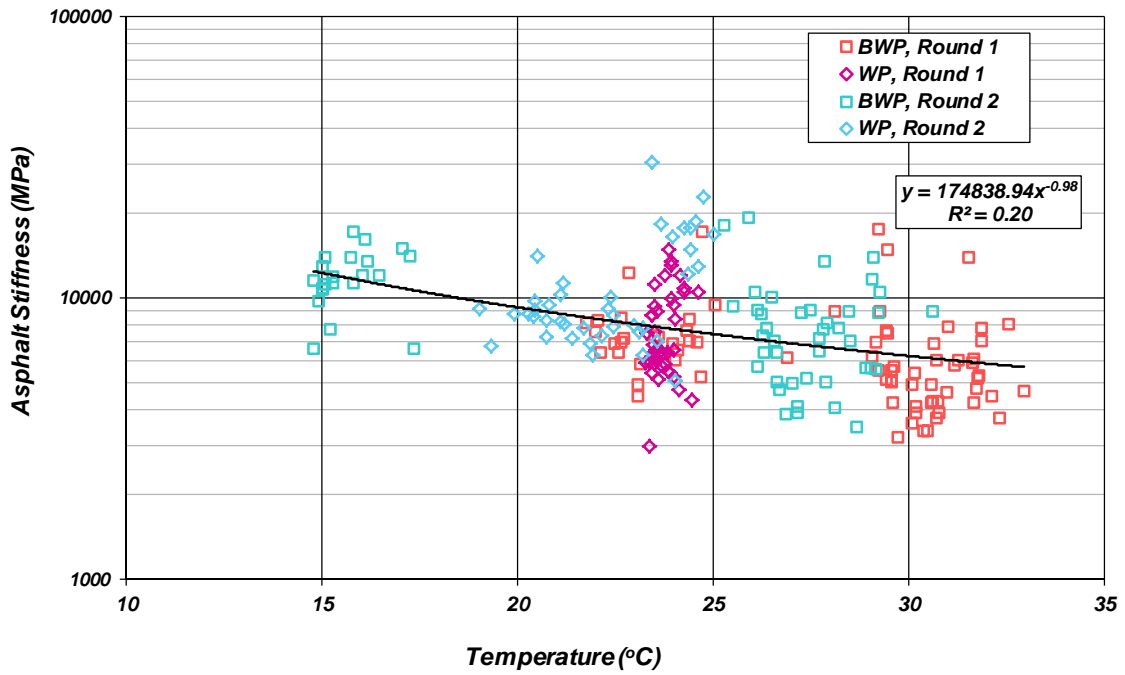


Figure B.10: Modoc 299 asphalt stiffness versus temperature.

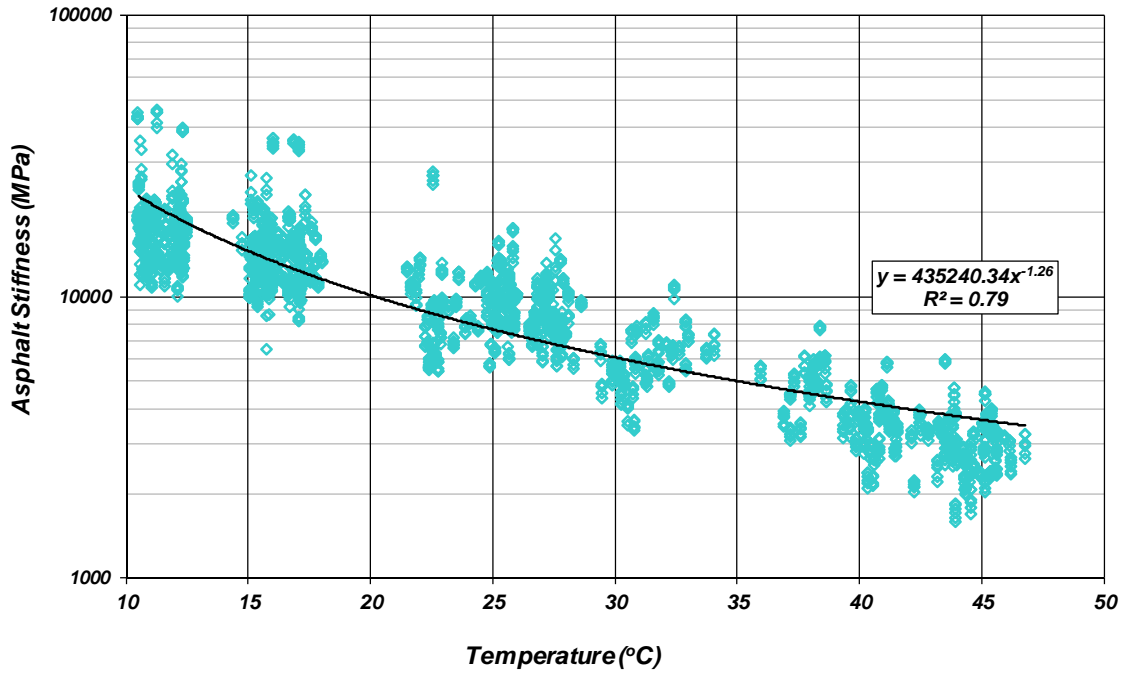


Figure B.11: Asphalt stiffness versus temperature for ATIRC.

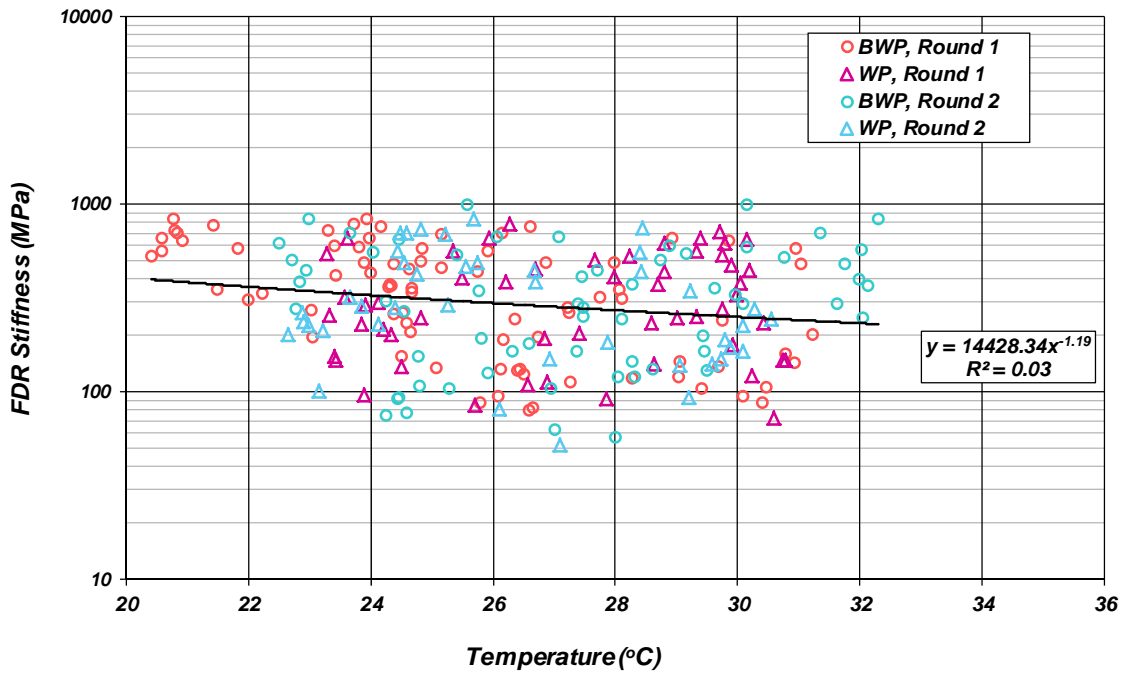


Figure B.12: Colusa 20 FDR-FA stiffness versus temperature.

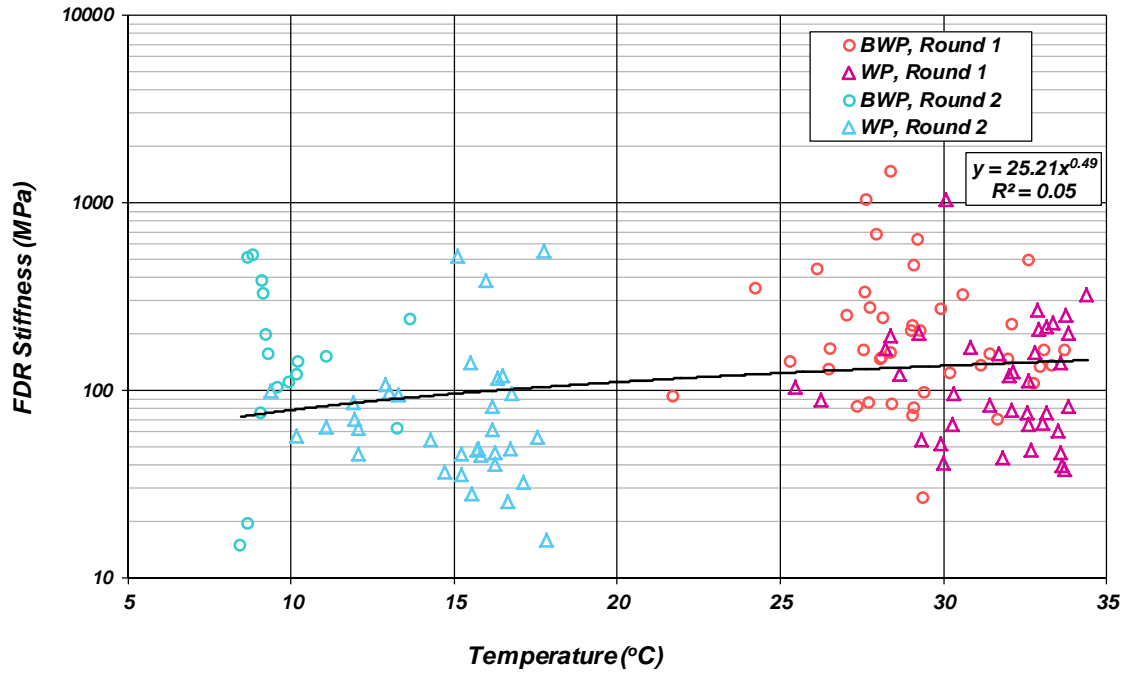


Figure B.13: Sierra 89 FDR-FA stiffness versus temperature.

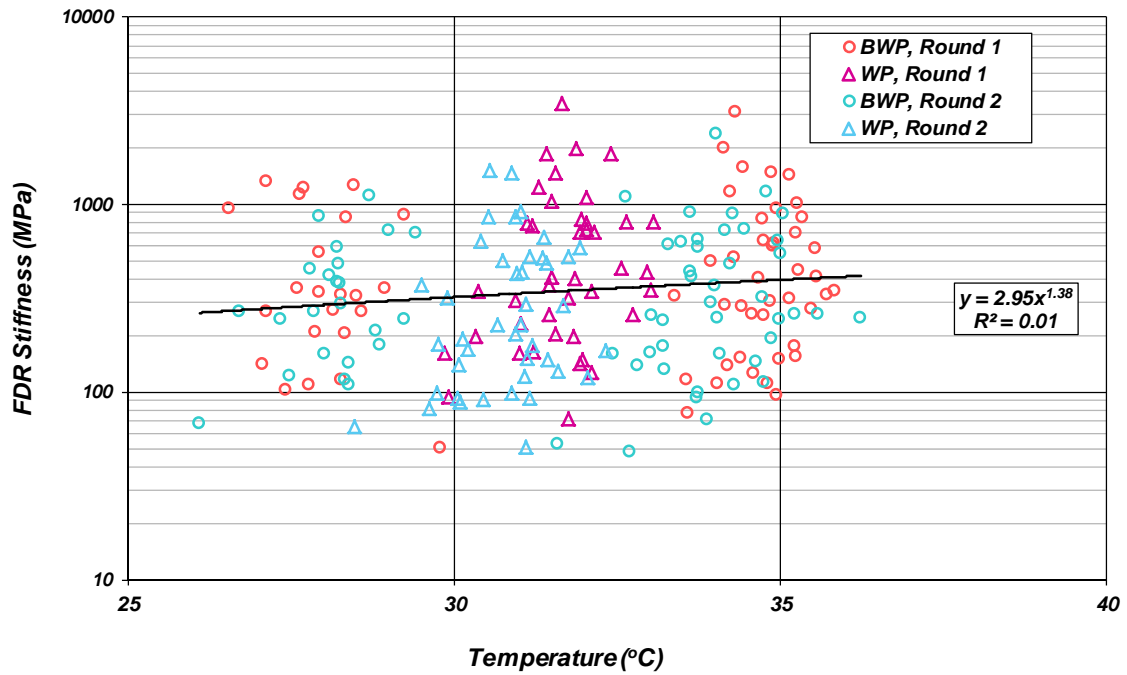


Figure B.14: Ventura 33 FDR-fly ash stiffness versus temperature.

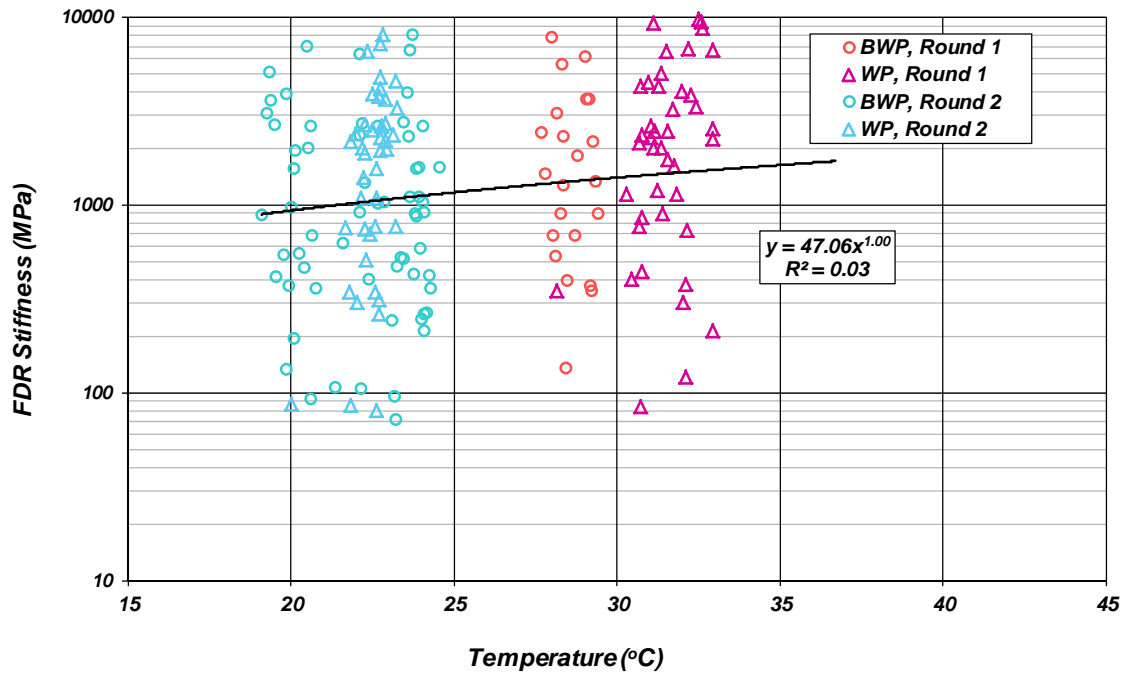


Figure B.15: Santa Barbara 166 FDR-FA stiffness versus temperature.

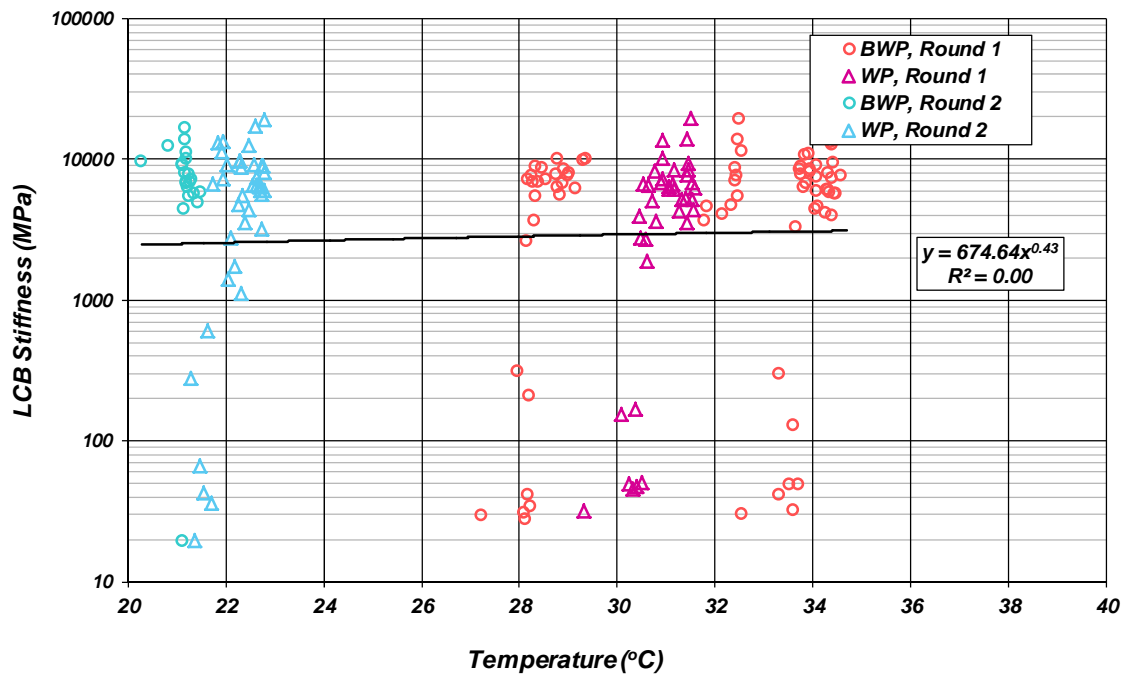


Figure B.16: San Luis Obispo 46 LCB stiffness versus temperature.

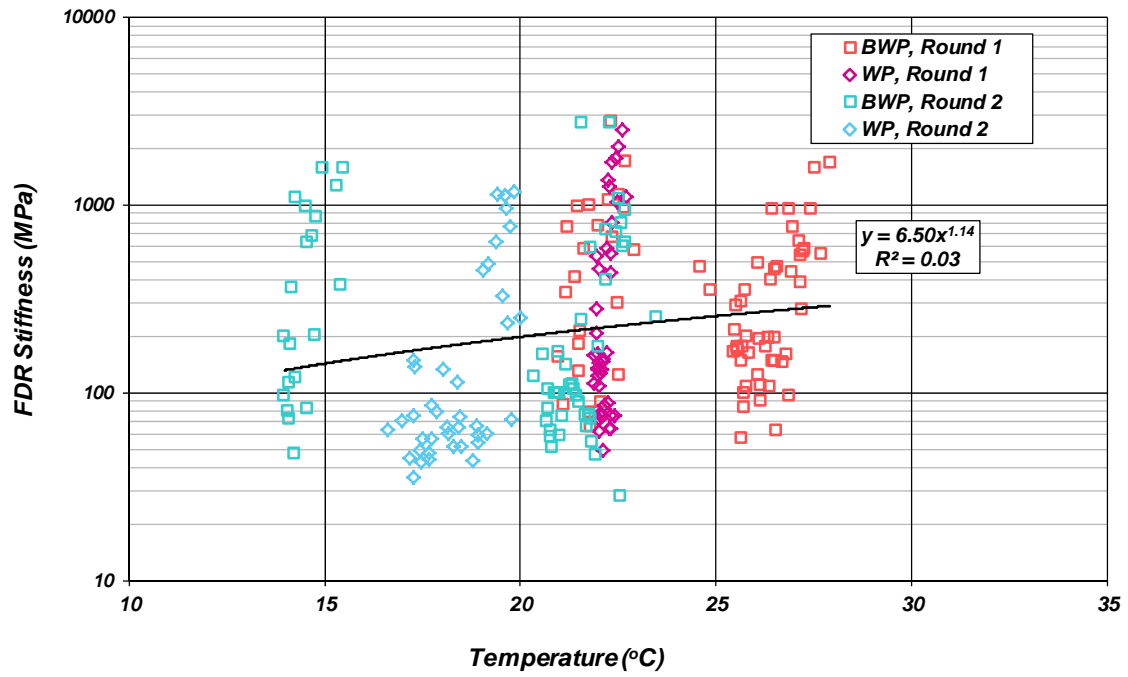


Figure B.17: Modoc 299 FDR-C stiffness versus temperature.